

**EXPERIMENTAL STUDIES ON HYDROGEN INDUCED
CRACK INITIATION IN FLAT ROLLED STEELS IN SOUR
SERVICE**

A thesis submitted to the
University of Petroleum and Energy Studies

For the award of
Doctor of Philosophy
in
Mechanical Engineering

By

Goutam Ghosh

June 2019

Supervisors

**Dr. Rajnish Garg
Dr. Ashoutosh Panday
Dr. Paul Rostron**



UNIVERSITY WITH A PURPOSE

Department of Mechanical Engineering
University of Petroleum & Energy Studies
Dehradun-248007, Uttarakhand

**EXPERIMENTAL STUDIES ON HYDROGEN INDUCED
CRACK INITIATION IN FLAT ROLLED STEELS IN SOUR
SERVICE**

A thesis submitted to the
University of Petroleum and Energy Studies

For the award of
Doctor of Philosophy
in
Mechanical Engineering

By

Goutam Ghosh
SAP ID 500018537
June 2019

Internal Supervisors

Dr. Rajnish Garg
Professor, Department of Mechanical Engineering
University of Petroleum and Energy Studies

Dr. Ashoutosh Panday
Professor, Department of Chemical Engineering
University of Petroleum and Energy Studies

External Supervisor

Dr. Paul Rostron
Assistant Professor, Department of Chemistry
Khalifa University, The Petroleum Institute, Abu Dhabi, UAE



UNIVERSITY WITH A PURPOSE

Department of Mechanical Engineering
University of Petroleum & Energy Studies
Dehradun-248007, Uttarakhand

DECLARATION

I declare that the thesis entitled “**EXPERIMENTAL STUDIES ON HYDROGEN INDUCED CRACK INITIATION IN FLAT ROLLED STEELS IN SOUR SERVICE**” has been prepared by me under the guidance of **Dr. Rajnish Garg**, Professor, Department of Mechanical Engineering, University of Petroleum and Energy Studies, Dehradun, **Dr. Ashoutosh Panday**, Professor, Department of Chemical Engineering, University of Petroleum and Energy Studies, Dehradun, and **Dr. Paul Rostron**, Asst. Professor of Chemistry, Khalifa University, The Petroleum Institute, Abu Dhabi, UAE.

No part of this thesis has formed the basis for the award of any degree or fellowship previously.

Goutam Ghosh

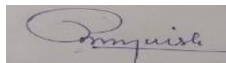
Department of Mechanical Engineering
University of Petroleum & Energy Studies
Dehradun-248007, Uttarakhand

Date:.....

THESIS COMPLETION CERTIFICATE

This is to certify that the thesis on “EXPERIMENTAL STUDIES ON HYDROGEN INDUCED CRACK INITIATION IN FLAT ROLLED STEELS IN SOUR SERVICE” by Mr. Goutam Ghosh in Partial completion of the requirements for the award of the Degree of Doctor of Philosophy (Science and Engineering) is an original work carried out by him under our joint supervision and guidance.

It is certified that the work has not been submitted anywhere else for the award of any other diploma or degree of this or any other University.

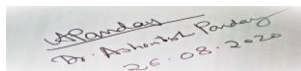


Internal Supervisor

Dr. Rajnish Garg

Professor, Department of Mechanical Engineering
University of Petroleum and Energy Studies
Dehradun, Uttakhand, India.

Date:



Internal Co-Supervisor:

Dr. Ashutosh Panday

Professor, Department of Chemical Engineering
University of Petroleum and Energy Studies
Dehradun, Uttakhand, India.

Date:

THESIS COMPLETION CERTIFICATE

(By External Supervisor)

This is to certify that the thesis on “**EXPERIMENTAL STUDIES ON HYDROGEN INDUCED CRACK INITIATION IN FLAT ROLLED STEELS IN SOUR SERVICE**” by **Mr. Goutam Ghosh** in Partial completion of the requirements for the award of the Degree of Doctor of Philosophy (Science and Engineering) is an original work carried out by him under my supervision and guidance.

It is certified that the work has not been submitted anywhere else for the award of any other diploma or degree of this or any other University.

External Supervisor:

Dr. Paul Rostron
Asst. Professor of Chemistry
Khalifa University, The Petroleum Institute,
AbuDhabi, UAE

Date:

Abstract

The damaging effect of hydrogen on mechanical properties of steels in hydrogen sulfide wet environment has been known over several decades and many equipment failures due to this effect were recorded in Oil & Gas Industry. Hydrogen sulfide or H₂S, has long been associated with the cause of corrosion, as well as, cracking of materials in Oil & Gas production, refining and chemical processing industries.

Atomic hydrogen is produced at local cathodic sites on the metal surface during corrosion reaction. In most corrosive environments, generally, atomic hydrogen recombines on the metal surface to form hydrogen gas (H₂) which evolves on the metal surface without any damaging effect on the material. However, in presence of sulfur containing species resulting from H₂S (dissolved H₂S, HS⁻ and S⁻²), recombination kinetics can be significantly retarded, resulting in substantial absorption of atomic hydrogen in the substrate metal. Sulfur acts as 'poison' in hydrogen recombination (similar to Sn, Sb, Pb and P) which increases efficiency of hydrogen charging in to the corroding metal.

Atomic hydrogen accumulates inside iron lattice and recombines to form molecular hydrogen. The internal pressure created by molecular hydrogen in the steel results in fissures and eventually forms cracks in the metal. The phenomena is commonly known as 'Hydrogen Induced Cracking' or 'HIC'.

Studies have shown that inclusions in steel is one of the responsible factors which beyond a certain level enhance HIC problem. Among the inclusions, Manganese Sulfide (MnS) is specifically the one which induce the HIC problem most. Accordingly, sulfur level is restricted in steels to curtail the HIC initiation in service, and HIC testing is carried out during fabrication or procurement of flat rolled steel products.

Several other metallurgical and environmental factors like alloying elements, strength of the metal, composition, thickness of the steel product, heat

treatment, microstructure, type and morphology of inclusions, partial pressure of H₂S and CO₂, temperature, pH of the solution and aggressive anions e.g. chlorides are known to contribute to HIC, but how the metallurgical factors and environmental parameters behave for different strength grades of steels to manifest HIC, remain largely inconclusive.

In view of above, the current research has considered different strength grades of pipeline steel as well as pressure vessel steels in several hydrogen sulfide containing environments to study the susceptibility of steels to HIC, and specifically focused on following aspects :-

1. Effect of environmental acidic condition or pH on HIC of steels,
2. Effect of exposure duration on HIC,
3. Behavior of different strength grades on HIC susceptibility of steels,

The present research is essentially an experimental research work. Experimental procedures and test methods followed in the present study for compositional analysis, microstructural characterization, ultrasonic testing, mechanical testing, HIC testing and Scanning Electron Microscopy for crack characterization of different specimens are described in detail. The tests identified that the materials conform to the specifications as ASTM A 234 Gr WPB 42" x 12.37mm (Cap), SA 234 WPB 30" x 9.55mm (Elbow) and API 5L Gr 60 – 36" x 19.05mm (Pipe). Nondestructive ultrasonic testing and metallographic study were carried out for each specimen to ensure that each specimen was free from defects for HIC testing. Twenty seven (27) HIC tests were conducted for three steel specifications in three different pH conditions coupled with three test durations in controlled laboratory conditions as per guiding standard NACE TM 0184. Ultrasonic testing of specimens was carried out subsequent to HIC testing. Hydrogen Induced Cracks were characterized using Optical and Scanning Electron Microscopy. Results of above tests were analyzed thoroughly and tendency of HIC cracking for different steel grades was evaluated for establishing relationship between HIC and environmental conditions along with strength grades of the steels. Extensive analysis of the test

results established following relationships for HIC in steels used for pressure vessels and pipelines fabrication-

- Relationship between Duration of Exposure and Hydrogen Induced Cracking (HIC)-
- Relationship between pH of Environment and Hydrogen Induced Cracking (HIC),
- Relationship between Tensile Strength and Hydrogen Induced Cracking (HIC),
- Microstructures and susceptibility to HIC, including types of inclusions and precipitates promoting HIC.

Significance of all test results and established relationships viz. Exposure Duration Vs HIC, pH Vs HIC, and Strength Vs HIC was discussed. Quantitative analysis of test results and established relationships among the variables provide in-depth understanding about effect of the above variables on HIC in steels

Research study achieves the set objectives and concludes with valuable outcome in terms of recommendation to use low strength grade steels with bainitic microstructure in hydrogen sulfide wet environment having pH above 2.7 and below 6.0 to avoid/minimize HIC. Some key parameters not considered in the present study but identified as future scope of this work include resistance of mixed microstructures, effect of banding and effect of thickness on HIC initiation and propagation in different steel microstructures

ACKNOWLEDGEMENTS

The research project presented herein “EXPERIMENTAL STUDIES ON HYDROGEN INDUCED CRACK INITIATION IN FLAT ROLLED STEELS IN SOUR SERVICE” would not have been possible without considerable support from my guides, Dr. Rajnish Garg and Dr. Ashoutosh Panday. I express my sincere gratitude to them.

I take this opportunity to thank my external guide, Dr. Paul Rostron, who supported me through all difficult terrains of the Ph. D. work.

I specially thank my friend Mr. Krishnan Sampath, (Senior Corrosion Engineer, Dragon Oil Holdings Limited, Dubai, and Ex-General manager, M/s. Global Vision Management Consultancy, Abu Dhabi), who facilitated the laboratory testing of samples and encouraged in the research work.

My sincere thanks to Mr. Syed S. Hussaini (General Manager, Lonestar Technical and Industrial Services - Abu Dhabi), who has shown extreme generosity by accommodating the testing work for the research within the busy schedule of the laboratory without any hesitation. I am especially thankful to the employees of the Lonestar Technical and Industrial Services, Abu Dhabi for assisting in conducting the tests reported in this thesis with utmost proficiency and diligence, a truly exemplary service towards such research project.

Finally, I am thankful to my family for consistently encouraging me to accomplish my PhD research work.

CONTENTS

Abstract	5
Abbreviations.....	11
List of Symbols	13
List of Figures.....	15
List of Tables	20
Chapter 1: Introduction	23
1.1 Research Motivation.....	27
1.2 Objectives.....	28
1.3 Research Methodology.....	28
1.4 Evaluation of Test Results.....	31
Chapter 2: Literature Survey	32
2.1 Introduction.....	32
2.2 Postulations of Cracking Mechanism (HIC)	34
2.3 Factors Affecting HIC	40
Chapter-3: Experimental Work	118
3.1 Preface.....	118
3.2 Introduction.....	119
3.3 HIC Experiment: Approach.....	120
3.4 Test Program.....	127
3.5 HIC Evaluation	131
3.6 Test Results	135
3.7 Quantitative Evaluation as per NACE TM 0284.....	140
3.8 Discussion	183
CHAPTER FOUR.....	202
4.1 Scanning Electron Microscopy	202
4.2 Conclusion.....	210
4.4 Future Work.....	213
References	214
APPENDIX-1	225
PUBLICATION-1:	225
ScienceDirect Engineering Fracture Mechanics journal.....	225
PUBLICATION-2:	227
International Journal of Applied Engineering Research.....	227
ISSN 0973-4562 Volume 13, Number 11 (2018).....	227
APPENDIX- 2	229

HIC TEST RESULT FOR EACH SPECIMEN.....	229
GLOSSARY.....	231

Abbreviations

API	American Petroleum Institute
ACC	Accelerated Cooling Curve
AIDE	Adsorption induced dislocation emission
BSE	Back scatter electron
CS	Carbon steel
CP	Cathodic protection
CAR	Crack area ratio
CLR	Crack Length Ratio
CTR	Crack Thickness Ratio
CSR	Crack Sensitivity Ratio
CLR	Crack Length Ratio
EDS	Electro Dispersive Spectroscopy
FEA	Finite Element Analysis
HIC	Hydrogen Induced Cracking
HAZ	Heat Affected Zone
HEDE	Hydrogen Enhanced Decohesion Effect
HELP	Hydrogen Enhanced Localized Plasticity
HEE	Hydrogen Environment Embrittlement
IHE	Internal Hydrogen assisted Embrittlement
HEDE	Hydrogen Enhanced Decohesion Effect
HELP	Hydrogen Enhanced Localized Plasticity
HEE	Hydrogen Environment Embrittlement
IHE	Internal Hydrogen assisted Embrittlement
ISO	International Standards Organization
LAS	Low alloy steel
MA	Martensitic Austenitic (compound)
NACE	National Association of Corrosion Engineers
PWHT	Post Weld Heat Treatment
PP	Partial Pressure
SEM	Scanning electron microscopy
SCC	Stress Corrosion Cracking

SSC	Sulfide Stress Cracking
SOHIC	Stress Oriented Hydrogen Induced Cracking
TMCP	Thermo-Mechanically Controlled Processing
TEM	Transmission electron microscopy
UNS	Unified Numbering System
Wt%	Weight percentage

List of Symbols

A	Alpha
CO ₂	Carbon di-Oxide gas
H ₂ S	Hydrogen Sulfide gas
Si	Silicone
CH ₄	Methane
O	Oxygen
NaCl	Sodium Chloride
H ₂ O	Water molecule
H ⁺	Hydrogen ion
°C	Degree Celsius
K	Stress Intensity factor
H _p	Hydrogen produced
H _A	Hydrogen absorbed
K _I	Stress Intensity factor for mode-I loading
K _{ISCC}	Stress Intensity Factor under Stress Corrosion Cracking
Fe	Iron atom
P	Phosphorus
S	Sulfur
Sb	Antimony
As	Arsenic
Mn	Manganese
HS ⁻	Hydrogen Bi-Sulfide
S ²⁻	Di-Sulfide
Fe ⁺	Iron ion
FeS	Iron-sulfide
Sn	Tin
Ti	Titanium
Zr	Zirconium
V	Vanadium
Ta	Tantalum
Mg	Magnesium

U	Uranium
Th	Thorium
SMYS	Specified Minimum Yield strength
YS	Yield strength
E	Electron
N/mm ²	Newton/ square mm
Jss	Permeability
Dapp	Apparent diffusivity
C _{app}	Apparent hydrogen solubility
C	Carbon
L	Thickness

List of Figures

FIGURE No.	DESCRIPTION	PAGE NO.
Figure 1.1	Hydrogen induced cracking (HIC) of carbon steel in H ₂ S environment.	26
Figure 1.2	Typical stepwise cracking (SWC) of steel.	27
Figure 1.3	Schematic diagram showing proposed tests for the study	30
Figure 2.1	Typical HIC morphology is shown.	33
Figure 2.2	Curves showing relative concentration of sulfide with respect to pH of solution.	35
Figure 2.3	Schematic diagram illustrating sites for hydrogen traps in materials	36
Figure 2.4	Micro dimples at crack site as observed by the researcher.	38
Figure 2.5	Cross section view of HIC initiation at M/A constituents in TMCP steel	39
Figure 2.6	Critical hydrogen concentration for HIC for different steels (schematic)	44
Figure 2.7(a)	Hydrogen permeation effect of H ₂ S partial pressure at pH	47
Figure 2.7(b)	Hydrogen permeation effect of solution pH at P _{H₂S} 1 atm.	47
Figure 2.8	Influence of partial pressure of H ₂ S on hydrogen permeation rates in gaseous and aqueous phase.	48
Figure 2.9	HIC in pipeline steel versus testing temperatures are seen.	49
Figure 2.10	Hydrogen permeation at different temperatures in hydrogen sulfide.	50
Figure 2.11	HIC with time of exposure and impact of pH at constant P _{H₂S}	51
Figure 2.12	Comparison of HIC at 1 bar P _{H₂S} and 0.1 bar P _{H₂S} at pH 5.5.	52
Figure 2.13	Modelling of H concentration at different pH values and critical H concentration for cracking.	53
Figure 2.14	Diagram showing TMCP, Normalized and Q & T steels	57
Figure 2.15	TMCP processing with different rolling and cooling schedules	62
Figure 2.16	Microstructure of conventional steel and HIC resistant steel	64
Figure 2.17	Microstructures due to variation of rolling temperature	65
Figure 2.18	Typical second phases DP, B and M/A with hardness values.	66
Figure 2.19	Relationship between diffusible hydrogen content and steel microstructure and (b) HIC susceptibility	67
Figure 2.20	Inclusions typically found in TMCP HIC resistant steels	70
Figure 2.21	Micrographs showing initiation of HIC at inclusions in steels	71
Figure 2.22	Embrittlement of M/A constituents and initiation of HIC.	72

Figure 2.23	HIC initiation sites near agglomerated M/A constituents and Crack propagation in quasi-cleavage manner	73
Figure 2.24	HIC initiation at oxide cluster and crack propagation in quasi-cleavage manner in X70 steel.	74
Figure 2.25	HIC nucleation sites in steels.	75
Figure 2.26	Propagation of HIC in centerline segregation zone in X60 steel	76
Figure 2.27	TEM bright field micrograph showing inclusions in X65 steel	77
Figure 2.28	BSE images of HIC for X80 steel and EDS showing inclusions.	78
Figure 2.29	SEM images of HIC propagation path in different microstructure of X80 steels.	79
Figure 2.30	Crystallographic Direction and Planes of a crystal	82
Figure 2.31	Crystal orientation and Crystallographic planes.	83
Figure 2.32	Stepwise cracks parallel to rolling direction and deflections at complex carbonitride inclusions (SEM and EDS).	84
Figure 2.33	Karnel Average Misorientation in grain along HIC region	85
Figure 2.34	Inverse Pole figure (IPF) mapping of HIC.	86
Figure 2.35	HIC susceptibility due to cold working, and effect of stress relief heat treatment.	91
Figure 2.36	HIC resistance of A516-70 plate with Stress Relief Heat Treatment	92
Figure 2.37	Occurance of HIC and segregation of C, Mn and P in steel	93
Figure 2.38	Microprobe curves of cracked segregation and uncracked segregation HIC tested secimen..	93
Figure 2.39	Effect of phosphorus content on HIC susceptibility	94
Figure 2.40	HIC susceptibility and S content for different heat treated steels	95
Figure 2.41	Change of shape parameter of inclusions with calcium treatment, and HIC susceptibility of calcium treated and untreated steels	96
Figure 2.42	Relative independence of S content versus HIC resistance	97
Figure 2.43	Influence of ‘under’ and over’ calcium treatment on HIC.	97
Figure 2.44	Influence of C/S ratio on CLR for plates with sulfur content \leq 0.001%.	98
Figure 2.45	Effect of Cu content on Hydrogen diffusion and Corrosion rate of API 5LX65 steel.	99
Figure 2.46	STEM image and EDS mapping showing Cu, Ni, Fe and S in scale deposited on steel.	100
Figure 2.47	Illustration of mechanism of formation of protective layers	100
Figure 2.48	Film formation on copper (>02%) bearing steels and EPMA Line Analysis of the protective layer.	102
Figure 2.49	Effect of Cu addition on HIC in Nb containing steel	103
Figure 2.50	Variation of inclusion’s aspect ratio with Nb content in steel	105
Figure 2.51	HIC initiation at interface between TiN inclusion and the matrix	106

Figure 3.1	Starting materials for specimen preparation.	122
Figure 3.2	Photograph showing sample specimens prepared for testing.	122
Figure 3.3	Sample A microstructure.	125
Figure 3.4	Sample D microstructure	126
Figure 3.5	Sample E microstructure.	127
Figure 3.6	HIC specimen extraction from base material	128
Figure 3.7	Specimen numbering for HIC testing.	129
Figure 3.8	The sketch showing sectioning and surfaces to be evaluated by metallography	131
Figure 3.9	Measurement and calculation of the ratios CSR, CLR and CTR to characterize HIC.	132
Figure 3.10	HIC test set-up in laboratory.	133
Figure 3.11	Photographs showing (a) specimens before, (b) after testing, and (c) sectioning for metallography	134
Figure 3.12	Metal sample-A, unetched surface showing HIC cracks	135
Figure 3.13	Metal sample-A, showing HIC cracks along centerline	136
Figure 3.14	Metal sample-D, unetched surface showing HIC cracks	137
Figure 3.15	Micrograph of metal sample-D after HIC testing,	137
Figure 3.16	Metal sample-E, unetched surface showing HIC initiation and progression in the material thickness	138
Figure 3.17	Micrograph of metal sample-E, after HIC testing showing cracks in different planes close to the centerline	139
Figure 3.18	HIC in sample-A in terms of average percentage of CLR, CTR and CSR% in testing.	142
Figure 3.19	Showing trend of average percentage CLR for sample A.	142
Figure 3.20	Showing trend of average percentage CTR for sample A.	143
Figure 3.21	Showing trend of average CSR percentage for sample A.	143
Figure 3.22	Curves representing CLR, CTR and CSR for sample D.	145
Figure 3.23	Trend of average percent CLR for sample D.	145
Figure 3.24	Trend of average percent CTR for sample D.	146
Figure 3.25	Trend of average percent CSR for sample D.	146
Figure 3.26	HIC of sample-E in terms of CLR, CTR and CSR	148
Figure 3.27	Showing average percent CLR trend for sample E.	148
Figure 3.28	Trend of average percent CTR for sample E.	149
Figure 3.29	Trend of average percent CSR of sample E.	149
Figure 3.30	Overall HIC parameters for duration of testing for samples A, D and E.	151

Figure 3.31	The overall trend of average percentage of CLR.	151
Figure 3.32	The overall trend of average percentage of CTR.	152
Figure 3.33	The overall trend of average percentage of CSR.	152
Figure 3.34	HIC parameters, as per table-3.21, are presented in the curves.	155
Figure 3.35	Trend of average percentage of CLR with respect to pH as derived from figure 3.34.	155
Figure 3.36	Trend of average percentage of CTR with respect to pH as derived from figure 3.34.	156
Figure 3.37	Trend of average percentage of CSR with respect to pH as derived from figure 3.34.	156
Figure 3.38	HIC in terms of average percentage of CLR, CTR and CSR tested in pH 1, 2.7 and 4 conditions	158
Figure 3.39	Trend of average percentage of CLR with respect to pH as derived from figure 3.24.	159
Figure 3.40	Trend of average percentage of CTR with respect to pH as derived from figure 3.24.	159
Figure 3.41	Trend of average percentage of CSR with respect to pH as derived from figure 3.24.	160
Figure 3.42	HIC in terms of average percentages of CLR, CTR and CSR tested in tested in pH 1, 2.7 and 4 condition as per table-3.27.	162
Figure 3.43	Trend of average percentage of CLR with respect to pH progression as derived from figure 3.42.	162
Figure 3.44	Trend of average percentage of CTR with respect to pH progression as derived from figure 3.42.	163
Figure 3.45	Trend of average percentage of CSR with respect to pH progression as derived from figure 3.42.	163
Figure 3.46	Overall HIC parametrs for samples of A-D-E.	167
Figure 3.47	Overall trend of CLR as found in HIC tested samples	167
Figure 3.48	Overall trend of CTR as found in HIC tested samples	168
Figure 3.49	Overall trend of CSR as found in HIC testing	168
Figure 3.50	CLR measured by Ultrasonic sonic means (UT) for sample A-D-E vs duration of exposure	171
Figure 3.51	Overall average UT crack length ratio plotted with respect to duration of exposure for sample A-D-E.	172
Figure 3.52	CLR measured by UT for sample A-D-E plotted with respect to each pH condition	173
Figure 3.53	Overall average UT crack length ratio plotted with respect to overall pH condition for sample A-D-E.	173
Figure 3.54	CLR as measured in test (1) Duration of Exposure (2) pH of solution and (3) UT method.	174
Figure 3.55	HIC parameters of sample D-A-E as found in tests against duration, are plotted against tensile values as per table 3.37	176
Figure 3.56	CLR trend against tensile strength of D-A-E samples	177
Figure 3.57	CTR trend against tensile strength of D-A-E samples	177

Figure 3.58	CSR trend against tensile strength of D-A-E samples	178
Figure 3.59	HIC parameters of sample D-A-E as found in tests against pH conditions are plotted against tensile values as per table 3.38.	180
Figure 3.60	CLR trend against tensile strength of D-A-E samples	181
Figure 3.61	CTR trend against tensile strength of D-A-E samples	181
Figure 3.62	CLR trend against tensile strength of D-A-E samples	182
Figure 3.63	CLR evaluated at different pH conditions, selected test durations and measured by UT against tensile strength of samples D-A-E	183
Figure 3.64	The figure shows relationship between average CLR% and Anisotropy index	195
Figure 3.65	The trend curve shows relationship between average CLR% and Anisotropy index	196
Figure 4.1	HIC in metal sample A is found originated/propagated along inclusions,	202
Figure 4.2	HIC in metal sample A is found originated/propagated along inclusions, identified mainly as oxide of silicon.	203
Figure 4.3	SEM image showing HIC originated/propagated along inclusions and propagated transgranularly in metal matrix.	203
Figure 4.4	SEM and EDX images HIC in metal sample D originated/propagated along inclusions, identified mainly as oxide of silicon.	204
Figure 4.5	Inclusion in HIC in metal sample D is shown to contain elements of sulfur and Mo.	205
Figure 4.6	Inclusion in HIC in metal sample D which might have transformed in morphology in steel making and rolling practice at high temperature.	206
Figure 4.7 A/B	HIC in metal sample E originated/propagated along inclusions and fractured M/A (martensite/austenite) constituents	207
Figure 4.8	HIC in metal sample E is found originated/propagated along inclusions constituting of oxides of silicon and fractured M/A constituents.	208

List of Tables

TABLE	DESCRIPTION	PAGE NO.
Table 2.1	Diffusible hydrogen amount reversibly trapped in steel	48
Table 2.2	Chemical composition of ASTM A516Gr 65	57
Table 2.3	Chemical composition of API 5L X65(H) (Thickness < 25.0mm)	58
Table 2.4	Restricted composition for manufacturing of HIC resistant steels	61
Table 2.5	Features of TMCP, Normalized and Q & T steels	63
Table 2.6	Chemical composition of X65 steel	64
Table 3.1	Material designation and sizes of two source materials for the research	121
Table 3.2	Chemical composition of source material samples	123
Table 3.3	Mechanical test result of starting materials	124
Table 3.4	Samples with numbering and test durations for testing	128
Table 3.5	Test condition for samples	130
Table 3.6	Showing material sample-A test conditions and HIC test results	135
Table 3.7	Test condition (solution pH and Exposure duration) and results of material sample-D.	136
Table 3.8	Test condition (solution pH and Exposure duration) and results of HIC test of material sample E.	138
Table 3.9	HIC in terms of CLR, CTR and CSR average percentage for sample A, for 48 hrs, 96 hrs. and 144 hrs., and overall average% as found in testing.	141
Table 3.10	Average percentage of CLR, CTR and CSR for 48 hrs., 96 hrs. and 144 hrs. extracted from table-3.9 are summarized below.	141
Table 3.11	HIC in terms of CLR, CTR and CSR average percentage for 48 percentage hrs., 96 hrs. and 144 hrs., and overall average for sample-D as found in testing.	144
Table 3.12	Average percentage of CLR, CTR and CSR for 48 hrs., 96 hrs. and 144 Hrs extracted from table-3.11 are summarized.	144
Table 3.13	Complete testing conditions and results, including overall average percentage for sample-E are mentioned in the table.	147
Table 3.14	Average percentage of CLR, CTR and CSR for 48 hrs., 96 hrs. and 144 hrs. extracted from table-3.13 for sample E.	147
Table 3.15	Overall average percentage of CLR, CTR and CSR for sample A.D and E. for test durations of 48 Hrs, 96 Hrs and 144 Hrs each for three pH conditions	150
Table 3.16	Overall HIC is indicated by average percentage of CLR, CTR and CSR for samples A-D-E.	150
Table 3.17	Table shows average percentages of CLR, CTR and CSR are indicated for metal A.	153

Table 3.18	Average percentage of HIC indicators (CLR, CTR & CSR) for sample-A at each pH condition as found in tests.	154
Table 3.19	Average values of CLR, CTR and CSR are summarized in below table for graphical representation.	154
Table 3.20	Showing average percentage of CLR, CTR and CSR for sample D.	157
Table 3.21	Average percentage of HIC indicators (CLR, CTR & CSR) for sample-D at each pH condition as found in tests	157
Table 3.22	Overall average percentage of CLR, CTR and CSR for sample-D, summarized from table-3.23 for graphical presentation.	158
Table 3.23	Average percentage of CLR, CTR and CSR as found for sample E	160
Table 3.24	Average percentage of HIC indicators (CLR, CTR & CSR) for sample-E at each pH condition	161
Table 3.25	Overall average percentage of CLR, CTR and CSR for sample-E, summarized from table-3.26 for graphical presentation	161
Table 3.26	Effect of pH on 48 Hrs testing for metal samples A, D and E are mentioned in terms of average percentages of CLR, CTR and CSR.	164
Table 3.27	Effect of pH on 96 Hrs testing for metal samples A, D and E are listed in terms of average percentages of CLR, CTR and CSR.	165
Table 3.28	Effect of pH on 144 Hrs testing for samples A, D and E are listed in terms of average percentages of CLR, CTR and CSR.	165
Table 3.29	Overall average values of CLR, CTR and CSR for samples A-D-E	166
Table 3.30	Overall average values of CLR, CTR and CSR for all samples in each pH condition listed.	166
Table 3.31	The crack lengths are measured by UT scanning of each sample of A-D-E before sectining as mentioned in the table.	169
Table 3.32	UT crack length ratios summarized from table 3.31	170
Table 3.33	Average UT crack length ratios for each test duration (HRS) are summarized for sample A-D-E and overall average from table 3.32.	171
Table 3.34	Average UT crack length ratios for each pH condition are summarized for sample A-D-E, including overall average from table 3.33.	172
Table 3.35	Average crack lengths (CLR) as found in evaluation with respect to Duration of exposure, pH solution, and UT measurement.	174
Table 3.36	HIC parameters (avg percentage CLR, CTR and CSR) calculations with reference to HRS of testing for sample A-D-E	175
Table 3.37	The overall average HIC parameters with tensile strength are listed.	176
Table 3.38	HIC parameters with reference to pH of testing for sample A-D-E are taken from table-3.18, 3.21 and 3.24	178
Table 3.39	The overall average HIC (against pH) as found in testing are summarized along with tensile and yield strength of the samples	180
Table 3.40	The overall average HIC (against pH) as found in testing are summarized along with tensile and yield strength of the samples	182
Table 3.41	Elements found in steel samples, and impact on HIC (ref table#3.2)	194
Table 3.42	Table lists Anisotropy Index for the metal microstructures.	195
Table 3.43	Shift in pH in HIC testing is shown in the table	201

This page is blank

Chapter 1: Introduction

Steel in contact with water will corrode producing hydrogen at its surface. In H₂S containing water, the sulfide species inhibits formation of hydrogen gas and promotes absorption of H₂ gas in to the steel. Below 200 degree Celsius, hydrogen atoms can become trapped in metal lattice which can lead to hydrogen related cracking of susceptible metals[1].

[H₂S environment is commonly encountered in Oil & Gas Industry which results in HIC. However, HIC may occur in few other environments also where hydrogen charging is possible].

Wet hydrogen sulfide cracking experience found in literature since 1950s related to petroleum industry equipment. The problem becomes more significant as fields rich in H₂S are explored and sensitive carbon-manganese (C-Mn) steel equipment are used[2].

Several types of cracking have been found related to hydrogen assisted cracking in wet H₂S environments for steels and alloys e.g., SSC, HIC, SOHIC, SZC, Blistering etc[3].

Product types and manufacturing processes have significant effect on susceptibility of materials to specific type of cracking[4]. Flat rolled steel products, i.e., plates are most susceptible to HIC in wet H₂S containing aqueous environment. HIC occurs due to hydrogen (H) ingress in steels from corrosion reaction between carbon steel and aqueous Hydrogen Sulfide (H₂S) containing environment. The absorbed hydrogen develops internal pressure as the hydrogen atoms recombine to form H₂ molecules. External stress is not a necessity for initiation or propagation of HIC. HIC are parallel to the surface. Linking of the parallel cracks reduce effective thickness of the material (ref- fig 1.1 and 1.2).

HIC are generally found in low strength steels having <700 MPa yield strength, the most common engineering material with which most of pressure

vessels and pipelines are fabricated. Internal H₂ pressure creates internal cracks in different planes due to high planar density of inclusions. Planar cracks also forms in regions of anomalous microstructure resulted from segregation of impurities and alloying elements in steels. The planar cracks link-up by transgranular plastic shear mechanism to form step-wise cracks, reduces load-bearing capacity of steels. Metallurgical cleanliness and sulfur level play big role in HIC initiation in metals[5].

For pressure vessel steels, improved HIC resistance is found in normalized steels with tensile strength less than 585 MPa (85 Ksi) and Hardness less than 200 BHN.

HIC cracks have been reported since 1940's in vessels and pipelines, and major incidents reported since 1976. Attention was paid towards environmental, fabrication and metallurgical parameters in research, to identify various cracking mechanisms. Several committees in different countries, evaluated the problem and provided guidelines to minimize incidents of HIC (and hydrogen related cracking problems) occurring in carbon manganese steels and other alloys.

Compilation of papers published by NACE in 1996 named "Wet H₂S cracking of carbon steels and weldments", which emphasized on several critical items as below[6]-

- Hydrogen permeation in steel & relationship of permeation to cracking of metal.
- Role of hard weld was examined as a relationship with cracking,
- Major metallurgical parameters contributing to HIC are, cleanliness of steel & microstructure.
- Environmental parameters related to increased severity of HIC is low pH (3-6), higher H₂S content and moderately higher temperature.

Several standards and guidelines have been accepted in manufacturing and testing of materials resistant to HIC, guidelines provided in following references are widely followed in the oil & gas exploration industry:

- MATERIAL STANDARDS[7][8]
 - o NACE 0175/ISO15156
 - o NORSOK M001
 - o ISO12457
 - o API 5L / ISO 3183
 - o DNV OS F 101
- TESTING STANDARDS [9][10]
 - o NACE TM-0284
 - o EFC 16
 - o OTI 95 635

NACE TM-0284 was developed to test steel (pipe) from 5mm to 30mm thickness, at pH 4.8-5.4 for 96 hrs. Crack Length Ratio (CLR), Crack Thickness Ratio (CTR) and Crack Sensitivity Ratio (CSR) are calculated for each section. Average of CLR, CSR and CTR are determined for each coupon which finally represent HIC of the steel.

Work in Canada by Centre for Mineral and Energy Technology and Canadian Standards Association (CSA) Sour Service task force evaluated following two parameters which were determined experimentally for each 19 line pipe steels-

1. Threshold H Concentration ($C_{th}H$) of diffusible H in the steel which cracking occurs and,
2. Threshold pH or pH below which cracking occurs.

Development of TMCP steels have reduced occurrences of HIC but could not eliminate it due to inherent sensitivity of TMCP process as explained in the relevant section of the thesis.

Atomic hydrogen (H) diffuses inside the material and recombines as molecular hydrogen, H_2 , at specific sites. This H_2 can develop high pressure at these sites. In ductile materials, these high pressures deform the material and produce blisters of gaseous molecular hydrogen H_2 . For less ductile material cracking can occur once the pressure exceeds a critical value.

Atomic hydrogen is usually produced by a corrosion reaction in H₂S containing environments. This type of failure is typical for medium or high strength carbon steel pipe transporting H₂S containing products.

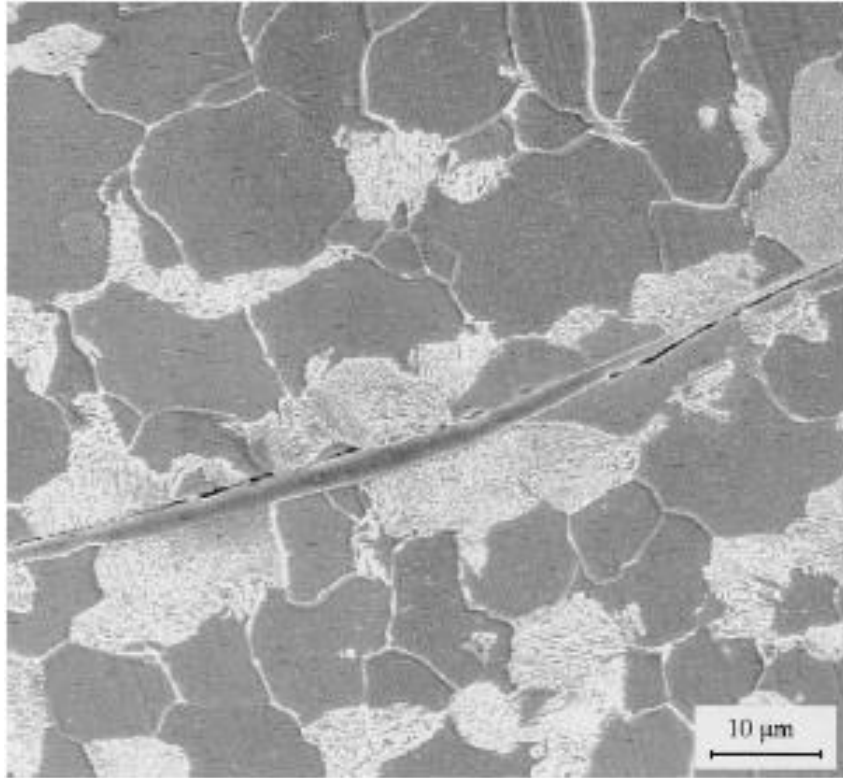


Figure 1.1: Hydrogen induced cracking of carbon steel in H₂S environment. Crack is associated to MnS inclusion

This type of damage occurs in the absence of applied stress. The stress is produced by the internal hydrogen pressure. HIC may propagate in a stepwise manner (stepwise cracking SWC), which is shown in Figure 1.2.

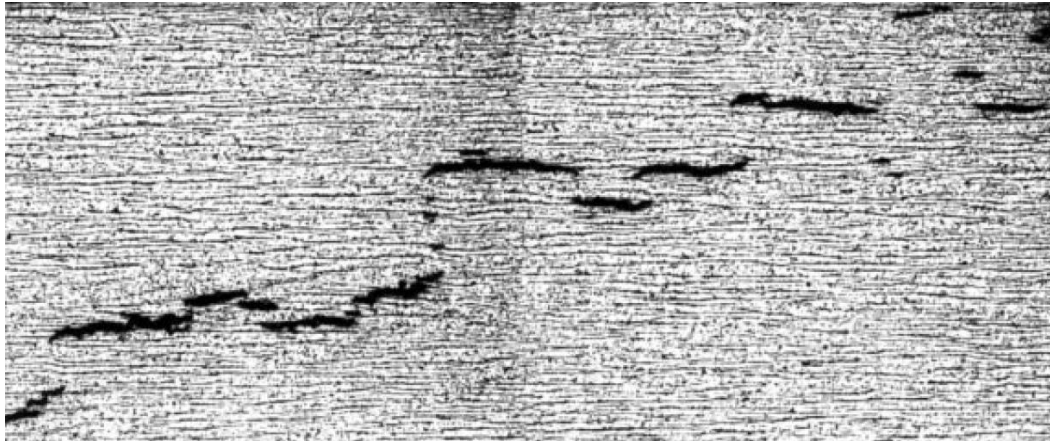


Figure 1.2: Typical stepwise cracking (SWC) of steel as seen in micrograph[11].

1.1 Research Motivation

The steel used in manufacturing pressure vessels and pipelines for processing & transmission of oil and gas, requires robust in quality to resist degradation by hydrogen sulphide in sour service applications. Among several types of cracking which occur in C-Mn steels in sour service, HIC is the most predominant mechanism that is found in flat rolled steels made for pressure vessels and pipelines (in general, flat rolled products).

It is probably difficult, if not impossible to manufacture steel plates which are not susceptible to HIC. Accordingly, codes & standards have provided limits for acceptance of HIC in steels in testing (which can be considered as engineering acceptance of flaws in materials), however no correlations have been established among the variables to denote initiation of HIC in steels. It has been found through research that there are several factors which contribute to HIC, viz., chemistry, cleanliness, homogeneity, microstructure, environment etc. Accordingly, C-Mn steels have been progressively improved in terms of chemistry, cleanliness, homogeneity, and microstructure but researches did not explicitly reveal how the metallurgical factors & environmental parameters, including duration of exposures impact different strength grades of steels to manifest HIC. In view of above, the

current research will focus on identifying behavior of different strength grades of steels to susceptibility to HIC in sour environments.

1.2 Objectives

The objectives of the current research are following-

1. To identify initiation of HIC in steel (flat rolled) with respect to three important variables:-
 - a. Exposure duration
 - b. pH of environment,
 - c. Strength grade,
2. To understand the mechanism of HIC initiation and to establish correlation among the variables to represent their combined effect on HIC.
3. To develop sets of operating conditions / material selection to avoid HIC in rolled steels.

1.3 Research Methodology

Two different grades of flat rolled steel samples was proposed to be collected for HIC testing for the experimental study. HIC testing would broadly follow ASTM 0284 guidelines; however, necessary modifications to test environments and coupons/specimens would carried out to achieve objective of the study. Important steps identified for the research program as described below.

- Extensive literature search carried out for following-
 - To identify & understand variables responsible for occurrences of HIC,
 - To specifically identify metallurgical variables,

- To identify duration of exposures and H₂S levels used in testing & rationale for the same in different standards/guidelines.
- Select steel grades for testing
 - Two strength grades of flat rolled steels, including fittings were proposed for testing (e.g., Gr 70, Gr 65, Gr 60 or Gr 52 etc.).
- Conduct mechanical testing and chemical analysis for determination of mechanical and chemical properties of specimens.
- Conduct HIC testing
 - Conduct testing in saturated H₂S condition (NACE TM0177),
 - Carry out HIC testing at three durations-
 - 48 hrs.
 - 96 hrs.
 - 144 hrs. in different pH conditions,
 - Starting pH conditions (before saturation) to be maintained in the following range-
 - pH 1.0-2.0,
 - pH 2.6-2.8,
 - pH 4.0-4.5

The summary of test program proposed are as follows-

Steel-1 (any of API 5L Gr-52, 60 or 65, ASTM A516 Gr 60 or 70, ASTM A234 etc. as available)

- HIC testing at pH#1 (pH1.0 -2.0)
 - Time 48 hrs. 96 hrs., 144 hrs.,
- HIC testing at pH#2 (pH2.6 – 2.8)
 - Time 48 hrs. 96 hrs., 144 hrs.,
- HIC testing at pH#3 (pH4 - 4.5)
 - Time 48 hrs. 96 hrs., 144 hrs.,

Steel-2 (any of API 5L Gr 52, 60 or 65, ASTM A 516 Gr 60 or 70, ASTM A234 etc.as available)

- HIC testing at pH#1 (1.0 -2.0)
 - Time 48 hrs. 96 hrs., 144 hrs.,
- HIC testing at pH#2 (2.6 – 2.8)
 - Time 48 hrs. 96 hrs., 144 hrs.,
- HIC testing at pH#3 (4 - 4.5)
 - Time 48 hrs. 96 hrs., 144 hrs.,

Other requirements of testing design will generally follow NACE TM 0284 requirements, necessary adjustment may be made keeping in focus objective of the study.

The proposed test matrix is schematically shown in figure 1.3 below.

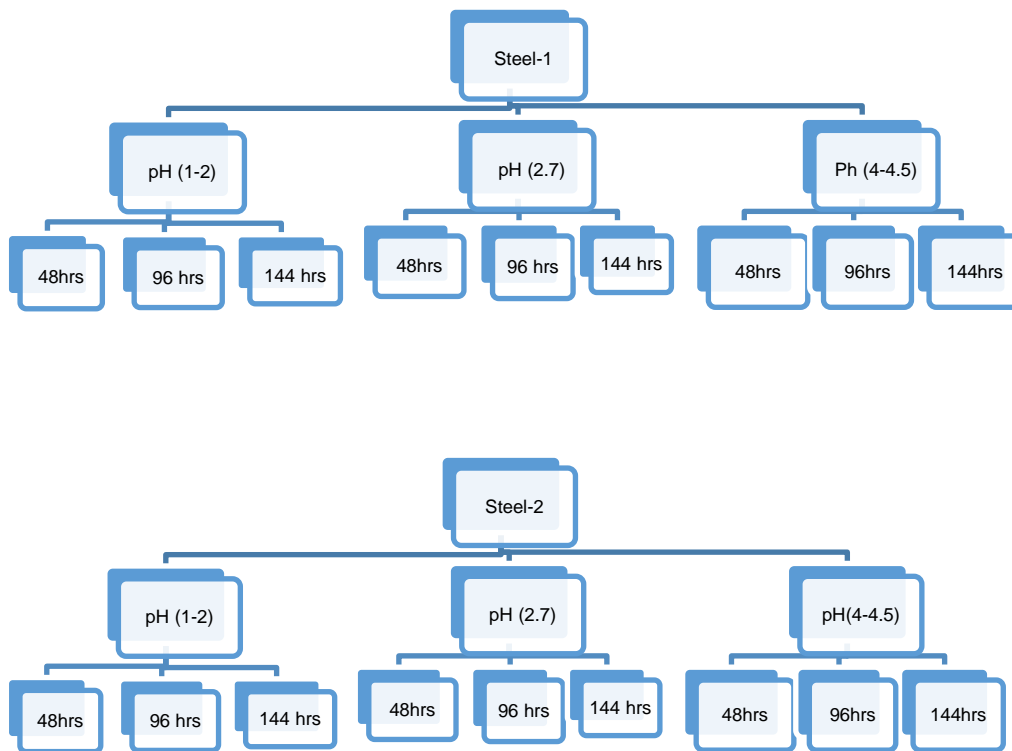


Figure 1.3: Schematic diagram showing proposed tests for the study

1.4 Evaluation of Test Results

Evaluation of the test results to follow as mentioned below-

- Identifying mechanical properties of different steel grades, and identifying any differences existing among different grades.
- Identifying chemical composition of each steel grade and differences, if existing among the samples selected.
- Primary evaluation of each specimen as per NACE TM0284 with optical microscopy for determination of following-
 - Existence of any cracks,
 - Crack Length ratio (CLR),
 - Crack Thickness Ratio (CTR),
 - Crack Sensitivity Ratio (CSR),
- Electron microscopy (SEM/EDX) for following-
 - Characterization of HIC,
 - Determination of crack morphology,
 - Identification microstructural defects e.g., inclusions etc.
- Evaluate effect of exposure on HIC susceptibility on steel grades,
- Evaluate effect of pH on cracking susceptibility,
- Study any other variables to find effect of the variables on cracking
- Determine HIC trend and relationship among strength grades.

Chapter 2: Literature Survey

2.1 Introduction

Among several types of cracking of steels in sour service, HIC is one of the common types of cracking encountered in the oil & gas industry. Flat rolled products, i.e., plates used in manufacturing of pressure vessels and pipes/pipelines etc. are commonly affected by HIC. Several metallurgical and environmental variables viz., metallurgical composition, manufacturing process, thickness of the products, pH of solution, hydrogen sulfide (H₂S) content etc. are known to affect cracking of steel products in presence of aqueous H₂S in oil & gas exploration environment [11].

Hydrogen (H) generates as a result of corrosion reaction on steel surface in aqueous environment, or as a result of cathodic reaction in cathodic protection (CP) or as a process gas (downstream high temperature hydro processing reactors or reactor effluent air coolers). Hydrogen diffuse in the steel, and can have damaging effect on properties of the material and result in cracking. Hydrogen degradation of equipment made of carbon steel and low alloy steel (LAS) in up-stream exploration condition, typically encompass acidic aqueous environment where Hydrogen generating from corrosion reaction causes degradation & cracking of steel which manifests in the form of Hydrogen Induced Cracking (HIC), Sulfide Stress Cracking (SSC) or Stress Oriented Hydrogen Induced Cracking (SOHIC). In all such cracking mechanisms, the initiation of crack is specific to the mechanism, but propagation essentially encompass degradation of mechanical properties of materials by hydrogen, e.g., SSC initiates at high hardness location, whereas HIC initiates at inclusions, but after initiation propagation of the crack is essentially guided by behavior of the hydrogen charged material ahead of the crack tip and associated stress around it.

Degradation of mechanical properties of materials due to presence of H, the elemental hydrogen, is termed as Hydrogen embrittlement. Therefore, essentially all the cracking mechanisms occur as a result of hydrogen

embrittlement although origin of the cracks may be at different locations, some at surface of the material and some are at internal thickness of the material, e.g., SSC is surface mechanism, whereas HIC is an internal cracking mechanism resulting in presence of Hydrogen.

International standards, e.g., NACE MR 0175/ISO 15156, and EFC-16 have addressed the problem of cracking in flat rolled steel products and provided metallurgical limits for acceptance for use in sour service [10]. The possible mechanisms, and effect of metallurgical & environmental factors are briefly discussed here [12]. Hydrogen Induced Cracking (HIC) is a type of hydrogen embrittlement which occurs in the form of surface blisters and/or internal cracks in absence of applied stress [13].

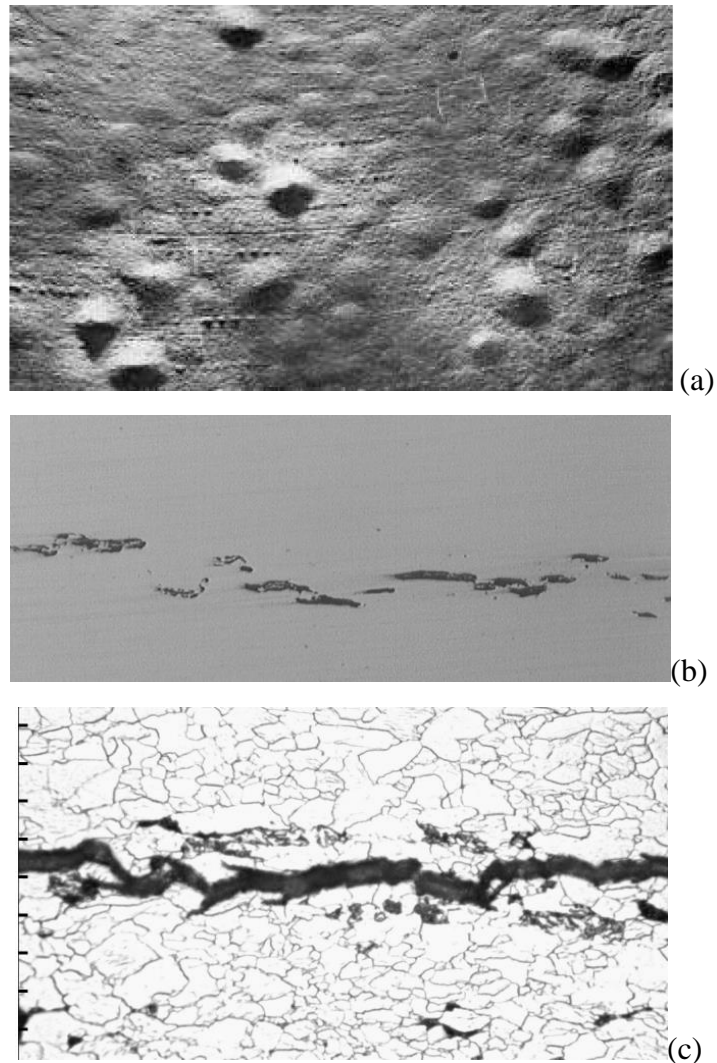


Figure 2.1: Typical HIC morphology is shown above in the form of (a) blisters, (b) stepwise cracks and (c) centerline segregation[14][15].

HIC generally initiates in thickness of the material and propagates parallel to rolling direction. HIC can form straight cracks or step-wise cracks depending on plastic deformation and shear stress distribution in the material. Centerline segregation provides a preferential location for HIC cracks in narrow band of centerline as shown in above micrograph.

2.2 Postulations of Cracking Mechanism (HIC)

HIC Morphology and Source of Hydrogen

HIC is generally developed by a sulfide corrosion process on the steel surface in the presence of hydrogen sulfide (H₂S) in solution. The corrosion reactions for steel exposed to an aqueous sour condition are as follows [16][17] :-

Anodic reaction: $\text{Fe} \rightarrow \text{Fe}^{+2} + 2\text{e}^-$

Dissociation Reactions: $\text{H}_2\text{S} \rightarrow \text{H}^+ + \text{HS}^-$



Cathodic reaction: $2\text{H}^+ + 2\text{e}^- \rightarrow 2\text{H}$ (atomic hydrogen)
 $\rightarrow \text{H}_2\uparrow$ (gas)

In acidic condition, H₂S is stable and can dissolve in water as shown in figure 2.2 below:-

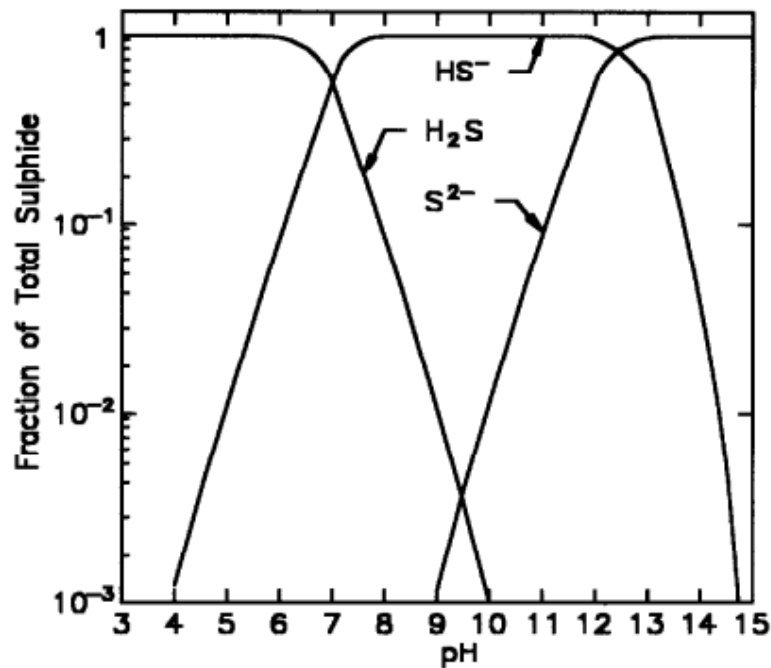


Figure 2.2: The curves showing relative concentration of sulfide with respect to pH of solution[11].

Kinetics of recombination reaction of H atom to molecule can be significantly retarded by sulfur species resulting from H₂S (dissolved H₂S, HS⁻, S²⁻ similar to Sn, Pb, Sb, P) resulting increased absorption of H in steel. The H⁺ ions present in acidic solution or produced by dissociation of reactions (in neutral and alkali solution) combine at the cathode with electrons released by the steel, to form atomic hydrogen on the steel surface. The hydrogen atoms combine to form molecular gaseous hydrogen. However, the presence of H₂S gas in acidic solution or hydrogen sulfide ions (HS⁻) in neutral and alkali solution is believed to reduce the rate of hydrogen gas formation on the steel surface [18]. Thus inducing diffusion of atomic H into the steel.

Several factors may affect environmentally assisted cracking as HIC which occur in aqueous medium. As the name suggests, HIC is caused by H in metal body which enters and resides at preferred locations in metal thickness and causes degradation of material properties, eventually causes cracking of the material. Diffused H in steels is trapped in reversible and irreversible trap sites which are metallurgical defects, such as nonmetallic inclusions, large

precipitates and bands of hard microstructures. Inclusions and metallurgical micro-defect sites in steels are considered as irreversible trap sites. H in interstitial locations of steel degrade mechanical properties and facilitates cracking of the material [19]-[20].

It is proposed that H molecules are physically adsorbed on the metal surface and then dissociate to atomic H resulting layer of atomic H on the surface and in few atomic layers in the metal which are considered as stronger trap sites than interstitial lattice sites [20].

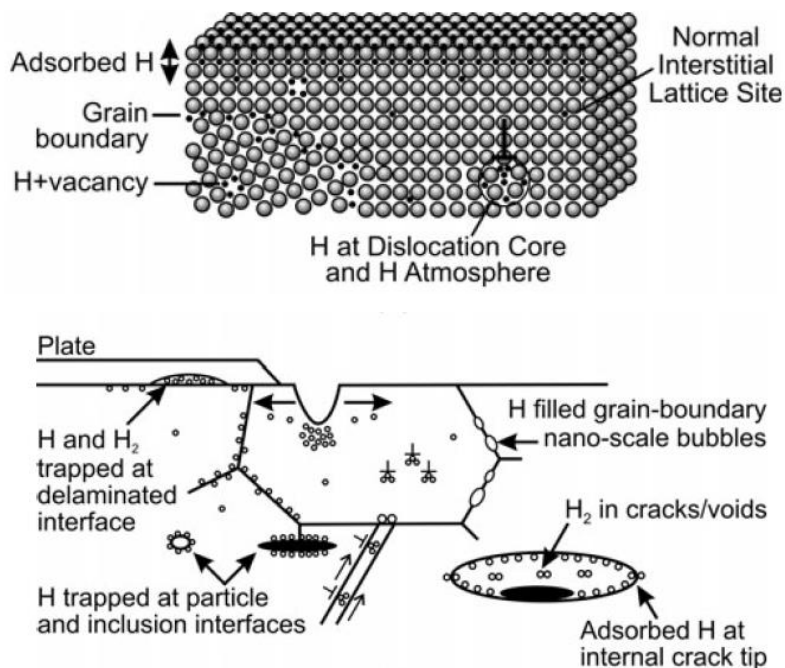


Figure 2.3: Schematic diagram illustrating sites for hydrogen traps in materials (a) the diagram on top shown on the atomic scale, (b) the bottom diagram is shown on a microscopic scale[21].

In figure 2.3, note that high concentration of hydrogen on and between the first and second layers at the surface (adsorbed hydrogen) at external and internal crack tips or hydrogen trapped at grain boundaries are responsible for hydrogen embrittlement.

Adsorption of H, involving charge transfer with substrate atoms may weaken interatomic bonding at crack tips which may facilitate cracking.

Several mechanisms of H embrittlement may occur conjointly or different mechanisms could predominate [20][22].

Following mechanisms have been proposed for HIC:-

- ‘Adsorption Induced Dislocation Emission’ (AIDE) or ‘Void Coalescence mechanism’ predominates for dimpled intergranular and dimpled transgranular cracking (including cleavage-like cracking when nano-scale dimples are present),
- ‘Hydrogen enhanced decohesion’ (HEDE) mechanism is proposed in which increase of H concentration reduces cohesive forces of Fe-Fe bonds in steel by forming Fe-H bonds. Reduced Fe-Fe cohesive force enhanced by interstitial H atoms and internal stress generated lead to cracking or H embrittlement.
- ‘Hydrogen-Enhanced-Localized-Plasticity’ (HELP) model was first proposed by Beachem in 1972 [20]. In case of HELP theory, elastic relaxation of dislocation-dislocation repulsion by interstitial H atoms is regarded as enhancing dislocation mobility leading to H embrittlement resulting slip-band cracking.

There are controversies about applicable theories for H embrittlement & cracking, The AIDE probably predominates for cleavage like and dimpled intergranular cracking, HEDE probably predominates for brittle intergranular cracks, and HELP may make a minor contribution in some cases [20][21][23]. HIC is most frequently explained with the help of gas-bubble model [24]. H atoms form molecular hydrogen at voids, at interfaces between steel matrix and nonmetallic inclusions. The pressure exerted by the molecular hydrogen causes a high stress field in the surrounding steel matrix, The steel matrix is then further embrittled by decohesion or by localized plasticity mechanism due to interstitial hydrogen atoms. Therefore, the parameters affecting HIC at nonmetallic inclusions can be said to be H pressure and hydrogen embrittlement of the surrounding microstructure while hydrogen embrittlement is affected by internal stress and interstitial H atoms[18][25].

Void nucleation often occurs ahead of crack tip in plastic zone in many cases. Voids are most easily nucleated by separation of particle-matrix interfaces or fracture of large particles or at dislocation cell walls, slip-band intersections, and vacancy clusters [20].

It has also been suggested that HELP can promote void growth and coalescence ahead of crack tip and may occur conjointly with AIDE.

In following SEM image HIC initiation location, it is postulated that micro dimples at crack site of about 1micrometer were observed which formed by HELP mechanism [18][20].

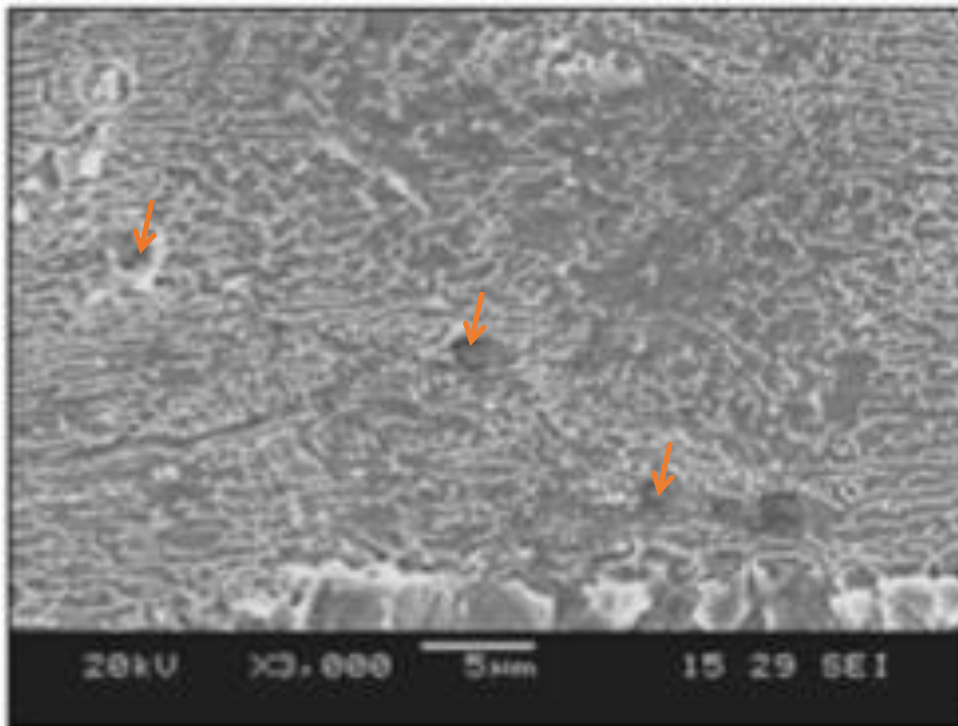


Figure 2.4: Micro dimples at crack site of about one micrometer were observed by the researcher in reference [17].

Generally, the defect sites are planer and oriented in the direction parallel to the rolling direction of the flat rolled steel product. As the H is collected at the trapping sites, the pressure developed causing a stress concentration at the edge of the site. Consequently, a crack is formed and it propagates parallel to the rolling direction [18]. Cracking occurs when pressure exceeds $1.013 \times 10^9 \sim 10^{10} \text{ N/m}^2$ ($10^4 \sim 10^5 \text{ atm}$) [26].

On the other hand, cracking at martensite/austenite or M/A constituents is not related to any voids between the steel matrix and M/A constituents, rather, it is associated with cracking of the M/A constituents themselves which is more likely of a decohesion effect. Internal stress during steel manufacturing also affects decohesion of M/A constituents. The steel matrix is then further embrittled by AIDE or Decohesion or HELP mechanism and cause cracking.

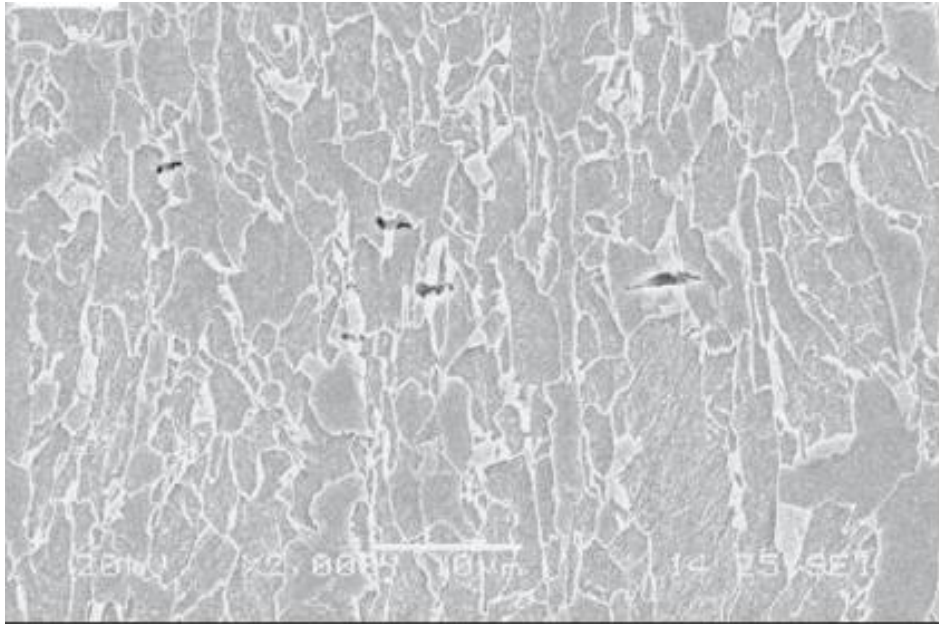


Figure 2.5: Cross section view of HIC initiation at M/A constituents in TMCP steel[17].

Even when inclusion level were low enough, clustering of M/A constituents could induce HIC irrespective of steel microstructure provided the M/A constituents were agglomerated to a certain degree e.g., 100 micro meter in length and 20% area localized along transverse direction to the rolling plane. M/ constituents were easily embrittled by hydrogen [25][27].

2.3 Factors Affecting HIC

Combination of following critical factors potentially drive HIC in materials-

- Environmental parameters
- Metallurgical parameters
- Duration of exposure

Environmental parameters primarily influence generation and charging of atomic hydrogen in steel, whereas, metallurgical factors are responsible for trapping of H atoms, forming H gas, and leading to cracking (HIC). Duration of exposure of material to sour environment for HIC to occur is also important and shall be reckoned with, in combination of other factors.

Researchers have found several metallurgical and environmental parameters which induce and influence HIC in steels [18][28][29].

Environmental parameters (relevant to oil & gas industry)-

- Composition of environment,
- H₂S
- CO₂, organic acids, arsenic etc.,
- Temperature
- Pressure

Among Metallurgical factors, following can be considered as important-

- Composition of steels
- Inclusions composition, shape & intensity
- Heat Treatment
- Microstructure
- Banding
- Homogeneity

Other important parameters may be listed as-

- Thickness of the item
- Strength Grade
- Exposure (one side / both side)
- Stress on/in the material

Important parameters of Environmental, Metallurgical and Exposure Duration, which influence HIC, are described in following sections.

Environmental Factors

Environmental factors which significantly control generation and charging of Hydrogen, eventually influencing HIC are, pH of solution, H₂S content, temperature and time of exposure [11][30].

Effect of H₂S – pH – Temperature & Time of Exposure

Experiment with high strength low alloy (HSLA) steel (equivalent to X70) shows that H₂S partial pressure is the key as sulfide content hinders recombination of H atoms to molecules, and thereby increasing diffusion of H in steel.

H permeation rate is affected by both H₂S partial pressure and pH of solution, whereas, H diffusivity is mainly determined by pH value in case of low P_{PH₂S} (<0.1 atm) [18].

Therefore, it is relevant to suggest that susceptibility to cracking increases with increase of H₂S content in acidic solutions with decreasing pH (acidic pH is more relevant to upstream oil & gas production, whereas, hydrogen charging is also significant at relatively high temperature alkaline environment in downstream processing units where additional HIC promoters e.g., cyanides etc. are found).

Charging & Solubility of Hydrogen in Steel

Relationship Among Variables

ISO-17081 [31] provides method for measurement of hydrogen permeation and uptake in metals by electrochemical technique. The Hydrogen (H) permeation curves provide important information regarding H diffusion and trapping such as Apparent Diffusivity (D_{app} , apparent lattice diffusivity, dissolved & reversibly trapped H), Permeability ($J_{ss}L$), Hydrogen Solubility in steel (C_{app} , H in lattice & reversible traps) and amount of Irreversibly Trapped H in steel. It is

often believed that decrease in D_{app} & $J_{ss}L$ and increase in C_{app} mean that more H can be trapped in steel. The relationship among different parameters are given in following equations [32]-

Hydrogen flux ($mol H m^{-1}S^{-1}$)

$$J_{ss} = i_{ss} / nF \quad i_{ss} = \text{steady current density to oxidize diffused H.}$$

Permeability ($mol H m^{-1}S^{-1}$)

$$J_{ss}L = i_{ss}L / nF \quad n = \text{no. electrons transferred, } F = \text{faraday's const.,}$$

$$L = \text{specimen thickness,}$$

$$J_{ss} = \text{steady state H flux.}$$

Apparent diffusivity

$$D_{app} = L^2 / 2\Pi^2 t_b \quad t_b = \text{breakthrough time when a diffused H was firstly oxidized on a Pd coated layer.}$$

If the surface H is in thermodynamic equilibrium with sub-surface H, the following is defined-

Apparent H solubility ($mol H m^{-3}$)

$$C_{aap} = J_{ss}L / D_{app}$$

HIC/SWC/Blistering damage mechanism always involves bulk metallurgical process related to concentration of dissolved H (internal process), whereas SSC/HSC are related to H charging rate, is a surface or external process. Concentration of dissolved H and charging rate can be related as-

$C_o = \sqrt{(J_{ch}/\alpha)}$; C_o is an internal parameter whereas J_{ch} is an external parameter [33].

Hydrogen In Steel (Critical H concentration)

Environmental parameters e.g., pH, H_2S & temperature are important which control H charging, and consequently, cracking mechanism [34]. Susceptibility increases with increase in H_2S concentration and decrease in pH. Susceptibility of stepwise cracking increases up to 50°C, and then decreases. This may be due

to change of H charging efficiency with temperature in aqueous acidic solutions. In alkaline environment, H charging efficiency is found more than in acidic environment which is relevant in downstream processing conditions in oil & gas industry. Corrosion reaction may produce different scale/products e.g., FeS, FeS₂, Fe₇S₈, Fe₉S₈ depending on pH/ P_{H₂S}/ oxidizing potential of the environment. A protective corrosion product also retards hydrogen charging. Under steady state condition, in absence of internal trapping, efficiency of H charging can be given by simple ratio of permeation current determined in a simple H permeation experiment and the corrosion current on the exposed surface. Overall severity of H charging can usually be represented by the product of corrosion current and efficiency of H charging which is proportional to the H flux. In most cases, H permeation flux reaches maximum (J_{max}) over a period of time and then decreases slowly to an intermediate steady state value (J_{ss}) as semi protective sulfide films form on the metal surface. However, periodic disruption of film will again increase H permeation. Apart from inhibitors to stabilize the film, metallurgical processing of an alloy/metal also has significant role in forming protective scale or corrosion product on the metal surface. Research has shown that subsurface H concentration (C_o) under the exposed surface, is an important parameter which is derived from steady state hydrogen permeation current (J_{ss}), given by-

- $J_{ss} = D_{eff}C_o / L$, where L = thickness of material, D_{eff} is effective diffusivity of H in metal,
- This allows determination of critical H concentration (C*) in steel for cracking of a particular material so that the role of metallurgical & processing can be understood to optimize service condition/performance [11].

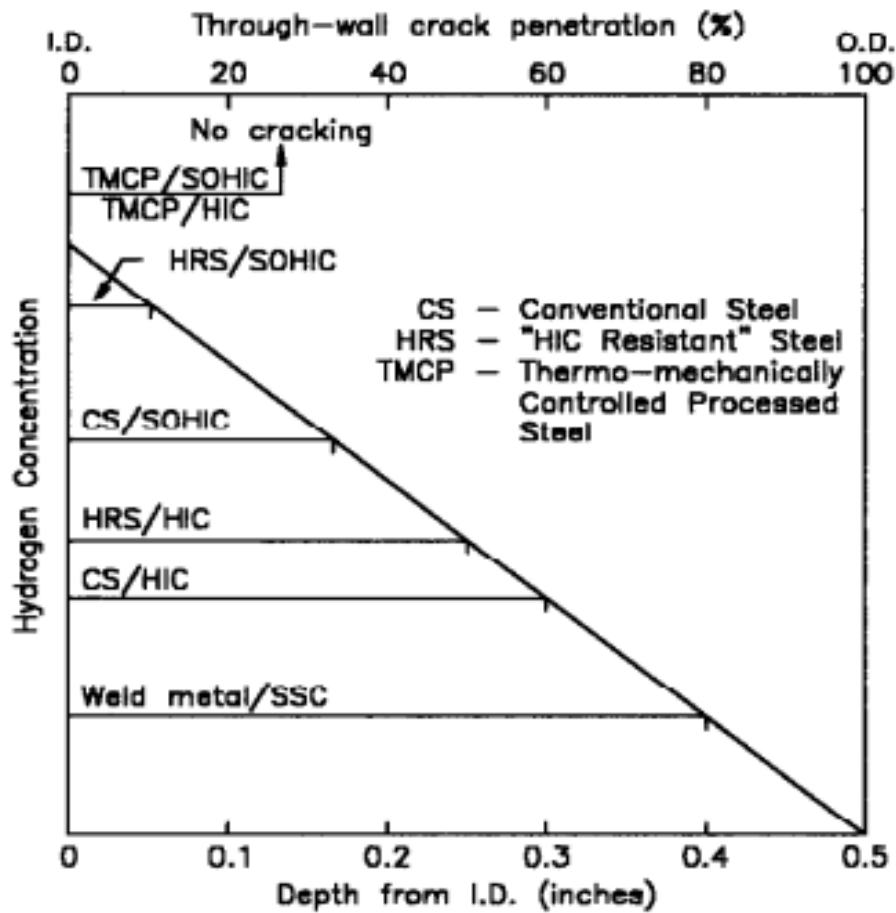


Fig-2.6: Critical hydrogen concentration for HIC for different steels (schematic)[11]

Hydrogen Charging and Trapping in Steel

Researchers observed that amount of H which can be introduced in steel (CH) and Critical concentration of H for cracking (CK) depends upon several parameters[35][36] as following:-

- Total system Pressure and Partial Pressure of Hydrogen (controls CH),
- pH of solution (controls CH),
- Solution composition (controls CH),
- Temperature (controls CH & CK),
- Time (controls CH),
- Residual stress (controls CH & CK),

- Applied stress (controls CH & CK),
- Inclusion content (controls CH & CK),
- Segregation (controls CH & CK)
- Hardness variation (controls CH & CK),

CH & CK values are inter dependent. Cracking can be reduced either by reducing CH value or increasing CK or both. Steel makers can act only on CK, as CH is largely environment related but fewer sites of trapping in steel will also reduce CH.

Threshold hydrogen concentration ($C_{th\ H}$) and threshold pH (pH_{th}) for hydrogen-induced cracking (HIC) were determined for commercial sour service line pipe steels exposed to H_2S saturated buffer solutions. Metallographic examination of the steel samples by optical and electron microscopy showed that ultrasonic C-scan is an effective method for detecting HIC and for locating cracks in exposed steel coupons. A banded microstructure was found to be detrimental to the HIC resistance of clean steels. The obtained pH_{th} values can be used to rank the steels with respect to HIC resistance[37].

Experiments were conducted in H_2S saturated buffered saline environment. The parameters show that diffusible hydrogen content/concentration (C_{thH}) > 1.0 ml/100 g of steel indicated good HIC resistance. Values could be used to rank steels With respect to HIC resistance. Recent work by Hay on line pipe steels to measure internal surface hydrogen concentration (C_{oH}) and quantify HIC resistance in terms of CTR (Crack Thickness Ratio) and CLR (Crack Length Ratio). The work involved laboratory measurement of H flux in specific line pipe steel used for sour service [38][39].

- Each specimen weighing 100grs were exposed to test solutions having pH 1.1/3.1/3.7/4.3 for 96 hrs. and diffusible H were checked by using Japanese standard method involving displacement of glycerol by H at $45^\circ C$ for 72 Hrs.
- Diffusion coefficient (C_o) was determined to calculate H concentration at inside surface of the steel. Diffusion coefficients

were determined at 25/40/60/70°C to check effect of FeS on internal surface.

- Ultrasound 'C' scan (5MHz) with recorder was used for checking cracks, however, no cracking was found, and therefore no threshold H conc. could be detected. Activation energy for diffusion of H in steel was found as 21 kJ/mol.

Role of P_{H_2S} and pH on Hydrogen Charging

It is considered that HIC is reduced when pH of environment increases and partial pressure of H_2S is reduced [40][41].

Diffusible hydrogen content which is reversibly trapped in steel indicate HIC sensitivity of steel rather than hydrogen permeation rate for the steel[18][42][43].

Experiment with several grades of API 5L steel showed that level of diffusible H significantly varied in acidic pH range (7.8 to 0.1 ml H / 100g steel in pH range of 1.1 to 5.9) [37][44].

The following curves indicate variations of hydrogen permeation rates for steel depending on pH as well as H_2S partial pressure [18]. Lower pH at constant P_{H_2S} and high P_{H_2S} with lower pH have effect of higher permeation of H in steel as seen in fig below-

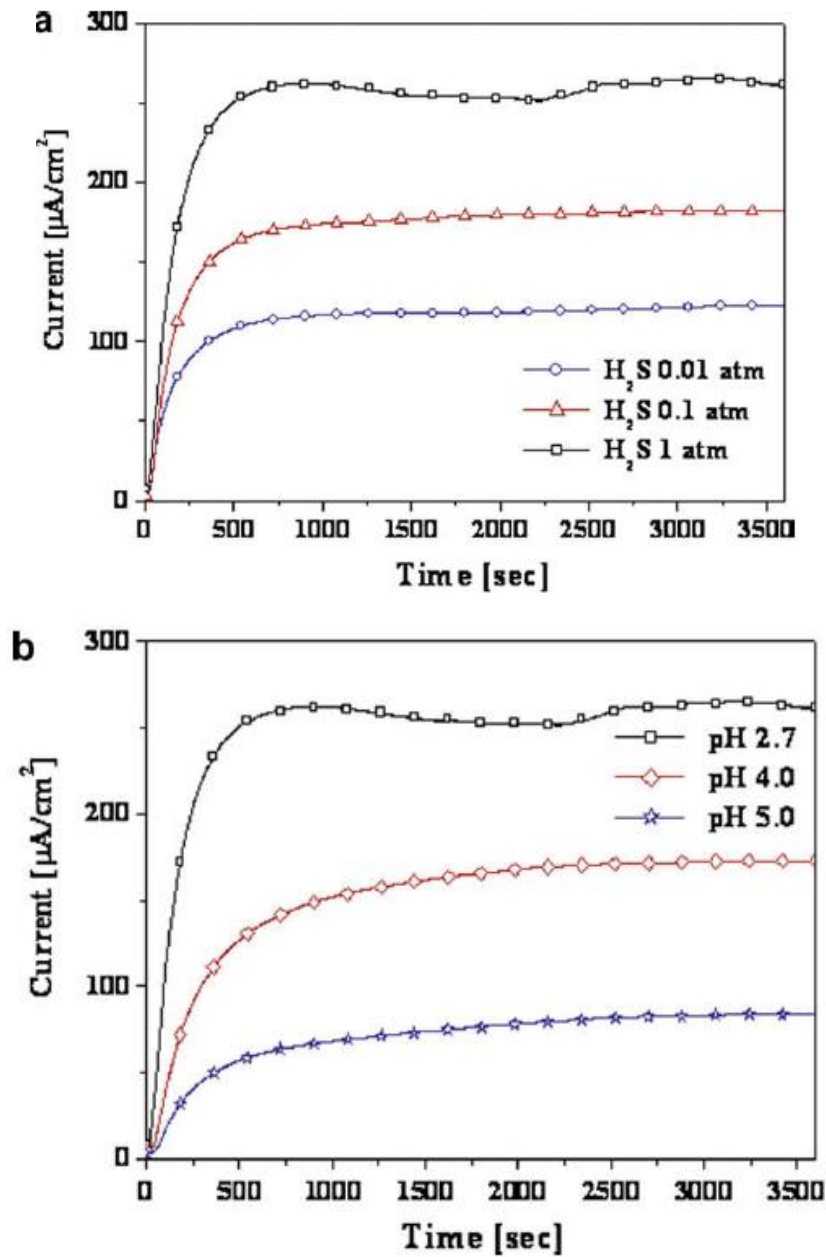


Figure 2.7: (a) Indicates hydrogen permeation effect of H_2S partial pressure at pH 2.7, (b) The bottom curve indicates effect of solution pH at P_{H_2S} 1 atm.[45]

However, studies found that diffusible hydrogen is more consistently affected by P_{H_2S} , rather than pH which is more representative of HIC sensitivity for steel as observed in experiment as per following table [18].

Table 2.1: Diffusible hydrogen amount reversibly trapped in steel

P_{H_2S} (atm)	1	1	1	0.1	0.1	0.1	0.01	0.01	0.01
pH	2.7	4.0	5.0	2.7	4.0	5.0	2.7	4.0	5.0
Diffusible hydrogen amount (weight ppm)	2.87	1.76	1.04	1.25	1.14	0.78	0.75	0.74	0.03

Two types of hydrogen permeation behaviors are found in full scale tests depending on partial pressures of Hydrogen sulfide (P_{H_2S}). There is a high peak value and a rapid decay with the higher P_{H_2S} , but a low peak value and slow decay with low P_{H_2S} depending on P_{H_2S} and medium i.e., gas or aqueous as seen in below figure [46].

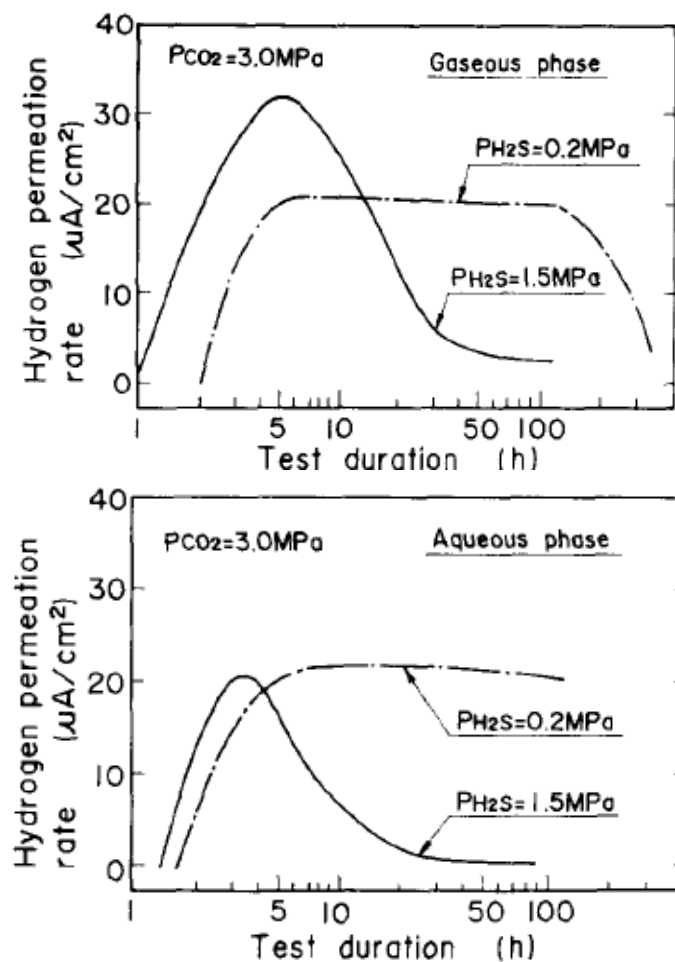


Figure 2.8: Influence of partial pressure of H_2S on hydrogen permeation rates in (top) gaseous and (bottom) aqueous phase shown in above curves[47].

Effect of Temperature on Hydrogen Charging

Effect of temperature, as found in laboratory studies that HIC cracking increases up to approximately 50°C. Above 50°C, the effect is found diminishing possibly due to change in hydrogen charging efficiency with temperature in aqueous solution [11].

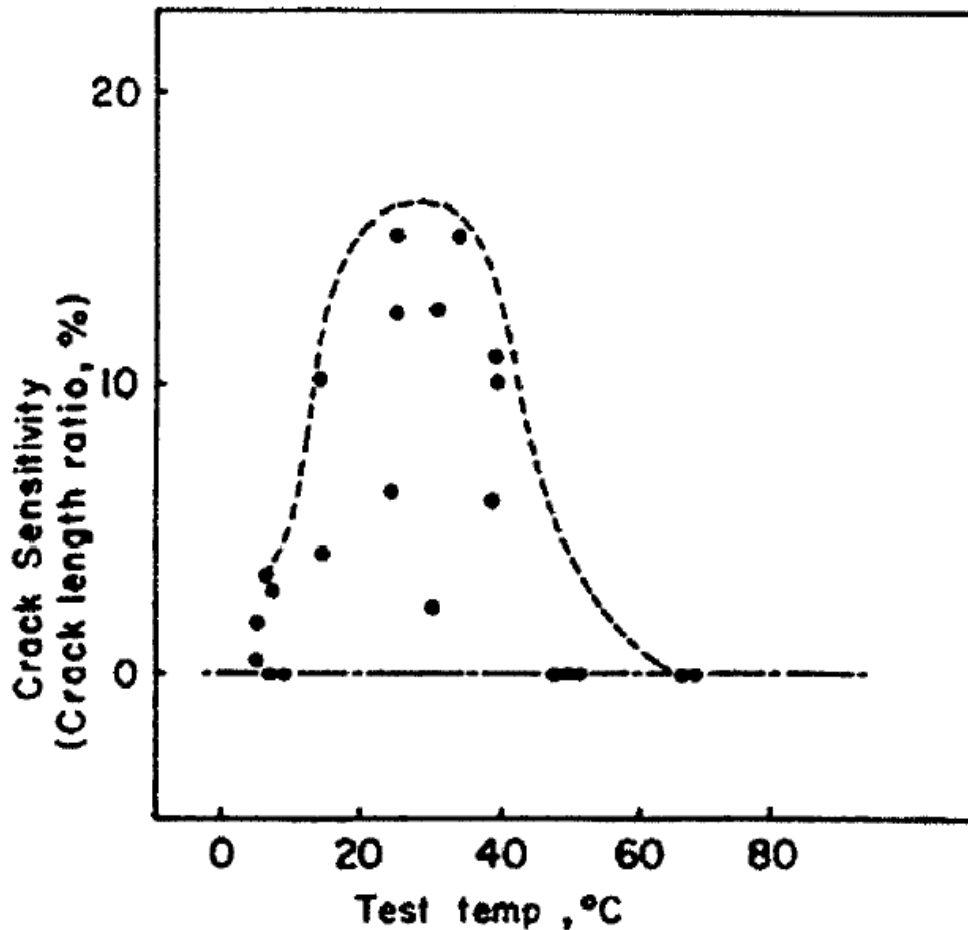


Figure 2.9: HIC in pipeline steel versus testing temperature as seen that severity of HIC increases with reduction in pH (in the range of 3 to 6), higher H₂S content and moderately elevated service temperature[11].

Crack growth rates are dependent on temperature and thus on stress intensity factor (K). The different growth rates indicate that the rate controlling factors are different for internal hydrogen embrittlement (IHE) and hydrogen environment embrittlement (HEE). IHE is probably controlled by hydrogen diffusion to hydrostatically stressed crack-tip region, and HEH is probably controlled by adsorption kinetics in most circumstances, but not all cases

Precipitous decreases in crack velocities above a critical temperature (which depends on steel composition etc.) for both IHE and HEE are probably best explained by in terms of abrupt reduction in concentration of adsorbed H (at surface and subsurface sites) which needs further understanding & work [48][47].

Effect of Duration of Exposure on HIC

Duration of exposure is also an important factor for initiation and propagation of cracks[49]-[3]. Hydrogen permeation flux versus time curve has the characteristic behavior as shown below. In most of the cases for sour environment, the hydrogen permeation flux increases with time and reaches maximum (J_{max}), then decreases to an intermediate steady state or slowly reduces as semi protective sulfide scale forms on the metal surface [11].

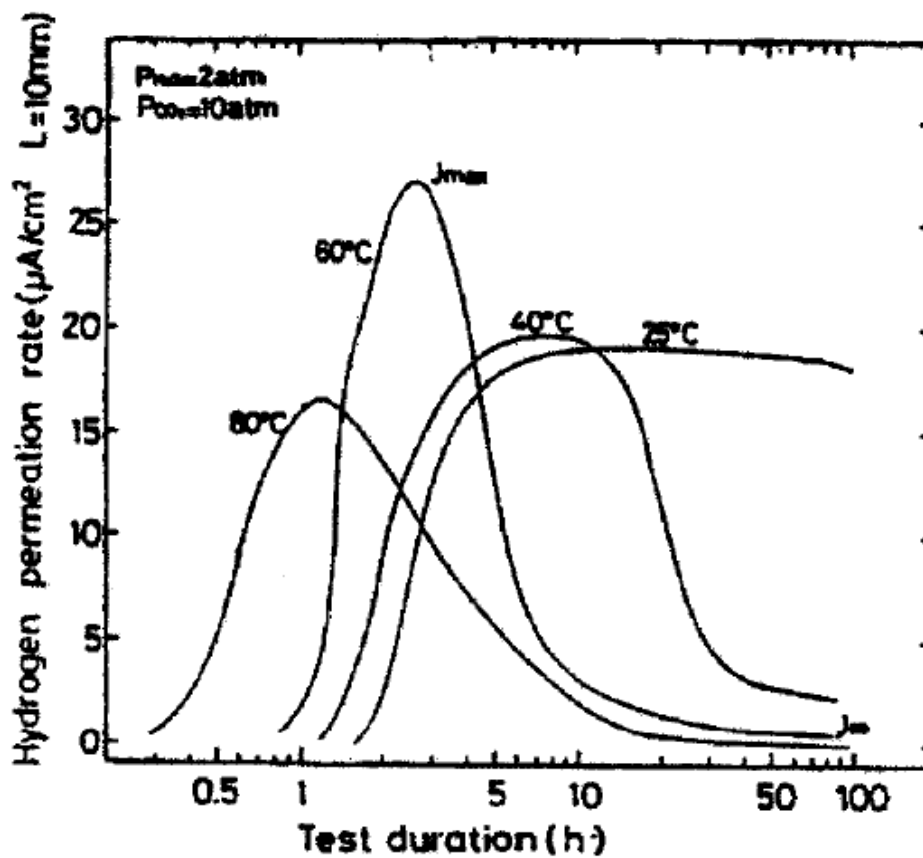


Figure 2.10: Hydrogen permeation at different temperatures exposed to hydrogen sulfide environments[11]

Crack area ratio (CAR) was analyzed against time of exposure in testing of API 5L X65 TMCP steel (C-0.09, S-0.28, Mn-1.56, S-0.001, Nb-0.04, V-0.05, Mo-0.01 Cu-0.02, Cr-0.05, Ni-0.03, ferrite/ferrite-pearlite structure sweet service steel). It was found that pH and P_{H_2S} have significant effect on time necessary for HIC to initiate. At constant P_{H_2S} , increasing pH leads to a delayed HIC initiation. It seems that P_{H_2S} has more pronounced influence than pH on maximum extent of HIC [50].

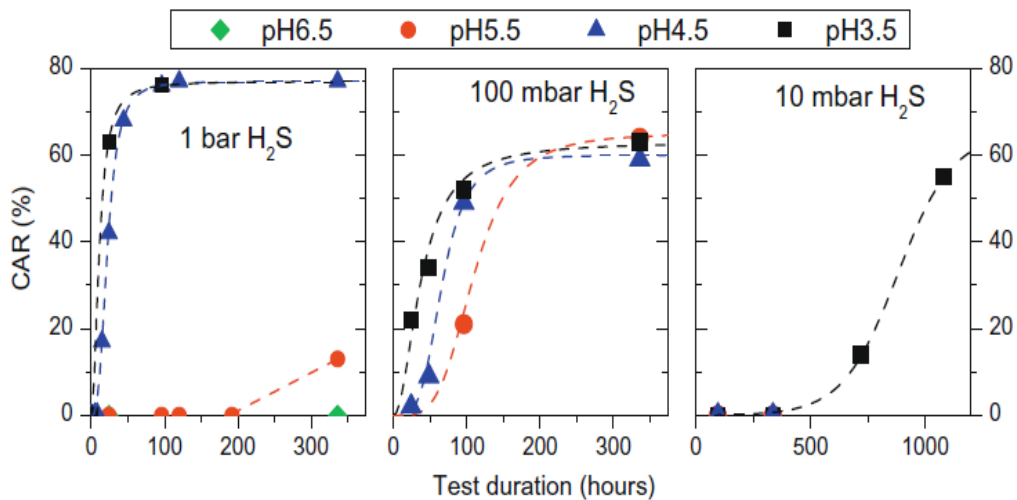


Figure 2.11: The curves showing evolution of HIC with time of exposure and impact of pH at constant P_{H_2S} [51]

One contradictory result was found that under 1 bar P_{H_2S} , it took longer to initiate HIC than 0.1 bar P_{H_2S} at pH 5.5 as shown in figure 2.12 below [50].

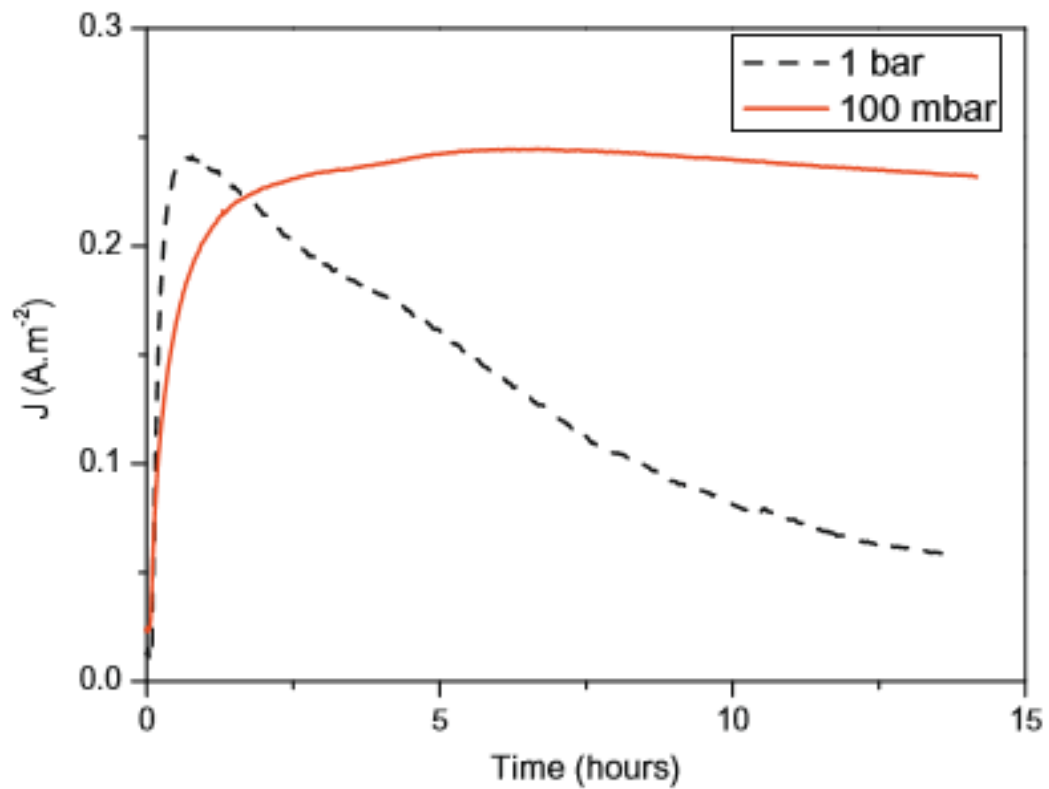


Figure 2.12: Under 1 bar P_{H_2S} , it took longer to initiate HIC than 0.1 bar P_{H_2S} at pH 5.5 [51]

Critical hydrogen concentration for initiation of HIC was studied at different pH and H_2S concentration. It was found that critical diffusible hydrogen concentration is a prerequisite for HIC initiation. It is found that critical hydrogen concentration is different for different steels which were studied separately by different researchers as presented in below curves[18][52].

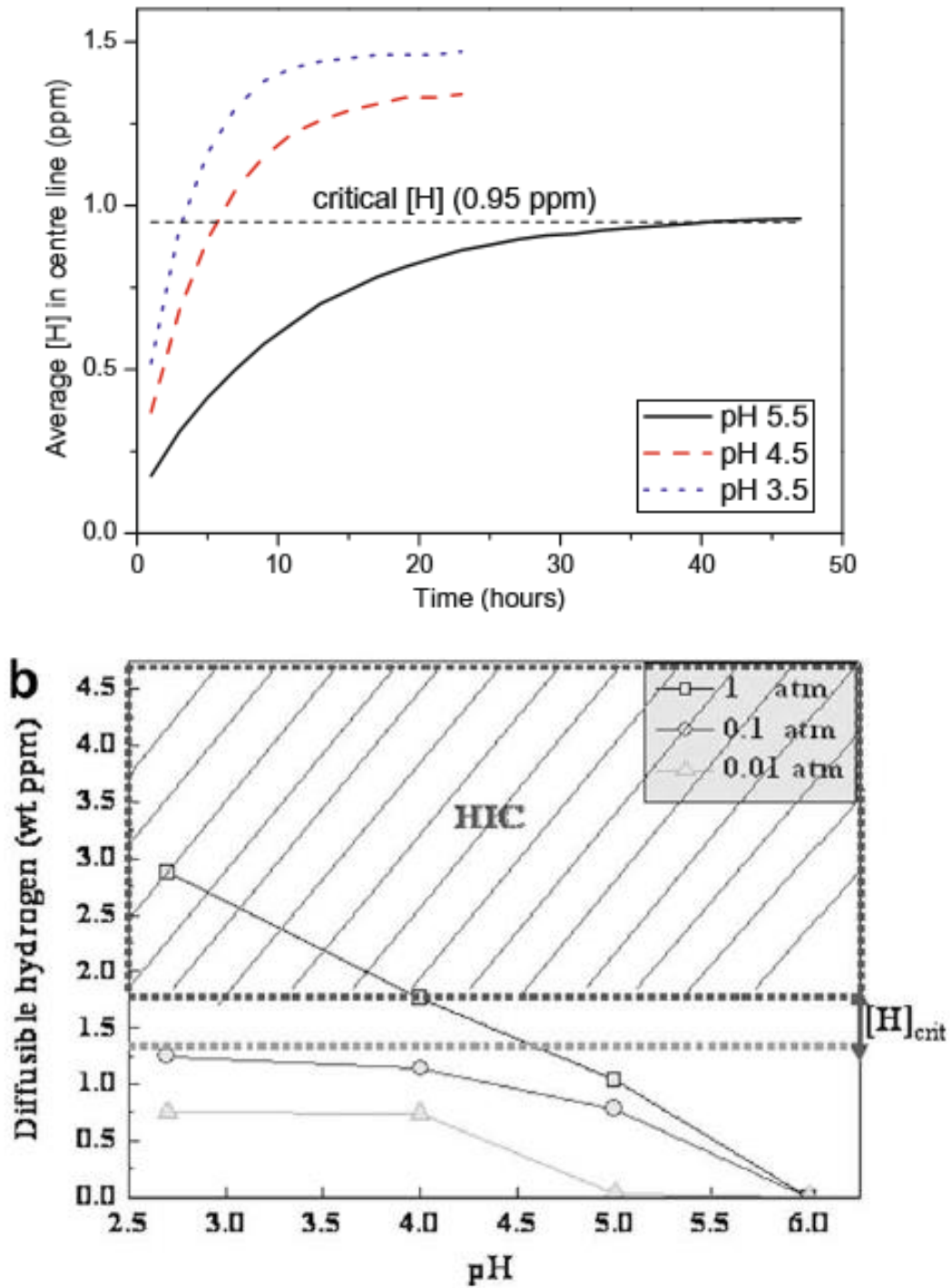


Figure 2.13: (Top) Modelling shows H concentration at different pH values and critical H concentration for cracking at 0.1 bar P_{H_2S} . (Bottom) Modelling of average concentration at centerline of a HIC specimen under 100 mbar H_2S and at different pH conditions for X70 steel [18].

Metallurgical factors

It is found that flat rolled steel products are mainly susceptible to HIC attack, whereas tendency of seamless or other type of manufacturing, are considerably less vulnerable.

Commonly, API 5L grades are used for manufacturing of pipeline steels whereas, ASTM A 516 grade of steel is used for manufacturing of pressure vessels. For restricting occurrences of HIC, steels are manufactured with controlled chemical composition, especially with restricted sulfur content.

It is relevant to mention here that difference between other forms of sour service cracking (SSC etc.) and HIC is that SSC is a solid state embrittlement reaction resulting from the interaction between the metal lattice and atomic hydrogen, whereas, HIC involves the recombination of atomic hydrogen to molecular hydrogen at internal defects. Hydrogen diffusion and accumulation in steel causing HIC initiation signifies that steels which retard hydrogen diffusion and accumulation in steel shall be superior in HIC resistance. Well known sinks for hydrogen in steel are matrix-inclusion interface (mainly elongated MnS), centerline segregation and shrinkage cavities. The appropriate steel design shall consider following-

- Minimize the quantity of harmful trap sites,
- Improve features of trap sites and
- Optimize the material fracture toughness

HIC initiation or, to-some-extent, propagation, are observed more in low strength steels (generally < 700 MPa) [11][28].

The metallurgical factors which significantly affect hydrogen diffusion & accumulation in steel and result in HIC are, metallurgical processing including heat treatment and impurity content [11][53]. There are several routes to manufacturing carbon (CS) and low alloy steels (LAS) which are acceptable to use in sour service according to standards e.g. ISO 15156, for resistance to sulfide stress cracking including HIC with restricted sulfur and/or oxygen

content. The accepted routes as mentioned in the standard(s) are hot rolled (CS only), annealed, normalized, normalized and tempered, normalized-austenitized-quenched-tempered, austenitized-quenched-tempered including casting[54].

Composition and processing history of steels influence formation of nonmetallic inclusions (size/type and morphology) and materials ability to accommodate H atoms and affect susceptibility of HIC. Large inclusions e.g. elongated MnS and stringers of oxides are found detrimental for HIC in steels. Domizzi et al showed that HIC depends on sulfur (S) content and average, as well as, total length per unit area of sulfide inclusions in steels [55]. Controlling S content in steel has been considered as one of the primary attributes to control HIC [28] [56][57].

Materials Performance Council (MPC) defined four types of steels from the perspective of hydrogen related cracking mechanisms, as follows-

- Conventional steels (CS): Commercially produced hot rolled or normalized steel with moderate to high level of impurities, specifically S (0.01%), has high susceptibility of HIC (A283C / A516-70),
- Low sulfur conventional steel (LSCS): Commercially produced low S steels (0.003-0.01%), show high susceptibility to HIC,
- HIC resistant steel (HRS): Metallurgically processed ultra-low S (<0.002%) with normalizing treatment to modify hot rolled structure & Ca treatment (A516-70) steel, may show some degree of HIC/SOHIC in severe environment (A516-70).
- Ultra-Low Sulfur Advanced Steels (AS): Ultra low sulfur (<0.002%) with low Carbon equivalent with ferritic or ferritic/bainitic microstructure having little or no banding produced by TMCP process (ASTM 841 steel) [58].
- Above sulfur contents are typically described in American and European specifications. Conventional steel is typically having

0.005-0.008% S (to ensure good through thickness and general toughness properties (LSCS)). In European convention, low S steel is probably $<0.008\%S$.

- It is felt that HIC can initiate in matrix interfaces which are stronger than inclusions e.g., pearlite colonies. Although stresses are not prerequisite for HIC, but in this case high stresses & H charging condition are required.

Manufacturing Process and Properties of Steels

Good HIC resistance requires not only impurity control, but also specially adapted steel making and plate heat treatment process. The use of so called “pseudo-HIC” steels is based solely on chemical composition and does not provide enough guarantee of HIC resistance. Following are commonly accepted steel making and heat treatment processes-

- Normalized,
- Quenched and Tempered (Q & T),
- Thermo-Mechanical Controlled Process (TMCP),

Figure 2.14 indicates heat treatment requirements for plate production which are followed for each manufacturing process i.e., Normalized, Quenched and Tempered (Q and T) and TMCP [4].

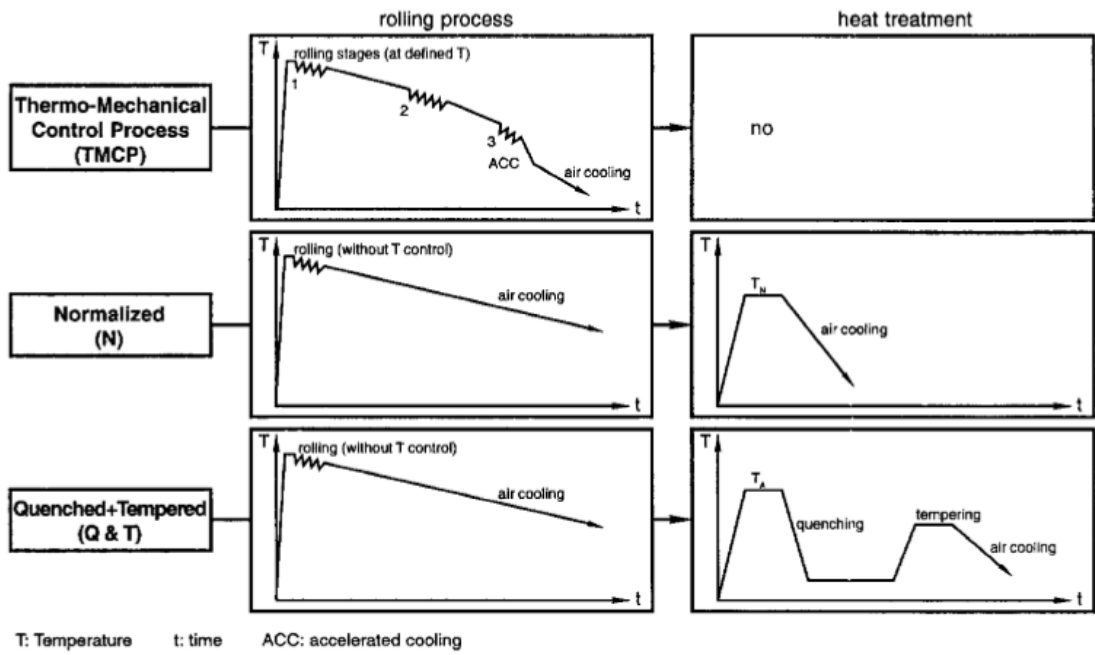


Figure 2.14: Diagram showing TMCP, Normalized and Q & T steels[4].

Nominal Composition of commonly used pressure vessel and pipeline steels i.e., ASTM A516Gr 65 and API 5L X65 (H) (Thickness <2 5.0mm, 0.984”) are given in Tables 2.2 and 2.3.

Table-2.2: Chemical composition of ASTM A516Gr 65 [59].

STEEL	C Max	Si Max	Mn Max	P Max	S Max
A516 Gr-65	0.24 - 0.29	0.13 - 0.45	0.55 - 1.3	0.025	0.025

Table-2.3: Chemical composition of API 5L X65(H) (Thickness < 25.0mm)[60]

STEEL	Welded / Seamless	C ^(b) Max	Si Max	Mn ^(b) Max	P Max	S Max	V Max	Nb Max	Ti Max	Others (c,d)	CE _{IIW} W (a)	CE _{Pcm} m
API 5L X65 (App-H)	SMLS & Welded pipes	0.16	0.45	1.65	0.02	0.003 ^(e)	0.09	0.05	0.06	(g,I,k)	0.42	0.22 ^h
API 5L X65 (App-H)	Welded pipe	0.1	0.45	1.60	0.20	0.002 ^(e)	0.1	0.08	0.06	(g,I,j)	--	0.22

a) Based on product analysis. The CE_{IIW} applies If C>0.12% and CE_{Pcm}<0.12,

b) For each reduction of 0.01% below the specified max for C, an increase of 0.05% above the specified max for Mn permissible up to a max increase of 0,20%

c) Al total<0.06%; N≤0.012%; Al/N≥2:1 (not applicable to titanium killed –killed steel); Cu<0.035% (if agreed, Cu ≤0.10%; Ni≤0.30%; Cr≤0.30%; Mo≤0.15%; B≤0.0005%.

d) For welded pipe where calcium is intentionally added, unless otherwise agreed, Ca/S≥1.5 if S>0.0015%. For SMLS and welded pipes, Ca≤0.006%...

e) The max limit for S may be increased to ≤0.008% for SMLS pipe and, if agreed, to ≤0.006% for welded pipe. For such higher S levels in welded pipe, lower Ca/S ratios may be agreed.

f) Unless otherwise agreed, Nb+V≤0.06%.;

g) Nb+V+Ti≤0.15%;

h) For seamless pipe, the listed CE_{Pcm} value may be increased by 0.03; (i). If agreed, Mo≤0.35%;

i) If agreed, Cr≤0.45%; (k). If agreed, Cr≤0.45% and Ni≤0.50%,

Pressure vessel steels QT have shown better HIC resistance for thicker plates. Wet H₂S cracking resistance requires heated ladle refining process under vacuum for inclusion control. Typically, following Carbon-Equivalent are maintained for various sizes and strength grades [61][28].

- <100mm thick plate-
 - 0.41 max for x65 for HIC / x70 for SOHIC, 0.45 for x70 for HIC,
 - 0.41 max for x65 for HIC / x70 for SOHIC,
 - 0.45 for x70 for HIC,
- 100-200mm thick plate-

- 0.41 max for x60 for HIC ,
- 0.43 max for x65 for HIC / x70 for SOHIC,
- 0.45 for x70 for HIC,

Following treatments are performed for specific purpose as described below[11][35][14] :-

- Ca for shape control of elongated inclusions. Ca treatment is effective if S > 0.002%,
- Cleanliness to reduce sites of initiation of cracks,
- Oxide manifests HIC in low S steels,
- Ca treatment in very low S steels will produce oxides as CaO formation tendency is high.
- Other Oxide inclusions are less harmful than CaO, but numerous little cracks can initiate from oxides which will pass in HIC test, but this will reduce mechanical properties.

Stringent control is required in slab manufacturing and secondary processing including continuous casting with dynamic soft reduction for ultraclean centerline production of pipeline steels[28].

Controlled cooling of slab is carried out for atomic hydrogen control below 2ppm. Atomic hydrogen dissolved in steel lattice interstices combine in preferred sites and initiates HIC. Pipeline steel in sour service cracks by hairline cracks or delayed cleavage fracture with residual H content. Preferred sites or H₂ are following-

- Matrix & inclusion (MnS) interface. If not shape controlled, inclusion gets elongated in hot rolling. Differential thermal expansion coefficient of MnS and steel leads to interface decohesion.
- Centerline segregation promotes shrinkage cavities and formation of hard micro-constituents which attract and act as sinks for atomic hydrogen. Hot rolling creates hairline cracks when excessive H accumulates in such cavities, Typical HIC cracks are found in centerline having hard micro-constituents & shrinkage cavities [62].

Therefore, cleanest matrix and shape controlled MnS with minimum dissolved H in cast slab before hot processing are critical.

After casting, (typically for X52-X65) slabs are controlled/slow cooled between 48 & 72hrs for removal of atomic H. Slab internal cross sections are checked by macro etching with 30% HCl by most of the manufacturers. Chemical segregation further checked with drilled samples at different depths across thickness (H in final slab is also measured using 5mm pin samples taken at various sections across thickness of the slab).

Following steel making sequence is typically followed-

- At ladle furnace, Argon (Ar) blowing is done with Fe-Al and lime addition for slag making, as well as, sulfur control.
- In second step, less Ar injection with fine compositional control.
- In 3rd phase, metallic calcium for sulfide shape control and Ar blowing for oxide control. Oxide is typically maintained <18ppm, ratio of Ca/S=2-3.
- After ladle treatment, metal is transported to RH degassing station (RH degassing is considered as superior to vacuum tank process, reduces segregation because retains super heat). This process produces typically H < 2ppm & N = 30-55ppm after RH degassing.
- Titanium (Ti) is added after degassing for better control over TiN stoichiometry,

Centerline segregation is found as one of the common problems related to HIC, caused due to continuous casting and alloy chemistry which act as sink for H entrapment. Following factors affect centerline segregation [11]-

- The last solidifying liquid is rich in alloy content, gets trapped between advancing columnar crystals in shrinkage cavities, formed by solidification shrinkage and lattice contraction from delta-gamma transformation.
- Chemically rich centerline may give rise to hard transformation products e.g., martensite. Microcracking may occur at martensite inclusion interfaces (TiN, TiNbCN, MnS etc.). ASTM E45 provides guidelines for inclusion measurement [64]
- C,Mn,S & P control reduces centerline segregation,

- Low superheat at Tundish (< 25 oC) and slow casting speed reduces centerline segregation,
- Use of dynamic soft reduction provides machine taper pattern, reduces segregation.
- Soft reduction 0.2-0.8mm/m is applied with split roller, instead of full body roller bulging of strand due to roll deflection is a major cause of centerline segregation.
- H < 2ppm is found to be safe from HIC up to 100 mm thick slabs,
- Slow slab cooling @ 5-6 °C/hr to diffuse H out is more effective at high temperature (in alpha iron region), stacking the slabs facilitate faster removal.

As stated, restricted composition is followed for HIC resistance in all manufacturing processes, in addition to specific requirements for each process i.e. Normalized, Q & T and TMCP as indicated in Table-2.4.

Table-2.4: Restricted composition for manufacturing of HIC resistant steels

<u>CONTROL FOR ALL PROCESSES (NORMALIZED, Q & T, TMCP STEEL)</u>		
• Vacuum Treatment, • S ≤ 0.001%, • Ca Treatment, • Cleanliness Treatment • O ≤ 0.002%, • P ≤ 0.010%		
<u>CONTROL FOR EACH PROCESS</u>		
<u>NORMALIZED</u>	<u>Q & T</u>	<u>TMCP</u>
Balanced addition of C and Mn	C≤0.06%, Mn Restricted, Micro alloyed (with Nb, V)	Balanced addition of C and Mn. Addition of Mo, Ni for hardenability

TMCP rolling schedule utilizes different metallurgical transformation to achieve required mechanical properties with desired HIC resistance. TMCP can have several combinations of rolling at specific temperature ranges (intermediate cooling IC) and finishing with air cooling or accelerated cooling (ACC), as shown in Figure 2.15.

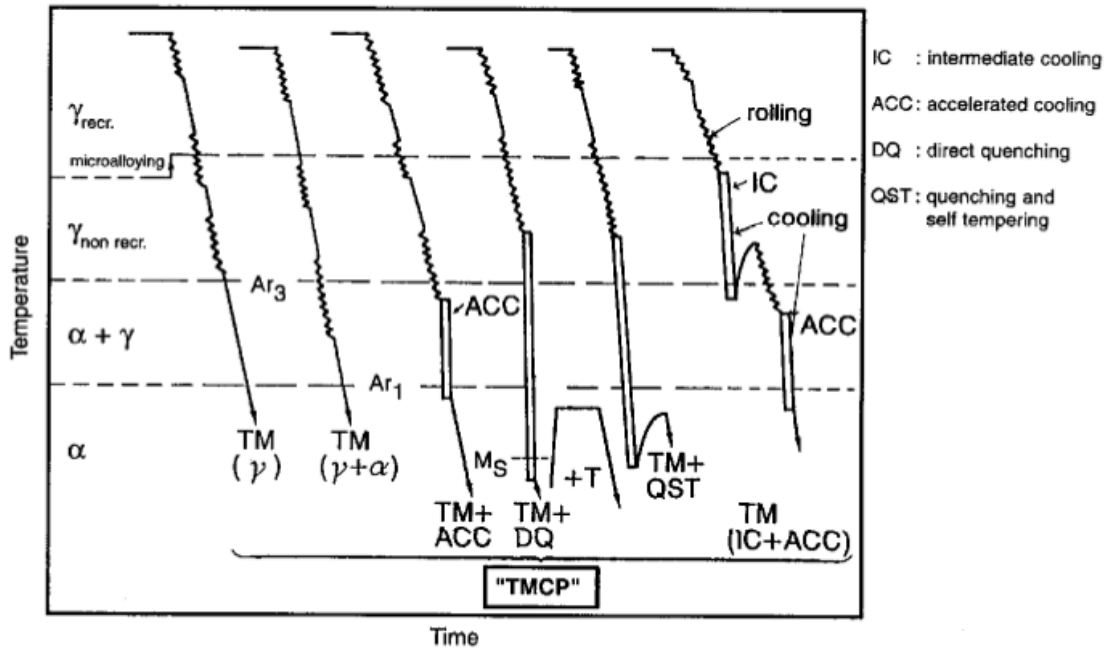


Figure 2.15: TMCP processing with different rolling and cooling schedules[4].

TMCP steels are produced by accelerated cooling (ACC), rolling schedule should be targeted to desired microstructure which shall constitute of fine grain, mixture of massive ferrite and low carbon bainite without pearlite or bainite bands. Reheating temperature is selected high enough ($\sim 1200^{\circ}\text{C}$) to provide full dissolution of large NbCN particles. Large deformation at the first stage is targeted at maximum austenite grain refinement by multiple recrystallizations. Critical requirement in second stage of rolling is to provide rolling finish temperature, $30\text{-}50^{\circ}\text{C}$ above Ar_3 ($\gamma \rightarrow \alpha$ transformation start temperature) to ensure ACC start temperature shall be higher than Ar_3 temperature to avoid structural banding. Typically, $25^{\circ}\text{C}/\text{Sec}$ is ACC cooling in bainitic transformation region for target microstructure formation. Microstructure with bainite transformation is more resistant to crack propagation due to deformed grain boundaries, devoid of cementite layers. The ferrite is responsible for further hardening and austenite promotes additional hardening by raising number of sites available for nucleation of ferrite. Rolling below recrystallization temperature develops pancake-shaped austenite grains, further transforming to polygonal ferrite[62].

After rolling, plates shall be stockpiled for retarded cooling to remove hydrogen. Controlled cooling of slabs has enabled control of hydrogen level below 2ppm which is considered as important for increase in HIC resistance of the steel.

Depending on type of processing, specific properties are developed in the steel. Table 2.5 present the effect of variation in processing for normalized, Q & T and TMCP steels.

Table-2.5. Features of TMCP, Normalized and Q & T steels[4]

TMCP – NORMALIZED - Q & T STEELS				
STEEL TYPE	CARBON EQUIVALENT	SUBSEQUENT PROCESSING	STRENGTH LEVEL	THICKNESS
TMCP	Low	Only cold or semi-hot forming	High	Restricted
NORMALIZED	Medium	Cold or hot forming	Restricted	High
Q & T	Low/Medium	Cold or hot forming + Q & T	High	Medium

Microstructure and HIC Susceptibility

Depending on processing and heat treatment, steels develop specific microstructures. HIC sensitivity depends on microstructure [63][27][43]. Precipitation of carbides occurs in tempering of steels which influence HIC behavior of the metal. Precipitation of coarse $M_{23}C_6$ and M_7C_3 particles is found to deteriorate HIC resistance [64].

Hot rolled structure is most susceptible to HIC degradation. Normalizing, quenching & tempering have shown to reduce susceptibility of steels to HIC initiation or cracking particularly in low S steel. Figure 2.16 shows the

microstructures of A516Gr 70 conventional steel and HIC resistant steel. Heavy banding can be seen in conventional steel.

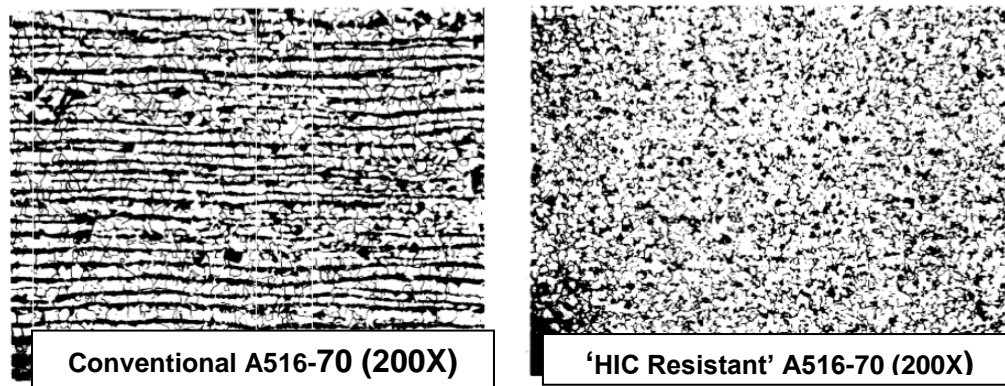


Figure 2.16: Microstructure of (a) A516Gr70 conventional steel (b) HIC resistant steel [65].

Thermo-mechanically controlled process, commonly called TMCP steels with low sulfur and low carbon equivalent, have shown significant resistance to HIC cracking. Reduction in ferrite/pearlite banding in steels produced by TMCP, is considered for such behavior. Carbide rich bands are also considered as secondary sites which initiate HIC in low sulfur containing steels[11].

TMCP X65 steel having chemical composition given in Table 2.6 has different microstructure with variation of finishing temperature above and below Ar₃ after reheating at 1180 °C hot rolled and accelerated cooling @ 12C/s. Finishing temperatures are varied as below [66].

A1 & A2: Start of ACC temperature after rolling above Ar₃

A3 & A4: Start of ACC temperature after rolling below Ar₃

Final cooling by normalizing for A1 & A3 was higher than A2 & A4.

Table 2.6: Chemical composition of X65 steel

C	Mn	Si	P	S	Al	Nb+Ti+V	Cu+Ni	Ca	Cr
0.05	1.25	0.2	0.005	0.002	0.1	0.1	0.4	0.002	0.1

The difference in microstructure due to variation in finishing temperature is shown in Figure 2.17. Microstructure consists of primary and secondary phases

including nonmetallic inclusions and precipitates. Micrographs 2.17 a and c consist of ferrite and dispersed pearlite (F/DP) for steels A1 and A3, micrograph 2.17 b has ferrite and acicular ferrite (F/AF) for steel A2, and micrograph 2.17 d has ferrite and bainite ferrite (F/BF) for steel A4.

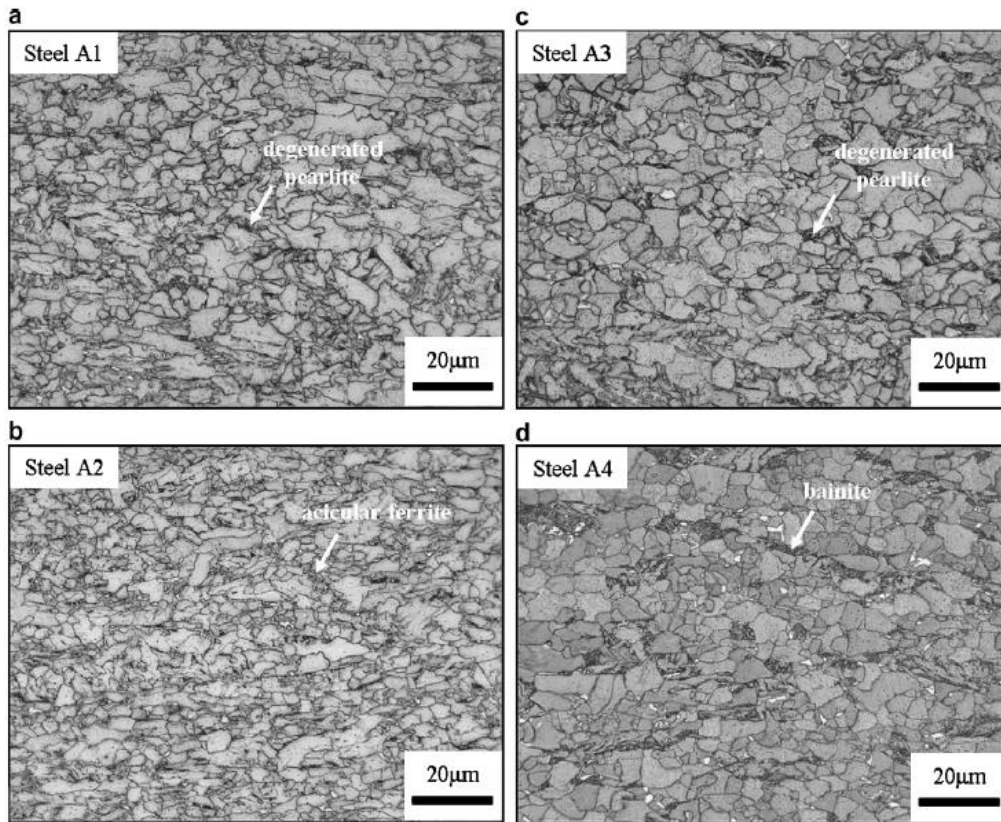
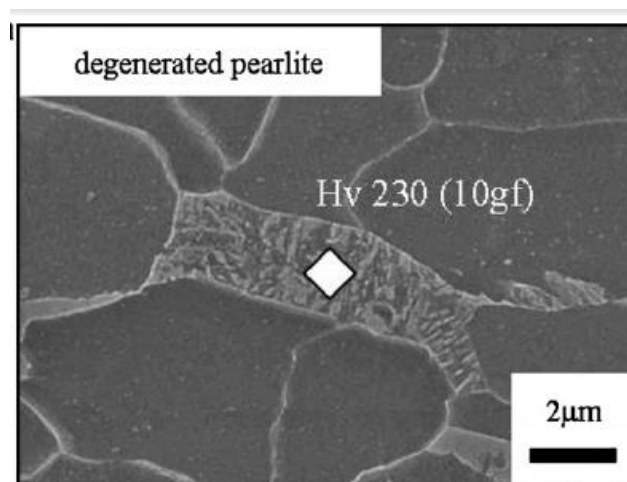


Figure 2.17: Different microstructures due to variation of rolling temperature[32]

Typical second phases are found to be DP, B and M/A constituents as shown in Figure 2.18.



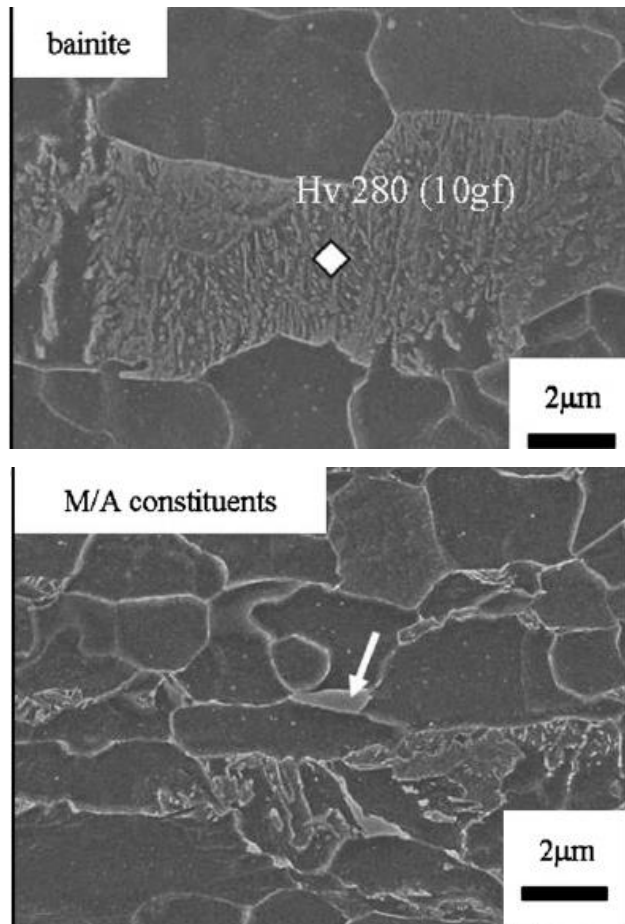


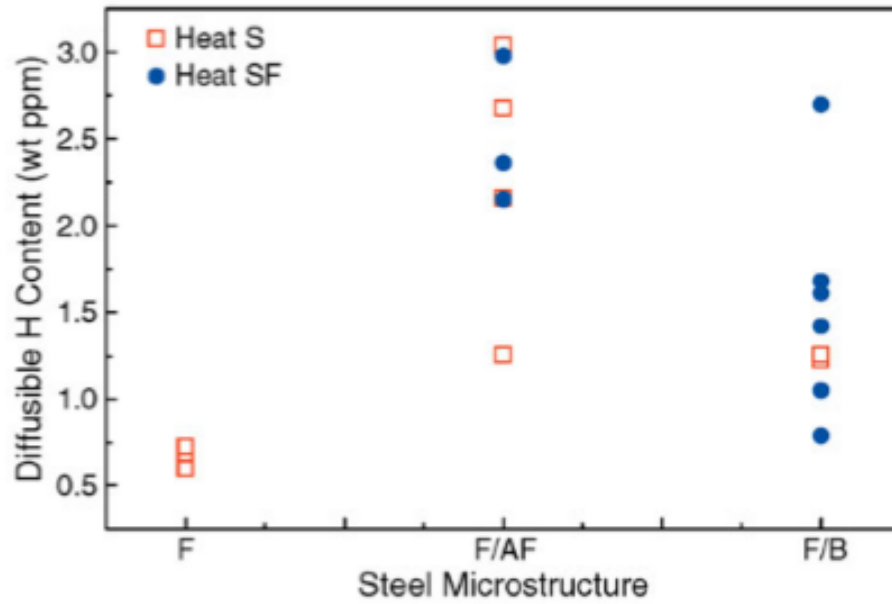
Figure 2.18: Typical second phases DP, B and M/A (top, middle and bottom) with hardness values[32].

Role of Microstructure on Diffusion and HIC Susceptibility

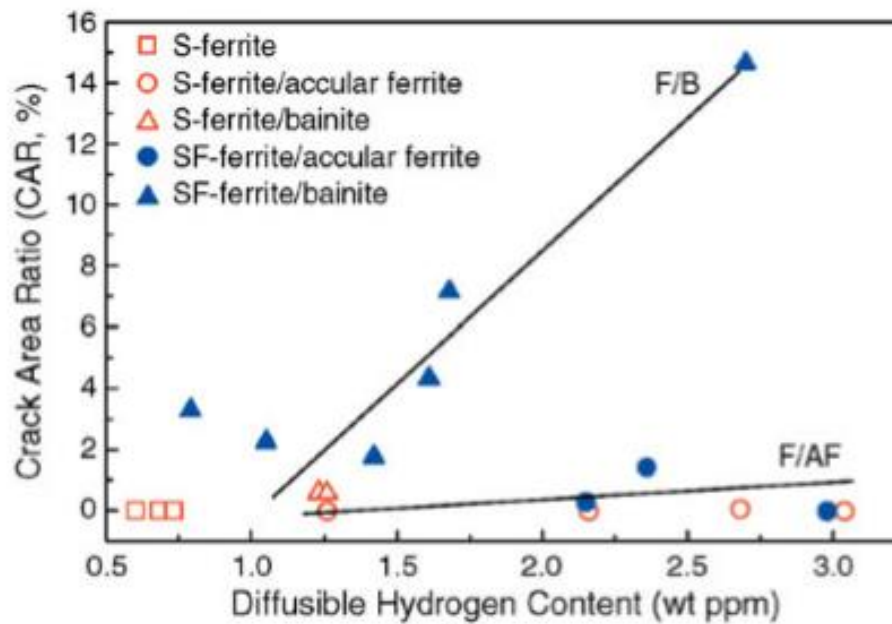
Rate of H diffusion in steel is influenced mainly by two factors i.e., concentration of hydrogen at the steel surface and microstructure of the material [55]. Steels having different microstructures as shown Figure 2.17 were subjected to HIC testing.. It is seen that steel with AF microstructure has smaller D_{app} , J_{ssL} and larger C_{app} than that of steel with F/DP microstructure[66].

Figure 2.19 (a) shows that there was no direct relationship between diffusible hydrogen content and primary microstructure, even internal inclusions does not affect the diffusible hydrogen content when compared with different heats of steels[25]. Fig 2.19 (b) shows that effect of diffusible hydrogen content on HIC as a function of microstructure (and inclusion level). It is seen that HIC does not occur in F/AF microstructure for a wide range of diffusible hydrogen content,

and HIC susceptibility was found proportional in F/B microstructure implying that F/B microstructure is prone to HIC by diffusible hydrogen.



(a)



(b)

Figure 2.19: Relationship between (a) diffusible hydrogen content and steel microstructure and (b) HIC susceptibility and diffusible hydrogen content [25].

Table-19 shows that F/DP microstructure have the maximum diffusion rate whereas, Figure 2.19 shows that F/B microstructure has maximum diffusion rate as well as, cracking tendency.

Carneiro et al, showed that refined and homogenously quenched and tempered bainite/martensite microstructure exhibits best performance against HIC and SSCC. On the other hand, other researchers found that acicular ferrite and ultra-fine ferrite have optimum HIC resistance and mechanical properties (SSCC resistance is better in ultrafine ferrite than acicular ferrite). Park et al studied effect of different microstructures on HIC of X65 steel, and found that acicular ferrite is the most efficient microstructure for H trapping whereas deformed pearlite was the least efficient[67]. Micro-cantilever beam testing of acicular ferrite showed that threshold stress intensity factor to initiate HIC in acicular ferrite is significantly lower than which is found in conventional steels, this implies that HAC in microscale could be significantly different than what is seen in macro scale [68].

Crack Initiation and Propagation

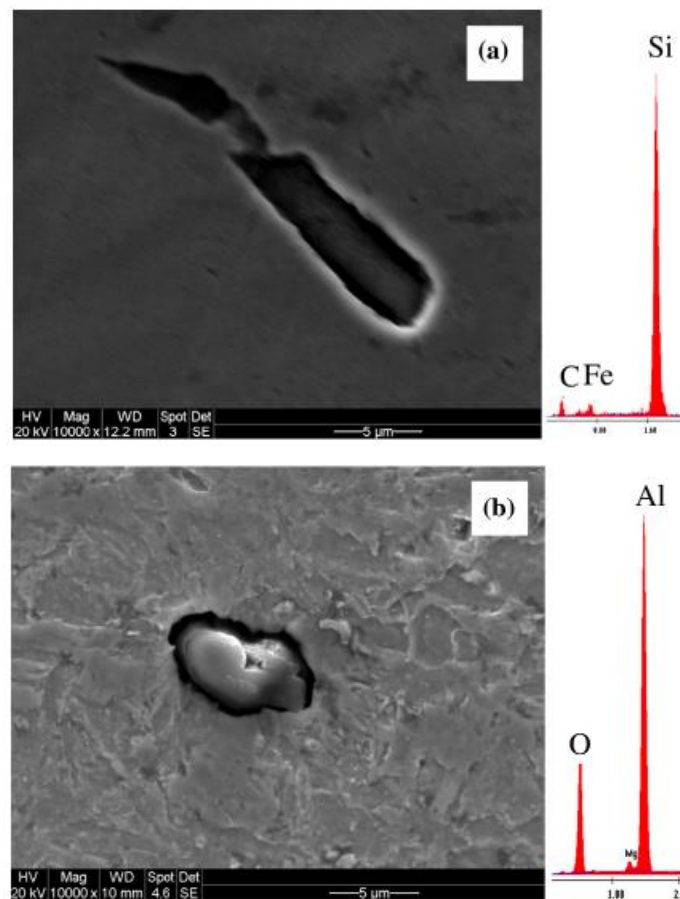
Role of Inclusions

It has been recognized that inclusions are one of the most dominant factors affecting HIC. Several types of inclusions are identified in steels. Types, amount, size & distribution of inclusions affect HIC susceptibility of steels in a significant way. Effect of inclusions on hydrogen cracking possibly cannot be isolated from the microstructure, it belongs to[69].

MnS inclusions are known as most detrimental defects promoting HIC in steels. MnS inclusions are relatively soft which get planer & elongated in flat rolling. Differential thermal expansion coefficient of steel and MnS leads to interface decohesion in steel[25]. In practical experience, it is believed that HIC initiates mainly from Type-II manganese sulfide (MnS) inclusions and propagates along the pearlite bands or bainite and martensite formed in the segregation zone of Mn and P [26][70].

In ultralow sulfur steels MnS inclusions are rarely found instead several kinds of inclusions are found in pipeline steels, which are enriched with silicon, aluminum oxide, magnesium and calcium oxide, ferric carbide, and manganese respectively [14][71][44].

Elongated inclusion enriched with Si, Al oxide with small amount of Mg and Ca, and mixture of Al-Mg-Ca-O are found typically in X80 pipeline steel (X80: C-0.07, Mn-1.86, Si-0.27, Cr-0.04, Mo-0.3, Cu-0.27, Al-0.26, S-0.01, P-0.015, Ti-0.01, Nb-0.079) as shown in fig-2.20 a, b & c.



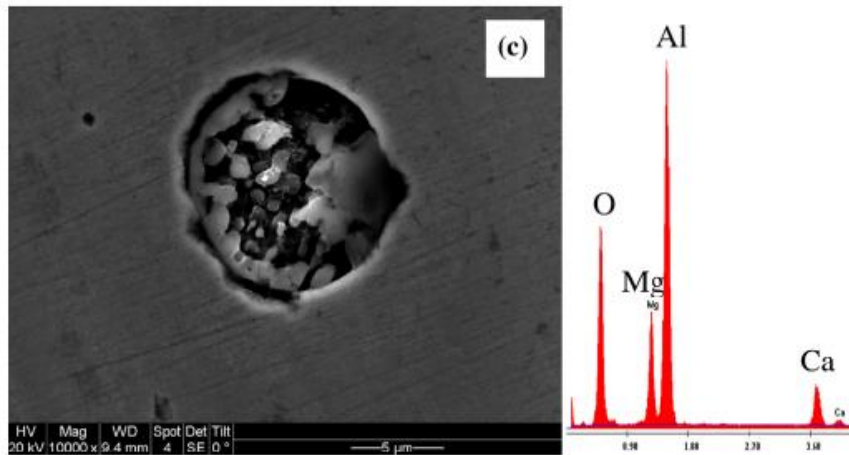


Figure 2.20 (a,b,c): Inclusions typically found in TMCP HIC resistant steels[14]

The inclusions enriched with Si and Al are hard and brittle and found to be incoherent to the metal matrix. There are micro-voids existing at the inclusion-steel interface and acts as sink for H. It is likely that H may diffuse into the interfacial channel and move along the interface towards point of lower chemical potential. H around inclusions markedly reduces interfacial cohesion. A big lattice deformation usually occurs near inclusions, consequently local stress concentration develops around inclusions. The stress concentration facilitates H ingress, as well as, accumulation for initiation of micro cracks. It is found that HIC initiates at inclusions enriching in Si and Al oxides rather than other types which are enriched with ferric carbide, Al-Mg-Ca-O and MnS as in fig-2.21 below [14][55].

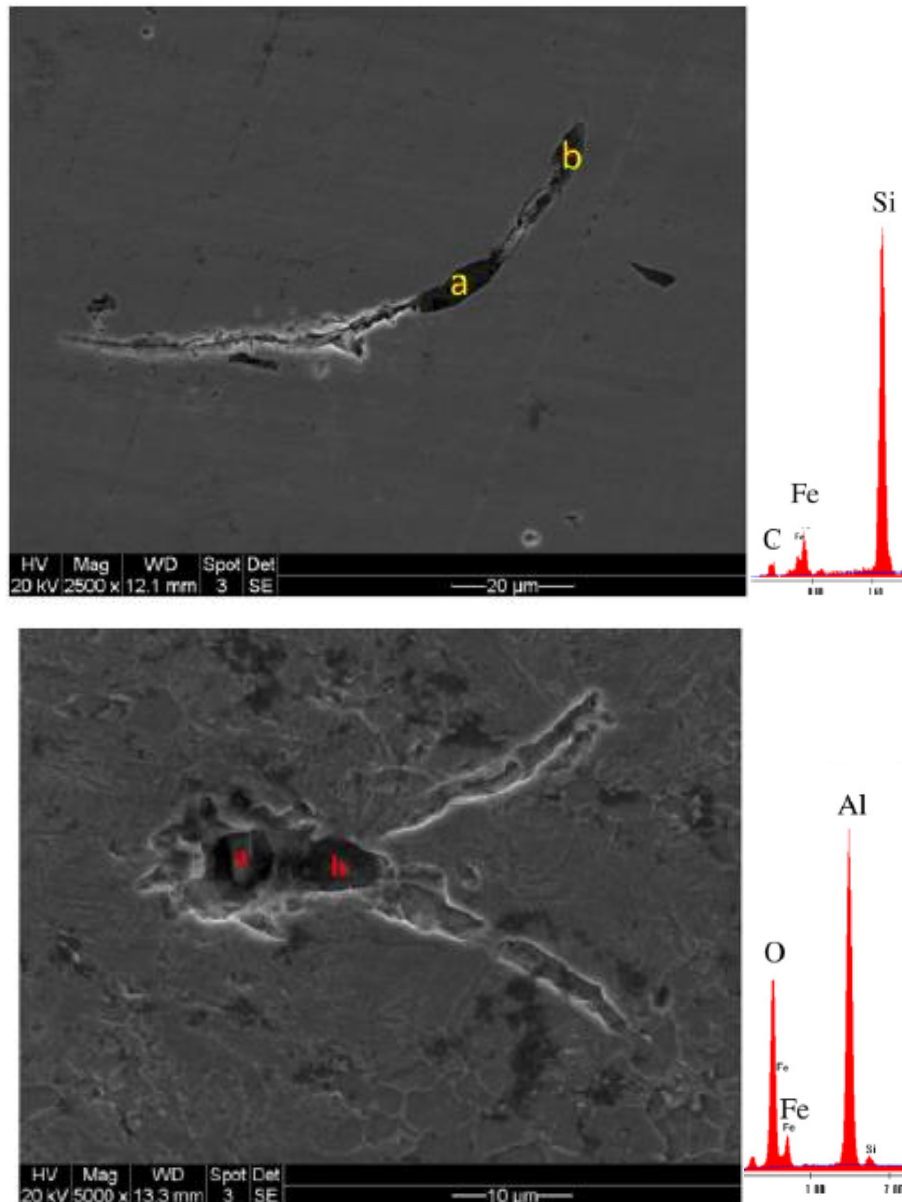


Figure 2.21: Micrographs showing initiation of HIC at inclusions in steels[14]

Kim et al found that HIC primarily nucleated at inclusions enriched with Al and Ca oxides. Inclusions longer than 20 μm in length were detrimental to HIC in steels which contained bainitic-ferrite structure [14]. It was also recognized that the resistance of HIC can be improved by controlling the nature and geometric characteristics of nonmetallic inclusions.

Effect of Martensite/Austenite (M/A) Constituents

In Thermo Mechanically Controlled Processing (TMCP) steels, it is found that cracking of M/A constituents do not require void formation, the M/A constituent is embrittled by H and disintegrates [25]. Crack propagation is in F/AF and F/B phases along M/A constituents are quite visible as shown in Figure 2.22.

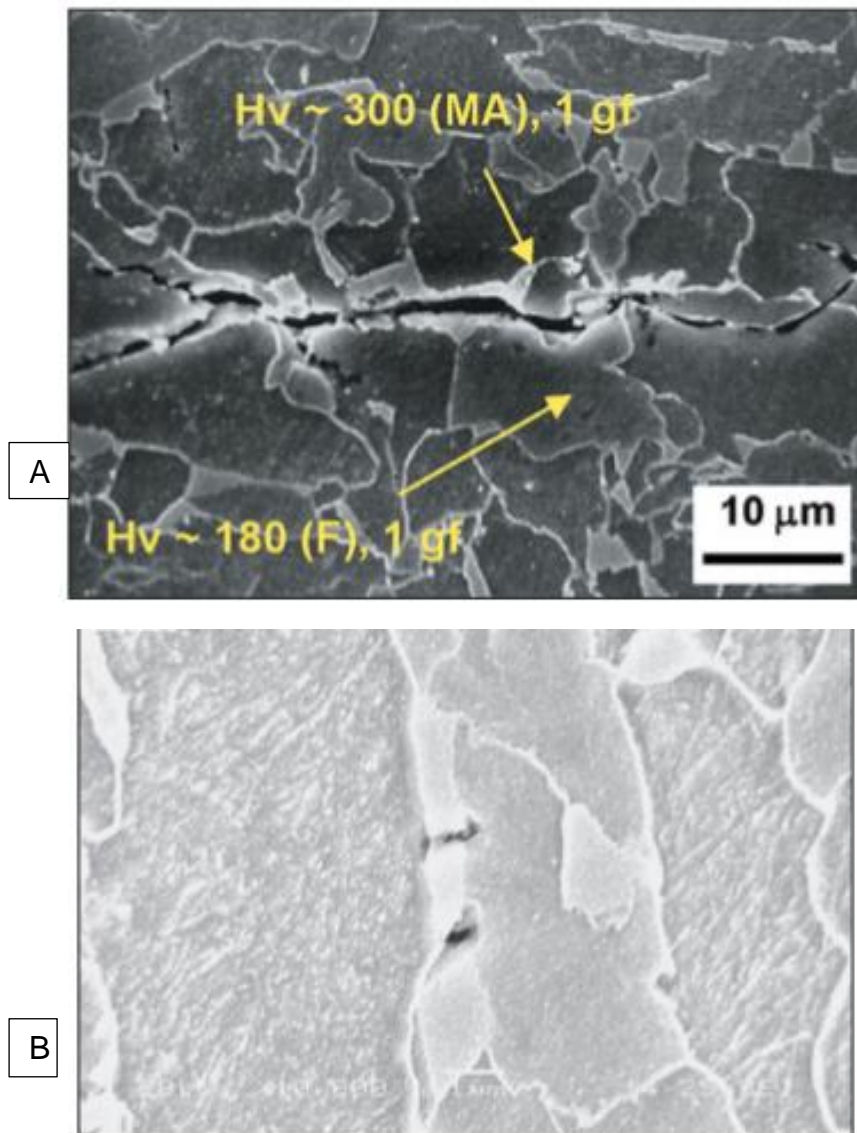


Figure 2.22 : Embrittlement of M/A constituents and initiation of HIC found in micrograph A & B.

Figure 2.23 shows that HIC nucleates where M/A constituents agglomerate which implies that HIC nucleates in areas where M/A agglomerates rather than where M/A is distributed.

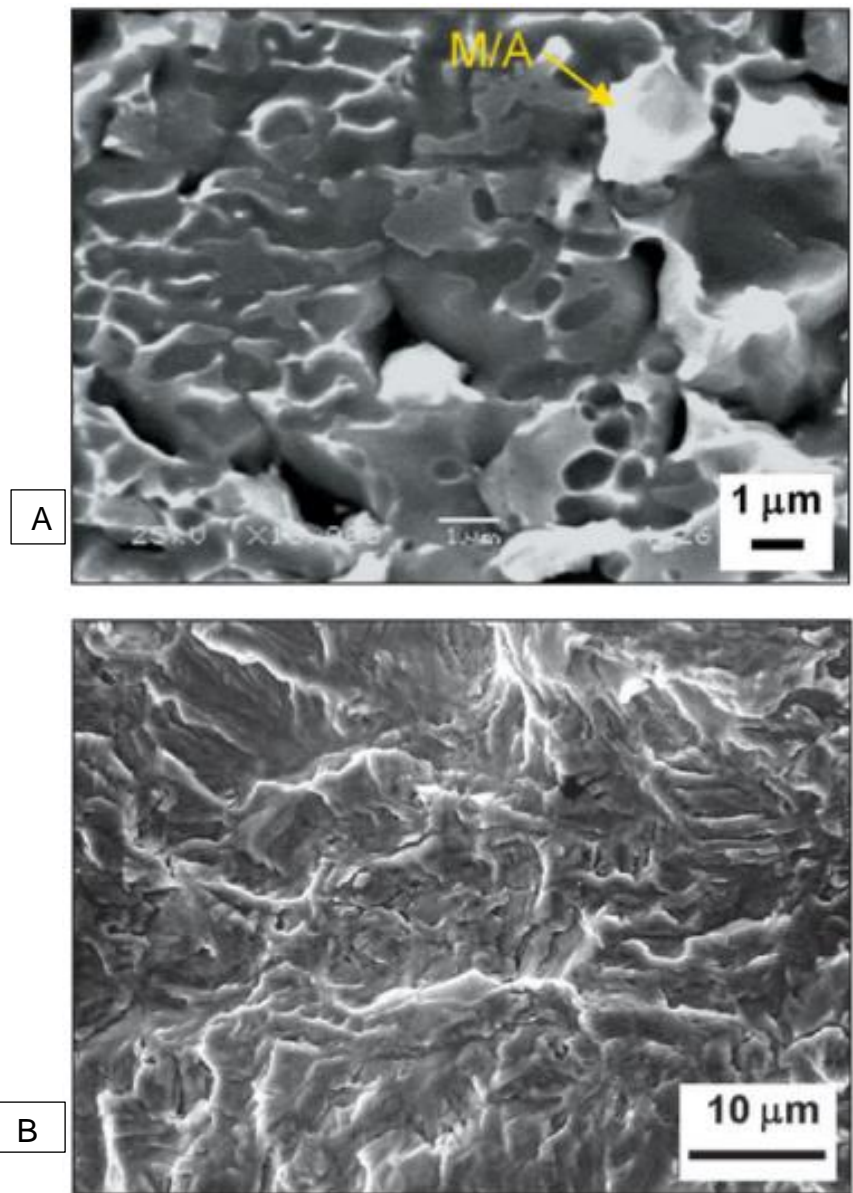


Figure 2.23: (A) HIC initiation sites near agglomerated M/A constituents and (B) Crack propagation in quasi-cleavage manner.

Figure 2.24 shows that HIC initiates from inclusion of oxide cluster in X70 steel and crack propagates in quasi cleavage manner [18].

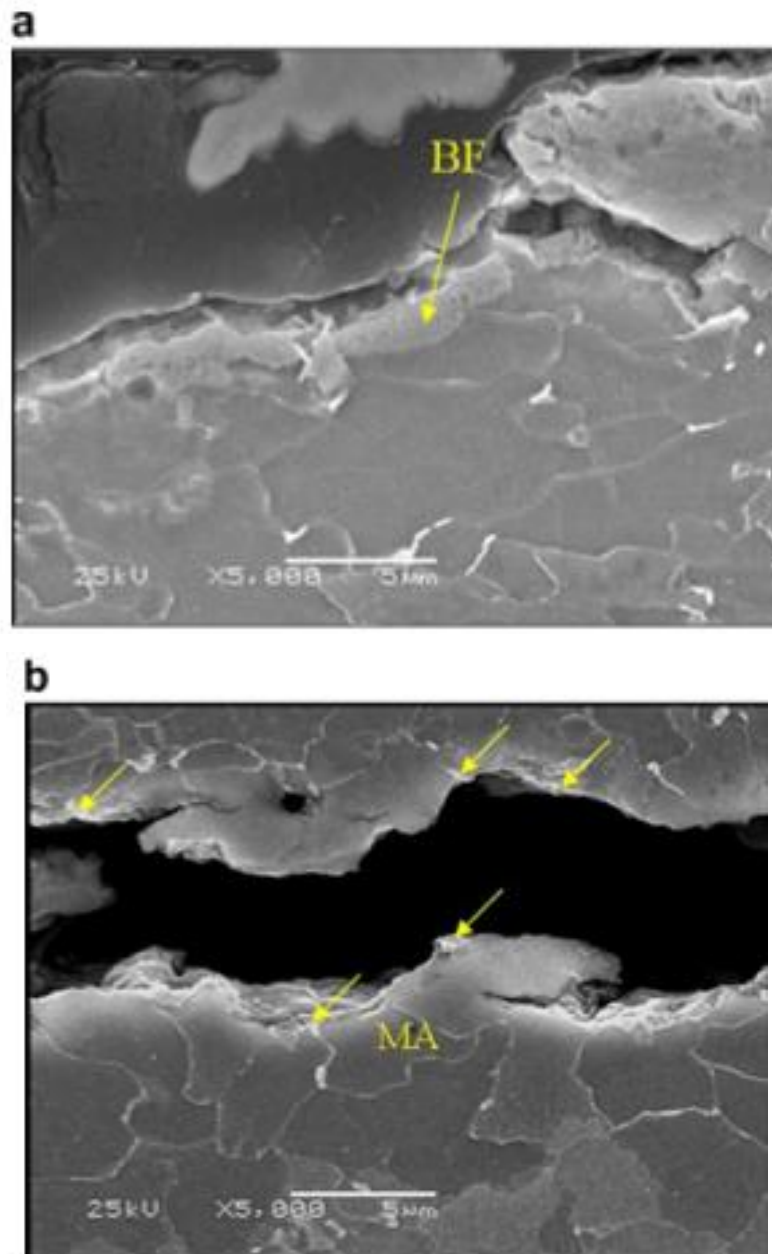
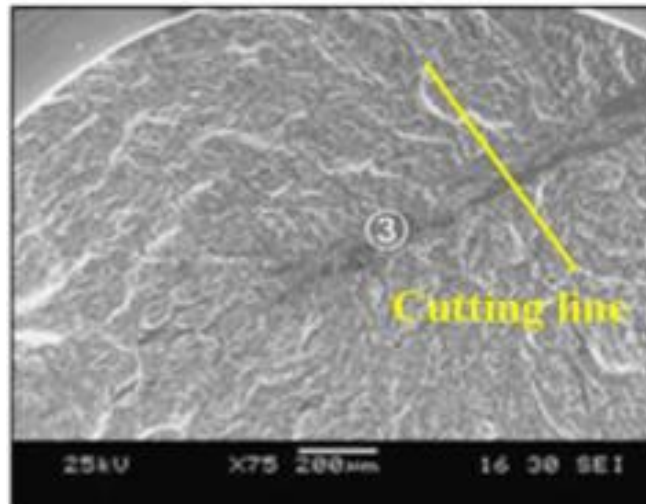


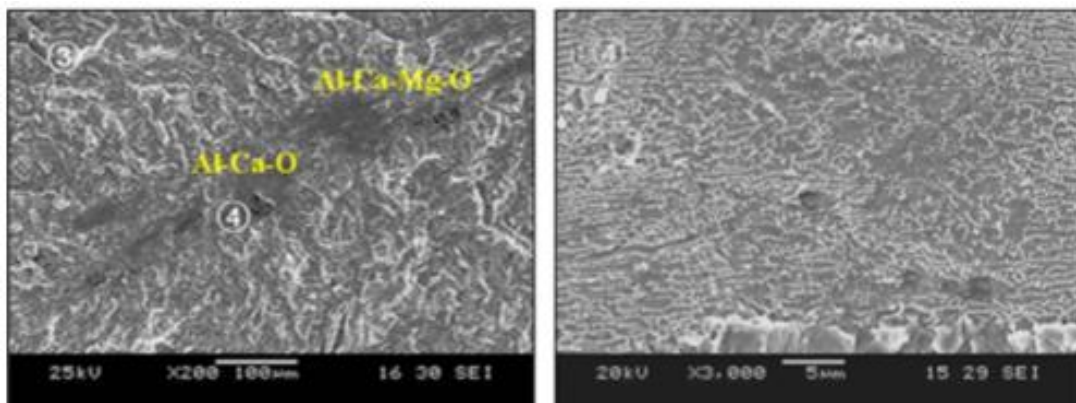
Figure 2.24: (a) HIC initiation at oxide cluster and (b) crack propagation in quasi-cleavage manner in X70 steel.

Figures 2.25(a) and (b) shows that HIC initiated from single oxide inclusion. Valley shown in Figure 2.25(b) results from interconnection of few nucleation sites. Micro-dimples of 1micron were observed at all sides of HIC nucleation sites as seen in Figure 2.25(c). This signifies that micro-dimples from nucleation sites propagate to the point where cleavage crack can advance which becomes critical crack size for quasi-cleavage crack. [Formation of micro-dimples seems to be due to hydrogen enhanced localize plasticity (HELP) mechanism. H

concentration is increased at crack tip which facilitates deformation at the crack tips so that crack growth occurs by more localized micro-void coalescence process than which occurs in inert environment].



(a)



(b)

(c)

Figure 2.25: (a) and (b) HIC initiated from single oxide inclusion, valley in Figure 2.25 (b) and Micro-dimples at all sides of HIC nucleation sites in Figure 2.25(c).

Carbonitride Particles and Centerline Segregation

Centerline segregation contributes to HIC. The centerline segregation is enhanced by continuous casting parameters, as well as, by alloy chemistry. The last liquid which solidifies, is rich in alloy content, and gets trapped in between advancing columnar crystals in shrinkage cavities due to solidification and also

lattice contraction from $\delta \rightarrow \gamma$ transformation [25]. It gives rise to shrinkage cavities and formation of hard micro constituents which are attractive sinks for atomic hydrogen. During hot rolling, accumulated hydrogen hinders annihilation of the cavities, instead creates pressure and forms hairline cracks. Typical HIC cracks are found at centerline of plates following hard constituents as shown in Figure 2.26 [28][62].

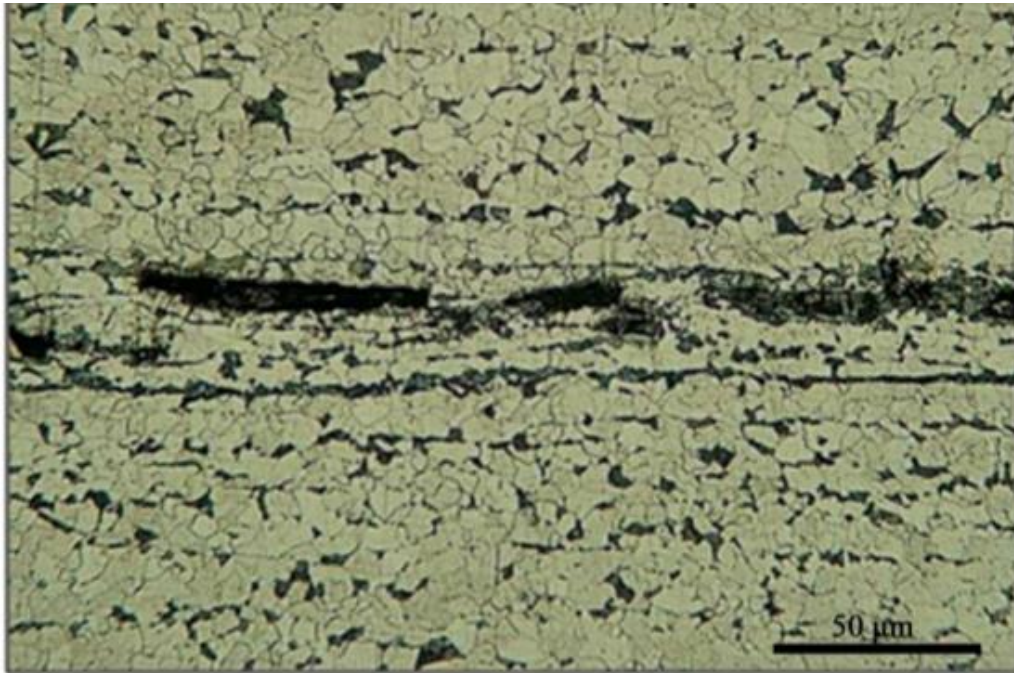


Figure 2.26: Propagation of HIC in centerline segregation zone in X60 steel

Centerline, rich with constituents, may promote hard transformation products such as martensite after hot rolling where micro cracks can initiate at martensite-inclusion interfaces (TiN, TiNbCN, MnS etc.).

In modern steel making of low sulfur steels, micro alloying elements (Nb, Ti) are highly susceptible to segregation, and tends to precipitate as large carbonitride particles in the slab centerline zone. Calcium treatment for shape control of MnS inclusions, as well as, Ti micro alloying less than stoichiometric ratio to nitrogen at minimum concentration of nitrogen prevents formation of large particles of Ti-Nitride in centerline of slabs. Additionally, reduced Nb micro alloying prevents large conglomerates of Nb (CN) or TiNb (CN) in centerline[62] [78, [72].

Carbonitride precipitates are generally medium sized precipitates (40-80nm), presumably TiNb(CN). No large cubic TiN particles were found in the microstructure as revealed from TEM micrograph shown in Figure 2.27. Hydrogen cracks are seen close to Ti Nb(C,N) particles in X65 steel.

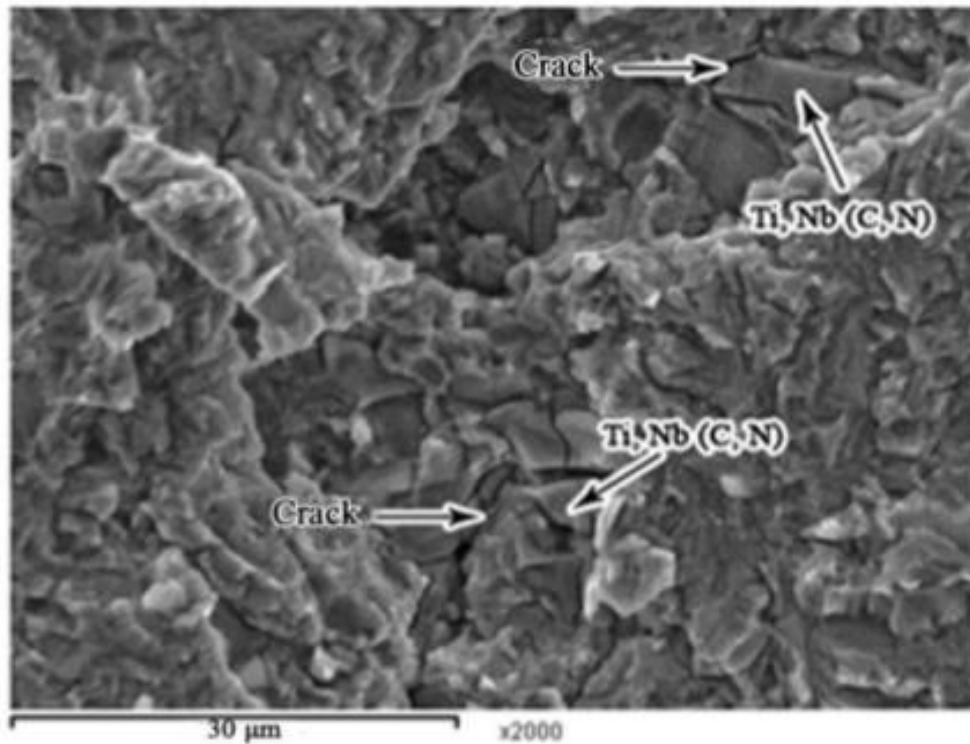


Figure 2.27: TEM bright field micrograph showing inclusions in X65 steel.

In HIC testing of X80 pipeline steel, precipitates of Ti, Nb(C,N) were found in size ranging from 20-50nm however, no cracks found around the precipitates. Zhao et al reported that Nano sized carbonitrides behave as innocuous hydrogen traps in micro alloyed steels which help in hydrogen redistribution in numerous sites (provides optimal cracking resistance). Smaller size precipitates cannot act as irreversible hydrogen trapping sites, and did not affect HIC resistance of the steels. However, it was reported that presence of inclusions is one of the dominant factors for HIC initiation[55].

Micrographs shown in Figure 2.28 reveal that cracks initiated or ran across MnS in F/AF and Al₂O₃ in polygonal ferrite and bainite structure, but not in Si

inclusions in martensite and retained austenite microstructure, suggesting that composition of inclusions have great effect on initiation of HIC. Al_2O_3 inclusions are hard, brittle and incoherent with the matrix. Micro-voids around MnS inclusions, caused by partial dissolution will provide site for H accumulation leading to crack initiation. In general, SiO_2 inclusions can be easily deformed relieving effectively residual stress. Moreover, SiO_2 inclusions are sphere shaped, cause relatively less lattice deformation, and no crack initiation is found around this inclusions.

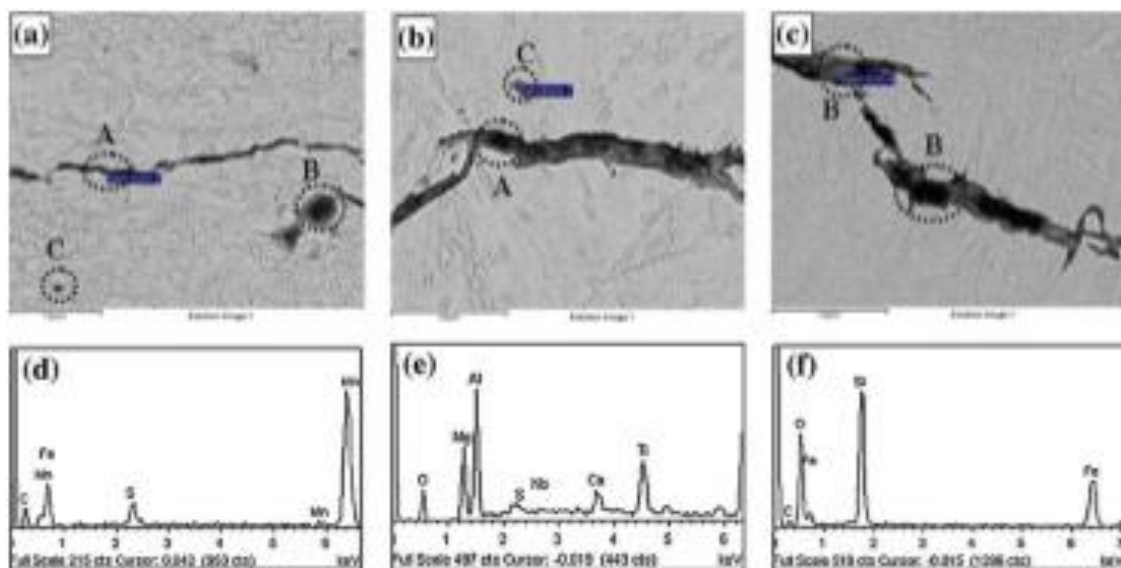


Figure 2.28: BSE images of HIC for X80 steel (a) original (b) air cooling and (c) water quenching and EDS on inclusions (d) A, (e) B and (f) C.

Micrographs shown in Figure 2.29 shows crack propagation path. In original and air cooled specimens crack propagates predominantly in trans-granular manner while crack propagation in water quenched steel is predominantly inter-granular accompanied by little trans-granular cracks. Air cooled and quenched microstructures seem to be more susceptible to HIC than original microstructure.

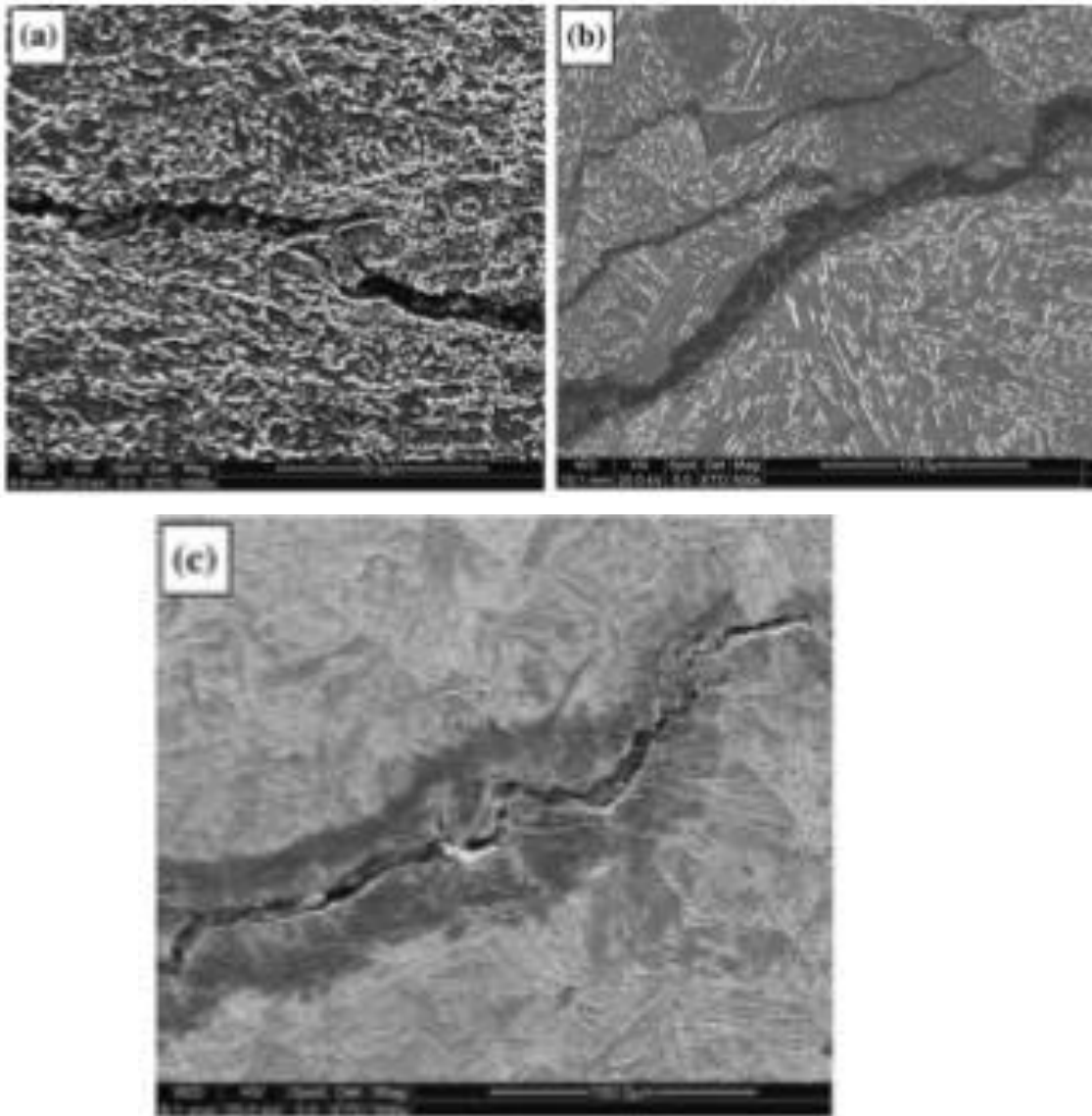


Figure 2.29: SEM images of HIC propagation path in different microstructure of X80 steels (a) Original (b) Air Cooling (c) Water Quenching.

Therefore, to have sufficient resistance of HIC, steel should have least inclusion without change in shape during rolling (min MnS) and minimum dissolved hydrogen content in cast slabs. It is found that clean steel with homogeneous microstructure without banding formed by severe deformation from high temperature to lower bainitic region without large cubic TiN with minimized carbon, sulfur, Mn and balanced micro alloying resists HIC in steel [62][33].

Crystallographic Texture on Crack Initiation & Propagation

Various measures are taken to reduce susceptibility to HIC by adding micro alloying elements (Ti/V/Nb), decreasing S & P content, inclusion shape control, eliminating segregation/precipitation zone, reducing H trapping sites etc., but all these measures could not eliminate occurrences of HIC. HIC cracked samples were analyzed under SEM and EDS. Inclusions e.g. complex carbonytride precipitates (Ti, Nb, V) were found near the cracks. Ferrite/pearlite phase boundaries also enhance crack spread. Hardness was found high at cracked location than other locations which indicated relation of HIC with hardness[73][13]. According to Hall-Petch relation, yield strength & hardness of metal increase with decreasing grain size leading to increased HIC susceptibility. Again, it is believed that grain boundaries act as obstacles to crack propagation, therefore large grains will promote HIC. Therefore, there is an optimum grain size for maximum HIC resistance. Further research led the way to crystallographic texture and grain boundary distribution engineering which is considered a step forward towards enhancing HIC resistance of steels [61].

Thermomechanical processing produces favorable crystallographic textures and significantly increased HIC resistance. It is observed that high angle grain boundaries and Kernel parameter values act as hydrogen trapping sites which increases HIC susceptibility and highest resistance to HIC is achieved by rolling isothermally at 850°C. Kernel Average Misorientation represents “relative average misorientation between any points that belong to the same grain”. High accumulation of grains with relative misorientation between 0.5-2.5° at grain boundaries created during manufacturing and service due to strain are preferred location for H accumulation and HIC. Regions near HIC showed lower Kernel values due to release of energy near crack tip which provides sufficient driving force for crack growth. Crack tends to propagate along grains with high Kernel values. The high dislocation density in the crack path promotes accumulation of misorientations inside the grains and distortion between neighboring lattices.

This increases the HIC susceptibility. It is deduced that there are three possibilities of crack propagation-

- Where dynamic recrystallization or recovery did not occur, crack tends to propagate through the deformed grains with high stored energy.
- Where the lack of sufficient slip systems has harmful effect on HIC resistance, crack propagates along grain oriented with $\{001\}$ //ND,
- Fine grains can trap more hydrogen and generate more internal energy to promote crack nucleation, as well as, propagation.

Grains oriented in preferred crystallographic directions during manufacturing can influence mechanical properties, as well as, HIC resistance. Crystallographic orientation is denoted by $\{hkl\} \langle uvw \rangle$; where $\{hkl\}$ is rolling plane and $\langle uvw \rangle$ is rolling direction. Figure 2.30 represents the crystallographic planes and directions of a cubic crystal.

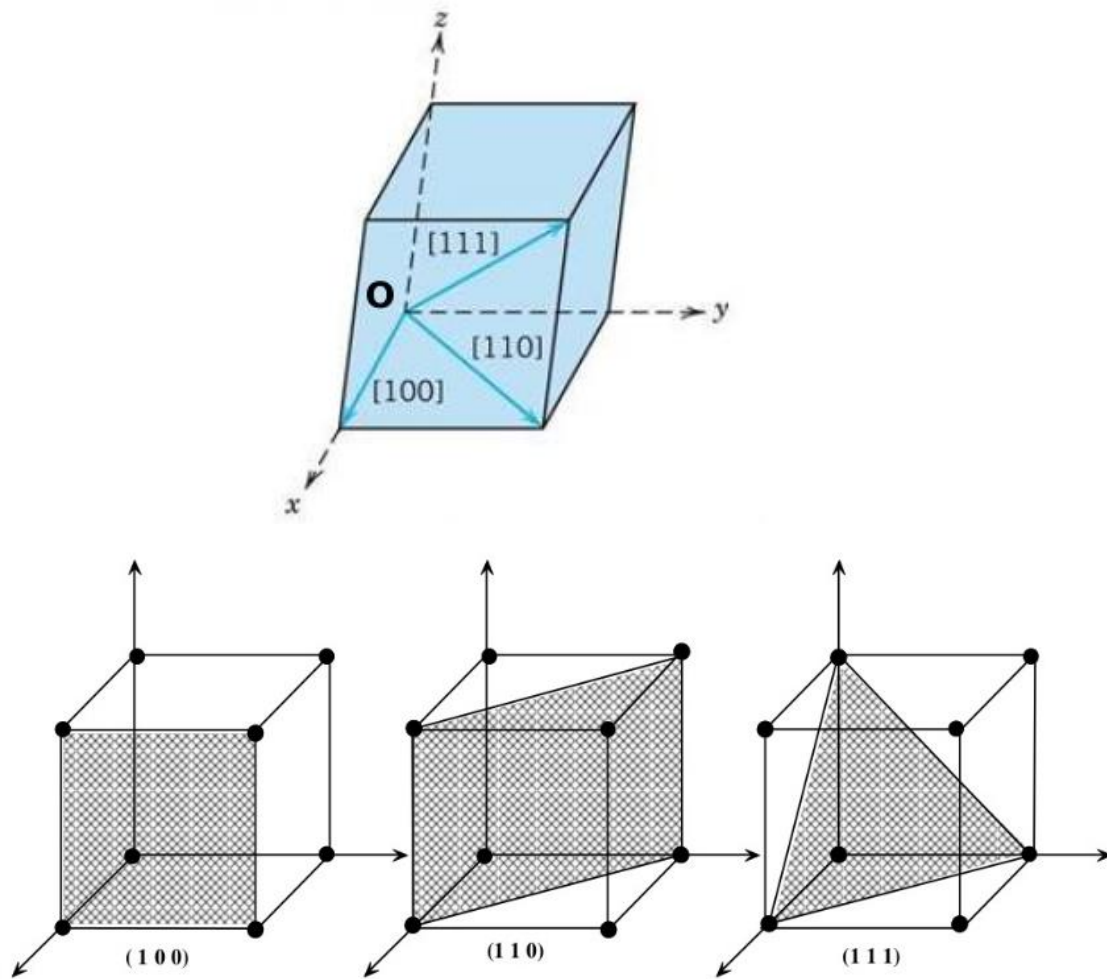


Figure 2.30: Crystallographic Direction and Planes of a crystal

Thermomechanical treatment produces favorable crystallographic textures and favorable grain boundary distribution which can significantly improve HIC resistance as well as mechanical properties. High ‘angle’ grain boundaries and high ‘Kernel parameter’ promote hydrogen trapping which increases HIC susceptibility. Texture in rolling is represented by a combination of crystallographic plane and direction $\{hkl\}\langle uvw \rangle$ which means that $\{hkl\}$ are the planes, parallel to the rolling plane and $\langle uvw \rangle$ are the planes, parallel to the rolling direction as shown in Figure 2.31 [61][74].

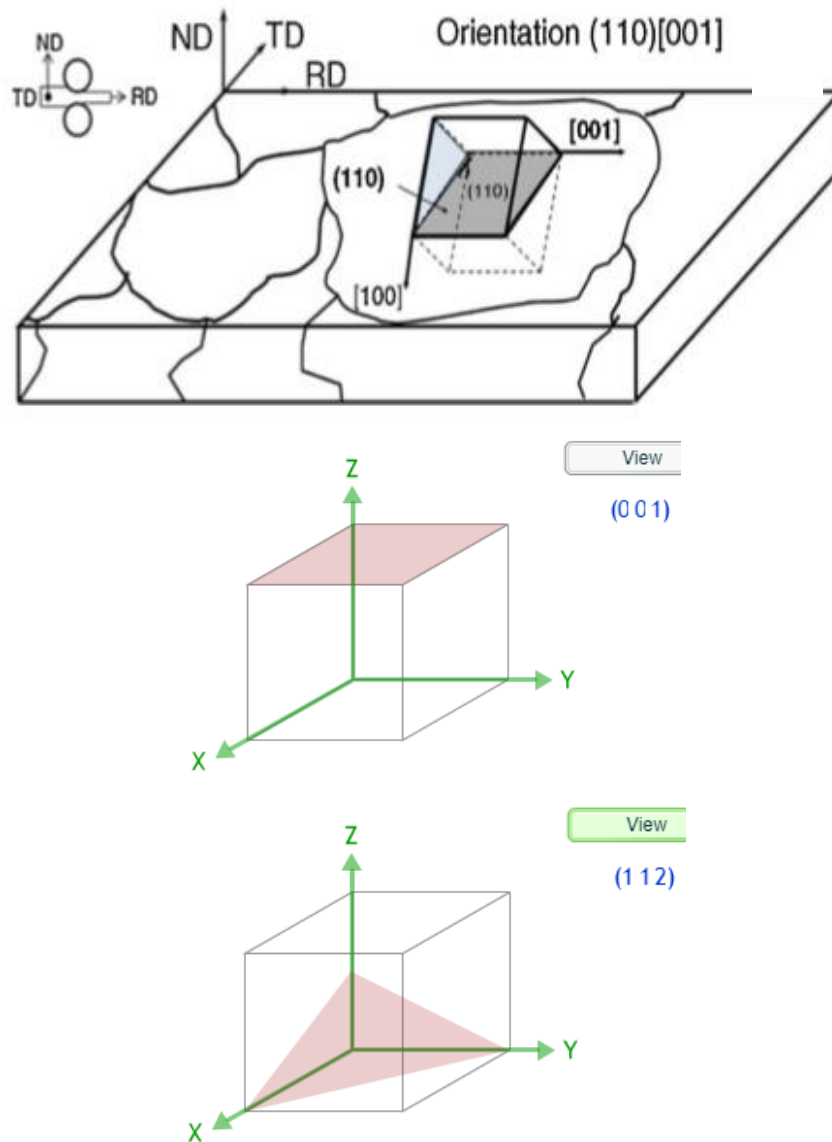


Figure 2.31: (Top) Crystal orientation with respect to sample axis, (Bottom left) and (Bottom right) represent Crystallographic planes (001) and (112) respectively.

Experiment with X70 sour service used steel with HIC cracks (pearlite/ferrite banded structure: 0.105C, 1.6Mn, 0.018P & 0.006S wt. %) and new steel with similar composition were carried out. Typical stepwise crack parallel to rolling direction besides some deflection to normal direction were observed, as shown in Figure 2.32.

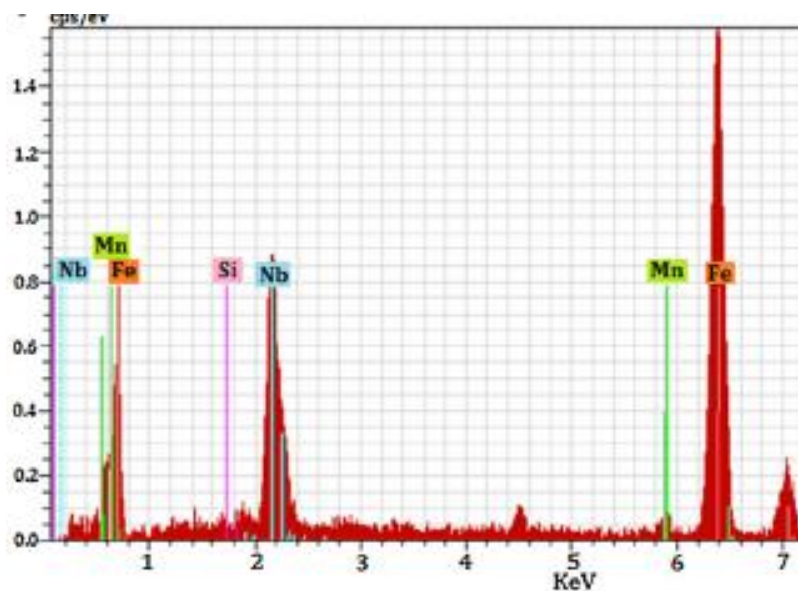
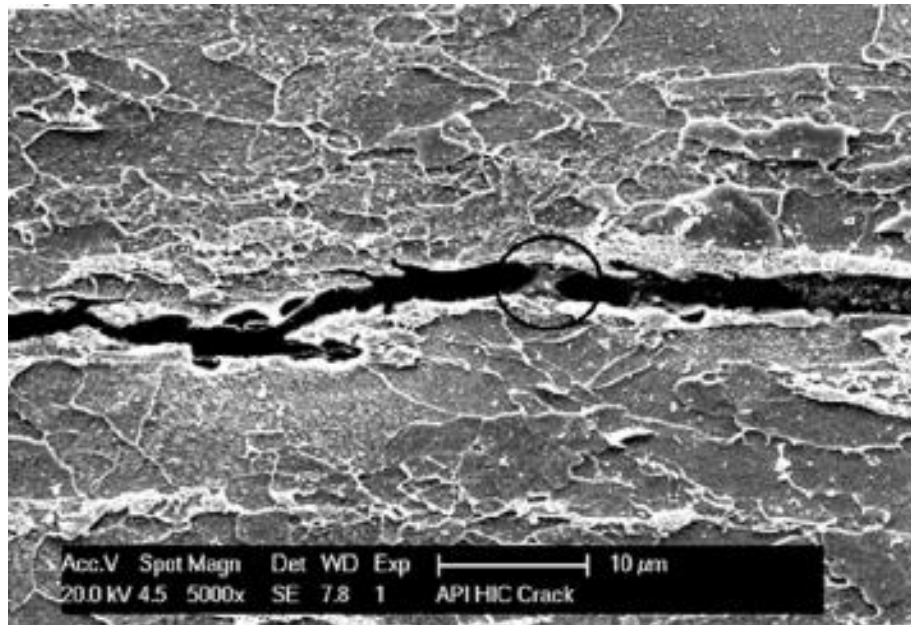


Figure 2.32: Stepwise crack developed parallel to rolling direction and deflections to normal direction at ferrite-pearlite phase boundaries having complex carbonitride inclusions (SEM and EDS).

Some different types of inclusions including complex carbonitride precipitates (Ti, Nb, V) (C, N) were identified in the vicinity of crack path. Ferrite-pearlite phase boundary is also found to enhance crack spread. High hardness favours cracking.

KAM map for the HIC cracked sample is shown in Figure 2.33. The misorientation observed demonstrates induced strain during manufacturing and service which provides easier path for crack propagation. The high dislocation

density around the crack path permits accumulation of misorientations inside grains and distortion between neighboring lattices, leading to an increase in HIC susceptibility, whereas, high amount of recrystallization with no stored energy provides high HIC resistance [75].

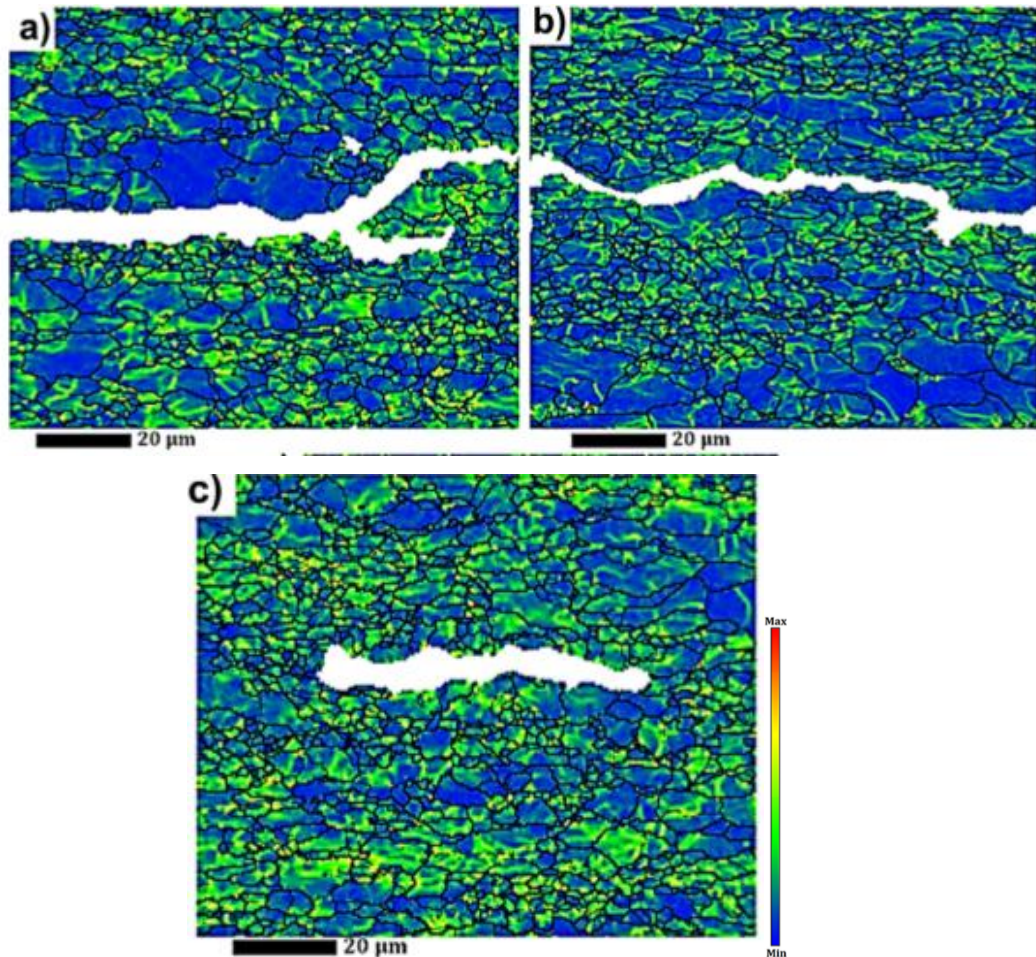


Figure 2.33: Fig a, b and c indicates Karmel Average Misorientation in grain along HIC region and in the vicinity of crack path. The regions near the crack show lower KAM values due to release of energy.

High KAM values prior to cracking are the driving force for the HIC to propagate along the plane and cracking results in lowering of KAM. ‘Inverse Pole figure’ (IPF) mapping of HIC cracks, as shown in Figure 2.34 reveals the propagation of cracks along the boundaries of grains oriented with $\{001\}$ //ND and $\{111\}$ //ND fibers (indicated in red and blue colors) respectively. High angle grain boundaries having higher internal energy are considered as main trapping sites for hydrogen that provide easy path for crack propagation.

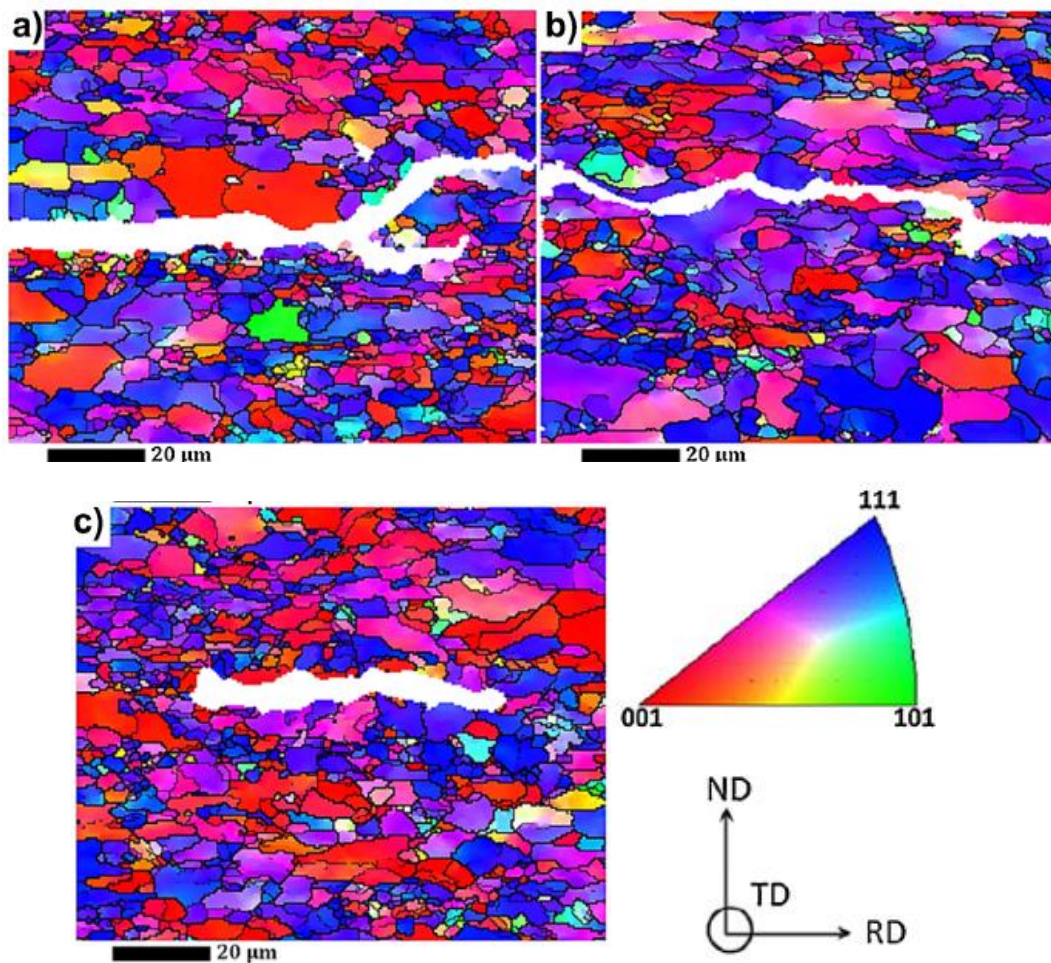


Figure 2.34: fig a, b & c shows Inverse Pole figure (IPF) mapping of HIC showing crack propagation along very small grains (<2microns in diameter).

In TMCP steel manufacturing process, high dislocation density generated during rolling is distributed among different slip systems and provide maximum shear stress ahead of crack tip. Thus, the crack path is zig-zag and not straight which is typical characteristics of HIC propagation. Main slip plane in the BCC lattice is oriented along (112) plane, dislocations are arranged along this slip plane which provides sufficient driving force for crack propagation. Highest HIC resistance was achieved by rolling isothermally below recrystallization temperature at 850°C due to the high proportion of grains oriented with {110} planes parallel to the normal direction and {111}//ND fibers accompanied by negligible fraction of grains oriented in cleavage planes {001}//ND. {110}, {111} and {112}//ND are desirable compact planes. Hot rolling (~1040°C) produces close to random textures, while warm rolling (850°C) increases the

intensity of the $\{111\}$ //ND fiber. Similar study by other researcher with API 5L X52 steel concluded that warm rolling in the range of 600-800C promotes dominant crystallographic texture of $\{111\}$ ND, $\{112\}$ ND, and $\{011\}$ ND. The lower the final rolling temperature, the larger the amount of strain and higher the strength of the latter fiber. Venegas et.al [74] studied the influence of texture on HIC susceptibility of X46 steel and found that preferred grain orientation was $\{111\}$ plane, parallel to normal direction ($\{111\}$ //ND) produced via warm rolling below recrystallization temperature. Ghosh et al. reported that cleavage in $\{001\}$ //ND grains generated during rolling at high temperature by recrystallization of austenite grains followed by ferrite transformation provides easy crack path and reduces significantly mechanical and HIC properties. Verdeja et al. reported that texture in $\{110\}$ //ND and $\{332\}$ //ND reduce sensitivity to HIC in ferritic-pearlite steel while $\{001\}$ //ND and $\{112\}$ //ND textures have the opposite effect. Recent studies showed that dislocation sliding during rolling at elevated temperature (above $T_m/4$) in BCC structure takes place largely on the $\{110\}$ and $\{112\}$ planes, leading to decreasing intensity of crystallographic texture. Rolling at relatively lower temperature (below A_r3) generates a higher dislocation density in steel. Dislocation accumulation inside grains leads to grain subdivision with highly stored energy which facilitates HIC. High temperature rolling (above $T_m/2$) reduces the degree of deformation of austenite phase, but dynamic recrystallization produces undesirable $\{001\}$ $[0\bar{1}0]$ cube texture components which reduce HIC resistance [74].

Mohtadi-Bonab et al have found that there is no preferred direction for hydrogen crack propagation, the crack can propagate in various directions. However, different factors, such as grain orientation, grain boundary distributions, special coincidence site lattice (SCL) boundaries and distribution of recrystallized grains play significant roles in HIC resistance by providing good lattice fit with low stored energy ahead of crack tip [82].

It is worth mentioning that equiaxed and strain free recrystallized grains surrounded by high angle grain boundaries produced during hot rolling have high resistance to crack nucleation and propagation. In contrary, elongated

grains with stored energy are prone to HIC. High angle grain boundaries with high disorder between neighboring grains and high density of dislocations and vacancies are considered as hydrogen trapping sites thereby promoting HIC in steel. It is also believed that high angle boundaries with high lattice distortion, having high stored energy, provide an easy path for crack nucleation and propagation. TMCP reduce proportion of high angle boundaries [61][76].

Grain Size and Angle

High angle grain boundaries have higher internal energy, are more preferable hydrogen trap sites which provide easier crack paths. HIC propagates along very small grains ($<2\mu\text{m}$). It is expected that fine grains with large fraction of high angle grain boundaries and with high stored energy increases the number of nascent hydrogen trapping sites. According to Hall-Petch relation, the yield strength and hardness increase with decreasing grain size, which increases HIC susceptibility. On the other hand, it is believed that grain boundaries act as obstacles to crack propagation. But the coarse grains with low fraction of grain boundaries, can facilitate crack propagation and increase HIC susceptibility[61][18]. For X70 TMCP steel, it was found that HIC nucleates at oxide clusters with size over hundreds of microns. Crack propagates in quasi-cleavage manner as soon as HIC initiated[26].

Therefore, there is an optimum grain size with which maximum HIC resistance can be achieved. It is deduced that there are three possible factors related to manufacturing process which promote HIC in steels-

- a. Cracks tend to propagate through deformed grains with high stored energy where dynamic recrystallization or recovery does not take place.
- b. Cracks propagate along grain oriented with $\{001\}$ //ND. Lack of sufficient slip systems with this plane is found to have a harmful effect on HIC resistance. Besides deformed grains oriented with $\{111\}$ //ND and $\{112\}$ //ND, high dislocation density can also provide easier paths to crack propagation.

- c. Very fine grains can trap more hydrogen and generate more internal energy to promote crack initiation, as well as, propagation.

Taylor factor demonstrates relation between yield stress and crystal orientation which is used to analyze level of plastic deformation by showing the distribution of grain orientation.

Some grains are aligned in the loading direction and can easily slip and deform, since the critical resolved shear stress is attained. Taylor factor is low for these grains. The grains which are not aligned with slip planes will require some kind of rotation to bring out minimum critical resolved shear stress to slip. These grains with moderate Taylor factor value are called, soft grains. Some grains which cannot rotate to bring the appropriate slip system are called hard grains. These are highly prone to cracking & propagation.

Transgranular crack propagation occurs through the grains with high Taylor factor and dislocation accumulation tends to be resistant to yielding while intergranular cracks propagate due to Taylor factor mismatch in neighbouring grains because of differences in active slip systems. Active slip systems depend on crystallographic orientation and the differences of local stresses near grain boundaries between adjacent grains.

Banding in Microstructure

Normalized, Quenched and Tempered steels have high HIC resistance, particularly in low sulfur steels. Microstructural banding (carbide rich) in such steels is considered as sites for HIC initiation in low sulfur steels[11]. Studies also found contradictory evidences that banding or absence of banding in steels does not have any effect on HIC for clean steel (A516-60) [77] . In general, banding is considered harmful for HIC resistance of steels.

Hardness and Strength of Materials

Hardness and microstructure influence low alloy steels to H assisted cracking. Cracking initiates and propagates more easily in less ductile microstructures[55].

Ferrite pearlite phase boundaries are found to promote spreading of cracks. Micro hardness measurements at locations having cracks showed higher values (235+-7 HV) than sound locations (200+-5HV) which indicates a correlation between HIC susceptibility and hardness. According to API 5L, hardness shall be 238+- 6HV (22HRC)[61].

Low strength steels (<700 MPa yield strength) are known to suffer more from HIC[5]. For pressure vessel steels, improved HIC resistance is found in normalized steels with tensile strength less than 585 MPa (85 Ksi) and Hardness less than 200 BHN .

Heat Treatment and HIC

Controlled cooling of slabs has enabled control of hydrogen level below 2ppm which is considered important for improving HIC resistance of the steel. HIC resistance of plate can be impaired by cold processing as shown in Figure 2.35 [28].

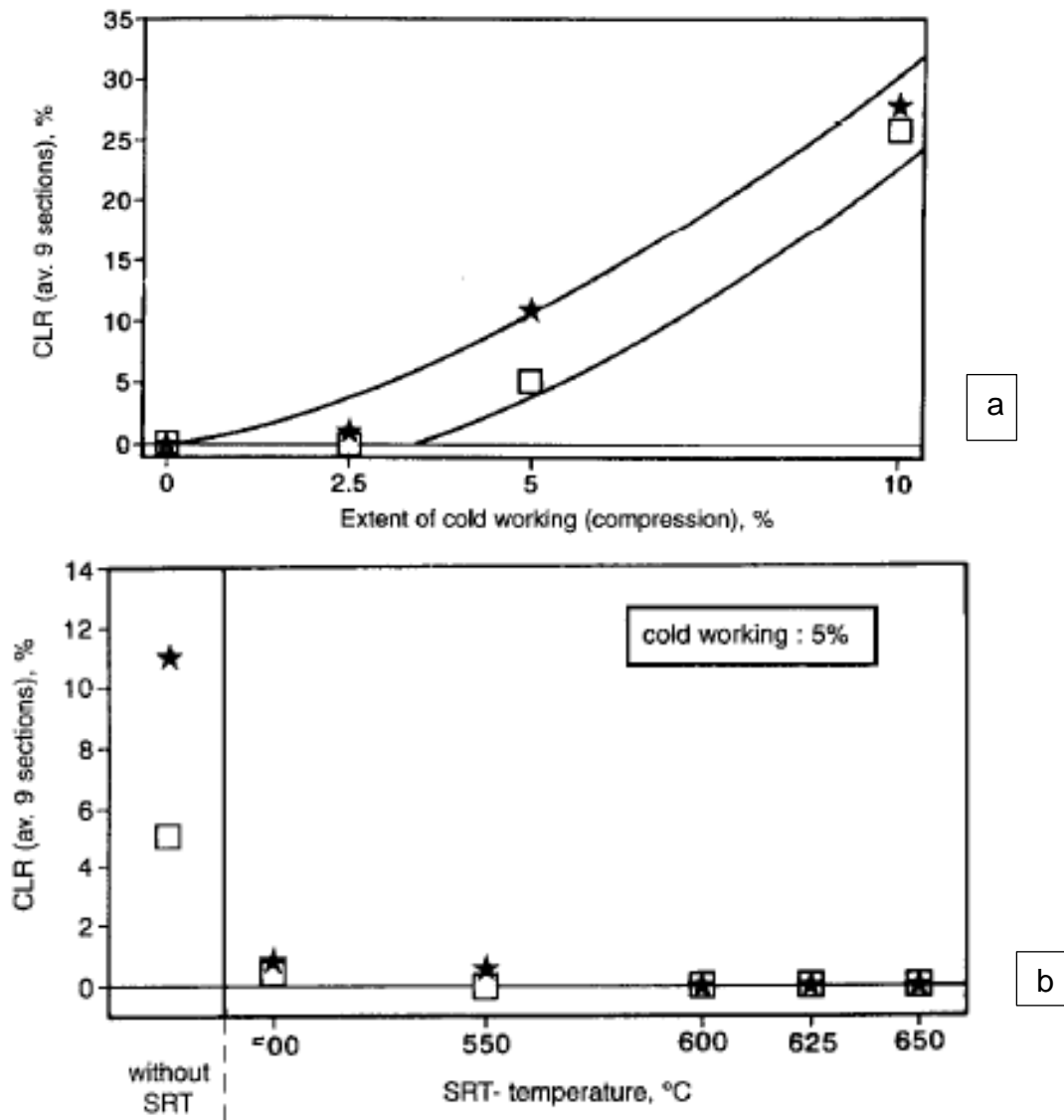


Figure 2.35: (a) HIC susceptibility of A516-70 with extent of cold working, (b) HIC resistance compensation by stress relief heat treatment.

Experiment on A516-70 plates shows that stress relief heat treatment (tempering effect) improves HIC resistance. Above 550°C, no further improvement can be seen for normalized steel as shown in Figure 2.36.

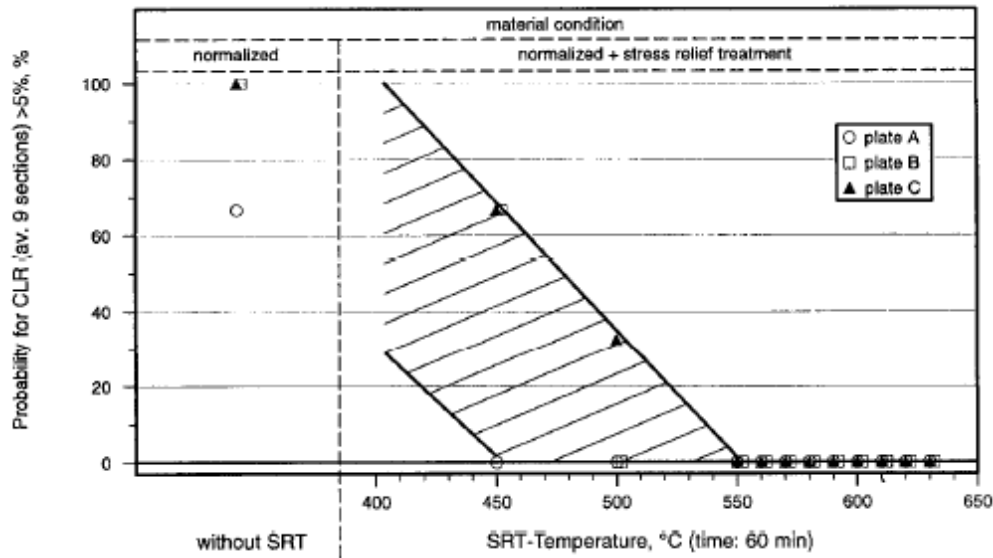


Figure 2.36: HIC resistance of A516-70 plate with Stress Relief Heat Treatment.

Experimental results also show that heat-treated specimens have lower hydrogen trapping efficiency, but more susceptible to HIC[55].

Effect of Composition and Alloying Elements on HIC

Elements present in steel influences the microstructure which in turn influences the propagation of HIC, once it is initiated in the material. Elements beyond a limit, alone or in combination with other elements, affect HIC susceptibility by influencing the microstructure[35].

Effects of specific alloying elements on HIC are discussed below.

Carbon (C), Manganese (Mn) and Phosphorus (P)

Carbon and Manganese have high tendency to segregate and form hard bainitic or martensitic in solidifying steel [11][35]. Segregated areas in bainitic and martensitic microstructure is found to be susceptible to HIC propagation. Segregation ratio of manganese depends on carbon content. Phosphorus also has shown strong segregation capability during solidification which is influenced by carbon and manganese content in steel as shown in Figures 2.37 and 2.38.

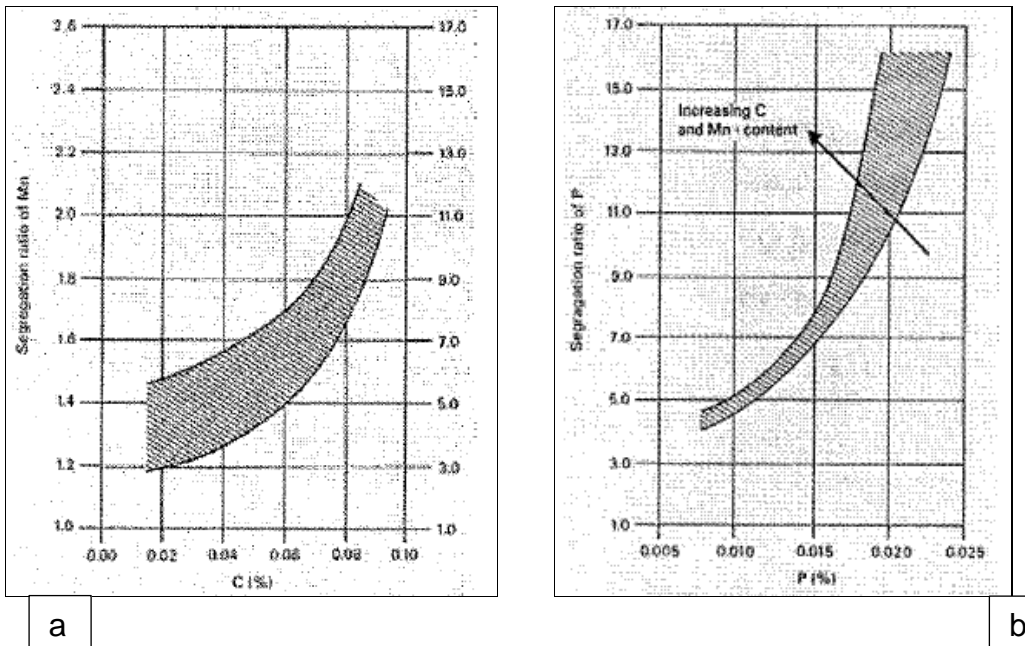


Figure 2.37: Fig a, b show occurrence of HIC and segregation of C, Mn and P in steel[1].

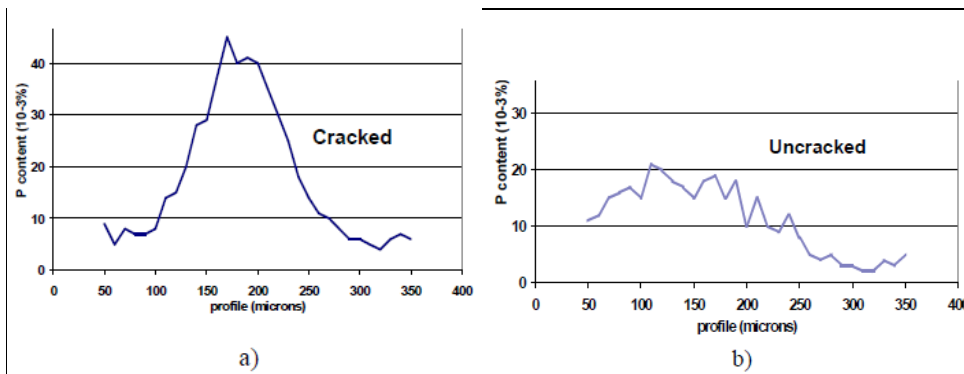


Figure 2.38: HIC test specimen's microprobe curves of P segregation (a) cracked segregation and (b) uncracked segregation.[1]

Figure 2.38 reveals that HIC is predominant in phosphorus segregated area rather than where phosphorus has not segregated. Effect of phosphorous content on HIC susceptibility of low sulfur normalized steel plates is shown in Figure 2.39. Phosphorus content should be below 0.008% for effective resistance to HIC in steel[35].

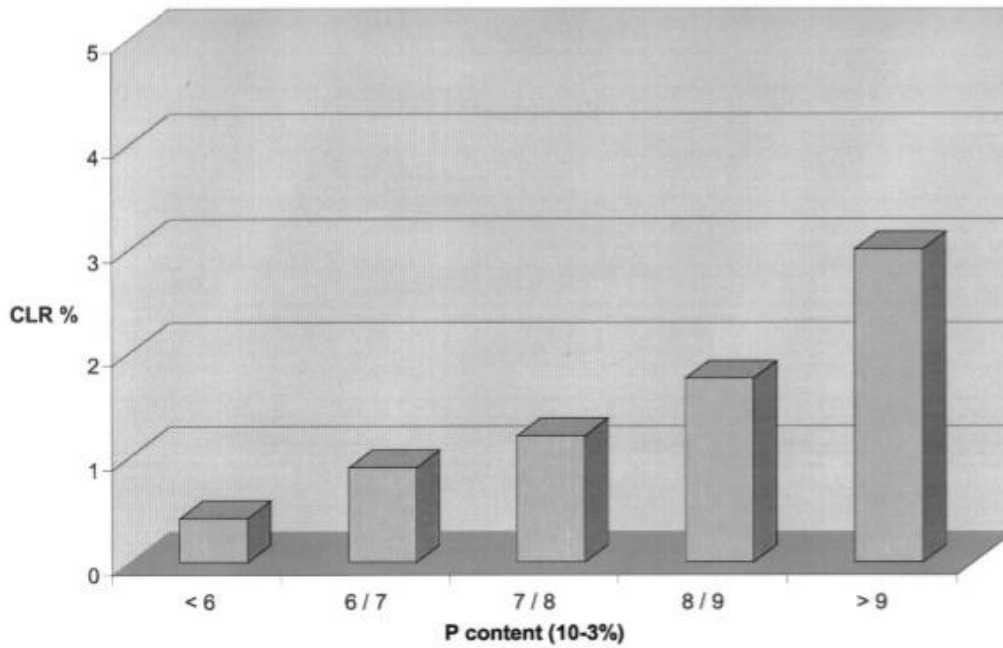


Figure 2.39: Effect of phosphorus content on HIC susceptibility [78]

Sulfur (S)

Effect of sulfur on susceptibility of steel to HIC is well known. Studies have found that carbon-manganese steels having elongated MnS inclusions are highly susceptible to HIC. Shape, size and number of inclusions are important parameters which influence HIC susceptibility [11]. Figure 2.40 shows that among various treatment of steels, Quenched and Tempered steel is more resistant to HIC.

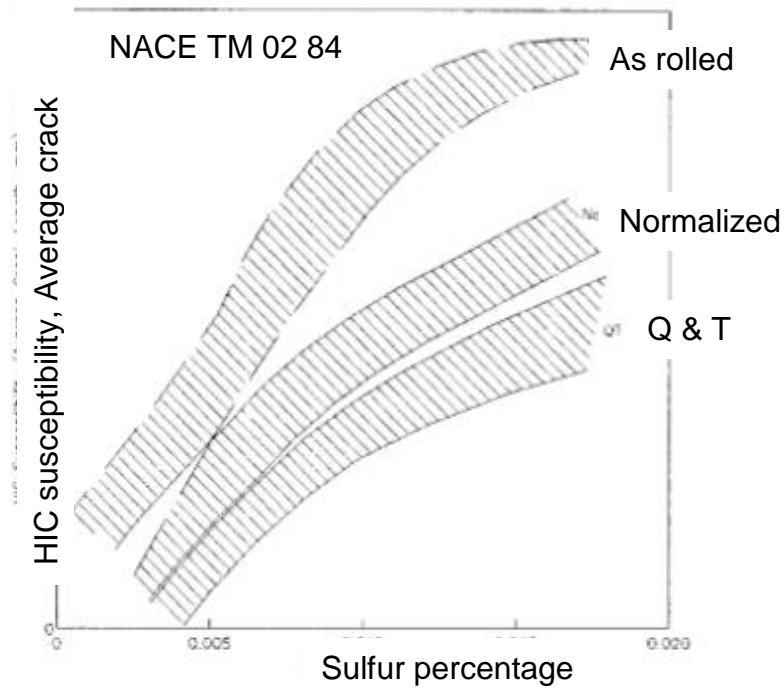


Figure 2.40: HIC susceptibility and S content for different heat treated steels [11].

Globular inclusions are resistant to deformation due to shape isotropy and reduces HIC occurrences. Calcium treatment is carried out in steel manufacturing to control the shape of sulfide inclusions [35][79]. The benefit of calcium treatment as well as, correlation between sulfur content and HIC behavior of steel is shown in Figure 2.41.

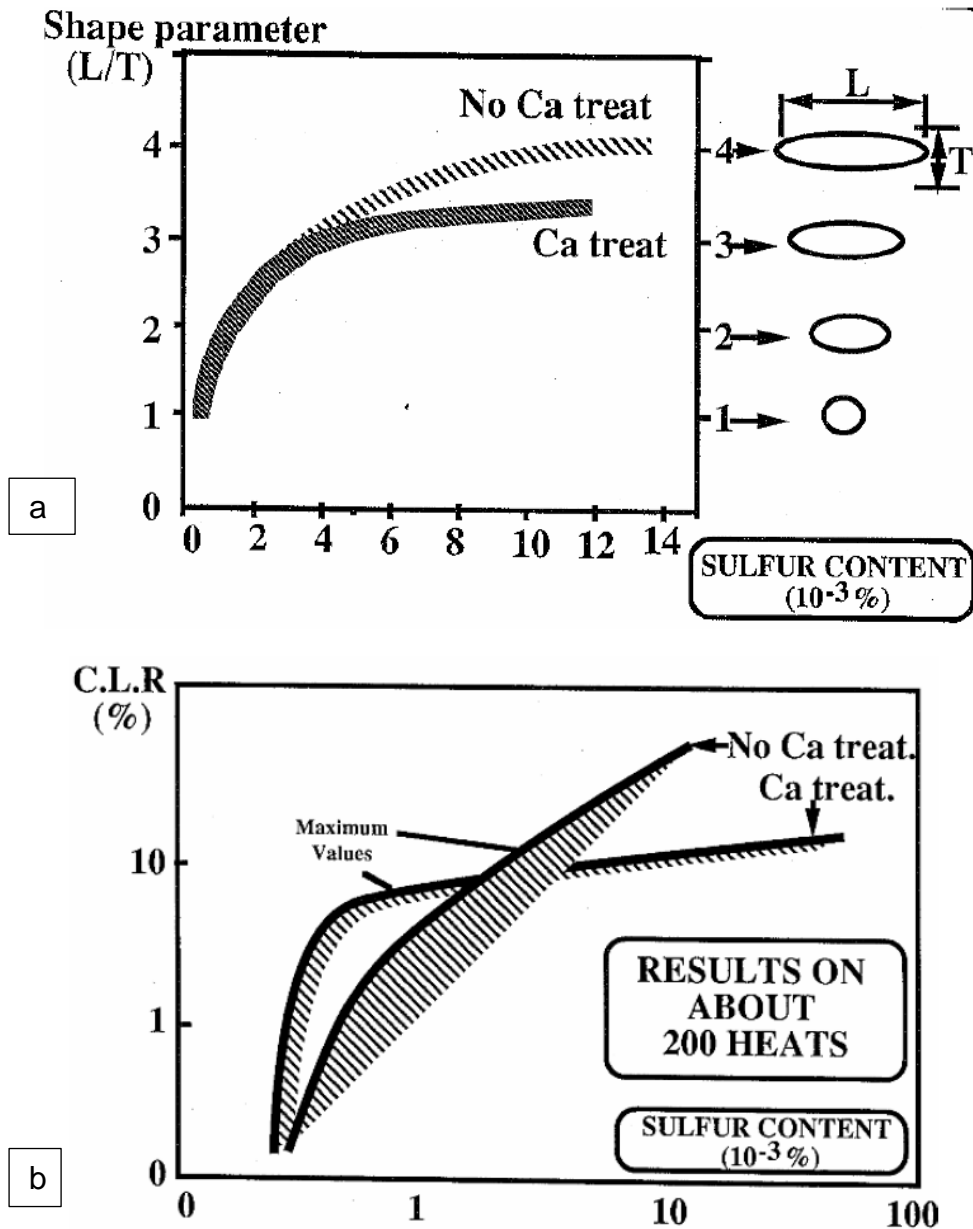


Figure 2.41:(a) Change of shape parameter of inclusions with calcium treatment and (b) HIC susceptibility of calcium treated and untreated steels [35].

It is found for X65 steels that reducing the sulfur content is not enough to control HIC susceptibility as shown in Figure 2.42. The CLR (crack length ratio in HIC test) is independent of sulfur content. Indeed, level of sulfur has an influence on sensitivity for HIC, but even for very low sulfur content, very high CLR is found which means that high sensitivity to HIC is possible with low sulfur content. Therefore, low sulfur content is a necessary condition but not a sufficient condition for good HIC resistance[80].

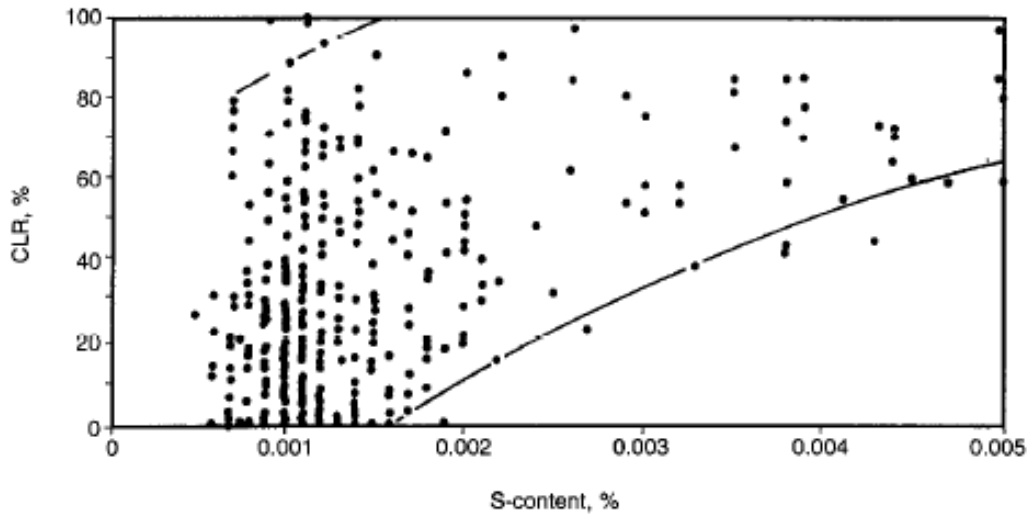


Figure 2.42: Relative independence of S content versus HIC resistance for X65 steel samples coming from different production routes[4].

Calcium treatment of steels is effective for sulfur content greater than 0.002% but ineffective for sulfur content below 0.001% as sulfide inclusions are considerably less. Calcium treatment for very low sulfur steels may cause harm by producing calcium oxide inclusions which may induce cracking in steels [11][35].

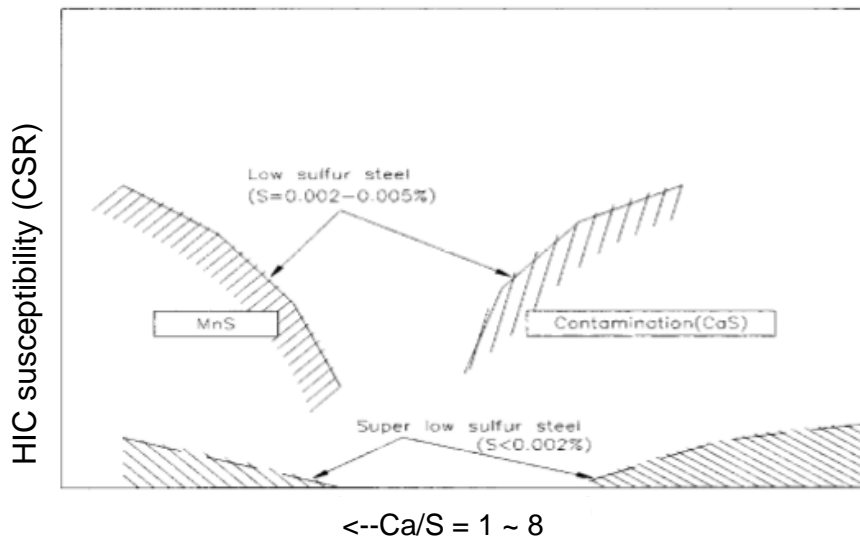


Figure 2.43: Influence of under/over calcium treatment on HIC susceptibility [11].

Similar results were obtained for API 5L and ASTM A 516 grades of steels having sulfur content less than 0.001% as shown in Figure 2.44. This study

reveals that Ca/S ratio is important for sulfur content $> 0.001\%$. The Ca/S ratio is irrelevant for sulfur content below 0.001% [80].

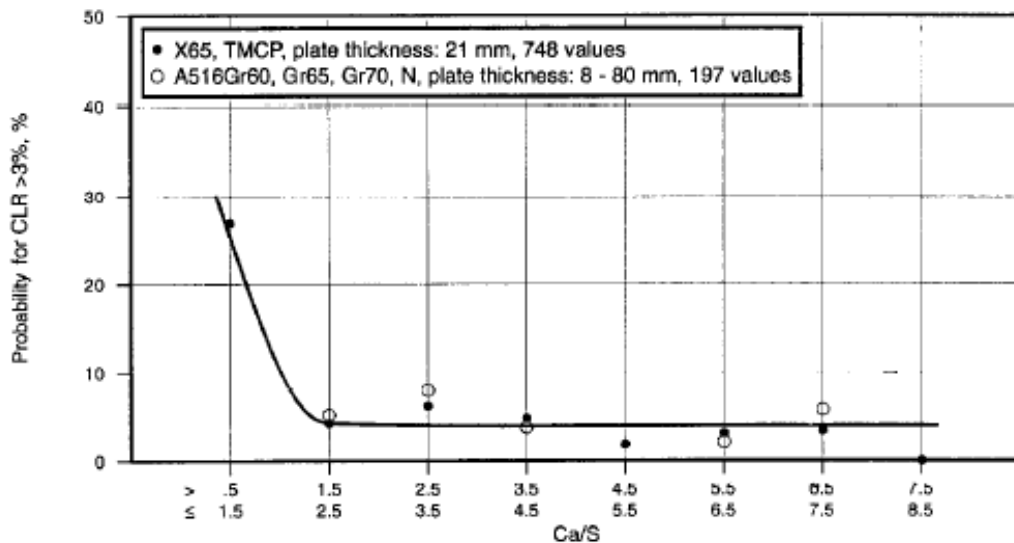


Figure 2.44: Influence of C/S ratio on CLR for plates with sulfur content $\leq 0.001\%$.

It is evident that a minimum level of Ca/S > 1.5 is desirable. Results with API and ASTM grades of steels are in good agreement to this fact, as there is no change in CLR for Ca/S ratio > 1.5 and ≤ 8.5 for $S \leq 0.001\%$.

Copper (Cu)

Addition of copper (Cu) is beneficial to minimize H charging and HIC. A study was conducted to evaluate the effect of Cu addition on diffusible hydrogen and corrosion rate of API 5LX65 steel. Steel samples with Cu (0.28%) and Cu free (Cu-F) were tested in H_2S wet environment of pH 5.3 and at H_2S partial pressure 0.1 MPa. Hydrogen permeability, diffusible hydrogen and corrosion rate decrease with addition of copper as shown in Figure 2.45 [81][26].

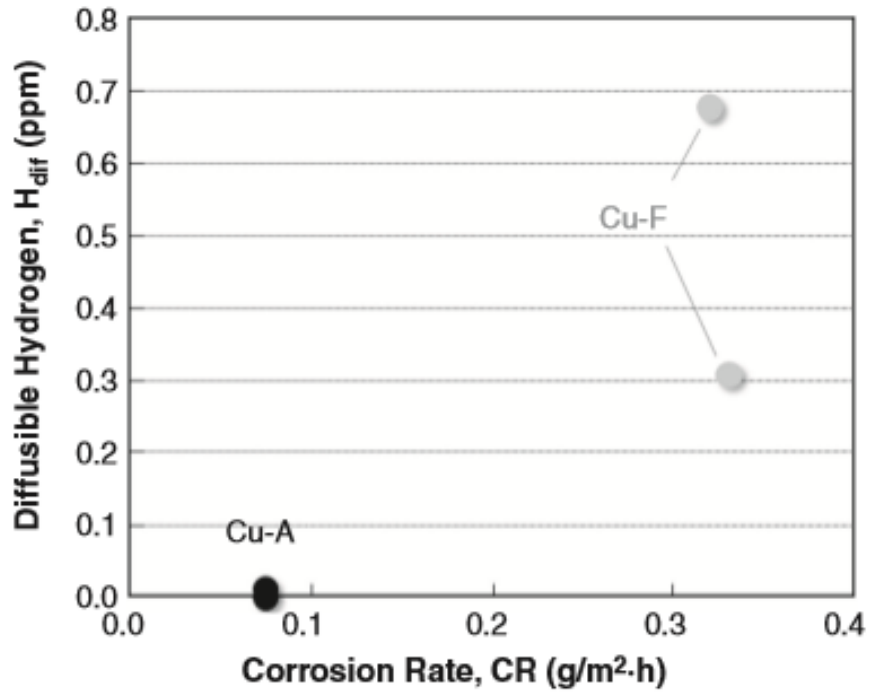


Figure 2.45: Effect of Cu content on H_{dif} and Corrosion rate of API 5LX65 steel.

Study shows that Cu tends to locally enrich the inner layer of corrosion product (within 100nm from the steel surface) as shown in Figure 2.46. There is a possibility that a complex sulfide viz. (Fe, Cu) S i.e. a dense iron sulfide or copper sulfide may form inner layer that has a protective effect against corrosion and H entry [82].

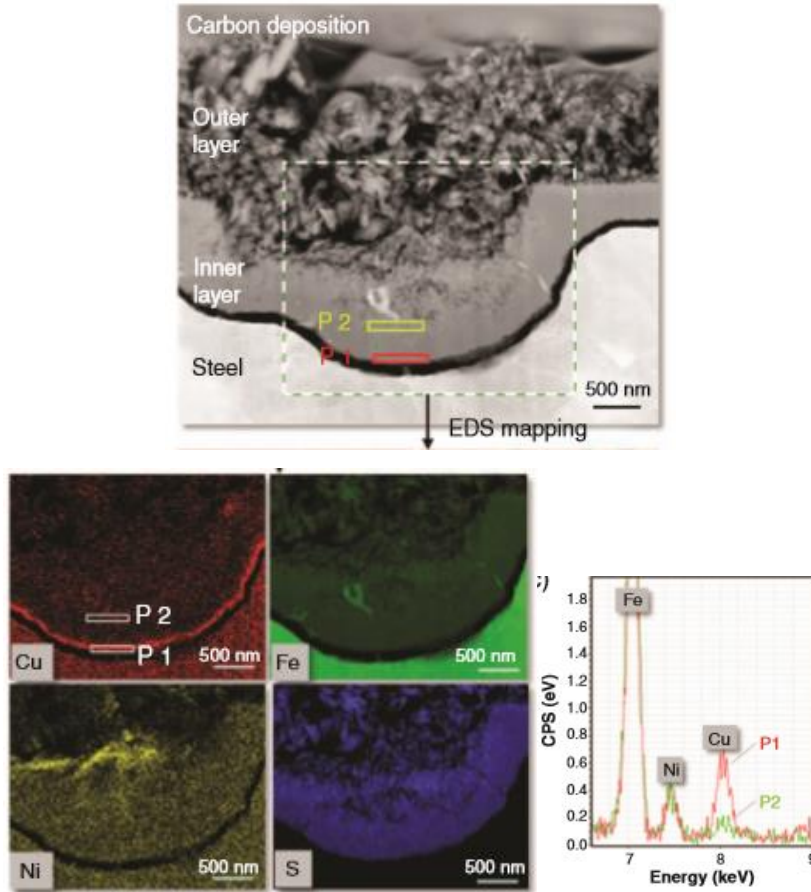


Figure 2.46.: STEM image and EDS mapping showing Cu, Ni, Fe and S in scale deposited on steel.

Sequence and mechanism of formation of different layers of scale deposited on copper containing steel which prevents hydrogen entry in sour environment is shown in Figure 2.47.

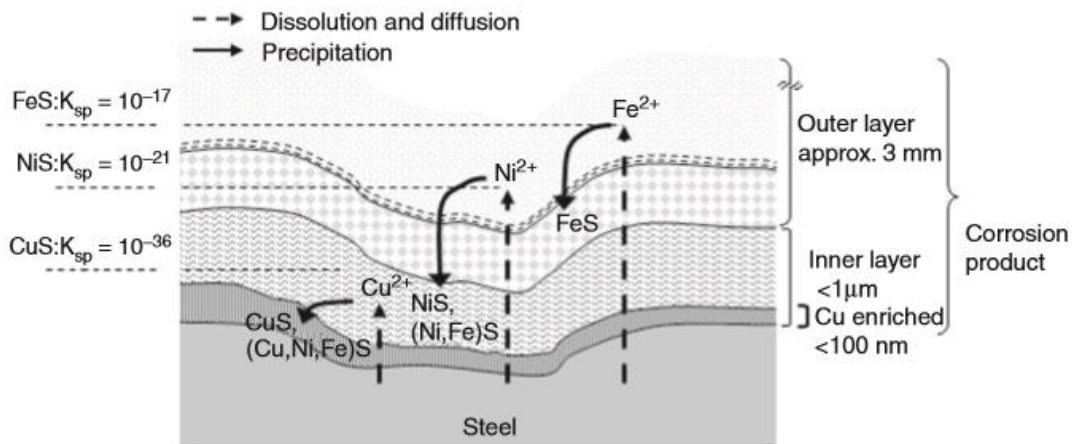


Figure 2.47: Schematic illustration of mechanism of formation of protective layers

It is seen that various kinds of iron sulfides are formed including Mackinawite, but dominance of CuS could not be established. Therefore, the question arises 'How Cu works as a protection for hydrogen entry in steel?'

The EDS mapping and spectra indicates that the dominating inside layers are made of Fe and S enriched with Cu. Possibly, due to low Cu content, it cannot form as a dominant/continuous layer of CuS, however, it can induce protection by two possible mechanisms; it forms complex sulfide scale such as (Fe, Cu)S which works as a barrier against hydrogen entry as it has very fine crystal structure and dense morphology. Other possibility is that it triggers precipitation of other sulfides such as FeS, which is a well recognized effect of co-precipitation (CPT). Due to more FeS precipitates near the steel surface, the inner layer of corrosion product becomes dense and can play an important role as barrier against corrosion and hydrogen entry. Ni possibly forms a eutectic without mutual solubility, as the interface is not enriched with Ni.

In BP solution, protective black surface film identified as mackinawite (FeS_{1-x}) containing Cu is developed on steel with $\text{Cu} > 0.2\%$. EPMA line scanning as shown in Figure 2.48 confirmed outer part of corrosion product to be as gamma Fe_2O_3 enriched with Cu and inner part containing FeS with high level of Sulfur, and some parts missing Cu, which may suggest random enrichment of film with Cu [26]. Results of Inagaki et al and Smith et al are contradictory, as both have reported the formation of FeS film enriched with copper.

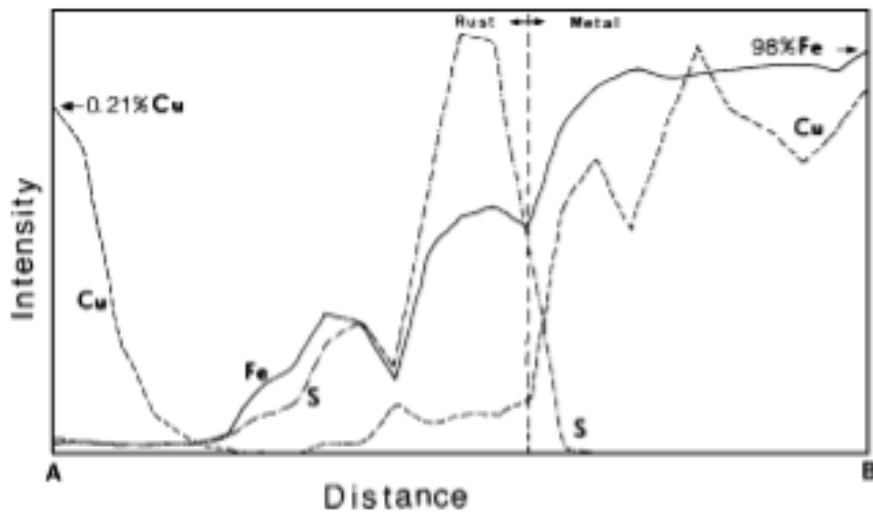
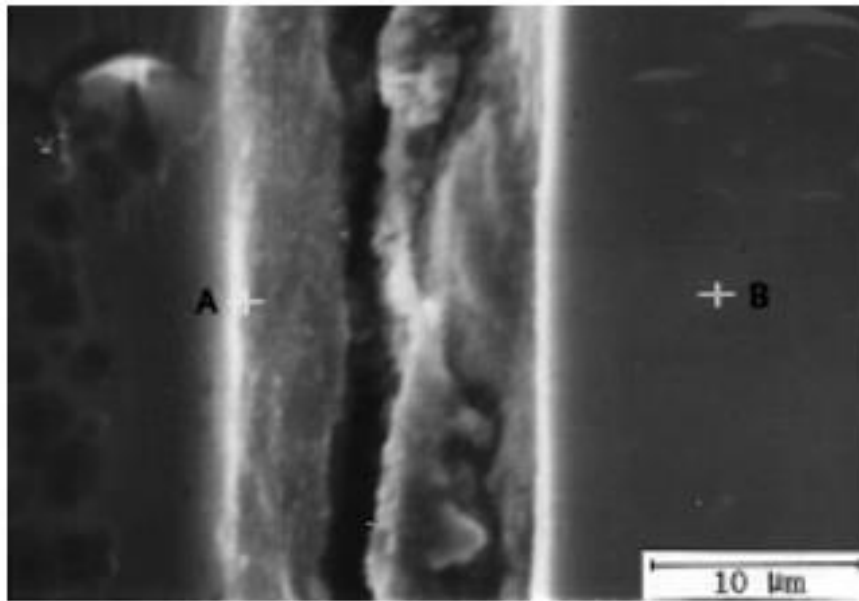


Figure 2.48: (Top) Black film formed on copper (>02%) bearing steels (Bottom) EPMA Line Analysis of the protective layer.

Similar effect of copper (> 0.2%) in reducing HIC in Nb bearing steel are also reported by researchers as shown in Figure 2.49.

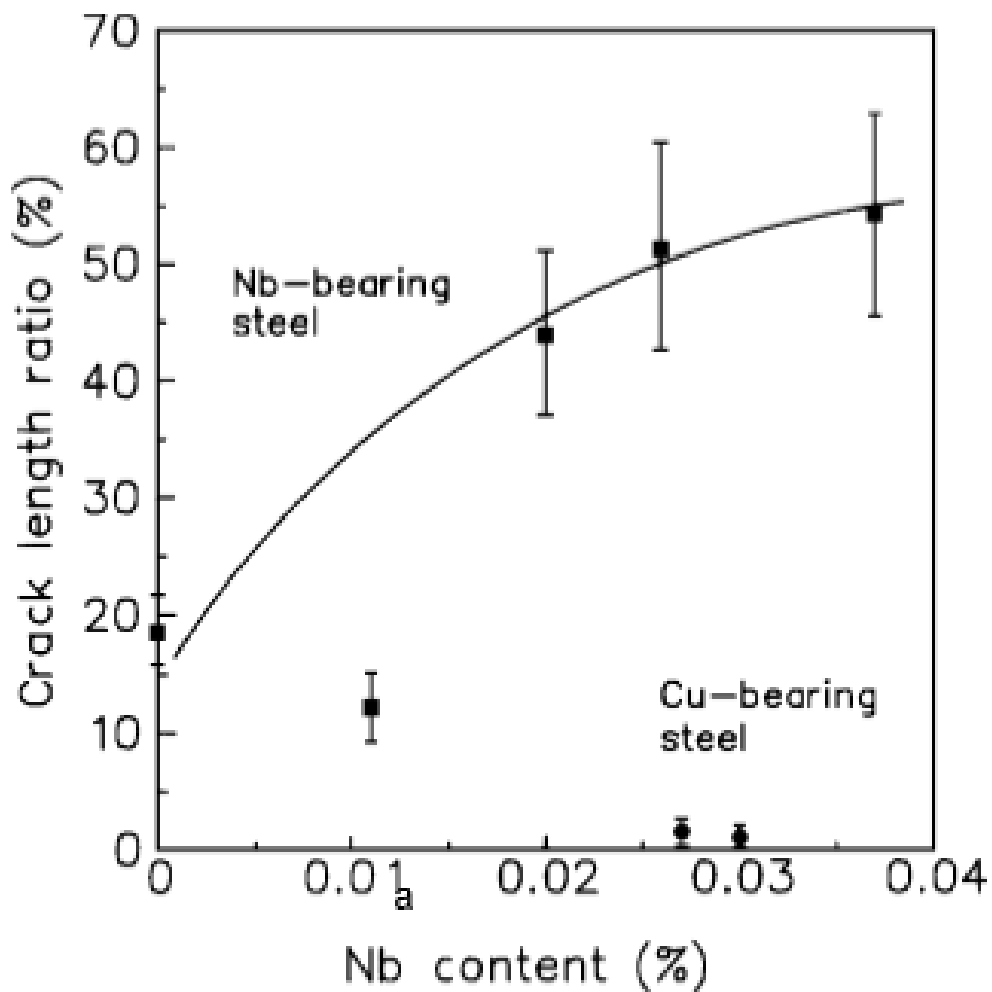


Figure 2.49: Effect of Cu addition on HIC in Nb containing steel [26].

Chromium (Cr), Molybdenum (Mo)

Cu, Cr and Mo are added for their corrosion resistance properties. Although the effect of these elements on HIC has been reported, but conclusions have not been consistent [26].

It is reported that Cr addition suppresses HIC and Mo addition impairs H absorption resistance. However, interaction between Cr and Mo is complex. Cr and Mo addition have considerable effect on microstructure. These elements (like Al, Si, V and W) can increase A_3 and decrease B_s and M_s temperatures thereby delay the transformation of ferrite and pearlite. This increases hardenability and promotes low temperature transformation products

(martensite/austenite constituent) in the steel. Increase in the Cr content leads to change of microstructure from ferrite-pearlite-small bainite to ferrite and bainite structure.

Parrini and DeVito have found that 0.3% Cr is most beneficial to HIC resistance in BP solution. Lino et al indicated that 0.6% Cr has the effect of lowering H absorption on steel surface in HIC testing, but addition of 0.4% Mo has contrary effect.

The relative effect of Cr and Mo is often analyzed with the help of International Institute of Welding's (IIW) Carbon Equivalent formula (CEQ) and Ito-Bessyo formula (Pcm) when added in combination of several other elements. In IIW, the parameters are applied as Cr/5 and Mo/5 whereas in case of Pcm, these are indicated as Cr/20 and Mo/15

As a combination, Cr and Mo values have synergistic effect on the properties of the material however, Mo has more pronounced effect on generating M/A-C in steel.

Hydrogen permeation and HIC full-scale tests on pipeline were conducted by HIC subcommittee of Iron and Steel Institute of Japan. The above subcommittee conducted full-scale tests on several pipelines (x42 – x65) of various compositions in various sour conditions. Alloy additions are found to reduce peak value and increasing decay rate [83].

Niobium (Nb)

Nb imparts the precipitation hardening and grain refinement effect. Addition of Nb has been found to decrease HIC resistance in steels. The mechanism may be explained as addition of Nb can retard the recrystallization of austenite and increase the nucleation sites and nucleation rates during ferrite transformation. This results in decrease of ferrite grain size but increases the deformation resistance of gamma (γ) phase at high temperature. However, deformation of

inclusions (MnS) during rolling is controlled by the relative strength between gamma phase and inclusions. The higher the deformation resistance of gamma phase, the more the inclusions are elongated. Figure 2.50 shows the increase in aspect ratio of inclusions with increase of Nb.

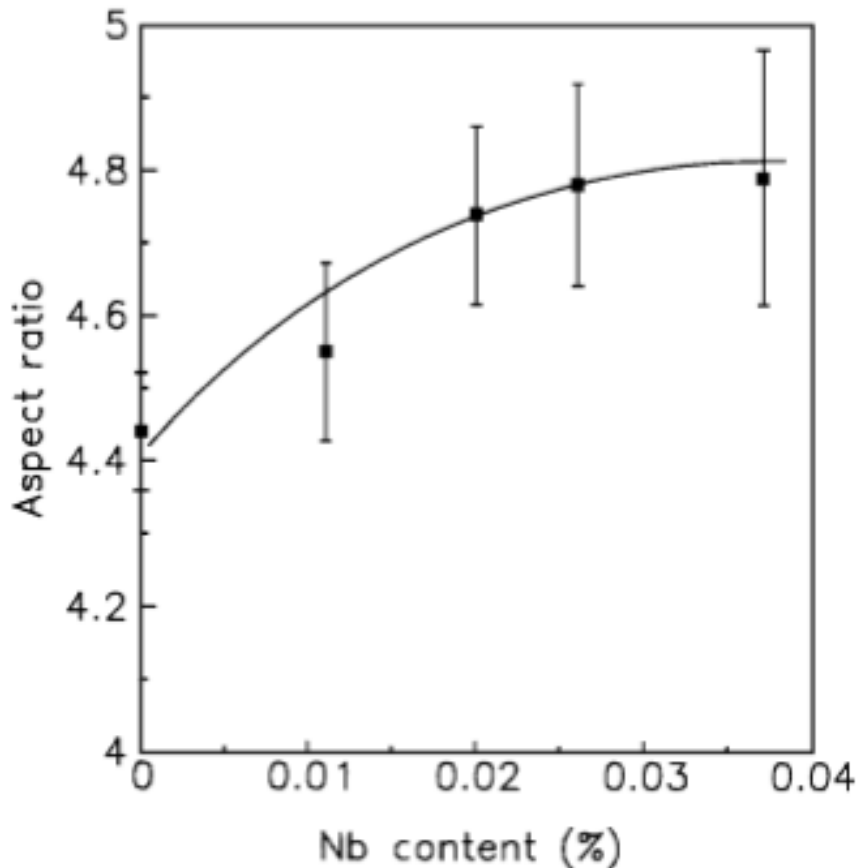


Figure 2.50: Variation of inclusion's aspect ratio with Nb content in steel

It is observed that HIC initiates mainly from the tips of elongated MnS inclusions. Nb increases the aspect ratio of the inclusions but large Nb(C, N) could not be found in testing with Nb < 0.037% [26]. Massive Nb carbonitride precipitates can act as initiation sites, but combined action of Nb and Boron increases HIC resistance.

Titanium (Ti)

Ti has primarily the grain refinement effect. The effect of Ti addition on HIC varies with the size of TiN and Ti(C, N) particles. HIC cracks are found to initiate at interface between rhombic TiN inclusion and the matrix as shown in Figure 2.51. Crack also penetrates through the inclusion. Some researchers have reported that Ti has a faint tendency to cohere with MnS and to form globular TiS inclusions. Study also found that TiN and MnS exist together and the combined inclusions cooperates to result in HIC [26]. Influence of Ti on hydrogen trapping efficiency is found to depend on microstructure [84].

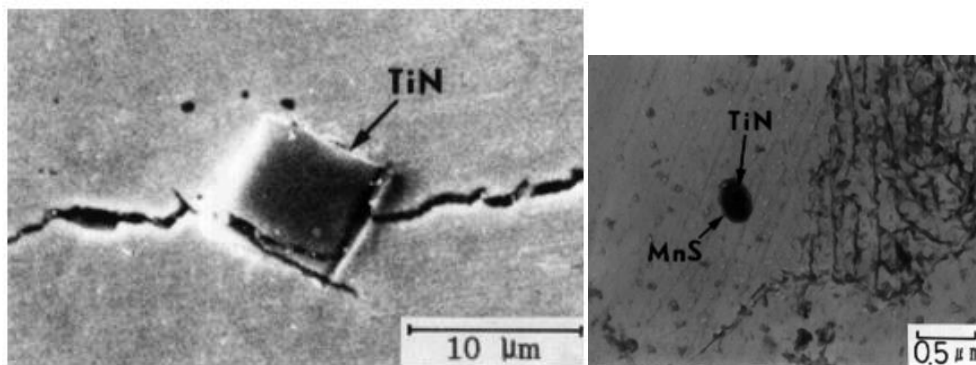


Figure 2.51: HIC initiation at interface between rhombic TiN inclusion and the matrix. The TEM micrograph showing the morphology TiN and MnS.

Wilde et al reported that major initiation site for HIC is elongated Type-II MnS inclusion. In addition, glassy silicate or massive Nb(C, N) precipitates act as initiation sites. However, Ti or other inclusions are not mentioned. Shimogoro et al found that fine and dispersed Ti(C, N) < 0.1 micrometer diameter decreases the H diffusion constant and thus, increases HIC resistance.

Shimizu et al found that fine and dispersed Ti(C, N) suppressed H segregation at the inclusion-matrix interfaces thereby decreases HIC. On the other hand, coarse Ti(C, N) and TiN precipitates are reported to act as HIC initiation sites.

HIC: Testing – Evaluation - Acceptance

NACE STD TM0284 was developed to evaluate the resistance of pipeline and plate steels to HIC and to provide a reliable test method for comparison of test data from different laboratories. The std. was developed by task group T-1F-20 in 1984 and revised in 1996 [35][30]. The following discusses background & theories, proper usage & some limitations of the standard and acceptance criteria used in the industry[56][85] [72][39].

- Two separate specimen removal criteria for pipes and plates.
- For pipes, set of three full thickness specimens are removed around the pipe diameter, removal location varies depending on manufacturing process.
- For steel plates, number & location of specimens depend on the thickness of the plate.
- Std HIC specimen is 100mmx20mmxthk, surface finish shall be 320 grit with all mill scale removed,
- 100% H₂S saturation test is for 96 hrs using solution A or B. Soln B is synthetic sea water,
- Blistering on wide surface may occur, but std does not have any provision for evaluation of this.
- Each of the three specimens to be sectioned in 4 sections and 3 internal surfaces to be polished, therefore, a total 9 surfaces are evaluated in each test upto x100.
- No guidance on metallography provided here, but ASTM E3 can be followed [30].
- Evaluation upto X100, light etching to distinguish cracks from inclusions, CSR/CTR/CLR are measured/evaluated.
- CSR characterizes cracked area wrt over all surface, CLR does sum of all crack lengths wrt over all width of the section, CTR does for sum of all crack widths wrt over all thk of the section. No pass fail criteria included in std.
- sampling frequency if not given by customer, one per heat of the thinnest plate is generally done,

- number of test specimens depends on plate thickness with a min of 3.
- the samples shall be cut from one plate's end at the middle of the width,
- if plate thk < 30mm, specimen thk = t-2mm, no. of specimens=3,
- if plate thk 30mm-88mm, specimen thk = 30mm, no. of specimens=3,
- if plate thk 88-146mm, specimen thk = 30mm, no. of specimens=5,
- if plate thk 146-204mm, specimen thk = 30mm, no. of specimens=7
- (30mm thk specimens shall cover the whole thickness of plate with a min overlap of 1mm),

Recently, several significant modifications have been made or proposed for the test procedure of this standard. Amongst others, these modifications affect the test solution chemistry, pH limitations and solution volume to specimen surface area ratio. Frequently, the acidified acetate buffer test solutions, as proposed in the EFC 16 recommendations and initially intended for use in sulfide stress cracking (SSC) tests, have been adopted for HIC testing. A frequent difficulty associated with the EFC 16 test solution A (pH 3.5) is the requirement of pH drift limitation within 0.1 pH units [11][39][50].

Industry Acceptance Limits

HIC free steels are probably impossible to manufacture, accordingly, different limits are mentioned in several standards / guidelines for different equipment [51-53]. Philosophically, acceptance shall have following criteria-

- Based on design requirement of the application,
- experience of user,
- data generated from past studies,
- understanding testing mechanism & relating results to intended application are important to set the acceptance criteria,

- Typical acceptance criteria as below, but acceptance criteria can significantly vary among users & applications

Four levels of quality of steel plates can be defined by the steelmakers [39][35][62]:

- HIC Level-1 will have CLR=5%, CTR=1.5% & CSR=0.5%,
- HIC Level-2 will have CLR=10%, CTR=3% & CSR=1%,
- HIC Level-3 will have CLR=15%, CTR=5% & CSR=1.5%,
- HIC Level-4 will have CLR>15%, NOT QUALIFIED FOR HIC.

HIC resistant= CLR<15%, CSR<3%, CTR<1.5%, in NACE solution A.

Discussion

Literature review indicates that studies have been carried out by researchers which cover several metallurgical aspects known to affect HIC susceptibility of steels. HIC is a complex and multivariable dependent phenomenon. Several important variables, including effect and sensitivity of the variables on HIC susceptibility were studied by researchers. Primarily, three factors predominantly influence HIC in steel i.e., microstructure, inclusions, and diffusion of hydrogen.

Some interesting, important, and sometimes contradictory observations mentioned in previous sections, are summarized below:

- Hydrogen Diffusion:
 - Diffusible H is one of the most important parameters to affect HIC as HIC is induced by absorption of Hydrogen in steel which can be evaluated subsequent to HIC testing [25].
 - Diffusible H content trapped reversibly in steel is more important than H flux permeating through steels because diffusible H (quantity) decides HIC sensitivity of steel. Accordingly, steels having similar inclusion levels will differ in HIC sensitivity based on difference of diffusible H content in steels [18].

- H permeation rate is affected by both H₂S partial pressure and pH of solution. Whereas, H diffusivity is mainly determined by pH value in case of low P_{H₂S} (< 0.1 atm.). It is found that HIC initiated mainly at Al and Ca oxide inclusions.
- Experiments with several grades of API 5L grades of steel show that level of diffusible H varies from 7.8 to 0.1 ml H / 100g steel in pH range of 1.1 to 5.9 [71][38].
- Each type of steels has a critical hydrogen concentration limit, beyond which precipitation occurs. Forced introduction of H causes lattice to expand inducing high stress, and the crack initiates at surface. Why severity of medium varies with P_{H₂S} can be explained depending on whether internal or surface H is the concern which is related to simultaneous charging and degassing of H in steel [86].
- Microstructure & Crack initiation in steels
 - No direct and convincing relationship could be found between primary microstructure and level of inclusions on diffusible H content in steel. Diffusible H measures the interstitial solubility of H in steel. H solubility in steel is closely related to reversible H trapping sites e.g. solute atoms or dislocations. Cold working reduces H diffusivity and increases H solubility in steel [25].
 - For a specific microstructure and associated defects, HIC initiates when a critical concentration of H locally exceeds due to hydrogen charging. Hydrogen charging varies with environmental factors e.g. partial pressure of H₂S and total pressure, pH of solution, solution composition, temperature, and time or duration of exposure. Metallurgical factors also affects H charging e.g. residual & applied stress, inclusion content, segregation, hardness variation etc. Critical H concentration for cracking depends on temperature, stress, local plasticity & stress concentration and defects in microstructure [35].
 - HIC apparently initiates at interfaces which are stronger than inclusions, such as pearlite colonies. High stress increases

solubility of H. Thus stress (residual) in the principal plane of rolling, may initiate cracks. In inhomogeneous materials, such as, welds, variations in strength can lead to development of in plane cracks.

- Microstructure - Homogeneity and cleanliness & composition of steels
 - Takahashi et al have shown by FE analysis that high through thickness stress can develop in the mid wall in a softened (HAZ) zone under transverse loading due to strain concentration. It was reported by Miyoshi et al that hydrogen cracking in a single crystal of pure iron occurs on a slip plane. Incidentally, Lino cited that cracking under SOHIC condition, where HIC is a component and part of cracking mechanism, decrease in sulfur level increases cracking in intense H charging condition. Dirty steels may accommodate more charged hydrogen and reduce cracking tendency where the steel gets rusted subsequently and H charging reduces. Cleaner steels suffer from other important microstructural factors to promote cracking. Several authors have shown that pearlite colonies can act as site for HIC, whereas, quenched & tempered heat treatment can significantly reduce cracking in TM0284 test on A516Gr-60 normalized steel. Some researchers found crack initiation (for SOHIC testing) resulting from micro phases e.g., martensite/austenite in HAZ, however, this has been contradicted by several other researchers who did not find any martensite at cracked zones and PWHT also did not reduce cracking tendency where martensite were present and the specimen cracked, some found crack initiation at pearlite region. Researchers found that nonmetallic inclusions, increases the trapping sites thereby increasing H solubility/diffusion in steels.
 - Carbide formers too play important roles (V, Mo, Nb, Ti, and Zr) and rolling through two phase regions would have more traps than rolled through austenite region only due to strain effect. Nb, above a certain size, may be more prone to contribute to cracking

or precipitation of Nb(CN) weakening grain boundaries, whereas, strengthening matrix, induce grain boundary cracking. In contrast, Kobayashi et al found that Nb free steels cracked more! [56].

- In case of large particles of carbonitrides in centerline zone in the slab, can cause HIC.
- Modern low S steels having microalloying elements, e.g. Ti, Nb are highly susceptible to segregation,
- Titanium micro alloying quantity should be less than stoichiometric ratio to nitrogen at minimum concentration of the latter for preventing formation of large particles of titanium nitride and reduce Nb micro alloying to prevent formation of large conglomerate of Nb (CN) or TiNb (CN) in centerline zone [62].
- Microstructural control to maximize bainitic structure by accelerated cooling for grain refinement for preventing centerline segregation in slab improved HIC resistance.
- Decrease in C, Mn, S, P and Ca treatment reduced inclusion content and segregation and banding ($S < 0.001\%$, $P < 0.006\%$,) in continuous casting of steels which improved HIC resistance.
- Heat Treatment
 - X80 steel showed that heat-treated specimens had lower trapping efficiency, but were more susceptible to HIC. Most of the HIC cracks initiated from the inclusions rich in Mn, Al, Ca, and Ti, and propagated trans granularly in the original and air cooled specimens, but mainly intergranular in water quenched specimens [25].
 - Less Si and Al with high finishing temperature improves HIC resistance of steels. Pipeline metallurgy transporting sour gas requires special consideration [62].
- Exposure condition
 - It has been found in MPC studies that short and very high hydrogen charging at initial stage when the steel is clean, can

result in more cracks than longer exposure less than peak charging level.

Following have shown improved HIC resistance in experiments by researchers-

- Manufacturing of slab by continuous casting with target microstructure i.e., fine grain mixture of massive ferrite and low carbon bainite without pearlite & bainite bands.
 - High temperature reheating to dissolve NbCN particles which precipitate during solidification mostly, at centerline zone.
 - Large deformation at first stage rolling to maximize austenite grain refinement by multiple recrystallizations. Finish rolling temperature 30-50 °C higher than Ar3 (gamma → alpha transformation start temp) to ensure ACC start temperature higher than Ar3 start temperature to avoid structural banding. Accelerated cooling (25 °C/s) favours the bainite formation.
 - Plates were stockpiled for retarded cooling for H removal.
- HIC testing in soln A, initial pH 3.30 & final 3.81 results in low HIC values as given below:
- $CLR \leq 3$, $CTR = 0.05$ and $CSR = 0$

Observation

Several important observations as discussed in previous sections are summarized below.

Presence of nonmetallic inclusions is considered as one of the dominant factors for HIC initiation. Area and volume fraction of inclusions, as well as, microstructure including M/A constituents, contributes to HIC cracking. Researcher also found inclusion free steel to suffer from HIC [25].

Studies found that hot rolled structure is most susceptible to HIC degradation. Normalizing-quenching and tempering has shown to reduce susceptibility particularly in low sulfur steels. Banded Ferrite Pearlite (BFP) is identified as one of the most susceptible microstructures in several studies [50]. Thermo-mechanically controlled processed (TMCP) steels with low sulfur content and low carbon equivalent has shown significant resistance to HIC cracking. The effect is considered as a result of reduction in ferrite/pearlite banding in steels[28] Research also found that there is no observed effect of microstructural banding on HIC for special clean steel (A516-60, S<0008%)[77].

Diffusible hydrogen content trapped reversibly in steel is considered more important than hydrogen flux permeating through steels. Steels having similar inclusion levels have different HIC sensitivity based on difference of diffusible hydrogen content in steel [38]. Reversible trapping is considered by many as most important factor in HIC susceptibility [49][14][72]. Diffusion of hydrogen in steel is affected by microstructure. Study shows that trapping efficiency for steel (X65) generally varies in the order as Acicular Ferrite (AF) > Bainite Ferrite (BF) > Degenerated Pearlite (DP), which is often considered as indicator of degree of cracking tendency of different microstructures in hydrogenated condition[43]. However, Mohtadi-Bonab et al concluded that higher amount of permeated hydrogen in steel is not a reliable measure for evaluation of HIC.

It was observed that bainite and tempered martensite have the highest susceptibility to HIC while acicular ferrite has the highest resistance against HIC [42]. Researcher (Carneiro et al) also found that refined and

homogeneously quenched and tempered bainite/martensite microstructure has the best performance against HIC and SSCC[55].

Investigation of acicular ferrite with micro cantilever structure demonstrated that mechanisms and resistance to HIC at micro-scale could be significantly different at macro-scale. It is found that effect of hydrogen on combination of different microstructures for the cracking nature of HIC/SSC has not been clearly explained in literature[87][68].

Inclusions and precipitates play important role in HIC in steel. Hydrogen diffusion in steel is dependent on the size, number and binding energy of trapping sites with hydrogen. Micro-alloying elements e.g., Cu, Ni, Mo and Ti are often added to low alloy steels to achieve required mechanical and corrosion properties of the material[88].

Researchers have found different inclusions to be responsible for crack initiation in presence of hydrogen. Traditionally, MnS is considered as the prime inclusion for initiating HIC in steels (without any shape control)[27][89][56]. Several types of inclusions were characterized e.g., MnS, Al, Si, and Ca-Al-O-S enriched inclusions and complex carbonitride particles (Ti, Nb, V)(C,N) in pipeline and pressure vessel steels[27][18]. TiC can be coherent, semi coherent or incoherent precipitate trap depending on the binding energy of the precipitate. However, some researchers consider TiC, NbC, VC and complex Ti,Nb(C,N), $Ti_4C_2S_2$ etc. as irreversible trap sites only [69][43]. Several researchers have contradictory considerations for MnS, i.e. strong irreversible, as well as, reversible trapping sites for hydrogen. It is also reported that trapping efficiency increases with sulfur content [49].

Guenter Herbsleb et al observed that cracks (HIC) in pipeline steels originates from MnS, as well as, Oxide inclusions, and concludes that, apparently composition of inclusions is not the decisive factor for originating HIC, rather, the shape and size of inclusions are responsible for initiation of cracks[90].

Calcium (Ca) treatment for shape control of MnS inclusions and Ti micro alloying less than stoichiometric ratio to nitrogen at minimum concentration of nitrogen for preventing large particles of TiN in centerline of slab, reduced Nb micro alloying to prevent large conglomerates of Nb(CN) or TiNb(CN) in centerline are imperative to resist HIC [62]. Fine M(C, N) (M: Nb or Ti) carbides (<100nm) can pin dislocations and decrease mobility thereby improving HIC resistance. Fine precipitates can belong to non-saturated hydrogen traps which can partake the hydrogen pressure [53]. It is postulated that in micro alloyed steels, Nano sized carbonitrides behave as innocuous hydrogen traps which help in hydrogen redistribution in numerous sites (provides optimal cracking resistance). Composition of inclusions have great effect on initiation of HIC [91]. It is suggested that further investigation is warranted on hydrogen trapping and characteristics of various precipitates, such as (Ti, Nb) (C,N) are more complex than binary carbides. Recent studies also suggested that Mo also affects micro-alloy precipitates' nucleation and growth process which may have implications on ferrite-precipitate interfacial energies and thus interaction of H with the interface[69].

It is also found that there is no difference in dislocation structure in crack sensitive and insensitive regions (welded samples) but crack sensitive region consistently contains relatively high concentration of 100-200 μ m diameter Nb rich precipitates. High concentration of <50 μ m or few more than 500 μ m precipitates did not apparently affect sensitivity[87].

It was observed by Escobar et al that there is no direct relationship between diffusible hydrogen content and primary microstructure, even internal inclusions do not affect the diffusible hydrogen content when compared with different heats of steels[92]. No direct relationship is found between primary microstructure and level of inclusions on diffusible hydrogen content in steel [91].

It was postulated that grain boundaries can have opposite effects i.e. either increase the diffusion of hydrogen by providing faster paths or reduce mobility

by acting as reversible hydrogen trapping sites at nodes and junction points [49][43] [61]. Correlation between hardness and HIC susceptibility was recognized. Role of reversible hydrogen trapping sites on HIC susceptibility and crack growth is found to be very important[42][93].

Various modifications of steel making processes such as addition of micro alloying elements to create non-detrimental trap sites, control of sulfur-carbon-nitrogen, control of morphology of inclusions and the level of residual stresses have been tried to improve microstructure and associated HIC performance, but it is felt that more innovative research is required to further reduce the level of occurrences of HIC in application.

Conclusion

Control of nonmetallic inclusions and uniformity of microstructure are considered as basic requirements for HIC resistance of steels. Accordingly, various modifications in steel making processes have been carried out to create no detrimental trap sites by following measures-

- Addition of micro alloying elements and control of sulfur –carbon-nitrogen content,
- Modifying morphology of inclusions by calcium treatment
- Preventing large particles of Ti-Nitride by micro alloying titanium less than stoichiometric ratio to nitrogen at minimum concentration of nitrogen, coupled with reduced Nb micro alloying to prevent large conglomerates of Nb (CN)/TiNb (CN).

Contrary to prevailing understanding, several studies have reported that HIC did occur beyond perceived limits of variables keeping focus on level of inclusions, as well as, level of hydrogen in steels. Therefore, further research is required to reveal the complex relationship and synergy among variables which lead to HIC occurrences in steels.

Chapter-3: Experimental Work

3.1 Preface

Hydrogen Induced Cracking, commonly known as HIC, is a well-known cracking problem of flat rolled steel products in sour service application in oil & gas industry. For over more than five decades there has been continual need for improvement in material technology to resist hydrogen related cracking in petroleum industry. Industry experience indicates that as much as 25% of failures of equipment in petroleum refining industry are related to hydrogen damage.

Typically, Hydrogen Induced cracking or HIC is caused by trapped hydrogen atoms at defect locations. The role of stress differs in different hydrogen assisted cracking mechanisms e.g., in Sulfide Stress Cracking (SSC) and Stress Oriented Hydrogen Induced Cracking (SOHIC) where additional stress is considered as necessary to initiate cracking, whereas, in case of HIC, external load is not considered as a prerequisite, rather, internal stress generated by the hydrogen molecules accumulated in defect locations inside the metal thickness, finally causes cracking.

Several studies have revealed important parameters which influence HIC in steels. Studies largely focused on microstructural parameters of specific steels, however effect of environmental parameters on different strength grades have not be properly studied. The current research focused on HIC in wide range of acidic conditions which is prevalent specifically in petroleum exploration industry with different strength grades of steels which are also commonly used in manufacturing of equipment in petroleum industry. The objectives of the research were following-

- To identify initiation of HIC in steel (flat rolled) with respect to three important variables-
 - strength grade,
 - exposure duration and

- pH of environment.
- To understand the mechanism of HIC initiation and to establish correlation among the variables to represent their combined effect on HIC.
- To develop sets of operating conditions / material selection to avoid HIC in rolled steels.

3.2 Introduction

Among several types of cracking of steels in sour service, HIC is one of the common types of cracking encountered in the oil & gas industry. Flat rolled products, i.e., plates used in manufacturing of pressure vessels and pipes/pipelines etc. are commonly affected by HIC. Several metallurgical and environmental variables, viz., metallurgical composition, manufacturing process, thickness of the products, pH of solution, hydrogen sulfide (H₂S) content etc. are known to affect cracking of steel products in presence of aqueous H₂S in oil & gas exploration environment.

Hydrogen (H) generates as a result of corrosion reaction on steel surface in aqueous environment, or as a result of cathodic reaction in cathodic protection (CP) or as a process gas (downstream high temperature hydro-processing reactors or reactor effluent air coolers). Hydrogen diffuse in the steel, and can have damaging effect on properties of the material and result in cracking. Hydrogen degradation of equipment made of carbon steel and low alloy steel (LAS) in up-stream exploration condition, typically encompass acidic aqueous environment where Hydrogen generating from corrosion reaction causes degradation & cracking of steel which manifests in the form of Hydrogen Induced Cracking (HIC), Sulfide Stress Cracking (SSC) or Stress Oriented Hydrogen Induced Cracking (SOHIC). In all such cracking mechanisms, the initiation of crack is specific to the mechanism, but propagation essentially encompass degradation of mechanical properties of materials by hydrogen, e.g,

SSC initiates at high hardness location, whereas HIC initiates at inclusions, but after initiation propagation of the crack is essentially guided by behavior of the hydrogen charged material ahead of the crack tip and associated stress around it.

Degradation of mechanical properties of materials due to presence of H is termed as Hydrogen embrittlement. Therefore, essentially all the cracking mechanisms occur as a result of hydrogen embrittlement although origin of the cracks may be at different locations, some at surface of the material and some are at internal thickness of the material, e.g., SSC is surface mechanism, whereas HIC is an internal cracking mechanism resulting in presence of Hydrogen.

International standards, e.g., NACE MR 0175/ISO 15156, EFC-16 etc. addressed the problem of cracking in flat rolled steel products and provided metallurgical limits for acceptance for use in sour service. The possible mechanisms, and effect of metallurgical & environmental factors are briefly discussed here.

An extensive literature survey has been conducted prior to deciding the research methodology. List of references are attached in 'Reference' section for information. HIC generally initiates in the inner part of steel and propagates parallel to rolling direction. HIC can form straight cracks or step-wise cracks. The difference is caused by plastic deformation and shear stress distribution. However, blistering is created because of stepwise cracking beneath the surface.

3.3 HIC Experiment: Approach

NACE standard TM 0284 provides quantitative approach to characterize internal HIC of metals. Standard HIC specimens are 100mm long and 20mm wide, thickness varies with product thickness up to maximum 30mm for a

specimen, surface finish shall be 320 grit with all mill scale removed. For the current study, test solutions were prepared to comply to specific requirement of the study and test durations were also selected with specific focus to the objective of the study. Tests were designed to be carried out in three pH conditions between pH 1 and 4.5. Three test durations were selected as 44Hrs, 96Hrs and 144 hrs, for each pH condition.

Materials for Testing

API 5L X65 flat rolled pipeline steel and a pipe bend (fitting) conforming to ASTM A234 Gr WPB[94] were sourced for the HIC study. The specification, sizes and identification for the study of the source materials are mentioned in table-3.1.

Table-3.1: Material designation and sizes of two source materials for the research

ID	MATERIAL TYPE & SIZE	PRODUCT	SPECIFICATION & GRADE
A	42" dia. X 12.37mm CAP	CAP	ASTM A 234 WPB
D	30" X 9.55mm ELBOW	ELBOW	SA 234 WPB
E	36" X 19.05mm PIPE	PIPE	API 5L GR 60 SAW*

*Submerged arc Welded pipe (SAW)

Following picture shows initial material sections, from pipe/fittings before specimen preparation.



Figure 3.1: Sections cut from respective product as starting material for specimen preparation.



Figure 3.2: Photograph showing sample specimens prepared for testing.

Chemical Composition

Chemical analysis was carried out using 'HILGER Analytical Polyvac 2000' Optical Emission Spectrometer. Chemical composition and specifications are mentioned in table-3.2.

Table-3.2 : Chemical composition of source material samples.

Chemical Analysis Report			
MATERIAL	SAMPLE- A	MATERIAL-D	MATERIA- E
PRODUCT	CAP	BEND	PIPE
DESIGNATION	ASTM A234 GR WPB	ASTM A234 GR WPB	API 5L GR 60
Carbon, wt. %	0.185	0.156	0.09
Sulfur, wt. %	0.012	0.013	0.012
Phosphorus, wt. %	0.007	0.008	0.008
Manganese, wt. %	1.45	1.09	1.38
Chromium, wt. %	0.067	0.083	0.076
Nickel, wt. %	0.022	0.029	0.02
Molybdenum, wt. %	<0.01	<0.01	< 0.01
Silicon, wt. %	0.336	0.188	0.27
Copper, wt. %	<0.01	0.022	0.011
Vanadium, wt. %	<0.002	<0.002	< 0.002
Niobium, wt. %	--	--	0.024
Titanium, wt. %	--	--	0.008
Boron, wt. %	<0.02	<0.02	< 0.02
Carbon Equivalent (IIW)	0.442	0.358	0.337
Carbon Equivalent (PCM)	0.278	0.224	0.175

Mechanical Properties

Tensile tests were carried out according to ASTM A370, results are shown in table-3.3 below. Sample preparation for HIC testing was carried out according to NACE TM 0284-2016.

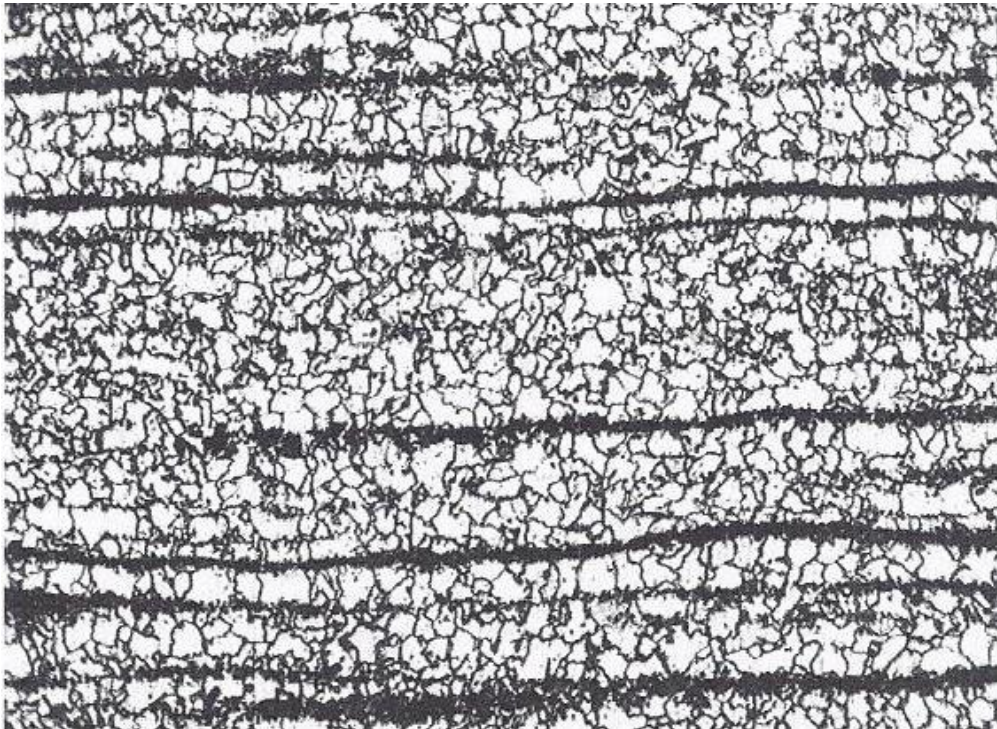
Table 3.3: Mechanical test results of starting materials.

Mechanical Test as per ASTM A370 [95]								
ID	Material Specification	Size	Hardness Average	Hardness max	Yield Strength, N/mm ² (0.2% offset)	Tensile Strength, N/mm ²	Elongation n%	Reduction in Area%
A	ASTM A234 GR WPB (CAP)	4 IN X 12.37 mm	147 BHN	153	384	531	38	77
D	SA 234 WPB (ELBOW)	30 IN X9.55 mm	128 BHN	133	304	475	40.00	77.00
E	API 5L x60 SAW (PIPE)	36IN X 19.05 mm	187 HV ₁₀	193.00	488	552	31.00	86.00

Microstructure

SAMPLE – A

Typical microstructure of as received sample A is produced below.



x200

Figure 3.3: Sample A consists of ferrite-pearlite microstructure having large inhomogeneous ferrite grains with heavy carbide banding as seen in micrograph.

SAMPLE – D

Typical microstructure of as received sample D is produced below.

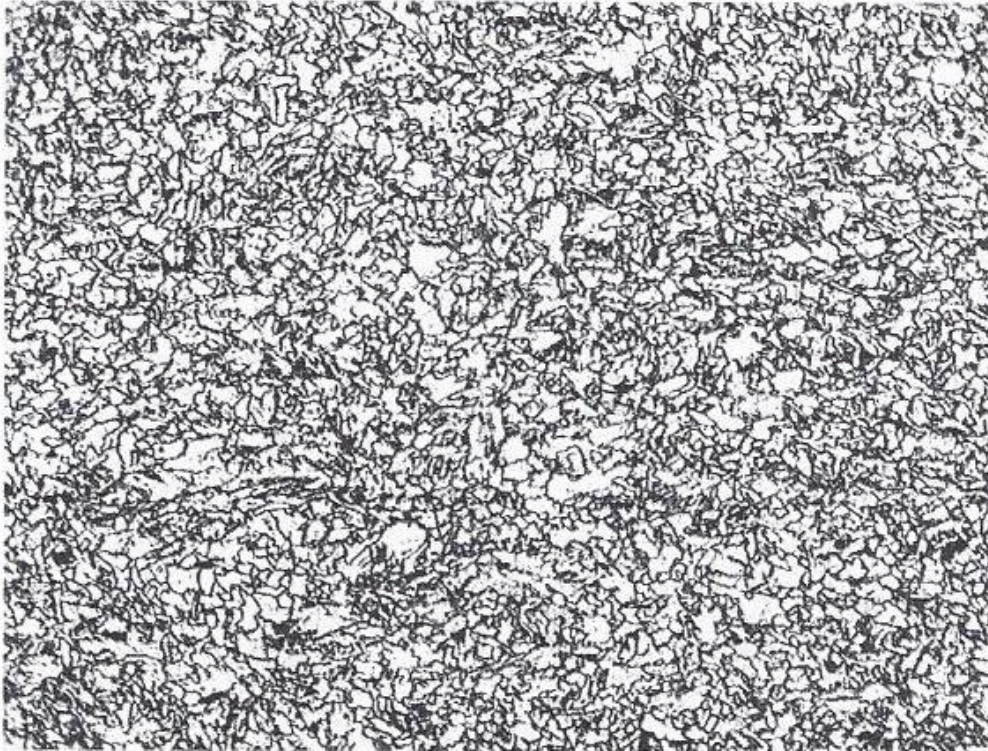


x200

Figure 3.4: Sample D consists of ferrite-pearlite microstructure having large ferrite grains with different degree of carbide banding and grain growth.

SAMPLE – E

Typical microstructure of as received sample E is produced below.



x100

Figure 3.5: Sample E, consists of bainitic microstructure, suggests that the steel received quench & tempered treatment in manufacturing.

3.4 Test Program

Standard glass vessels were used in experiment. All tests followed general requirement of NACE TM-0284 with exception of following-

- a. pH values were designed to cover from 1 to 4. No pH adjustment was made during test.
- b. Three exposure durations were chosen as 48, 96 and 144 Hrs.

Volume to surface ration was maintained greater than 3 ml/Cm². Initial pH was measured, and test was performed without interruption or adjustment of pH, pH were recorded at the end of the test.

Nine test conditions for sample D and eight test conditions for sample E, having three exposure durations were selected to achieve objective of the study as mentioned in table 3.4. Three pH ranges i.e., 1-2, 2-3 and 3-4 were designed for the study. Three sets of specimens were exposed in each pH range for three different exposure durations i.e., 48 Hrs, 96 Hrs, and 144 Hrs.

Table-3.4: Samples with numbering and test durations for testing

TEST ID	A1/ D1/ E1	A2/ D2/ E2	A3/ D3/ E3	A4/ D4/ E4	A5/ D5/ E5	A6/ D6/ E6	A7/ D7/ E7	A8/ D8/ E8	A9/ D9* & E9*
pH RANGE	1- 2			2- 3 (2.7)			4-4.5		
HRS TESTING	48	96	144	48	96	144	48	96	

A set of three test specimens are extracted from base section as per NACE TM 0284, as shown in figure 3.6, below.

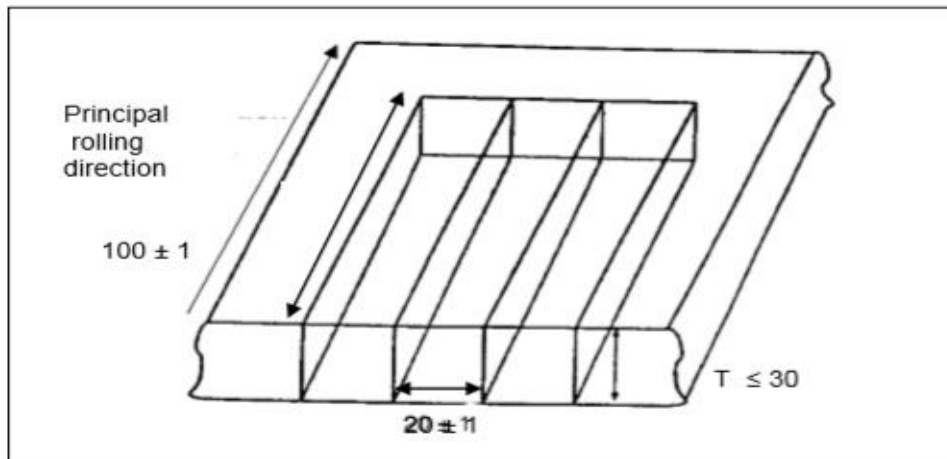


Figure 3.6: Sketch showing a set of HIC specimen extraction from base material.

Test specimen preparation for HIC testing and numbering of the same is shown in fig-3.7 below, the numbering shown as example which were targeted for

48hrs testing at pH 1 to 2 as per test condition indicated in table 3.4. The specimens numbering A1, A2 and A3 are exposed to test condition and subsequently sectioned for HIC evaluation, therefore each section has a number as shown in figure 3.7 below.

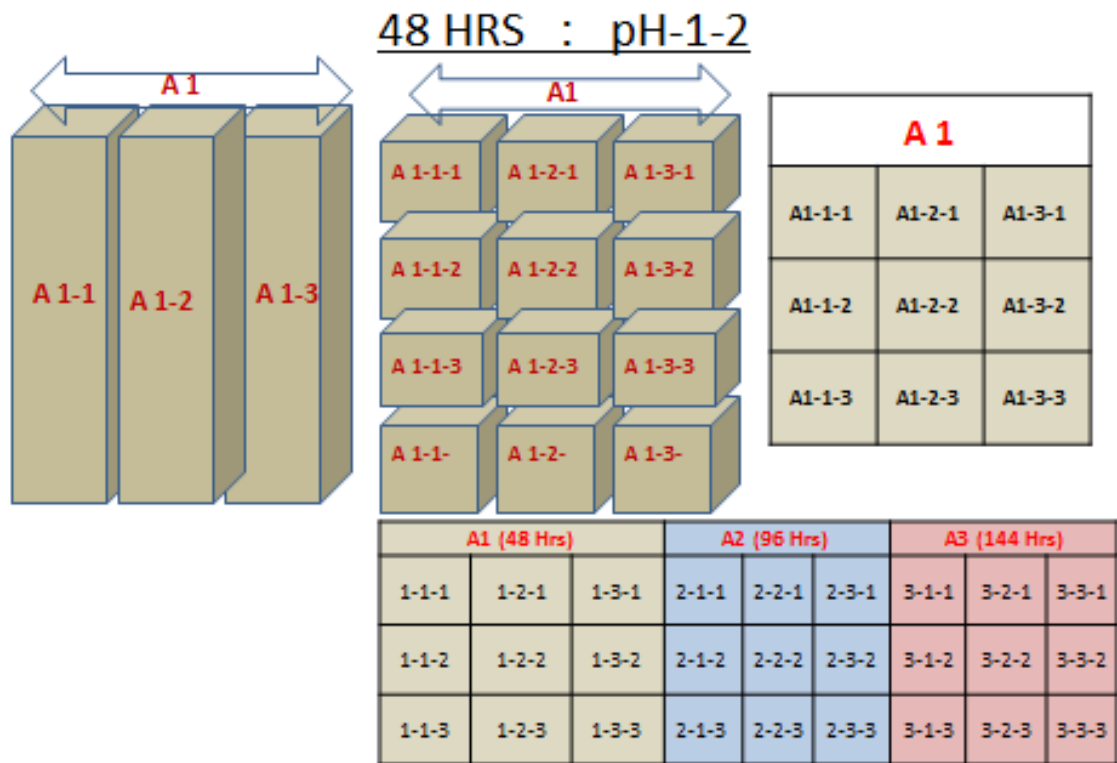


Figure 3.7: Showing specimen numbering system in HIC testing.

The above figure 3.7 shows from left corner as follows-

- Three 100mm x 20mm x Thickness constitutes one set of HIC specimens for testing,
- Each specimen is cut in four equal sections after exposure,
- A1 specimens represent one test condition for one duration of testing,
- A1, A2 and A3 represent all three exposure conditions (48 hrs, 96 hrs and 144 hrs) for one pH condition of sample – A.

The following table-3.5 indicates samples which were tested along with duration of testing. Table summarizes all testing carried out with numbering of specimens for metal sample A, D and E.

Table-3.5 : Test condition for samples.

Table summarizes all testing carried out with numbering of specimens for metal samples

A1-48 HRS			A2 -96 HRS			A3 -144HRS			A4- 48 HRS			A5 -96 HRS			A6 -144HRS			A7- 48 HRS			A8 -96 HRS			A9 -144HRS		
1-1-1	1-2-1	1-3-1	2-1-1	2-2-1	2-3-1	3-1-1	3-2-1	3-3-1	4-1-1	4-2-1	4-3-1	5-1-1	5-2-1	5-3-1	6-1-1	6-2-1	6-3-1	7-1-1	7-2-1	7-3-1	8-1-1	8-2-1	8-3-1	9-1-1	9-2-1	9-3-1
1-2-1	1-2-2	1-3-2	2-1-2	2-2-2	2-3-2	3-1-2	3-2-2	3-3-2	4-1-2	4-2-2	4-3-2	5-1-2	5-2-2	5-3-2	6-1-2	6-2-2	6-3-2	7-1-2	7-2-2	7-3-2	8-1-2	8-2-2	8-3-2	9-1-2	9-2-2	9-3-2
1-3-1	1-2-3	1-3-3	2-1-3	2-2-3	2-3-3	3-1-3	3-2-3	3-3-3	4-1-3	4-2-3	4-3-3	5-1-3	5-2-3	5-3-3	6-1-3	6-2-3	6-3-3	7-1-3	7-2-3	7-3-3	8-1-3	8-2-3	8-3-3	9-1-3	9-2-3	9-3-3
D1- 48 HRS			D2 -96 HRS			D3 -144HRS			D4- 48 HRS			D5 -96 HRS			D6 -144HRS			D7- 48 HRS			D8 -96 HRS			D9 -144HRS		
1-1-1	1-2-1	1-3-1	2-1-1	2-2-1	2-3-1	3-1-1	3-2-1	3-3-1	4-1-1	4-2-1	4-3-1	5-1-1	5-2-1	5-3-1	6-1-1	6-2-1	6-3-1	7-1-1	7-2-1	7-3-1	8-1-1	8-2-1	8-3-1	9-1-1	9-2-1	9-3-1
1-2-1	1-2-2	1-3-2	2-1-2	2-2-2	2-3-2	3-1-2	3-2-2	3-3-2	4-1-2	4-2-2	4-3-2	5-1-2	5-2-2	5-3-2	6-1-2	6-2-2	6-3-2	7-1-2	7-2-2	7-3-2	8-1-2	8-2-2	8-3-2	9-1-2	9-2-2	9-3-2
1-3-1	1-2-3	1-3-3	2-1-3	2-2-3	2-3-3	3-1-3	3-2-3	3-3-3	4-1-3	4-2-3	4-3-3	5-1-3	5-2-3	5-3-3	6-1-3	6-2-3	6-3-3	7-1-3	7-2-3	7-3-3	8-1-3	8-2-3	8-3-3	9-1-3	9-2-3	9-3-3
E1- 48 HRS			E2 -96 HRS			E3 -144HRS			E4- 48 HRS			E5 -96 HRS			E6 -144HRS			E7- 48 HRS			E8 -96 HRS			E9 -144HRS		
1-1-1	1-2-1	1-3-1	2-1-1	2-2-1	2-3-1	3-1-1	3-2-1	3-3-1	4-1-1	4-2-1	4-3-1	5-1-1	5-2-1	5-3-1	6-1-1	6-2-1	6-3-1	7-1-1	7-2-1	7-3-1	8-1-1	8-2-1	8-3-1	9-1-1	9-2-1	9-3-1
1-2-1	1-2-2	1-3-2	2-1-2	2-2-2	2-3-2	3-1-2	3-2-2	3-3-2	4-1-2	4-2-2	4-3-2	5-1-2	5-2-2	5-3-2	6-1-2	6-2-2	6-3-2	7-1-2	7-2-2	7-3-2	8-1-2	8-2-2	8-3-2	9-1-2	9-2-2	9-3-2
1-3-1	1-2-3	1-3-3	2-1-3	2-2-3	2-3-3	3-1-3	3-2-3	3-3-3	4-1-3	4-2-3	4-3-3	5-1-3	5-2-3	5-3-3	6-1-3	6-2-3	6-3-3	7-1-3	7-2-3	7-3-3	8-1-3	8-2-3	8-3-3	9-1-3	9-2-3	9-3-3

*Due to material constraint, two sets of specimens, instead of three were tested in E-9 condition

3.5 HIC Evaluation

According to NACE TM 0284, three specimens (100mm x 20mm) constitute a test set. Each of the three specimens is sectioned into four equal length sections and three internal surfaces are polished for examination as shown in below picture.

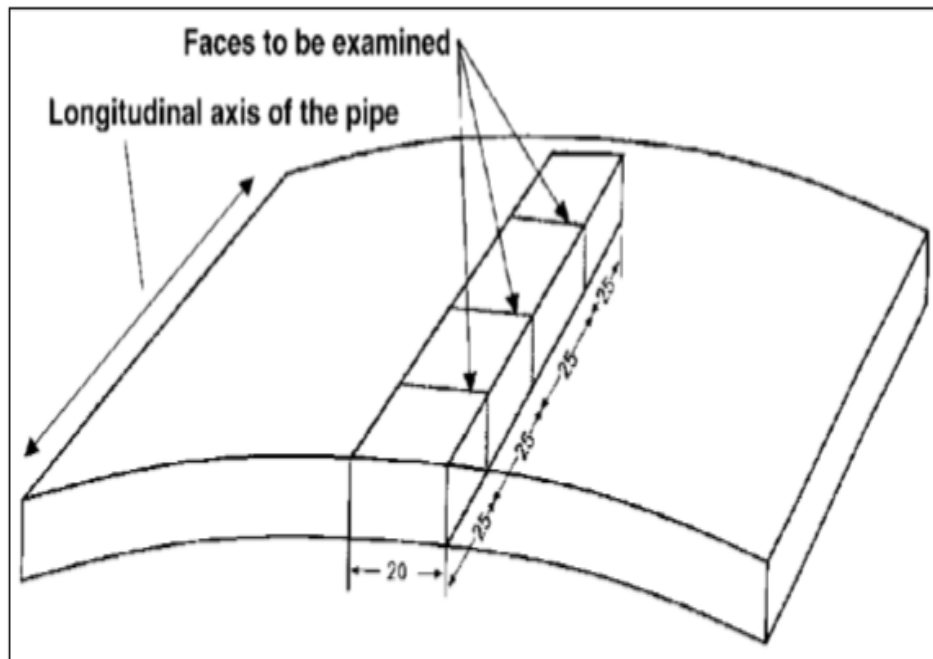
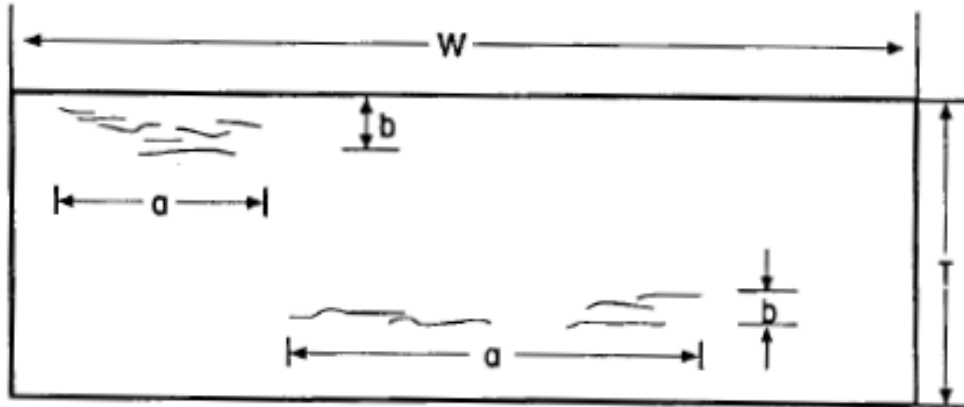


Figure 3.8: The sketch shows section of HIC tested specimen and surfaces to be evaluated by metallography.

Therefore, a total lot of at least nine surfaces (sections) are evaluated for each material for one test. Metallography of polished surfaces are carried out as per ASTM E3 standard and evaluated at X100 magnification under microscope.

The length and width of each individual crack in each section is measured according to the standard. Based on crack measurements, three parameters are determined i.e., Crack length ratio (CLR), Crack Thickness Ratio (CTR) and Crack Sensitivity Ratio (CSR) for each section and averaged for each specimen, as well as, set of specimens as shown in below sketch.



$$CSR = \frac{\Sigma (a \times b)}{(W \times T)} \times 100\%$$

$$CLR = \frac{\Sigma a}{W} \times 100\%$$

$$CTR = \frac{\Sigma b}{T} \times 100\%$$

Figure 3.9, Illustrates measurement and calculation of the ratios CSR, CLR and CTR to characterize HIC.

CSR is a ratio which characterizes the cracked area with respect to overall section surface area.

CLR is a ratio which characterizes sum of all crack lengths with respect to overall width of the section. CTR is a ratio which characterizes sum of all cracks with respect to overall thickness of the section.

The above three ratios are used for quantitative characterization of HIC, for a material as per standard procedure of NACE TM-02 84. Detection of blisters near the surface (within 1mm) are usually ignored.

HIC test set-up is shown in below picture.



Figure 3.10: Photograph shows HIC test set-up in laboratory. Test specimens are placed in glass vessel immersed in test solution, H₂S gas is continuously bubbled through the solution during testing.

Following figure 3.11, shows HIC specimens (a) before testing, (b) after exposure, and (c) marked for sectioning for metallography.

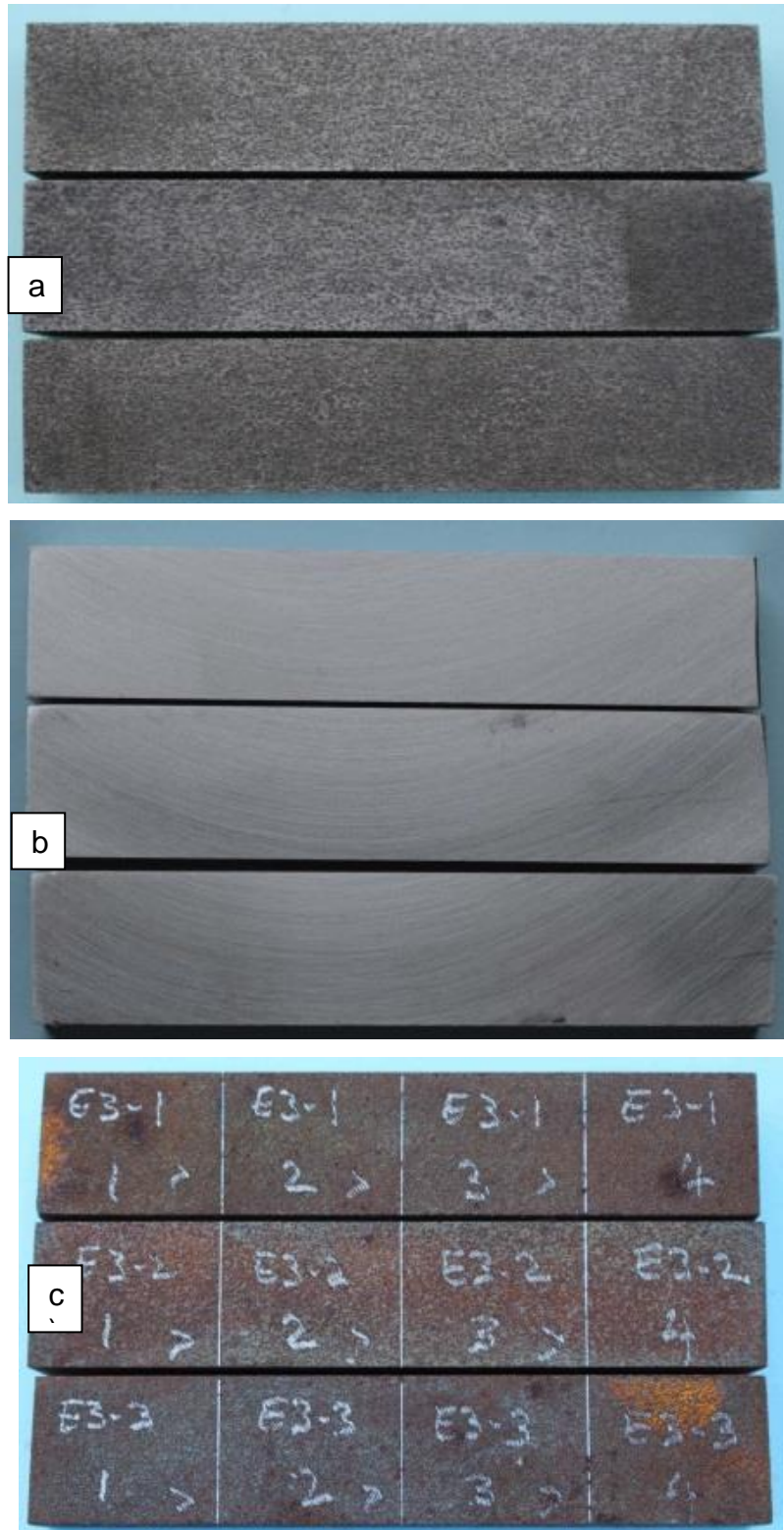


Fig-3.11, Photographs showing (a) specimens before, (b) after testing, and (c) marking for sectioning for metallography.

3.6 Test Results

Material sample - A:

Material sample 'A' was tested for nine (9) conditions as mentioned in table-3.6. HIC tests were carried out as per procedure mentioned in NACE TM 0284 and as described in the previous section. The test results indicated as average percentage of CLR, CTR and CSR by metallographic measurement (refer figure #3.9).

Table-3.6: Showing material sample-A test conditions and HIC test results

	HIC TEST RESULT FOR MATERIAL SAMPLE – A								
HRS TESTING	48	48	48	96	96	96	144	144	144
pH	1	2.7	4	1	2.7	4	1	2.7	4
CLR AVG(%)	16.90	16.30	1.93	12.96	15.87	3.52	8.66	9.13	24.58
CTR AVG(%)	2.39	4.63	0.23	1.65	2.92	0.37	1.74	1.43	7.14
CSR AVG(%)	0.22	0.63	0.01	0.28	0.39	0.02	0.13	0.14	0.97

Following unetched micrograph (fig-3.12) shows HIC cracks in the middle of thickness of the HIC tested sample-A. HIC often initiates and propagates along the centerline segregation in the flat rolled products.

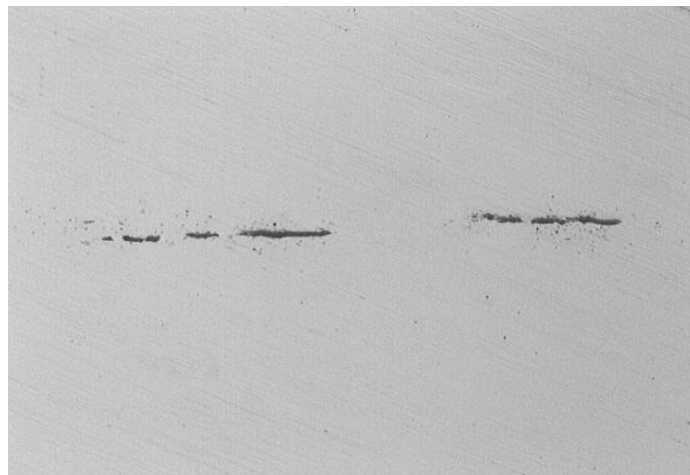


Figure 3.12: Metal sample-A, unetched surface showing HIC cracks (x100) at centerline of the specimen.

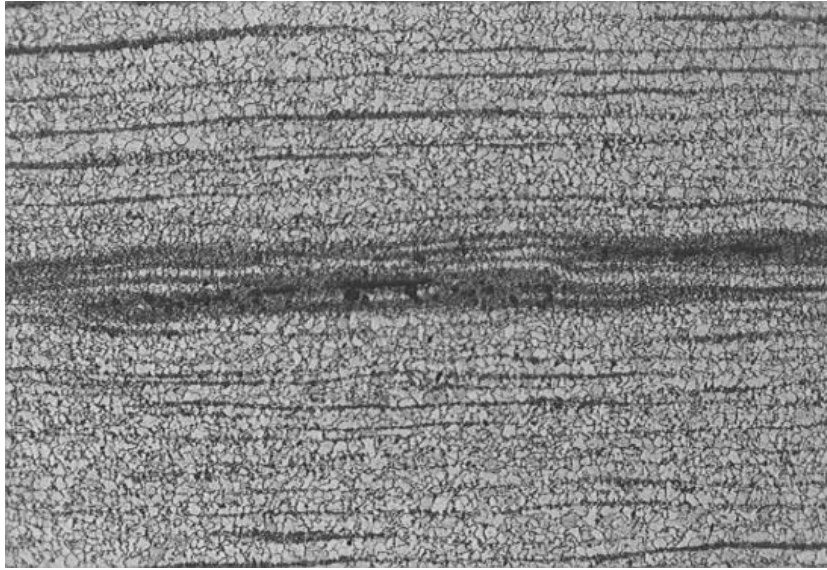


Figure 3.13: Above Metal sample-A, after HIC testing etched surface showing HIC cracks along centerline in the banded ferrite-pearlite microstructure (x100). The centerline segregation is evident in the micrograph.

Material sample - D

Material D was tested for nine (9) conditions as mentioned in table-3.7. The test results indicated as CLR, CTR and CSR average percentages, measured as explained in fig-3.9.

Table-3.7: Test condition (solution pH and Exposure duration) and results of material sample-D.

	HIC TEST RESULT FOR MATERIAL SAMPLE – D								
HRS TESTING	48	48	48	96	96	96	144	144	144
pH	1	2.7	4	1	2.7	4	1	2.7	4
CLR AVG(%)	19.11	1.43	2.35	3.06	22.58	12.67	6.44	72.86	60.47
CTR AVG(%)	8.78	0.3	0.86	1.38	11.24	4.18	17.31	24.16	15.87
CSR AVG(%)	0.68	0.01	0.03	0.07	2.03	0.83	0.26	8.82	8.84

Following unetched micrograph shows HIC cracks in tested specimen from metal sample-D.



Figure 3.14: Metal sample-D, unetched surface showing HIC cracks (x100)

The cracks in figure 3.14, initiated at different planes across the material thickness and the propagation showing classic HIC phenomenon. The edges of the cracks have typical linking pattern for HIC propagation. The morphology of the cracks indicate that the material and the test conditions were highly conducive to HIC degradation.

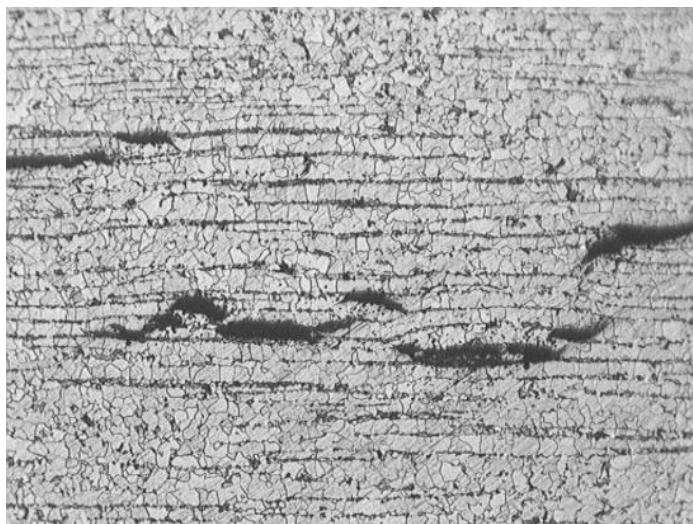


Figure 3.15: Optical micrograph of metal sample-D, after HIC testing, etched surface showing typical HIC cracks in the banded ferrite-pearlite microstructure (x100).

Material Sample - E

Material E was tested for eight (8) conditions as mentioned in table-3.8. The test results indicated as CLR, CTR and CSR average percentages, highlighted in figure 3.9.

Table-3.8: Test condition (solution pH and Exposure duration) and results of HIC test of material sample E.

	HIC TEST RESULT FOR MATERIAL SAMPLE – E							
HRS TESTING	48	48	48	96	96	96	144	144
pH	1	2.7	4	1	2.7	4	1	2.7
CLR AVG(%)	8.09	4.7	16.37	27.38	24.96	32.59	26.69	33.55
CTR AVG(%)	0.74	0.36	1.07	2.15	2.65	3.05	4.71	2.57
CSR AVG(%)	0.05	0.05	0.12	0.33	0.37	0.44	0.84	0.34

The following micrograph of unetched tested specimen from metal sample-E.

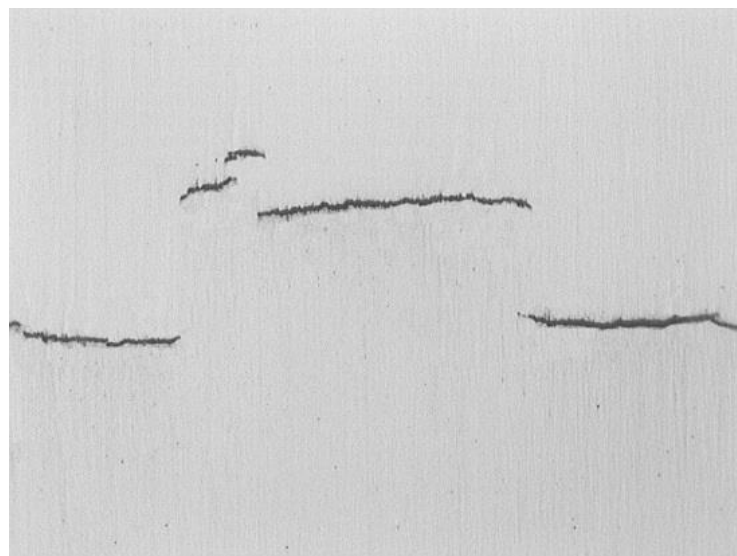


Figure 3.16: Metal sample-E, unetched surface showing HIC initiation and progression in the material thickness (x100).

Cracks are more towards the center of thickness of the specimen and flat in nature. Cracks also have sharp inclined edges, typical linking characteristics of HIC.

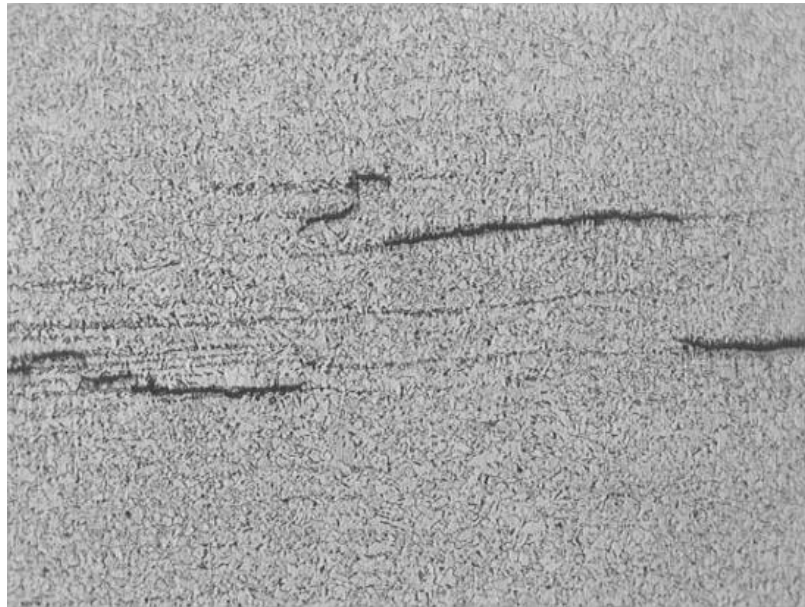


Figure 3.17: Optical micrograph of metal sample-E, after HIC testing etched surface showing flat HIC cracks in different planes close to the centerline of the thickness of the specimen. Micrograph indicates fine bainitic microstructure of the steel sample with some banding at centerline along the rolling plane (x100).

Observation & Discussion

Composition:

Composition of all the samples (A, D and E), meet respective ASTM specification as indicated in table-3.2.

Microstructure:

Sample-A: Equaxed ferrite pearlite grains are observed with heavy banding structure. HIC developed along centerline of the thickness.

Sample-D: Equaxed ferrite pearlite grains are observed with heavy banding structure. HIC developed along banding lines.

Sample-E: Fine grain ferrite bainite structure is observed. HIC developed along rolling direction, as well as, rolling plane.

Mechanical Properties:

Tensile, yield and hardness values are indicated in table-3. All the mechanical properties are found within limits of the specifications for all the materials A, D and E, including hardness values less than 237 BHN or 248 Hv10, which comply to requirement for SSC resistance according to NACE MR-0175 requirements. The Tensile Strength values measured were following-

Sample – A : 531 N/mm²

Sample – D : 475 N/mm²

Sample – E : 552 N/mm²

3.7 Quantitative Evaluation as per NACE TM 0284

Materials, A, D and E are found to exhibit extensive cracking in the form of HIC as indicated in table 3.6-3.8, signifying that the materials were susceptible to HIC in all test conditions.

HIC progression has been analyzed in terms of Crack Length Ratio (CLR), Crack Thickness Ratio (CTR) and Crack Sensitivity Ratio (CSR) to establish relationship of HIC with following parameters as described previously-

- Exposure duration,
- pH of environment,
- Strength grade,

Effect of Exposure Duration on HIC: Sample - A, D & E.

SAMPLE – A

Sample A has been tested in three test durations and three pH conditions for each test duration. The test conditions represented by pH of solution, as well

as, HIC as evaluated for each test duration represented by CLR-CTR-CSR, are described in table-3.9.

Table-3.9: HIC in terms of CLR, CTR and CSR average percentages for sample D tested for different durations for sample-A are shown in table.

SAMPLE - A						
HRS	pH	AVERAGE%			EACH TEST HR AVERAGE	OVERALL TEST HRS AVERAGE
		CLR	CTR	CSR	CLR / CTR / CSR	CLR / CTR / CSR
48	1	16.9	2.39	0.22	11.71 / 2.41 / 0.29	12.20 / 2.49 / 0.30
	2.7	16.3	4.63	0.63		
	4	1.93	0.23	0.01		
96	1	12.96	1.65	0.28	10.78 / 1.64 / 0.23	
	2.7	15.87	292	0.39		
	4	3.52	0.37	0.02		
144	1	8.66	1.74	0.13	14.12 / 3.43 / 0.41	
	2.7	9.13	1.43	0.14		
	4	24.58	7.14	0.97		

The cracking ratios as found in 48 Hrs, 96 Hrs and 144 Hrs testing (table #3.9), are further summarized in below table-3.10 to facilitate graphic presentation for sample A.

Table 3.10: Average percentage of CLR, CTR and CSR for 48 Hrs, 96 Hrs and 144 Hrs extracted from table-3.9 are summarized below.

AVERAGE HRS TESTING vs HIC (A)			
HRS TESTING	48	96	144
HRS TESTING (X48)	1	2	3
CLR% AVG	11.71	10.78	14.12
CTR% AVG	2.41	1.64	3.43
CSR% AVG	0.29	0.23	0.41

Following curves in figure3.18 showing average percentages of CLR, CTR and CSR of sample-A, as per values indicated in table-3.10.

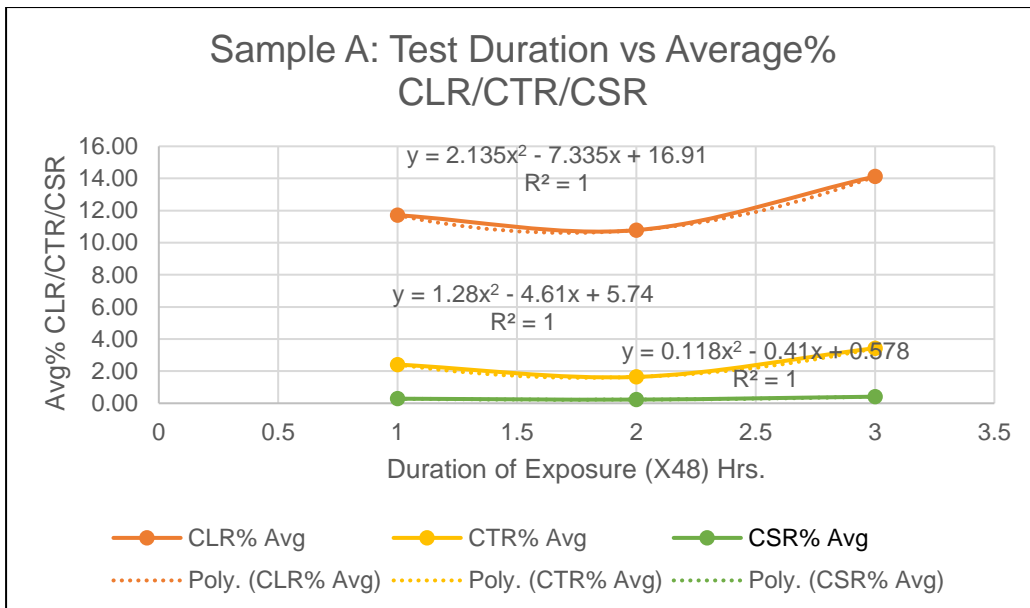


Figure 3.18: The curves represent HIC in sample-A in terms of average CLR%, CTR% and CSR%, tested for 48 hrs, 96 hrs and 144 hrs (1-2-3 in X axis).

Following curves in figures 3.19, 3.20 and 3.21 showing trend analysis of CLR, CTR and CSR of sample-A derived from curves in fig-3.18.

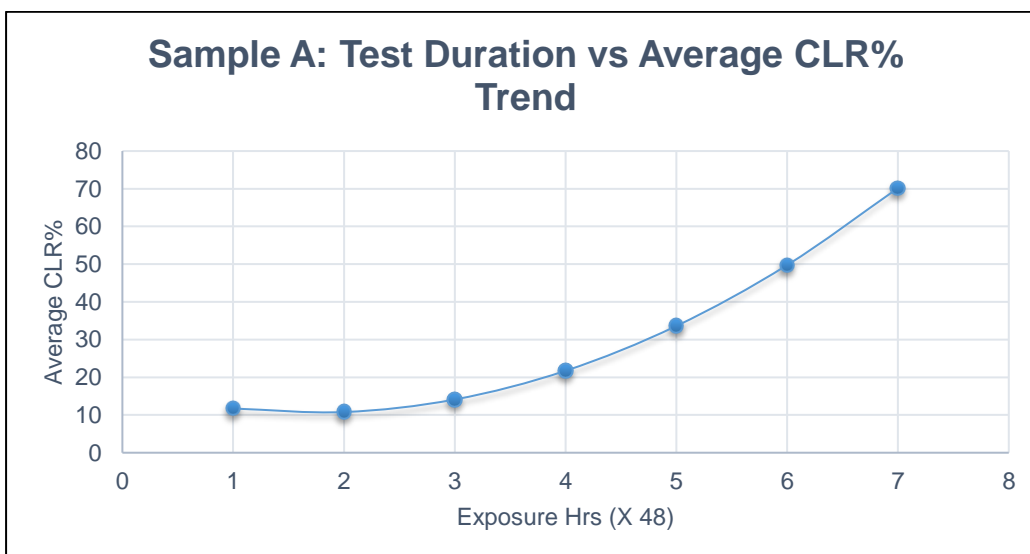


Figure 3.19: Showing trend of average CLR% for sample A. It is observed that an Initial marginal down-slope prevailed up to 96 Hrs (2x48 hrs, approx.), subsequently, exponential increase in rate of CLR is found with respect to test duration.

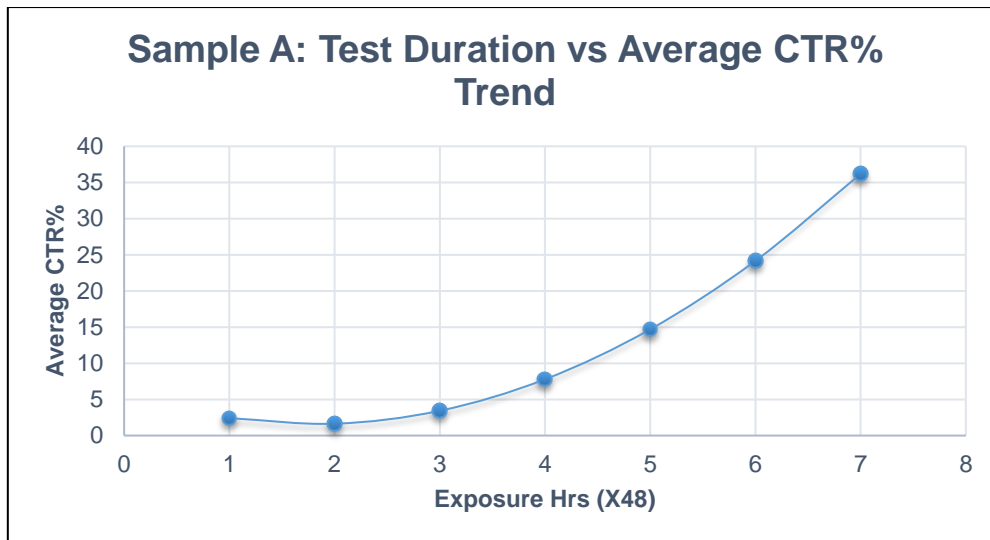


Figure 3.20: Showing trend of average CTR% for sample A. Initial marginal down-slope prevailed up to 96 Hrs (2x48 hrs, approx), subsequently parabolic increase in rate of CTR is found with respect to test duration.

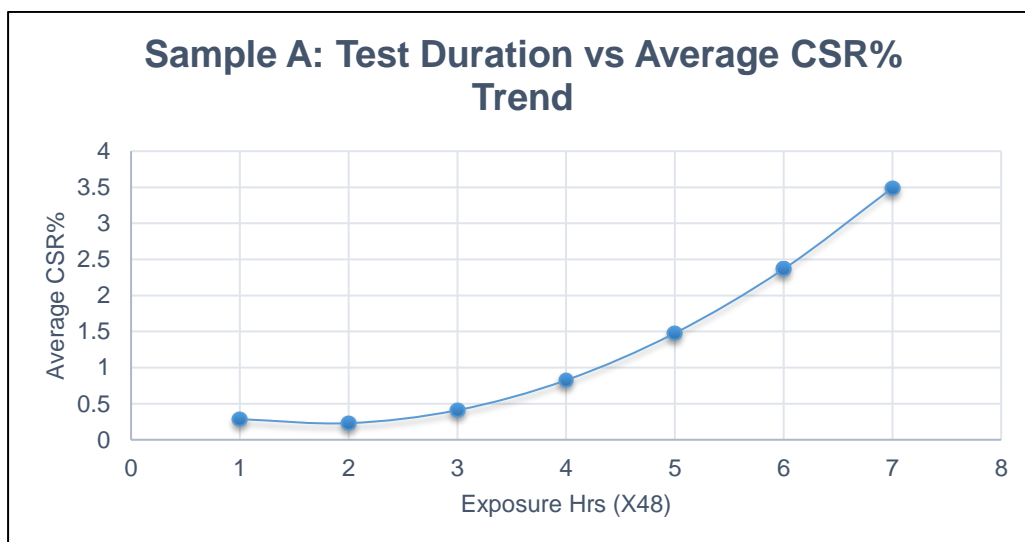


Figure 3.21: Showing trend of average CSR% for sample A. Initial marginal down-slope prevailed up to 96 Hrs (2x48 hrs, approx), subsequently exponential increase in rate of CSR is found with respect to test duration.

As evident from the curves and data from table-3.9, all the parameters CLR, CTR and CSR have parabolic upward trend in cracking with respect to duration of exposure. The trend indicates that initiation of the crack needed about 96 hrs. but once initiated, the propagation is extremely fast. Therefore, the severity of cracking for such banded ferrite and pearlite material can be expected to be considerably high, whereas HIC tendency of bainitic steels are low.

SAMPLE - D:

Sample D has been tested for three test durations, and three pH conditions for each test duration. The test conditions, as well as HIC evaluation for each test duration is described in table-3.11 below.

Table-3.11: HIC in terms of CLR, CTR and CSR average percentages for sample D tested for for different durations for sample-D are shown in table.

SAMPLE - D						
HRS	pH	AVERAGE%			EACH TEST HR AVERAGE	OVERALL TEST HRS AVERAGE
		CLR	CTR	CSR	CLR / CTR / CSR	CLR / CTR / CSR
48	1	19.11	8.78	0.68	7.63 / 3.31 / 0.24	22.33 / 9.34 / 2.39
	2.7	1.43	0.3	0.01		
	4	2.35	0.86	0.03		
96	1	3.06	1.38	0.07	12.77 / 5.6 / 0.97	
	2.7	22.58	11.24	2.03		
	4	12.67	4.18	0.83		
144	1	6.44	17.31	0.26	46.59 / 19.11 / 5.97	
	2.7	72.86	24.16	8.82		
	4	60.47	15.87	8.84		

Cracking ratios found in 48 Hrs, 96 Hrs and 144 Hrs testing, is further summarized in below table-3.12 for sample D.

Table 3.12: Average percentage of CLR, CTR and CSR for 48 Hrs, 96 Hrs and 144 Hrs extracted from above table are summarized.

AVERAGE HRS TESTING vs HIC (D)			
HRS TESTING	48	96	144
HRS TESTING (X48)	1	2	3
CLR% AVG	7.63	12.77	46.59
CTR% AVG	3.31	5.6	19.11
CSR% AVG	0.24	0.97	5.97

Following curves in figure-3.22 showing average percentages of CLR, CTR and CSR of sample-D.

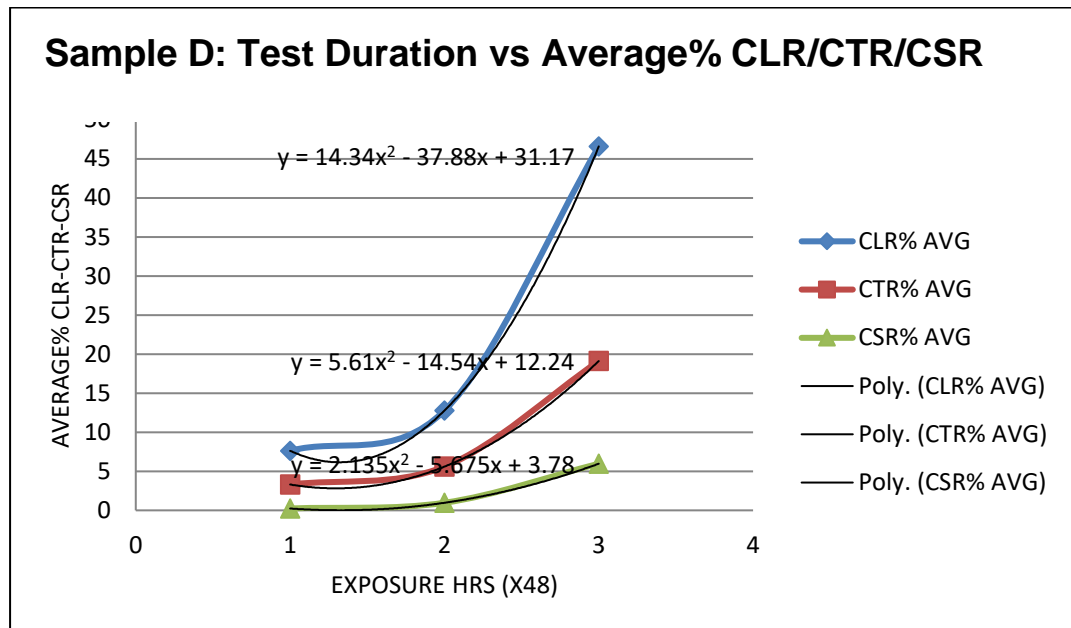


Figure 3.22: Curves representing CLR, CTR and CSR tested for 48 Hrs, 96 Hrs and 144 Hrs for sample-D.

Trend analysis of each CLR, CTR and CSR average% are shown in following Figure 3.23, 3.24 and 3.25, derived from curves in figure 3.22.

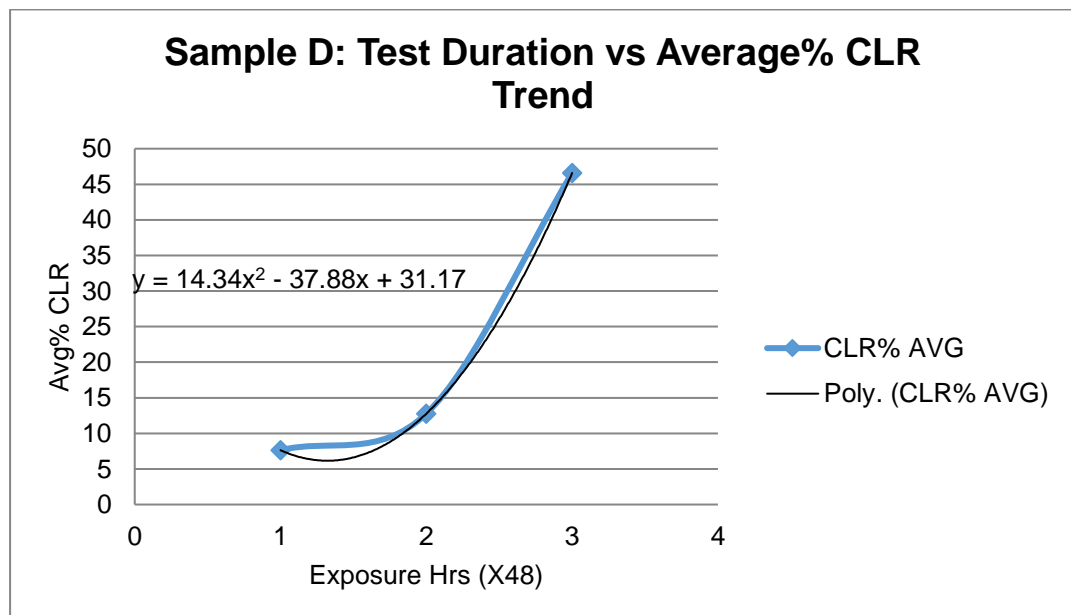


Figure 3.23: Showing trend of average CLR% for sample D. A parabolic increase in rate of CLR is found with respect to test duration according to the curve.

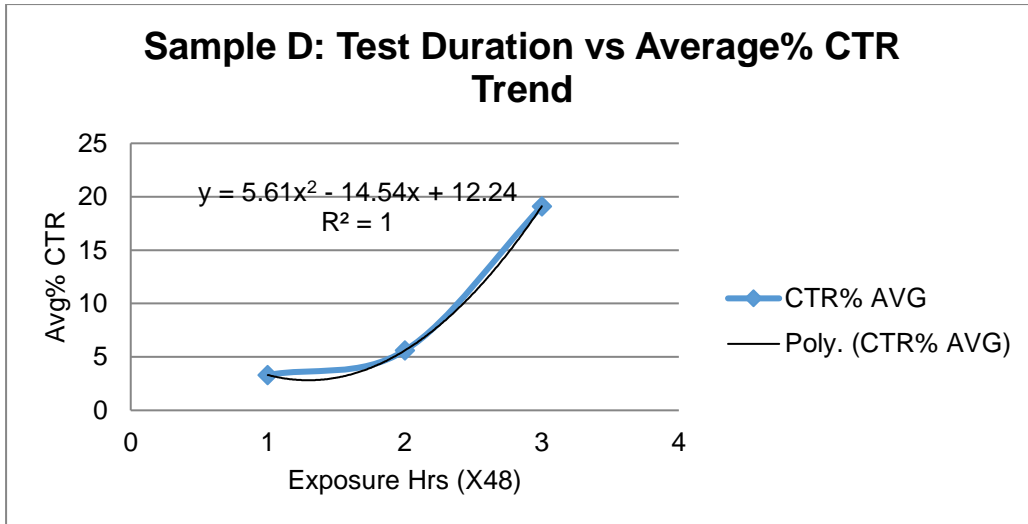


Figure 3.24: Showing trend of average CTR% for sample D. An increase in rate of CTR is found with respect to test duration according to the curve.

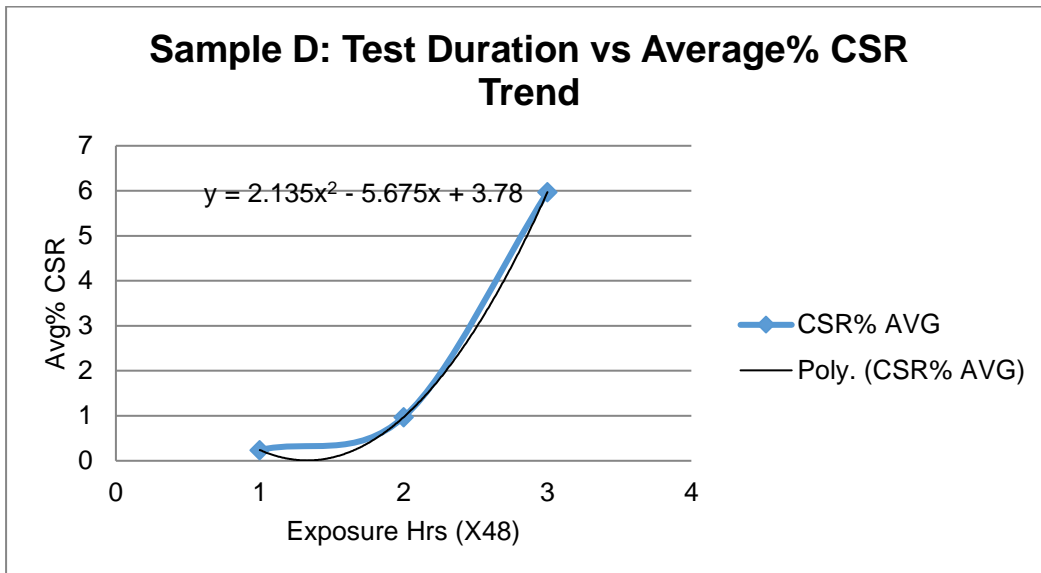


Figure 3.25: Showing trend of average CSR% for sample D. A steady exponential increase in rate of CSR is found with respect to test duration.

As evident from the curves (fig:3.23-3.25) and data from table-3.12, all the parameters CLR, CTR and CSR have upward trend of cracking with time after initial exposure of about 96 Hrs. Similar to sample-A, the trends indicate that, to achieve the threshold concentration of hydrogen accumulation in samples, it required approximately 96 hrs, but after initiation the propagation is considerably fast. Therefore, the severity of cracking for such banded ferrite and pearlite can be expected to be considerably high.

SAMPLE - E:

Sample E has been tested in three test durations and three pH conditions for each test duration. The test conditions, as well as HIC evaluation for each test duration is described in table-3.13 below.

Table-3.13: Complete testing conditions and results, including overall average percentages for sample-E are mentioned in the table.

SAMPLE - E						
HRS	pH	AVERAGE%			EACH TEST HR AVERAGE	OVERALL TEST HRS AVERAGE
		CLR	CTR	CSR	CLR / CTR / CSR	CLR / CTR / CSR
48	1	8.09	0.74	0.05	9.72 / 0.72 / 0.073	22.71 / 2.32 / 0.34
	2.7	4.7	0.36	0.05		
	4	16.37	1.07	0.12		
96	1	27.38	2.15	0.33	28.31 / 2.61 / 0.38	
	2.7	24.96	2.65	0.37		
	4	32.59	3.05	0.44		
144	1	26.69	4.71	0.84	30.12 / 3.64 / 0.59	
	2.7	33.55	2.57	0.34		

Cracking ratios found in 48 Hrs, 96 Hrs and 144 Hrs testing, are further summarized in below table-3.14 for sample E.

Table 3.14: Average percentage of CLR, CTR and CSR are mentioned as found in HIC testing for 48 Hrs, 96 Hrs and 144 Hrs for sample-E. Data source- table-3.13.

AVERAGE HRS TESTING vs HIC (E)			
HRS TESTING	48	96	144
HRS TESTING (X 48)	1	2	3
CLR% AVG	9.72	28.31	30.12
CTR% AVG	0.72	2.61	3.64
CSR% AVG	0.07	0.38	0.59

HIC in terms of CLR, CTR and CSR average percentages are represented in curves from data taken from table-3.14 for sample-E.

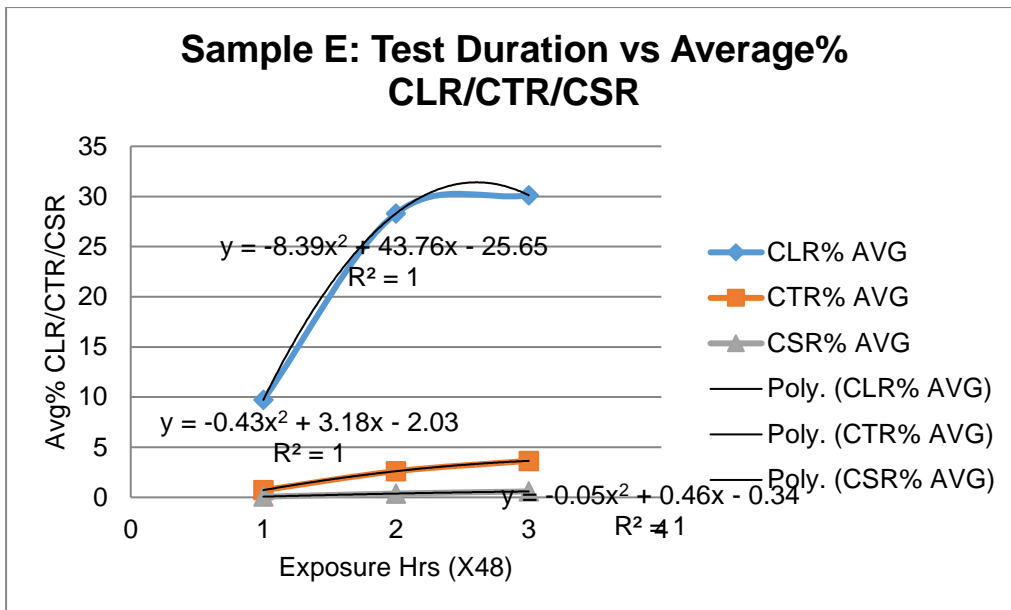


Figure 3.26: Representing HIC of sample-E in terms of CLR, CTR and CSR average percentages tested for 48 Hrs, 96 Hrs and 144 Hrs (indicated as 1-2-3 in X axis).

The trends of CLR, CTR and CSR are further analyzed in fig-3.27 –3.29.

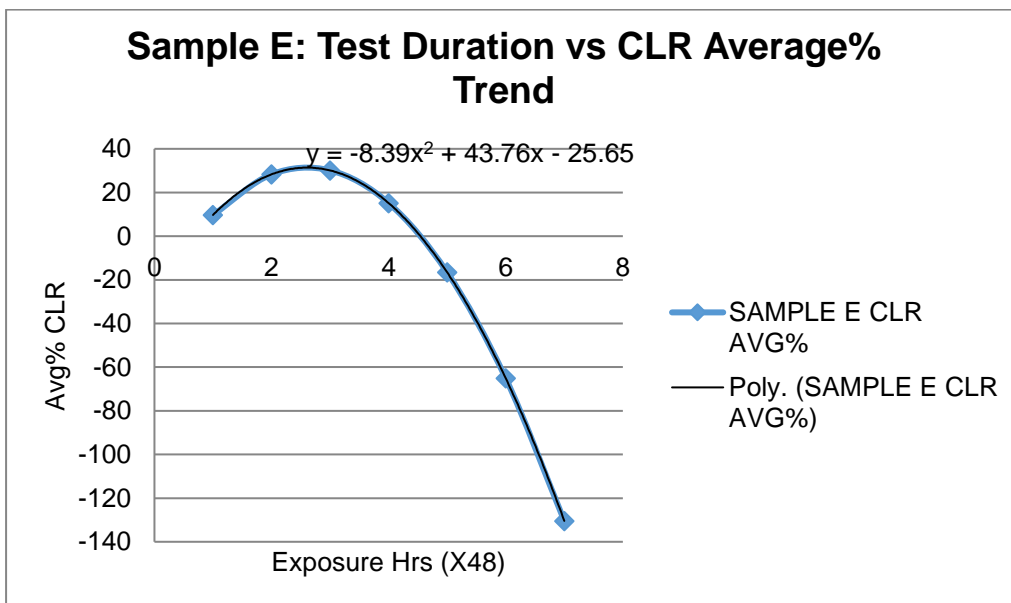


Figure 3.27: Showing average% CLR trend for sample E.

The CLR trend curve in Fig-3.27 indicates that unlike sample A & D, there has been an initial parabolic rise of CLR with respect to exposure duration in testing which reached peak at approximately 125 Hrs (2.6x48). Negative value of CLR is not a reality, therefore, shall not be considered below the X axis.

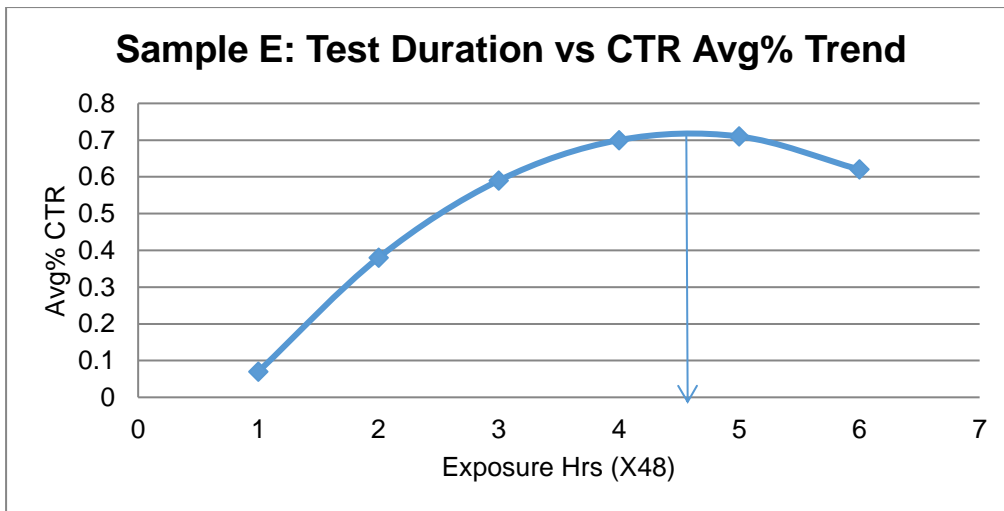


Figure 3.28: The trend curve of average% CTR indicates that the number of cracks across thickness of the specimens grows up to approximately 204 (4.25x48) Hrs of exposure.

Truly, the downtrend part from the peak in above curve (figure 3.28) also shall be considered not relevant because, thickness of cracks will not decline once cracks have developed in a specimen. Therefore, the trend up to peak value shall be considered as relevant in evaluation.

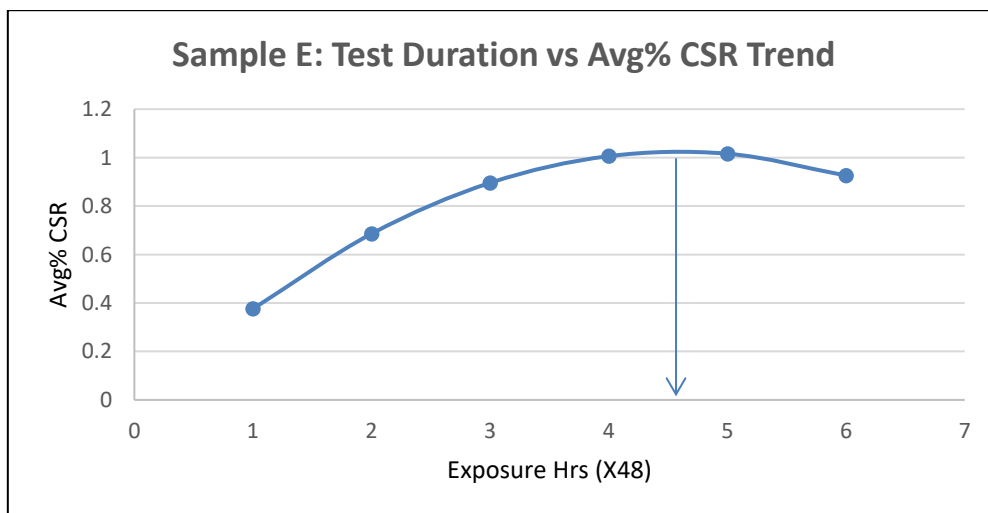


Figure 3.29: Showing CSR trend of sample E rise of crack sensitivity up to 220 hrs (4.6x48 approximately), closely resembling the trend of CTR curve.

The above curves show that CLR values maintain an increasing trend approximately up to, 2.5 unit values in X axis, which should approximately correspond to 120 hrs (2.5x48=120) in testing. The CTR and CSR trend curves similarly show upward trend up to approximately up to 204 - 220 hrs.

Overall Effect of Duration of Exposure on HIC

Overall effect of duration of exposure has been derived from effect of exposure of individual samples i.e., A, D and E as described in previous sections.

Following table-3.15 indicate average percentage of HIC in terms of CLR, CTR and CSR values for samples of A, D & E derived from Table-3.9, 3.11 & 3.13.

Table – 3.15: Overall average percentage of CLR, CTR and CSR for sample A,D and E for test durations of 48 Hrs, 96 Hrs and 144 Hrs each for three pH conditions.

SAMPLE A-D-E							
HRS	pH	AVERAGE%			AVERAGE% FOR A /D /E		
		CLR	CTR	CSR	CLR	CTR	CSR
48	1	14.7	3.97	0.32	9.69	2.15	0.20
	2.7	7.48	1.76	0.23			
	4	6.88	0.72	0.05			
96	1	14.47	1.73	0.23	17.29	3.29	0.53
	2.7	21.14	5.6	0.93			
	4	16.26	2.53	0.43			
144	1	13.93	7.92	0.41	31.66	9.61	2.81
	2.7	38.51	9.39	3.1			
	4	42.53	11.51	4.91			

Following table-3.16 summarizes HIC indications from table-3.15 overall test duration with respect to HIC cracking.

Table-3.16: Overall HIC is indicated for samples A-D-E.

OVERALL HIC FOR SAMPLE A-D-E			
DURATION (HRS)	AVERAGE%		
	CLR	CTR	CSR
48	9.69	2.15	0.20
96	17.29	3.29	0.53
144	31.66	9.61	2.81

Curve in Figure 3.30 indicate relationship of overall test duration with overall HIC parameters (CLR/CTR/CSR average%) for samples A, D & E.

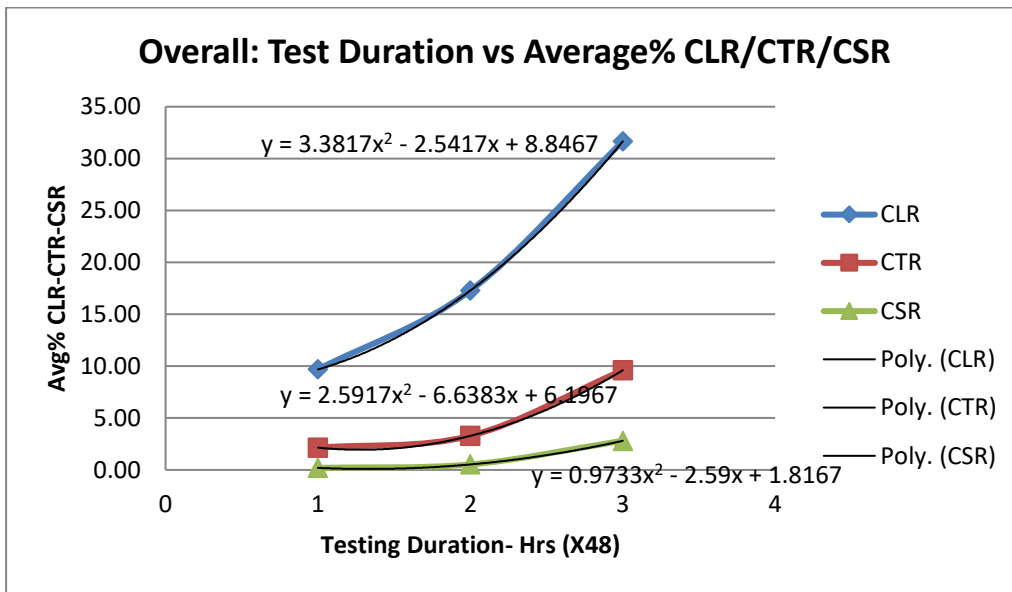


Figure 3.30: shows overall HIC parameters i.e., CLR, CTR and CSR with respect to duration of testing for samples A, D and E as obtained from testing.

The trends of average% of CLR, CTR and CSR are further analyzed in following curves.

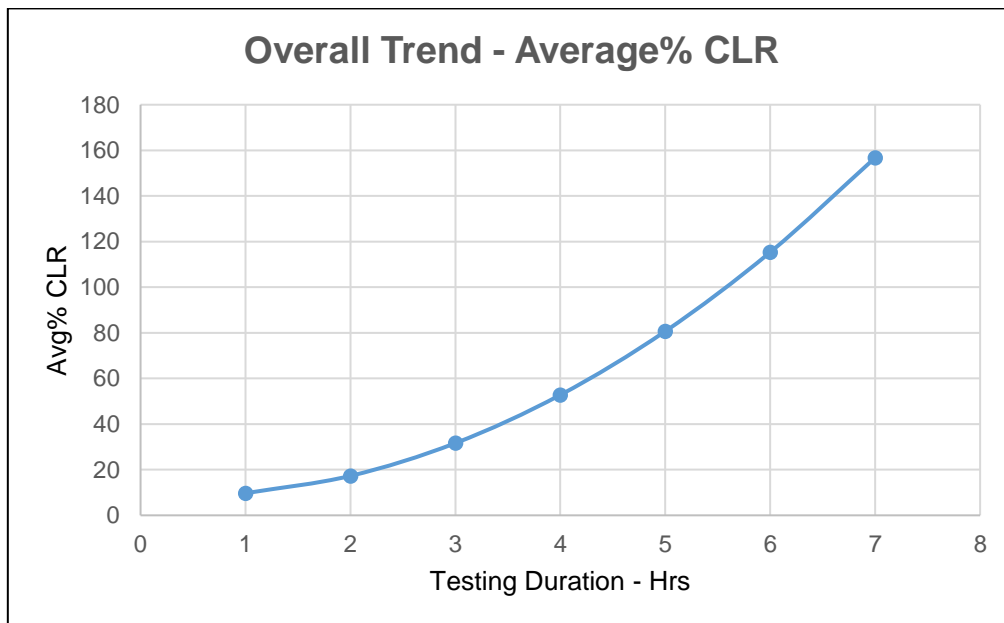


Fig-3.31: The overall trend of average% of CLR is indicated by the curve.

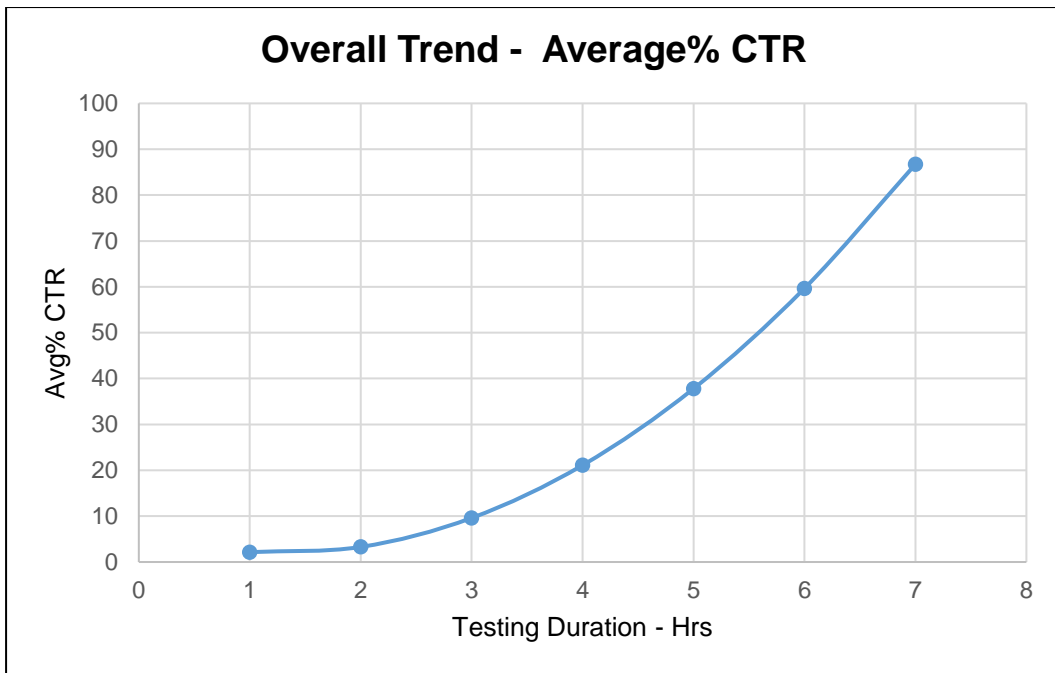


Figure 3.32: The overall trend of average% of CTR is indicated by the curve.

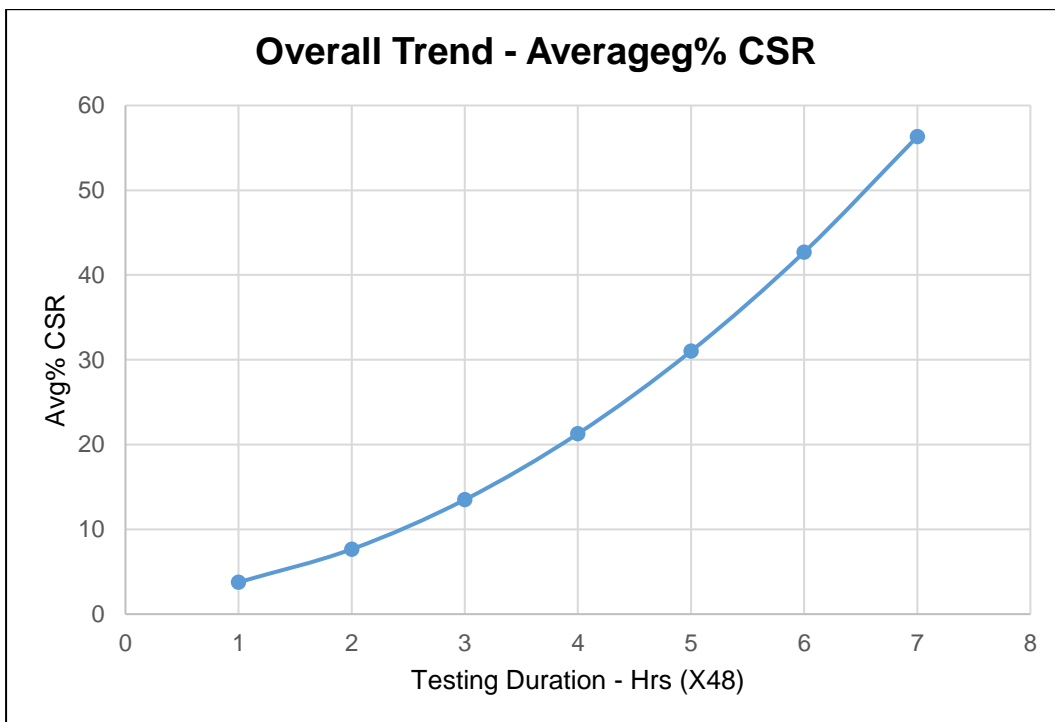


Fig-3.33: The overall trend of average% of CSR is indicated by the curve.

Relationship of Solution pH and HIC

The following section describes trend analysis for indicating effect of pH on HIC as found in each set of tests for A, D and E at different test conditions.

Effect of pH on HIC for sample – A

Solution pH can be considered as one of the main environmental variables which has significant effect on corrosion and HIC in steels. In the following section, the effect of pH on HIC has been evaluated from various data obtained in 26 number of tests for sample A, D and E (ref: table-3.4).

Following table-3.18 indicates average percentage of CLR, CTR and CSR values obtained in the tests for samples A at pH 1, 2.7 and 4 for testing durations of 48 Hrs, 96 Hrs., and 144 Hrs.

Table-3.17: Average percentage of CLR, CTR and CSR are indicated for metal-A

	AVERAGE% CLR / CTR / CSR FOR METAL SAMPLE – A								
SAMPLE-A	pH-1	pH-1	pH-1	pH-2.7	PH-2.7	pH-2.7	pH-4	PH-4	pH-4
HRS x 48	1	2	3	1	2	3	1	2	3
CLR	16.90	12.96	8.66	16.30	15.87	9.13	1.93	3.52	24.58
CTR	2.39	1.65	1.74	4.63	2.92	1.43	0.23	0.37	7.14
CSR	0.22	0.28	0.13	0.63	0.39	0.14	0.01	0.02	0.97

Effect of pH has been analyzed for each pH condition. The trends have been evaluated considering all test durations in each test condition.

Table-3.18: Average percentage of HIC indicators (CLR, CTR & CSR) for sample-A at each pH condition as found in tests.

SAMPLE – A					
pH	HRS	AVERAGE%			
		HIC IN EACH pH & HR			HIC IN EACH pH CONDITION
		CLR	CTR	CSR	CLR / CTR / CSR
1	48	16.9	2.39	0.22	12.84 / 1.92 / 0.21
	96	12.96	1.65	0.28	
	144	8.66	1.74	0.13	
2.7	48	16.3	4.63	0.63	13.76 / 2.99 / 0.38
	96	15.87	2.92	0.39	
	144	9.13	1.43	0.14	
4	48	1.93	0.23	0.01	10.01 / 2.58 / 0.33
	96	3.52	0.37	0.02	
	144	24.58	7.14	0.97	

Table-3.19: Average values of CLR, CTR and CSR are summarized in below table for graphical representation.

SAMPLE-A			
pH	CLR	CTR	CSR
1	12.84	1.92	0.21
2.7	13.76	2.99	0.38
4	10.01	2.58	0.33

Following curves in figure 3.34 indicate trend for CLR, CTR and CSR for sample A.

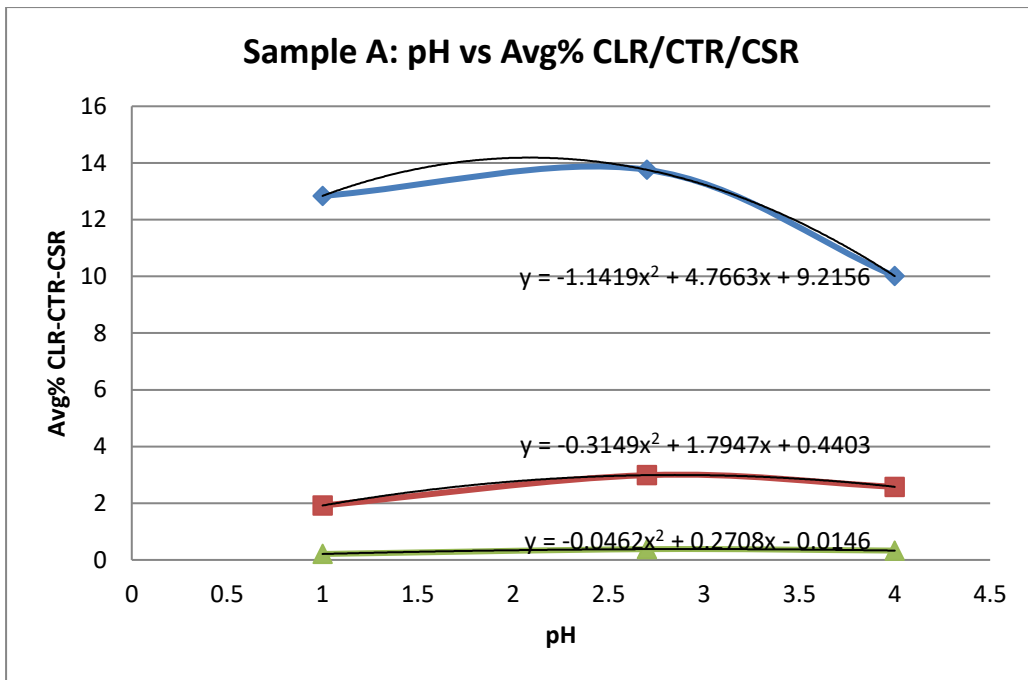


Figure 3.34: The values of HIC parameters i.e., average percentage of CLR, CTR and CSR, as per table-3.21 are presented in the curves.

Trend of above curves for CLR, CTR and CSR from figure 3.34 are further analyzed in following diagrams in figure 3.35-3.37.

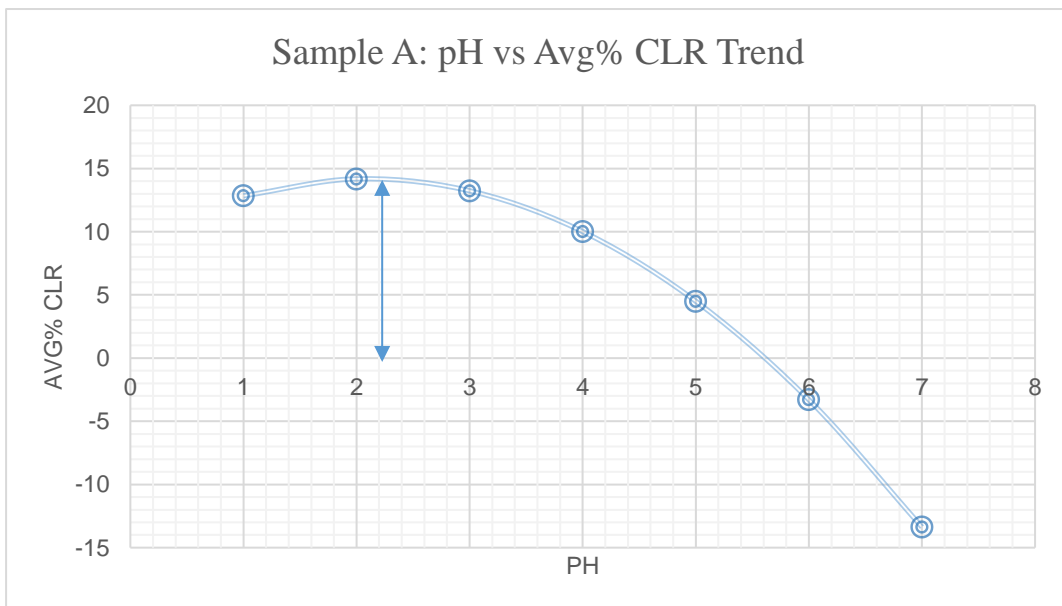


Figure 3.35: Showing trend of average percentage of CLR with respect to pH progression as derived from figure 3.34.

The trend shows that maximum average CLR value is reached at approximately pH 2.3, the CLR value declines with increase of further pH.

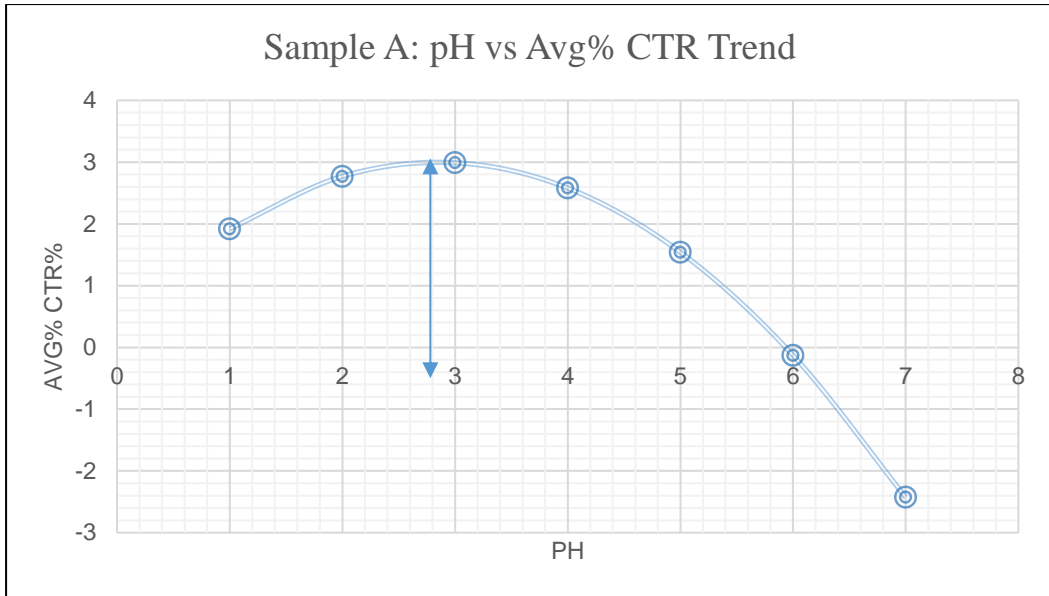


Figure 3.36: Showing trend of average percentage of CTR with respect to pH progression as derived from figure 3.34.

The trend shows that maximum average CTR value is reached at approximately pH 2.8, the CTR value declines with increase of further pH.

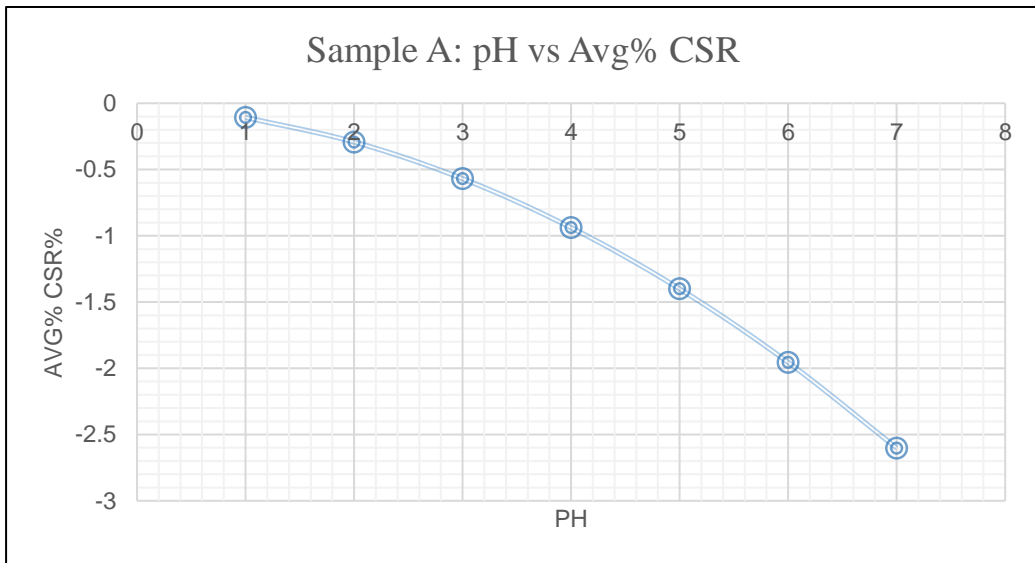


Figure 3.37: Showing trend of average percentage of CSR with respect to pH progression as derived from figure 3.34.

The trend shows an outright decline of CSR with respect to progression of pH starting from pH 1.

Effect of pH on HIC for Sample - D

Following table-3.21 indicates average percentage of CLR, CTR and CSR values obtained in the tests for sample D for pH 1, 2.7 and 4 for testing durations of 48 Hrs, 96 Hrs., and 144 Hrs.

Table3.20: Showing average percentage of CLR, CTR and CSR for sample D.

AVERAGE PERCENTAGE OF CLR/CTR/CSR FOR METAL – D									
SAMPLE - D	pH-1	pH-1	pH-1	pH-2.7	pH-2.7	pH-2.7	pH-4	pH-4	pH-4
HRS x 48	1	2	3	1	2	3	1	2	3
CLR	19.11	3.06	6.44	1.43	22.58	72.86	2.35	12.67	60.47
CTR	8.78	1.38	17.31	0.3	11.24	24.16	0.86	4.18	15.87
CSR	0.68	0.07	0.26	0.01	2.03	8.82	0.03	0.83	8.84

Effect of pH has been analyzed for each pH condition. The trends have been evaluated considering all test durations in each test condition.

Table-3.21: Average percentage of HIC indicators (CLR, CTR & CSR) for sample-D at each pH condition as found in tests are mentioned in the table.

SAMPLE – D					
		AVERAGE%			
pH	HRS	HIC IN EACH pH & HR			HIC IN EACH pH CONDITION
		CLR	CTR	CSR	CLR / CTR / CSR
1	48	19.11	8.78	0.68	
1	96	3.06	1.38	0.07	9.54 / 9.16 / 0.34
1	144	6.44	17.31	0.26	
2.7	48	1.43	0.3	0.01	
2.7	96	22.58	11.24	2.03	32.29 / 11.90 / 3.62
2.7	144	72.86	24.16	8.82	
4	48	2.35	0.86	0.03	
4	96	12.67	4.18	0.83	25.16 / 6.97 / 3.23
4	144	60.47	15.87	8.84	

Table-3.22: Showing overall average percentage of CLR, CTR and CSR for sample-D, summarized from table-3.23 for graphical presentation.

SAMPLE-D			
pH	CLR	CTR	CSR
1	9.54	9.16	0.34
2.7	32.29	11.9	3.62
4	25.16	6.97	3.23

Curves in figure 3.38 indicate trend of CLR, CTR and CSR for sample-D.

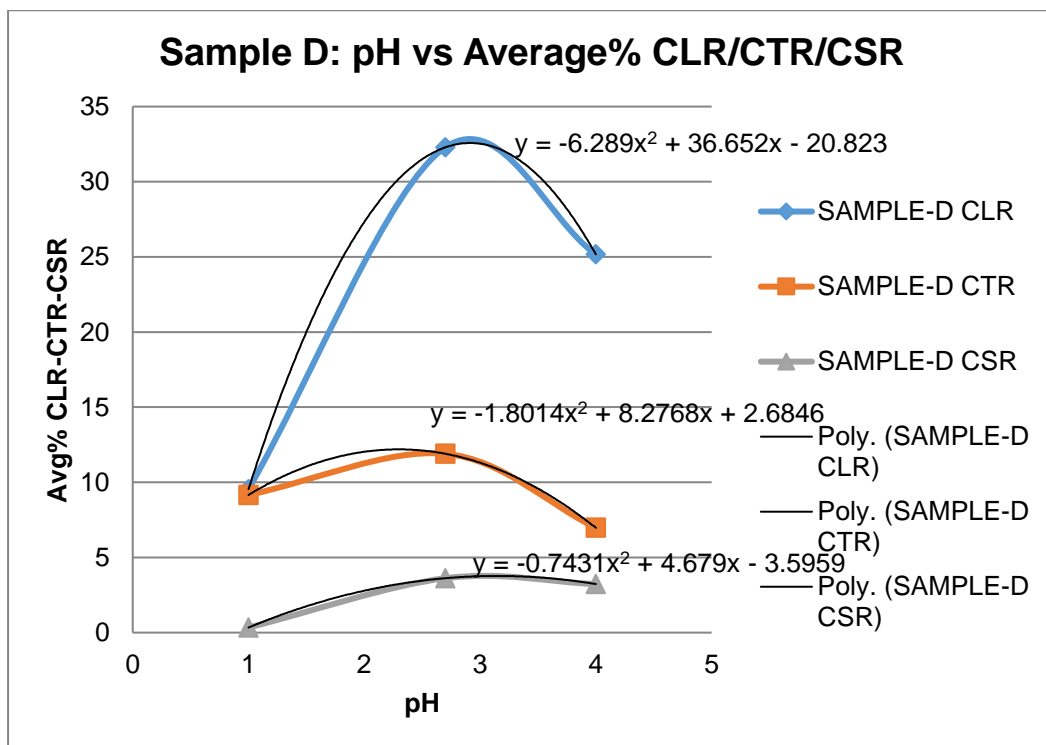


Figure 3.38: Shows HIC in terms of average CLR%, CTR% and CSR% tested in tested in pH 1, 2.7 and 4 condition as per table-3.24. X-axis representing pH of the test solution.

The trend of CLR, CTR and CSR are further analyzed in figure 3.39-3.41 below.

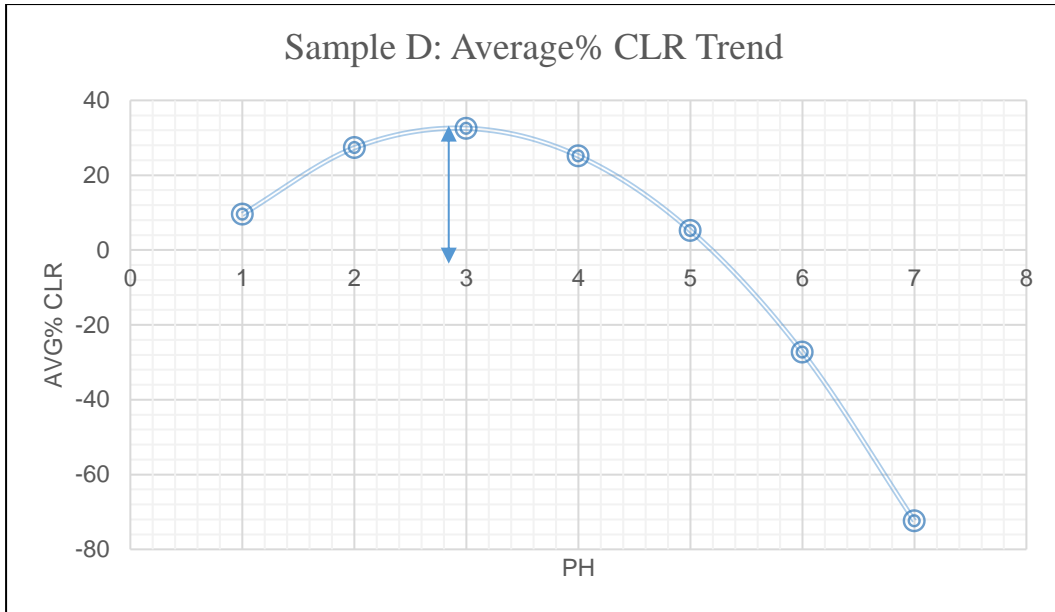


Figure 3.39: Showing trend of average percentage of CLR with respect to pH progression as derived from figure 3.24.

The trend shows that maximum average CLR value is reached at approximately pH 2.8, the CLR value declines with increase of further pH.

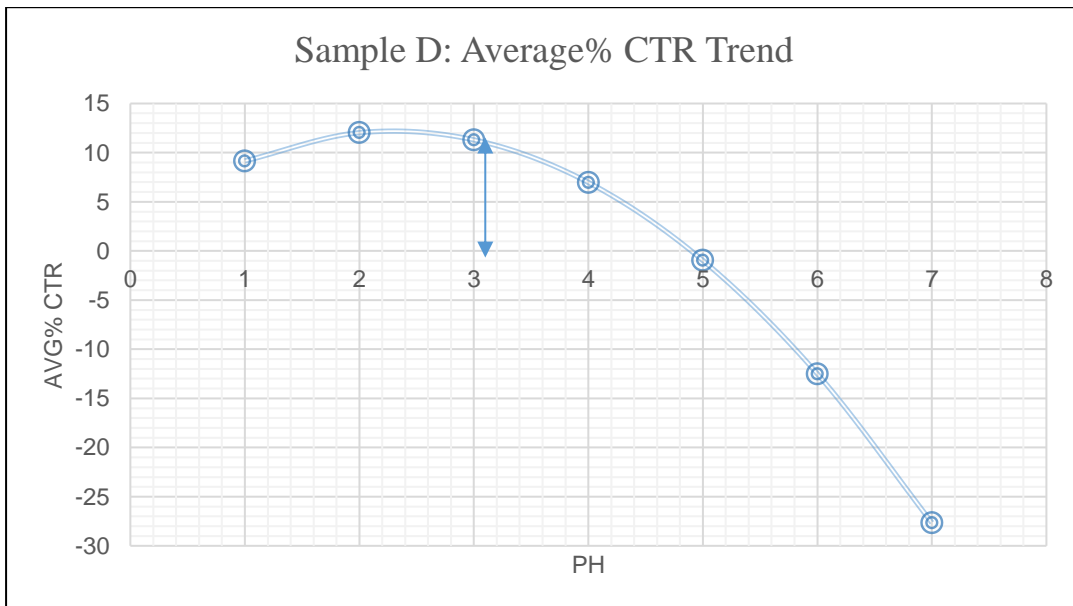


Figure 3.40: Showing trend of average percentage of CTR with respect to pH progression as derived from figure 3.24.

The trend shows that maximum average CTR value is reached at approximately pH 2.4, the CTR value declines with increase of further pH.

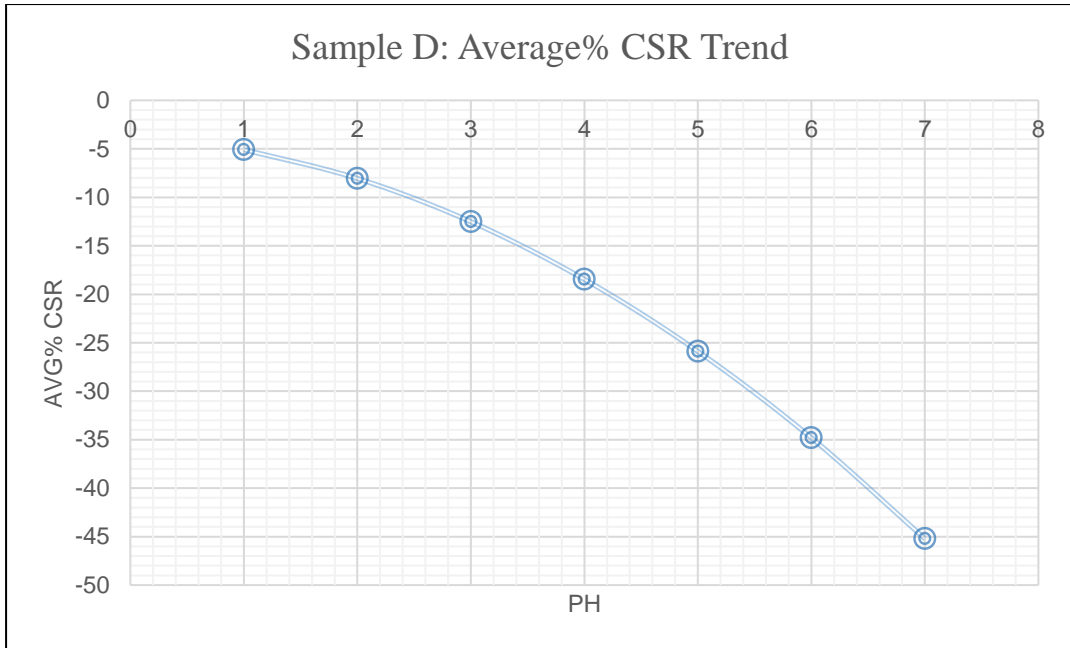


Figure 3.41: showing trend of average percentage of CSR with respect to pH progression as derived from figure 3.24. The trend shows an outright decline of avg% CSR value with increase of pH.

EFFECT OF pH ON HIC FOR SAMPLE – E

Table-3.23: Average percentage of CLR, CTR and CSR for sample E

SAMPLE-E	AVERAGE PERCENTAGE OF CLR/CTR/CSR FOR METAL – E								
	pH-1	pH-1	pH-1	pH-2.7	pH-2.7	pH-2.7	pH-4	pH-4	pH-4
HRS X 48	1	2	3	1	2	3	1	2	3
CLR	8.09	27.38	26.69	4.7	24.96	33.55	16.37	32.59	--
CTR	0.74	2.15	4.71	0.36	2.65	2.57	1.07	3.05	--
CSR	0.05	0.33	0.84	0.05	0.37	0.34	0.12	0.44	--

Table-3.24: Average percentage of HIC indicators (CLR, CTR & CSR) for sample-E at each pH condition as found in tests are mentioned in the table.

SAMPLE – E					
pH	HRS	AVERAGE%			
		HIC IN EACH pH & HR			HIC IN EACH pH CONDITION
		CLR	CTR	CSR	CLR / CTR / CSR
	48	8.09	0.74	0.05	
1	96	27.38	2.15	0.33	20.72 / 2.53 / 0.40
	144	26.69	4.71	0.84	
	48	4.7	0.36	0.05	
2.7	96	24.96	2.65	0.37	21.07 / 1.86 / 0.25
	144	33.55	2.57	0.34	
	48	16.37	1.07	0.12	24.48 / 2.06 / 0.28
4	96	32.59	3.05	0.44	

Table-3.25: Showing overall average percentage of CLR, CTR and CSR for sample-E, summarized from table-3.26 for graphical presentation.

SAMPLE-E			
pH	CLR	CTR	CSR
1	20.72	2.53	0.4
2.7	21.07	1.86	0.25
4	24.48	2.06	0.28

Curves in figure 3.42 indicate trend of CLR, CTR and CSR for sample-E.

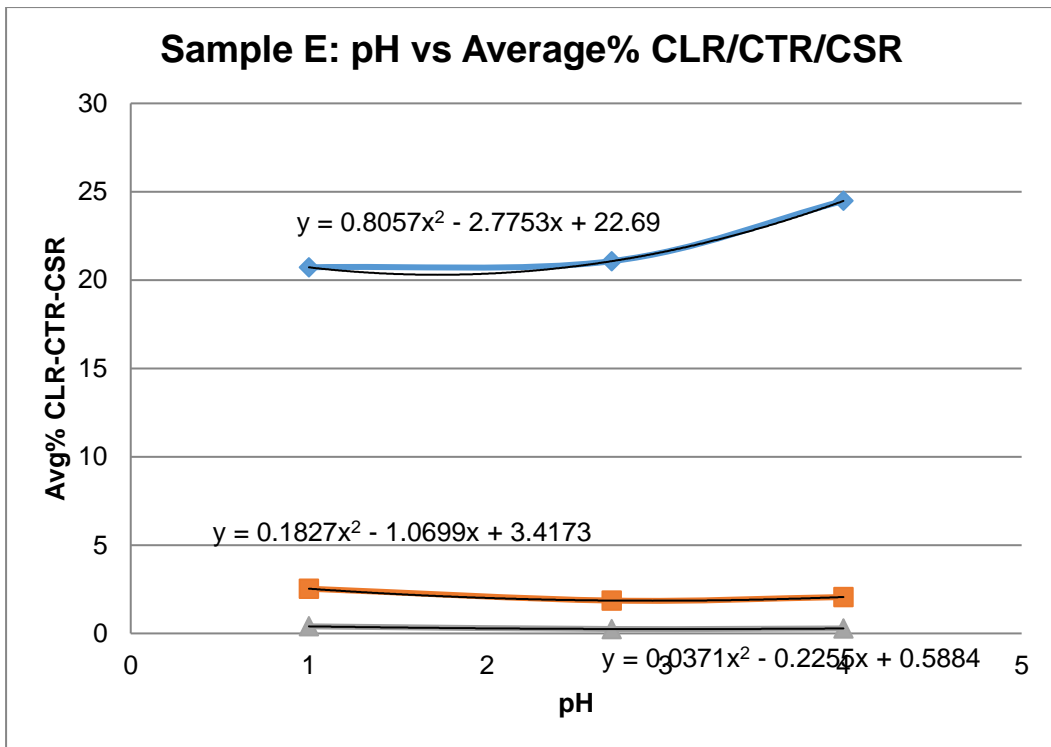


Figure 3.42: shows HIC in terms of average CLR%, CTR% and CSR% tested in tested in pH 1, 2.7 and 4 condition as per table-3.27. X-axis representing pH of the test solution.

The trend of CLR, CTR and CSR are further analyzed in figures 3.43 - 3.45 below.

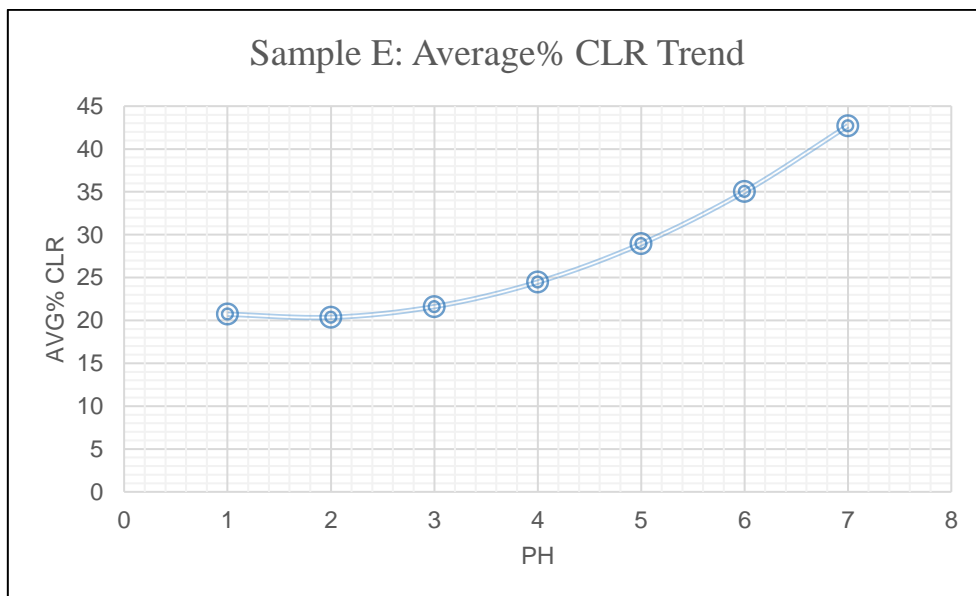


Figure 3.43: showing trend of average percentage of CLR with respect to pH progression as derived from figure 3.42.

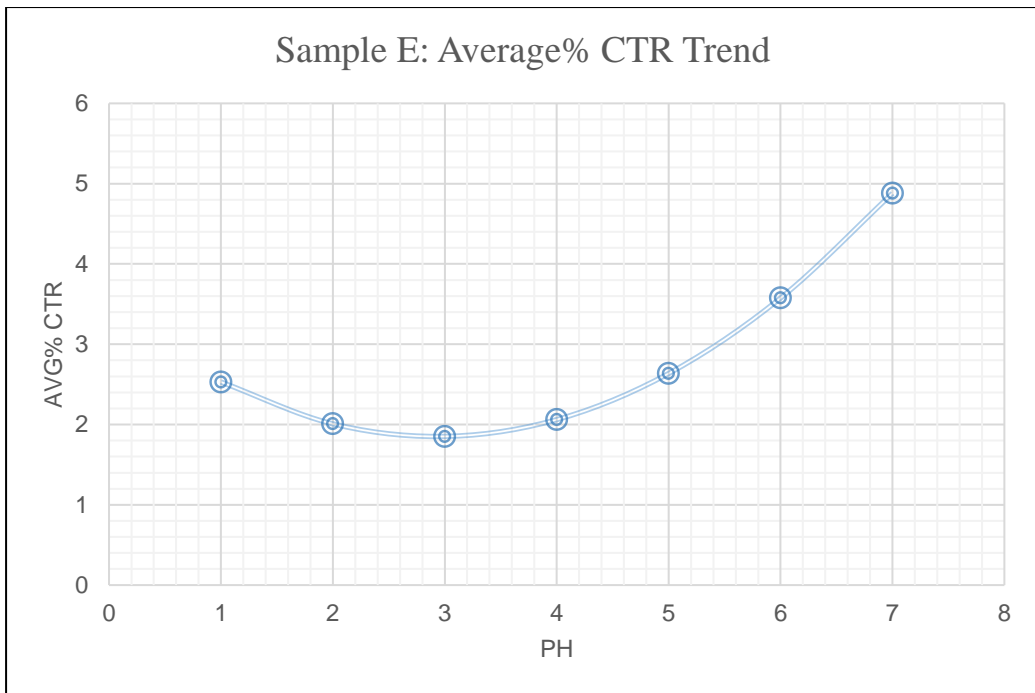


Figure 3.44: showing trend of average percentage of CTR with respect to pH progression as derived from figure 3.42.

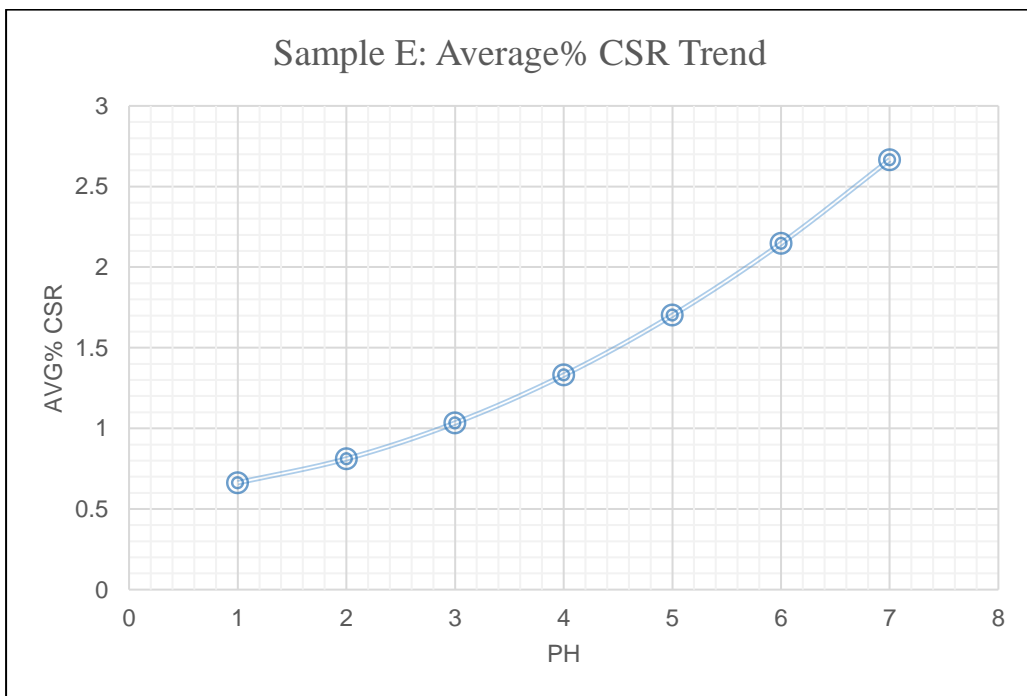


Figure 3.45: Trend of average percentage of CSR with respect to pH.

The trend curve for CLR% Average in figure 3.43, Shows increasing trend of average percentage of crack length with increase in pH. The locus follows parabolic curve in the overall trajectory.

The trend curve for CTR% Average in figure 3.44, Shows initial decrease in average percentage of crack thickness with increase in pH up to 2.8 (approx.), followed by increasing trend. The locus follows parabolic curve in the overall trajectory.

The trend curves for CSR% Average in figure 3.45, Shows outright increase in average percentage of crack sensitivity ratios with increase in pH.

Overall pH vs HIC

Overall effect of pH on HIC has been evaluated by summing-up effect of pH on metal samples-A, D and E and averaging the cumulative effect.

Effect of pH on Individual metal samples for differet duration of exposures are listed in tables 3.26 – 3.28.

Table-3.26: Effect of pH on 48 Hrs testing for metal samples A, D and E are mentioned in the table in terms of average perentages of CLR, CTR and CSR for each metal sample. Collective average of HIC parameters for the conditions for A-D-E are listed in the last column.

48 HRS pH-1				
	SAMPLE-A	SAMPLE-D	SAMPLE-E	AVERAGE
CLR AVG%	16.90	19.11	8.09	14.70
CTR AVG%	2.39	8.78	0.74	3.97
CSR AVG%	0.22	0.68	0.05	0.32
48 HRS pH-2.7				
CLR AVG%	16.30	1.43	4.70	7.48
CTR AVG%	4.63	0.30	0.36	1.76
CSR AVG%	0.63	0.01	0.05	0.23
48 HRS pH-4				
CLR AVG%	1.93	2.35	16.37	6.88
CTR AVG%	0.23	0.86	1.07	0.72
CSR AVG%	0.01	0.03	0.12	0.05

Table-3.27: Effect of pH on 96 Hrs testing for metal samples A, D and E are listed in the table in terms of average percentages of CLR, CTR and CSR for each metal sample.

96 HRS pH-1				
	SAMPLE-A	SAMPLE-D	SAMPLE-E	AVERAGE
CLR AVG%	12.96	3.06	27.38	14.47
CTR AVG%	1.65	1.38	2.15	1.73
CSR AVG%	0.28	0.07	0.33	0.23
96 HRS pH-2.7				
CLR AVG%	15.87	22.58	24.96	21.14
CTR AVG%	2.92	11.24	2.65	5.60
CSR AVG%	0.39	2.03	0.37	0.93
96 HRS pH-4				
CLR AVG%	3.52	12.67	32.59	16.26
CTR AVG%	0.37	4.18	3.05	2.53
CSR AVG%	0.02	0.83	0.44	0.43

Table-3.28: Effect of pH on 144 Hrs testing for metal samples A, D and E are listed in the table in terms of average percentages of CLR, CTR and CSR.

144 HRS pH-1				
	SAMPLE-A	SAMPLE-D	SAMPLE-E	AVERAGE
CLR AVG%	8.66	6.44	26.69	13.93
CTR AVG%	1.74	17.31	4.71	7.92
CSR AVG%	0.13	0.26	0.84	0.41
144 HRS pH-2.7				
CLR AVG%	9.13	72.86	33.55	38.51
CTR AVG%	1.43	24.16	2.57	9.39
CSR AVG%	0.14	8.82	0.34	3.10
144 HRS pH-4				
CLR AVG%	24.58	60.47		42.53
CTR AVG%	7.14	15.87		11.51
CSR AVG%	0.97	8.84		4.91

The over-all average values of HIC parameters for pH-1, pH-2.7 and pH 4 are taken from above tables 3.27-3.29 are reflected in following table 3.30 for all metal samples of A, D and E.

Table-3.29: Overall average values of CLR, CTR and CSR for samples A-D-E are listed in table.

SAMPLE A-D-E							
pH	HRS	AVERAGE%					
		HIC IN EACH pH & HR			HIC IN EACH pH CONDITION		
		CLR	CTR	CSR	CLR	CTR	CSR
1	48	14.7	3.97	0.32	14.37	4.54	0.32
	96	14.47	1.73	0.23			
	144	13.93	7.92	0.41			
2.7	48	7.48	1.76	0.23	22.38	5.58	1.42
	96	21.14	5.6	0.93			
	144	38.51	9.39	3.1			
4	48	6.88	0.72	0.05	21.89	4.92	1.80
	96	16.26	2.53	0.43			
	144	42.53	11.51	4.91			

Table 3.30: Overall average values of CLR, CTR and CSR for all samples of A-D_E in each pH condition are listed in table.

OVERALL	CLR AVG%	CTR AVG%	CSR AVG%
pH-1	14.37	4.54	0.32
pH-2.7	22.38	5.58	1.42
pH-4	21.89	4.92	1.80

The following curves in Figure 3.46, show overall HIC parametrs as measured in testing for samples of A-D-E.

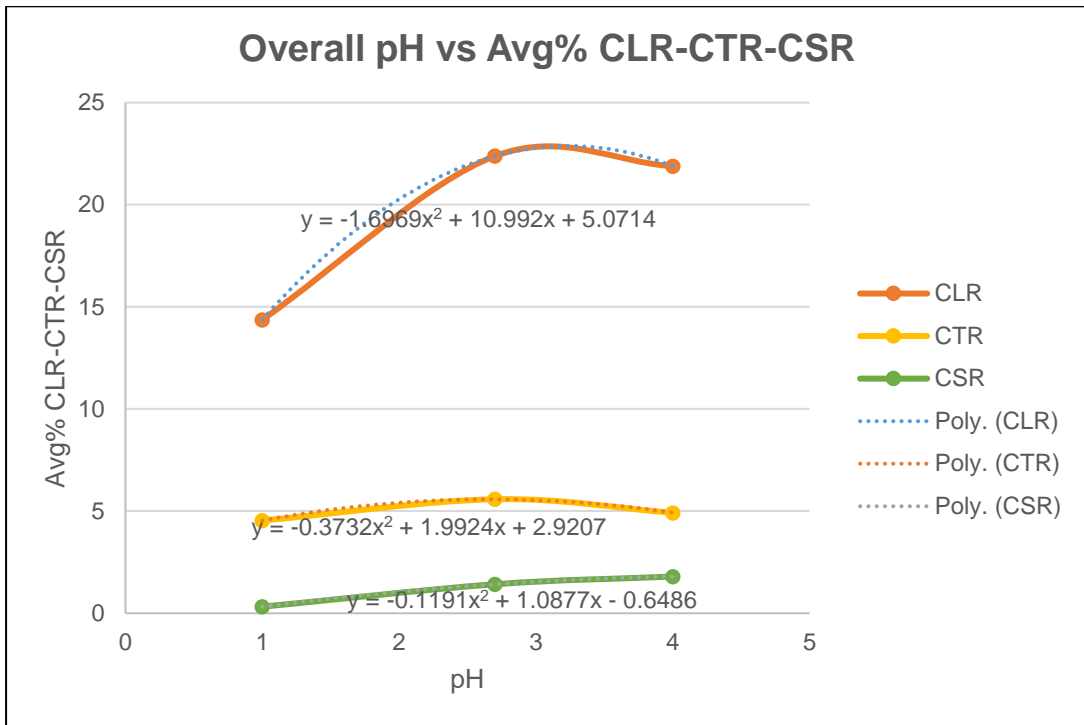


Figure 3.46: Show overall HIC parametrs for samples of A-D-E.

The trend of CLR, CTR and CSR are further analyzed in following curves (figure 3.47 - 3.49).

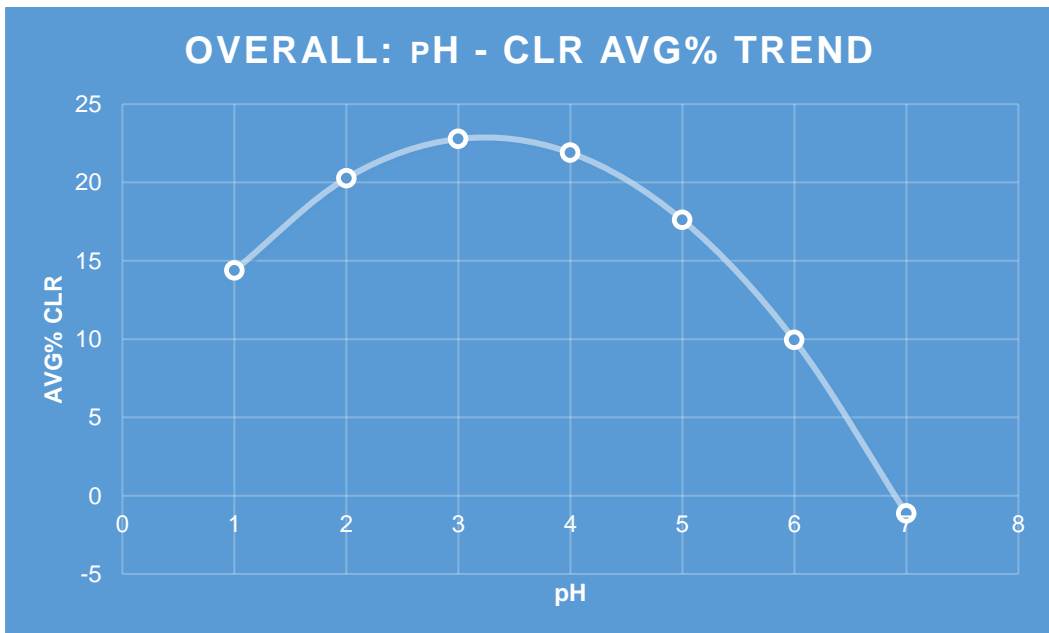


Figure 3.47: Showing overall trend of CLR as found in HIC testing

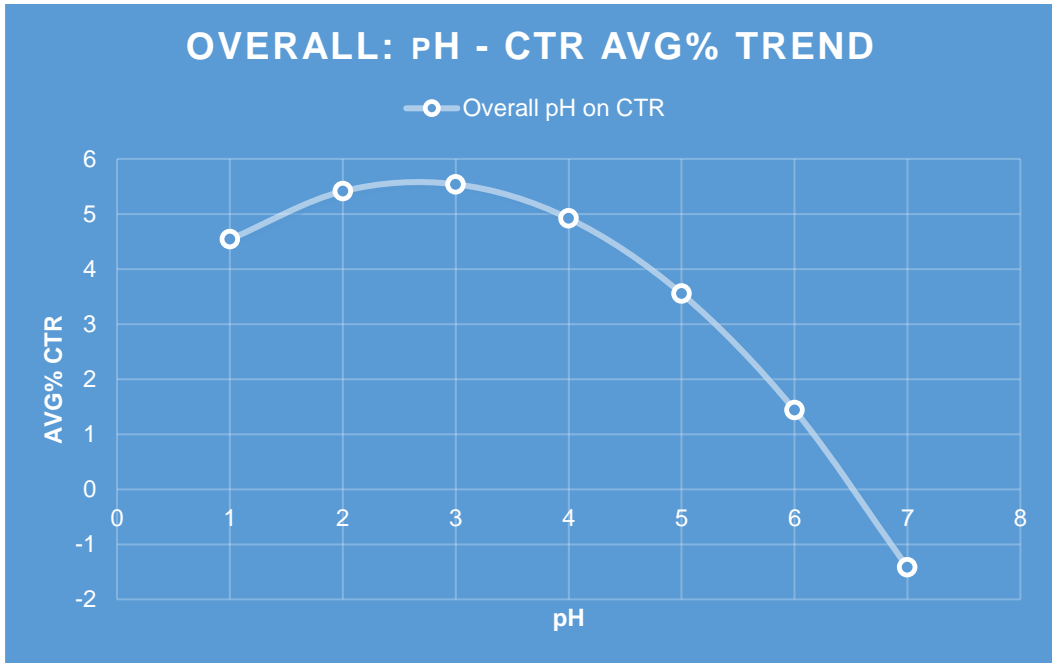


Figure 3.48: Showing overall trend of CTR as found in HIC testing

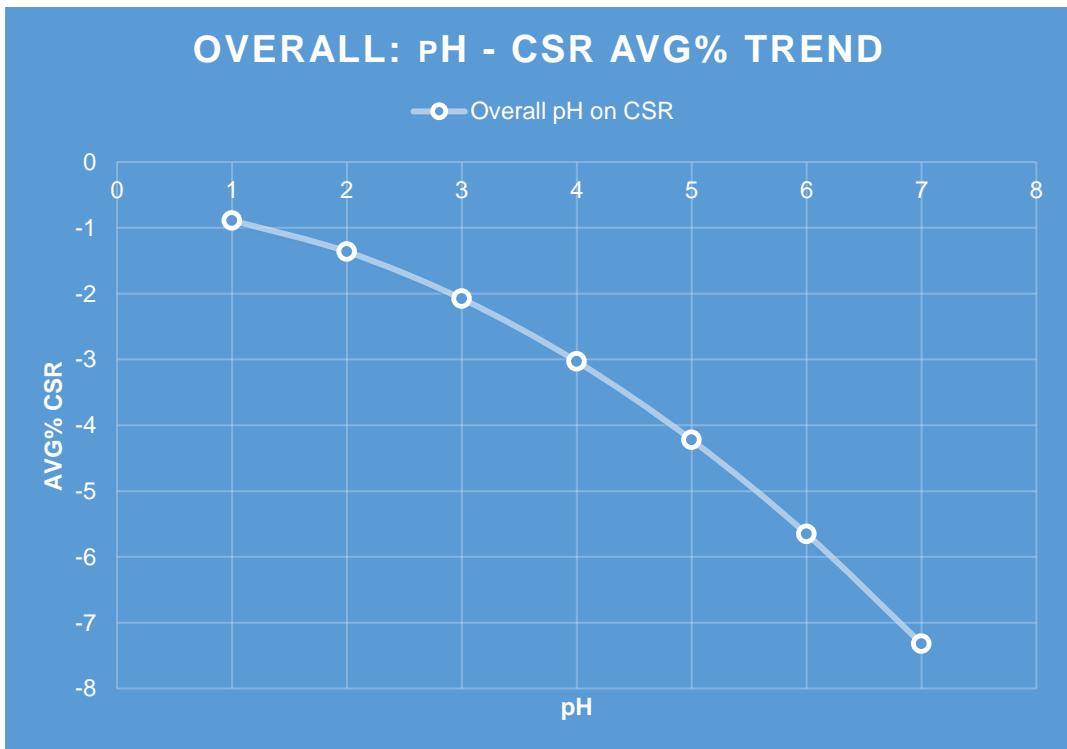


Figure 3.49: Showing overall trend of CSR as found in HIC testing

Verification of Crack Length by Ultrasonic Technique (UT)

The crack length which is checked for calculating Crack Length ratio (CLR) according to NACE TM 0284, is measured on the sectioned surfaces of specimens which enumerate a statistical measurement of cracks in specimens, however, the true crack length of HIC are planer cracks along the lenth of the specimens which are not required to be measured as per procedure of NACE TM 0284. Therefore, attempt was made to check true HIC crack length of each specimen by Ultra-Sonic Method (scan-A) from the surface perpendicular to the rollong plane and determine CLR and compare observed CLR obtained by NACE TM 0284 mthod. Following table-3.33 Shows total and average UT crack lengths of specimen A, D and E tested for 48 hrs, 96 hrs and 144 hrs at pH 1, 2.7 and 4 conditions.

Table-3.31: The crack lengths are measured by UT scanning of each sample of A-D-E before sectining as mentioned in the table.

		UT - CRACK LENGTH FOR EACH TEST										
		pH-1			pH-2.7			pH-4				
HRS	48	96	144		48	96	144		48	96	144	
SAMPLE #	A-1	A-2	A-3		A-4	A-5	A-6		A-7	A-8	A-9	
UT-CL (MM)	218	143	244		237	89	133		24	54	233	
UT-CLR	0.73	0.48	0.81		0.79	0.30	0.44		0.08	0.18	0.78	
TOTAL UT-CL				605				459				311
TOTAL UT-CLR				0.67				0.51				0.35
SAMPLE #	D-1	D-2	D-3		D-4	D-5	D-6		D-7	D-8	D-9	
UT-CL (MM)	145	53	213		41	186	300		45	57	174	(D9:2sp avg)

UT-CLR	0.48	0.18	0.71		0.14	0.62	1.00		0.15	0.19	0.87	
TOTAL UT-CL				411				527				276
TOTAL UT-CLR				0.46				0.59				0.35
SAMPLE #	E-1	E-2	E-3		E-4	E-5	E-6		E-7	E-8	(no test)	
UT-CL (MM)	187	216	244		75	251	300		289	300		
UT-CLR	0.62	0.72	0.81		0.25	0.84	1.00		0.96	1.00		
TOTAL UT-CL				647				626				589
TOTAL UT-CLR				0.72				0.70				0.98

Following table 3.32 Shows UT Crack Length Ratios of specimen A, D and E tested for 48 hrs, 96 hrs and 144 hrs at pH 1, 2.7 and 4 conditions. Data summarized from table-3.31.

able-3.32: UT crack length ratios summarized from table 3.31.

SAMPLE ID	UT - CRACK LENGTH RATIO FOR EACH TEST											
	A				D				E			
	48 HRS	96 HRS	144 HRS	A AVG	48 HRS	96 HRS	144 HRS	D AVG%	48 HRS	96 HRS	144 HRS	E AVG%
pH	CLR- 1	CLR- 2	CLR- 3		CLR- 1	CLR- 2	CLR- 3		CLR- 1	CLR- 2	CLR- 3	
1	0.73	0.48	0.81	0.67	0.48	0.18	0.71	0.46	0.62	0.72	0.81	0.72
2.7	0.79	0.30	0.44	0.51	0.14	0.62	1.00	0.59	0.25	0.84	1.00	0.7
4	0.08	0.18	0.78	0.35	0.15	0.19	0.87	0.35	0.96	1.00	-	0.98
Overall Average				0.51				0.46				0.8

Table-3.33: Average UT crack length ratios for each test duration (HRS) are summarized for sample A-D-E and overall average from table 3.32.

UT MEASUREMENT				
HRS	AVERAGE CLR			OVERALL CLR AVG
	A	D	E	
48	0.53	0.26	0.61	0.46
96	0.32	0.33	0.85	0.50
144	0.68	0.86	0.91	0.81

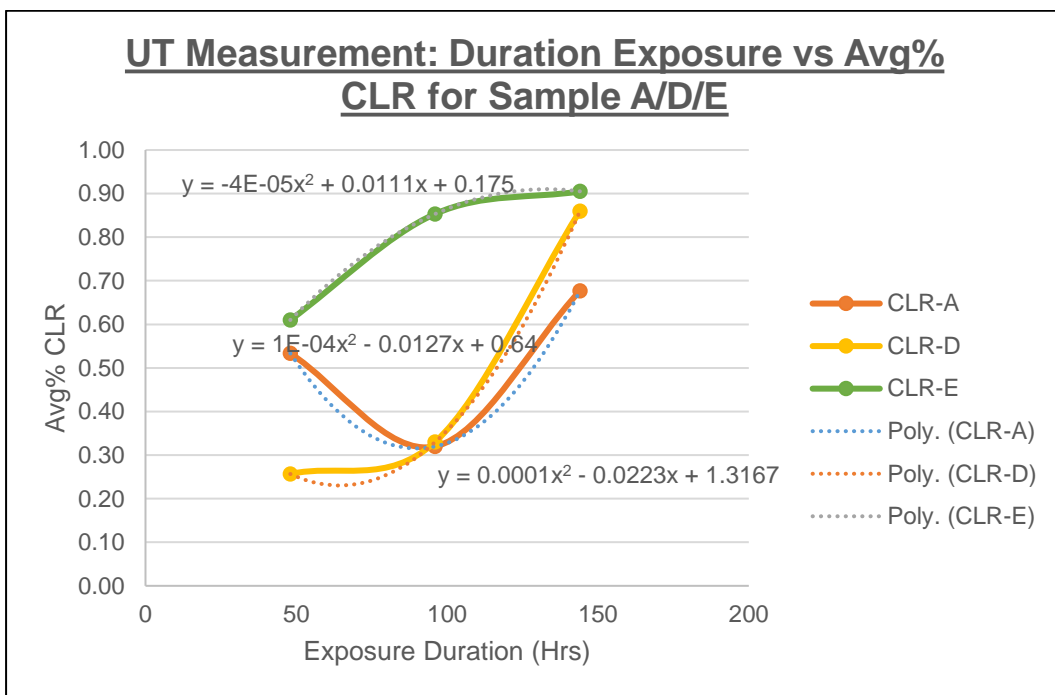


Figure 3.50: CLR by UT for sample A-D-E plotted with respect to duration of exposure.

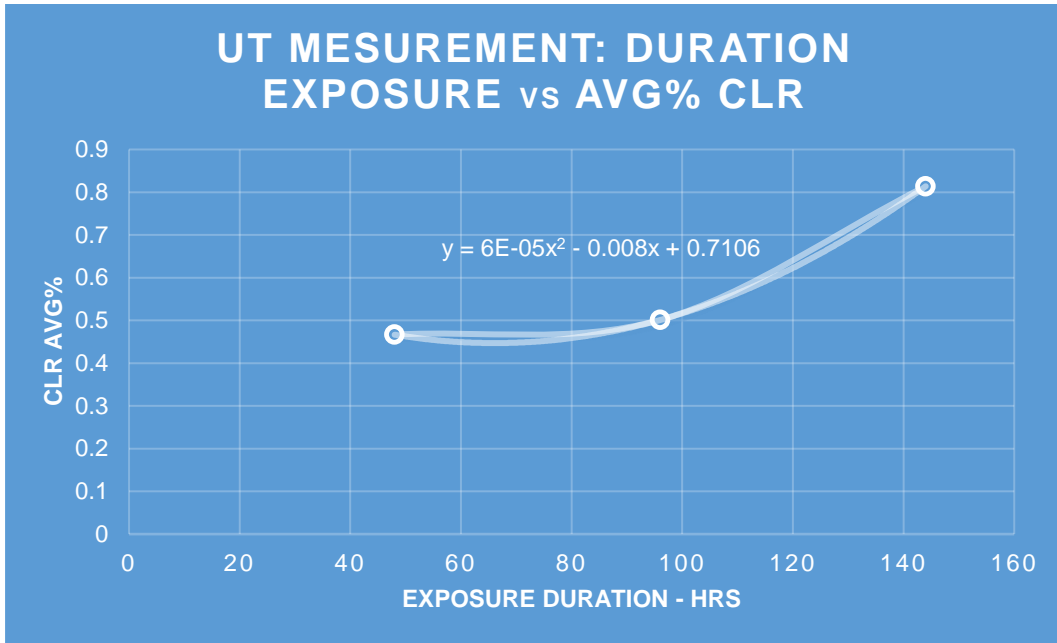


Figure 3.51: Overall average UT crack length ratio plotted with respect to duration of exposure for sample A-D-E.

Table-3.34: Average UT crack length ratios for each pH condition are summarized for sample A-D-E, including overall average from table 3.33.

UT MEASUREMENT				
pH	AVERAGE CLR			OVERALL CLR
	A	D	E	AVG
1	0.67	0.46	0.72	0.62
2.7	0.51	0.59	0.7	0.60
4	0.35	0.35	0.98	0.56

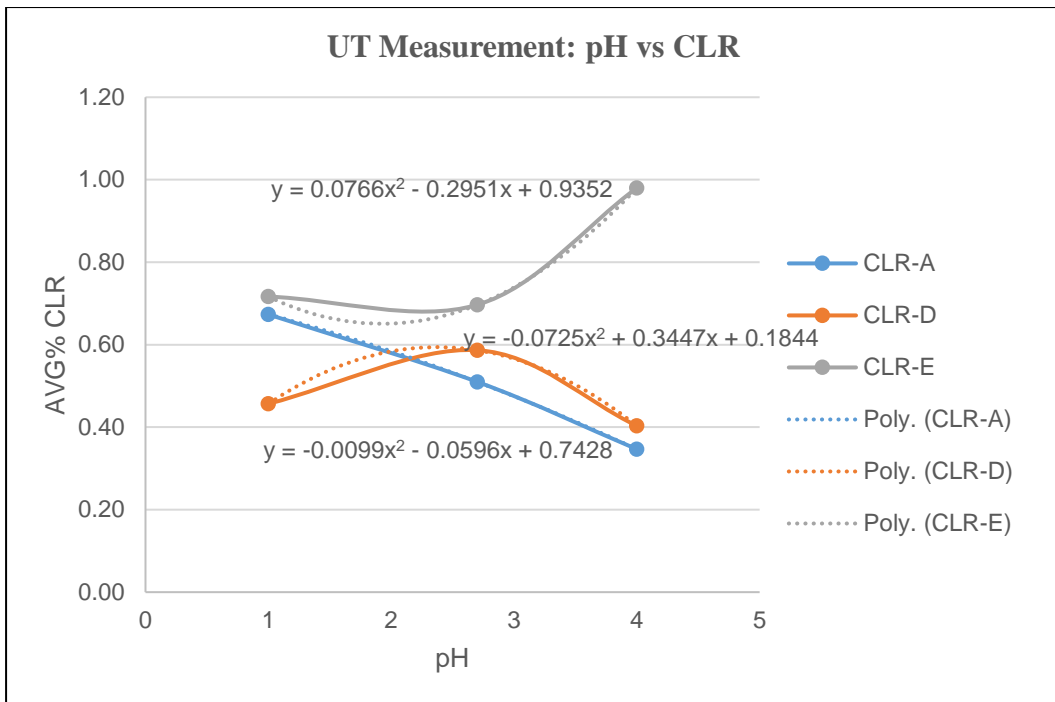


Figure 3.52: CLR measured by UT for sample A-D-E plotted with respect to each pH condition.

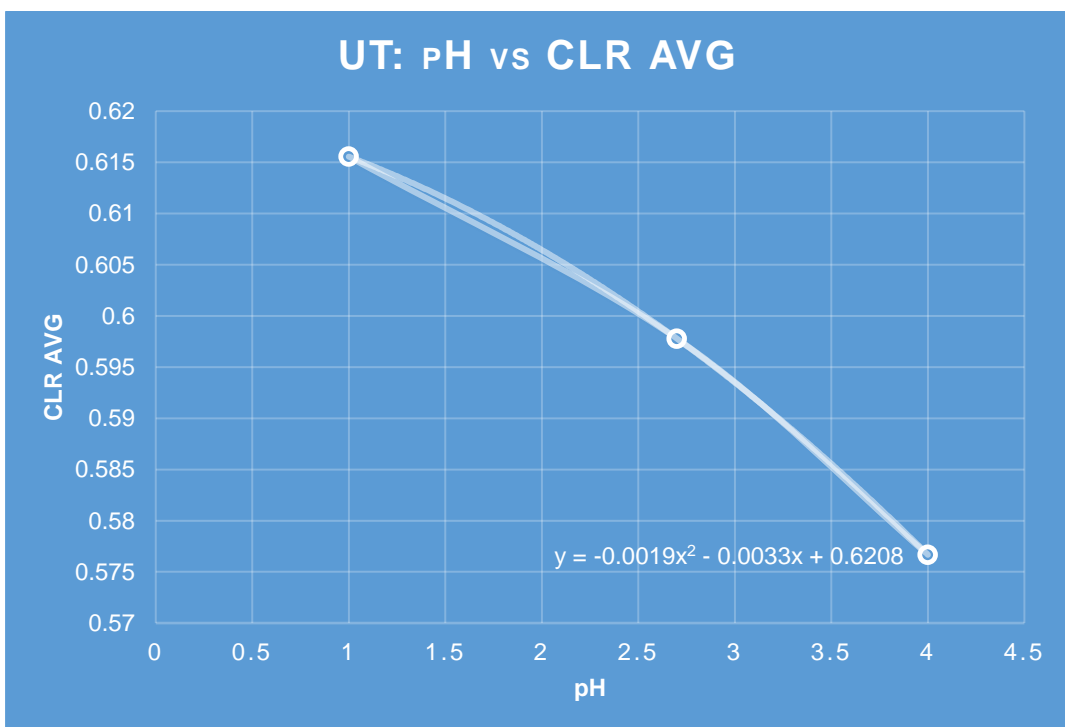


Figure 3.53: Overall average UT crack length ratio plotted with respect to overall pH condition for sample A-D-E.

In following table and curve, comparison has been made among average CLR values found by different methodologies, i.e., Duration of Exposure, pH of solution, and UT measurement described in previous sections.

Table 3.35: Average crack lengths (CLR) as found with respect to Duration of Exposure, pH of solution, and UT measurement are mentioned in table.

AVERAGE CLR			
	HRS-CLR	pH-CLR	UT-CLR
D	22.33	22.33	46.6
A	12.2	12.2	51
E	22.71	22.09	80

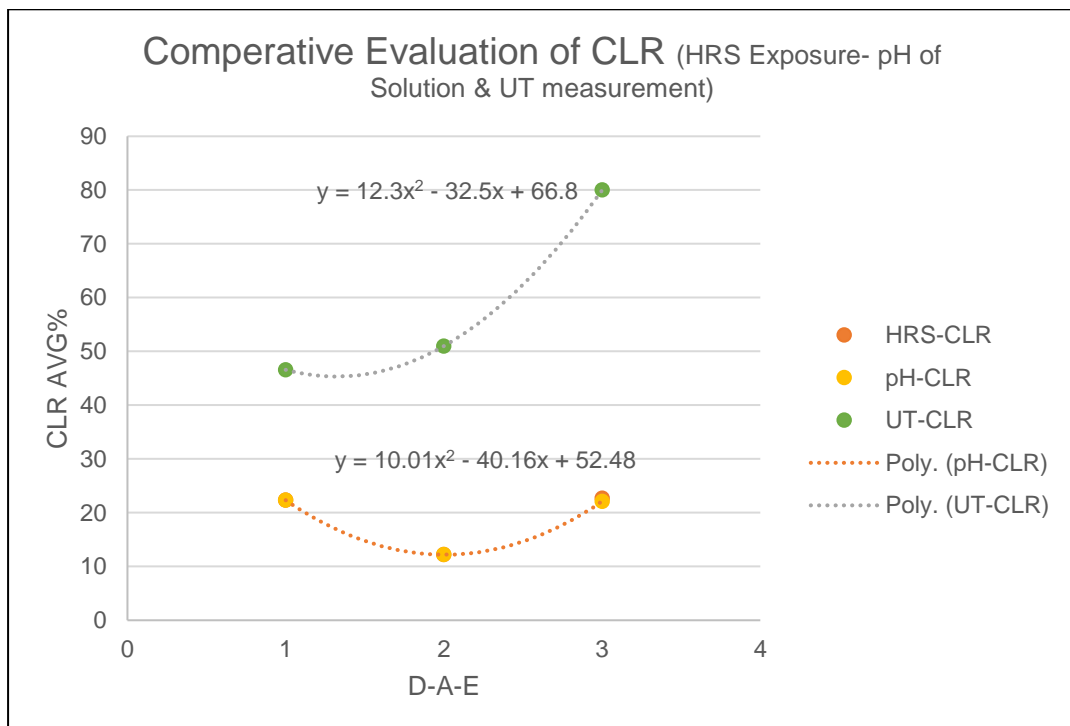


Figure 3.54: Comparative evaluation of CLR as measured in test for (1) Duration of Exposure (2) pH of solution and (3) Measured by UT is shown in curves

Tensile Strength vs HIC

Relation of tensile strength with HIC has been evaluated with reference to HIC evaluation with respect to pH as well as, duration of exposure in following sections for sample A,D and E.

Table 3.36: HIC parameters (avg% CLR, CTR and CSR) calculations with reference to HRS of testing for sample A-D-E. The table prepared based on tables #3.9, 3.11 and 3.13.

AVERAGE HIC CALCULATIONS FOR SAMPLE A-D-E BASED ON HRS OF TESTING						
SAMPLE – A						
HRS	pH	AVERAGE%			EACH TEST HR AVERAGE	OVERALL TEST HRS AVERAGE
		CLR	CTR	CSR	CLR / CTR / CSR	CLR / CTR / CSR
	1	16.9	2.39	0.22		
48	2.7	16.3	4.63	0.63	11.71 / 2.41 / 0.29	
	4	1.93	0.23	0.01		
	1	12.96	1.65	0.28		
96	2.7	15.87	292	0.39	10.78 / 1.64 / 0.23	12.20 / 2.49 / 0.30
	4	3.52	0.37	0.02		
	1	8.66	1.74	0.13		
144	2.7	9.13	1.43	0.14	14.12 / 3.43 / 0.41	
	4	24.58	7.14	0.97		
SAMPLE – D						
HRS	pH	AVERAGE%			EACH TEST HR AVERAGE	OVERALL TEST HRS AVERAGE
		CLR	CTR	CSR	CLR / CTR / CSR	CLR / CTR / CSR
	1	19.11	8.78	0.68		
48	2.7	1.43	0.3	0.01	7.63 / 3.31 / 0.24	
	4	2.35	0.86	0.03		
	1	3.06	1.38	0.07		
96	2.7	22.58	11.24	2.03	12.77 / 5.6 / 0.97	22.33 / 9.34 / 2.39
	4	12.67	4.18	0.83		
	1	6.44	17.31	0.26		
144	2.7	72.86	24.16	8.82	46.59 / 19.11 / 5.97	
	4	60.47	15.87	8.84		
SAMPLE – E						

HRS	pH	AVERAGE%			EACH TEST HR AVERAGE	OVERALL TEST HRS AVERAGE
		CLR	CTR	CSR	CLR / CTR / CSR	CLR / CTR / CSR
	1	8.09	0.74	0.05		
48	2.7	4.7	0.36	0.05	9.72 / 0.72 / 0.073	
	4	16.37	1.07	0.12		
	1	27.38	2.15	0.33		
96	2.7	24.96	2.65	0.37	28.31 / 2.61 / 0.38	22.71 / 2.32 / 0.34
	4	32.59	3.05	0.44		
	1	26.69	4.71	0.84	30.12 / 3.64 / 0.59	
144	2.7	33.55	2.57	0.34		

Table-3.37: The overall average HIC parameters summarized along with tensile strength.

	CLR	CTR	CSR	TS/100
D	22.33	9.34	2.39	4.75
A	12.2	2.49	0.3	5.31
E	22.71	2.32	0.34	5.52

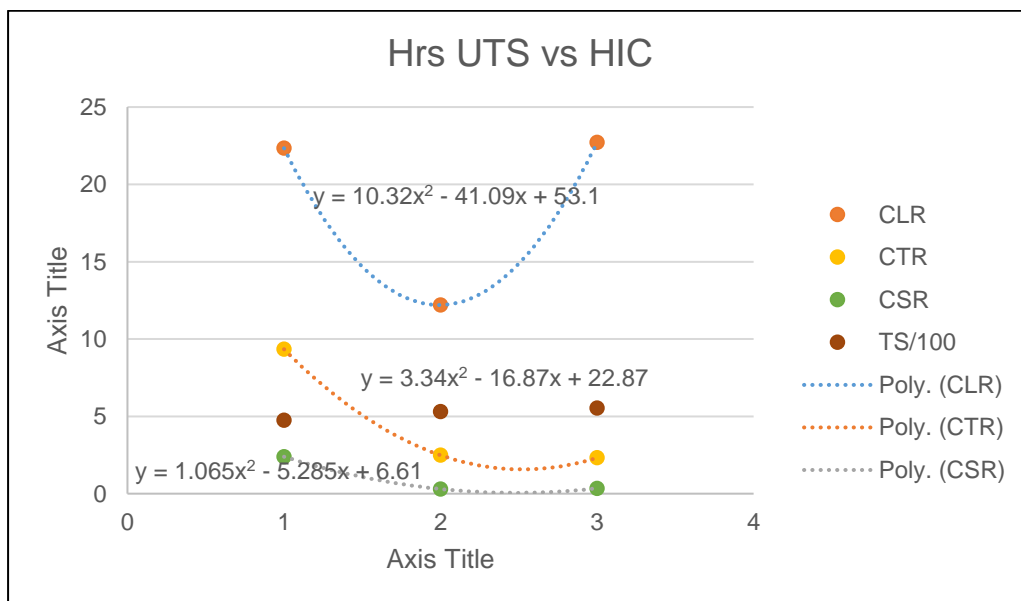


Figure 3.55: HIC parameters of sample D-A-E as found in tests against duration, are plotted against tensile values as per table 3.37

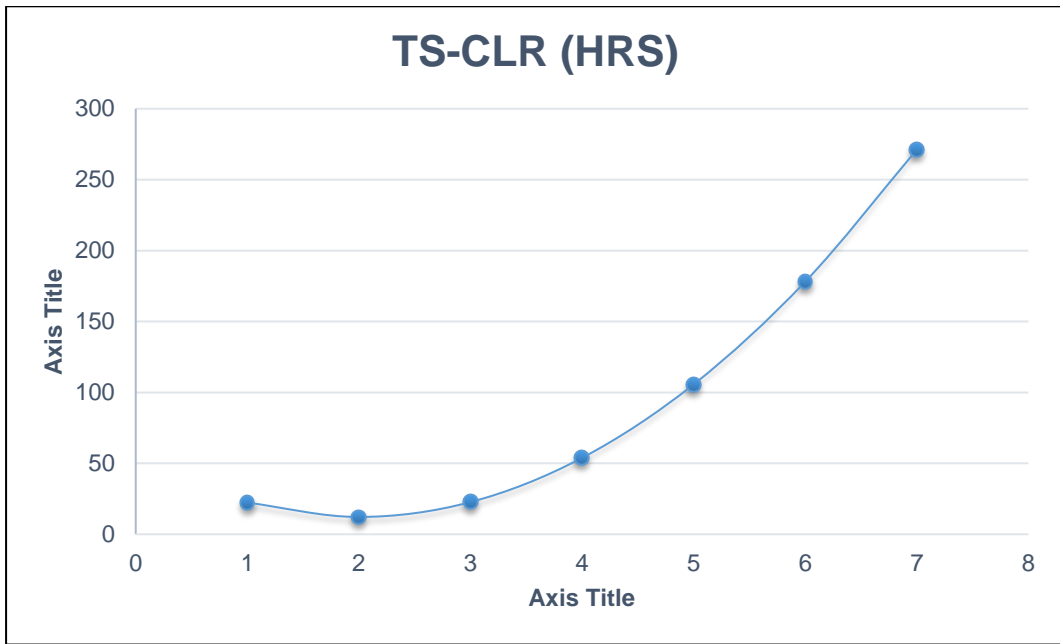


Figure 3.56: The curve shows CLR trend against tensile strength of D-A-E samples (divided by 100).

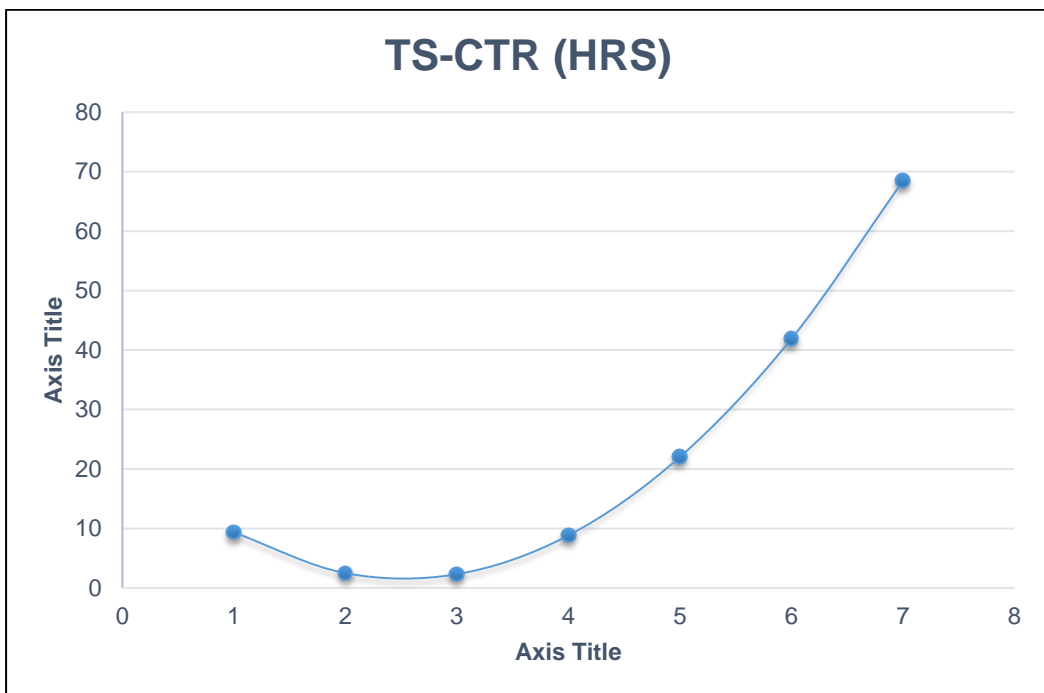


Figure 3.57: The curve shows CTR trend against tensile strength of D-A-E samples (divided by 100).

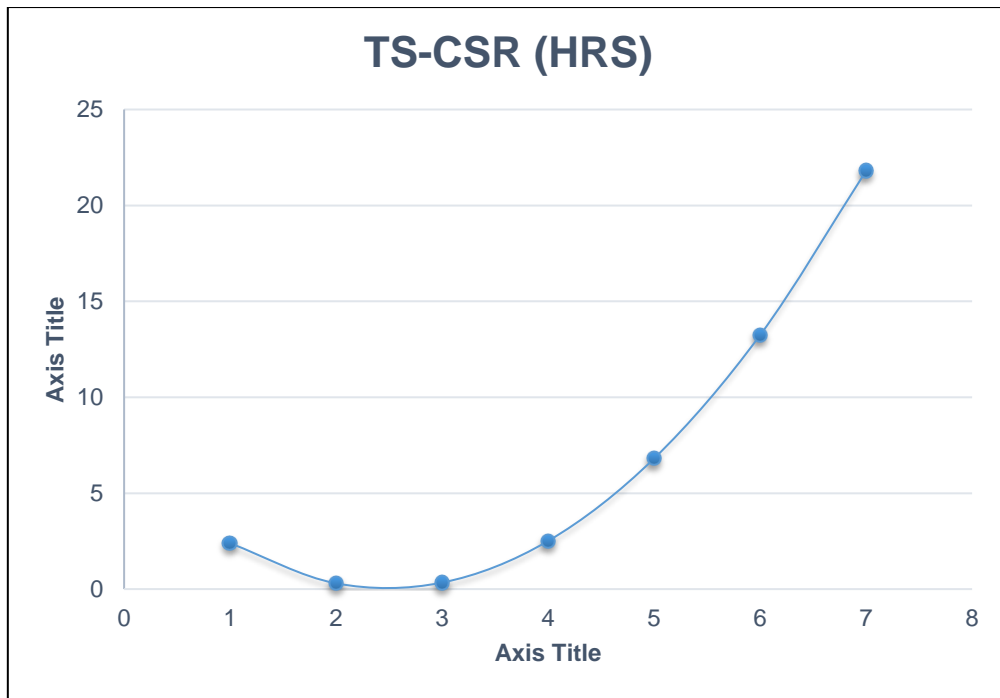


Figure 3.58: The curve shows CSR trend against tensile strength of D-A-E samples (divided by 100).

The trend analysis suggests that there has been reduction in HIC for sample 'A' i.e., at tensile strength of 5.31 N/mm², whereas HIC maintained upward trends on either directions, lower, as well as, higher tensile strengths than 5.31 N/mm².

Table 3.38: HIC parameters with reference to pH of testing for sample A-D-E are taken from previous sections ref table-3.18, 3.21 and 3.24.

AVERAGE HIC CALCULATIONS FOR SAMPLE A-D-E BASED ON pH OF TESTING										
SAMPLE – A										
pH	HRS	AVERAGE%								
		HIC IN EACH pH & HR								
		CLR	CTR	CSR	CLR	CTR	CSR	CLR	CTR	CSR
	48	16.9	2.39	0.22						
1	96	12.96	1.65	0.28	12.84	1.92	0.21			
	144	8.66	1.74	0.13						
	48	16.3	4.63	0.63						

2.7	96	15.87	292	0.39	13.76	2.99	0.38	12.20	2.50	0.31
	144	9.13	1.43	0.14						
	48	1.93	0.23	0.01						
4	96	3.52	0.37	0.02	10.01	2.58	0.33			
	144	24.58	7.14	0.97						
SAMPLE - D										
pH	HRS	AVERAGE%								
		HIC IN EACH pH & HR								
		CLR	CTR	CSR	CLR	CTR	CSR	CLR	CTR	CSR
	48	19.11	8.78	0.68						
1	96	3.06	1.38	0.07	9.54	9.16	0.34			
	144	6.44	17.31	0.26						
	48	1.43	0.3	0.01						
2.7	96	22.58	11.24	2.03	32.29	11.9	3.62	22.33	9.34	2.40
	144	72.86	24.16	8.82						
	48	2.35	0.86	0.03						
4	96	12.67	4.18	0.83	25.16	6.97	3.23			
	144	60.47	15.87	8.84						
SAMPLE - E										
pH	HRS	AVERAGE%								
		HIC IN EACH pH & HR								
		CLR	CTR	CSR	CLR	CTR	CSR	CLR	CTR	CSR
	48	8.09	0.74	0.05						
1	96	27.38	2.15	0.33	20.72	2.53	0.4			
	144	26.69	4.71	0.84						
	48	4.7	0.36	0.05						
2.7	96	24.96	2.65	0.37	21.07	1.86	0.25	22.09	2.15	0.31
	144	33.55	2.57	0.34						
	48	16.37	1.07	0.12	24.48	2.06	0.28			
4	96	32.59	3.05	0.44						

Table-3.39: The overall average HIC (against pH) as found in testing are summarized below along with tensile and yield strength of the samples.

HIC PARAMETERS MEASURED AGAINST pH-SOLUTION					
	CLR	CTR	CSR	TS/100*	YS/100*
D	22.33	9.34	2.4	4.75	3.04
A	12.2	2.5	0.31`	5.31	3.84
E	22.09	2.15	0.31	5.52	4.88

*→ The actual value is divided by 100 to accommodate in scale in the figures

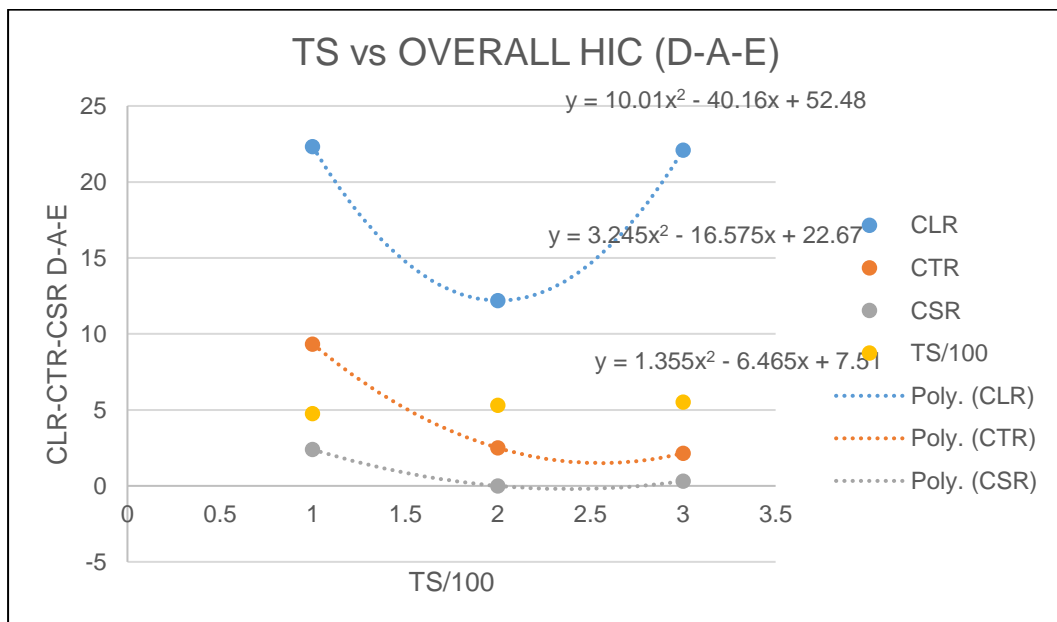


Figure 3.59: HIC parameters of sample D-A-E as found in tests against pH conditions are plotted against tensile values as per table 3.38.

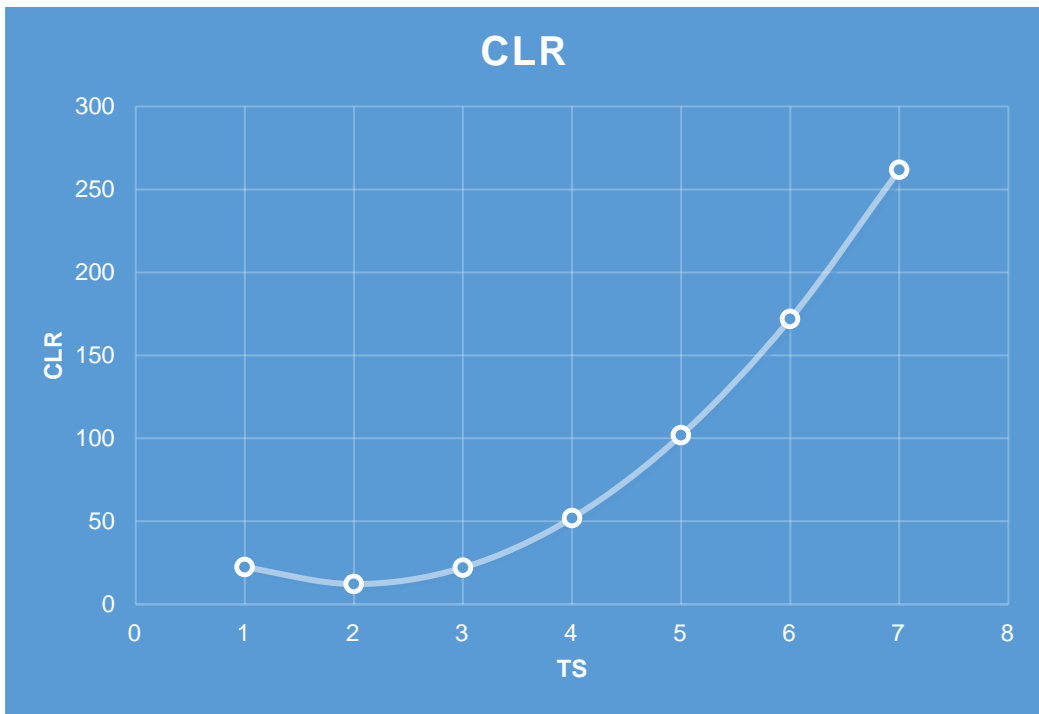


Figure 3.60: The curve shows CLR trend against tensile strength of D-A-E samples (divided by 100).

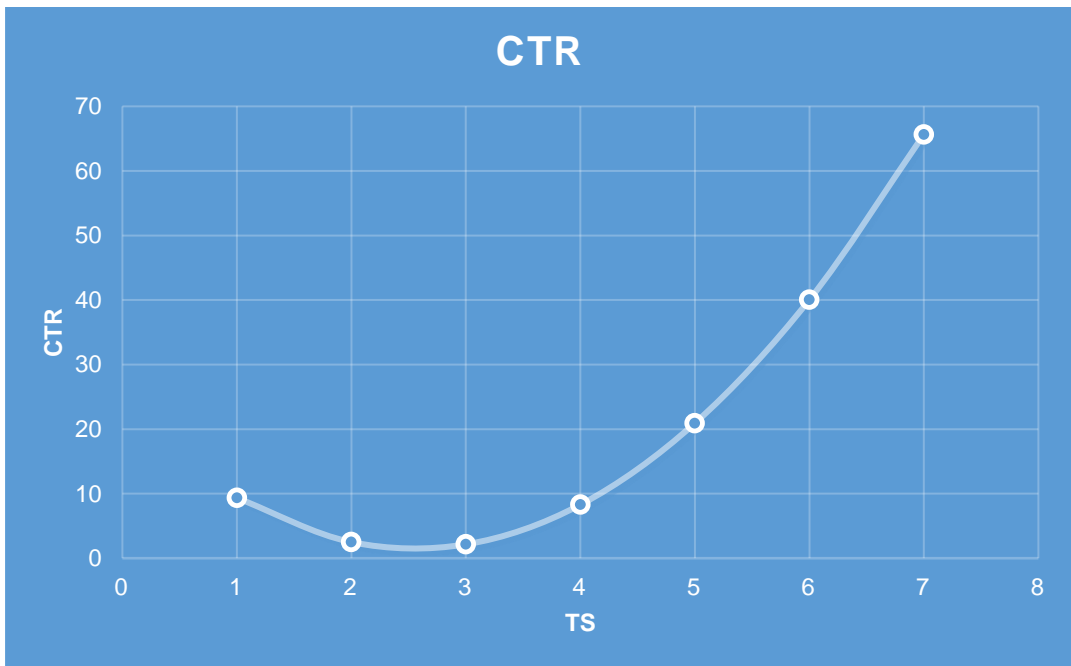


Figure 3.61: The curve shows CTR trend against tensile strength of D-A-E samples (divided by 100).



Figure 3.62: The curve shows CLR trend against tensile strength of D-A-E samples (divided by 100).

The overall trend analysis indicates increase of HIC with increase strength of the materials based on HIC – pH relationship on HIC as per above curves. The trend analysis suggests that there has been reduction in HIC for sample ‘A’ i.e., at tensile strength of 5.31 N/mm², whereas HIC maintained upward trends on either directions, lower, as well as, higher tensile strengths than 5.31 N/mm².

Table-3.40: Showing CLR values found in different evaluation methods with reference to tensile strength for samples D, A and E.

CLR VALUES EVALUATED BY DIFFERENT METHODS				
	HRS-CLR	pH-CLR	UT-CLR	TS/100
D	22.33	22.33	46.6	4.75
A	12.2	12.2	51	5.31
E	22.71	22.09	80	5.52

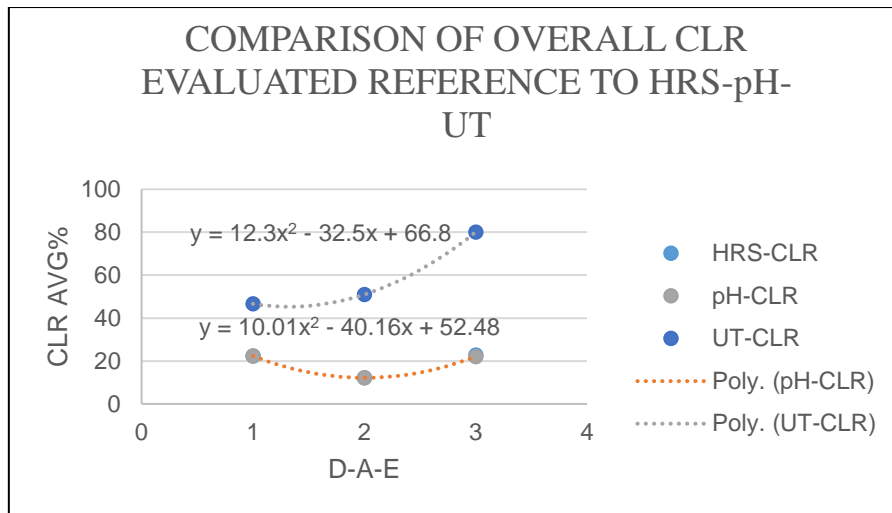


Figure 3.63: The curve shows CLR evaluated at different pH conditions, selected test durations and measured by UT against tensile strength of D-A-E samples (divided by 100).

Above figures, 3.59-3.63 clearly indicate that cracking tendency for all the samples A, D and E showed an increasing trend with increase in tensile as well as yield strength of the materials.

3.8 Discussion

General

HIC evaluation is carried out by metallographic method as per NACE TM 0284, and as described in section ‘HIC Evaluation’ in this thesis. The CLR, CTR and CSR are determined by metallography of the cross section of the specimens.

The discussion in the following section will elaborate results of all mechanical and physical testing and explain impact of the above results on probable HIC susceptibility or failure of the specimens in HIC testing. Metallographic evaluation which constitute an important part of the evaluation has been explained separately in Chapter-4. Conclusions are based on evaluation of all test results as explained in this section and chaopter-3.

It is to be also noted that samples A, D and E have been selected from materials actually used in the industry where threats for degradation of the materials by way of HIC prevails. Therefore, evaluation of HIC threats are relevant to actual industry scenario.

Characterization of properties of sample A, D and E by chemical, mechanical and metallographic evaluation are as follows-

- **Microstructure & Manufacturing Process**: Various microstructures, as observed in pressure vessel and pipeline steels, and their resistance or susceptibility to HIC cracking has been discussed at length by the research scholar in published paper, ref-[*G. Ghosh et al. Engineering Fracture Mechanics 199 (2018) 609–618 610*], the relevant section is reproduced below in this context (*in italic fonts*), and results of current research are discussed subsequently-

“Steels, used in manufacturing of pressure vessels and pipelines are produced by various manufacturing processes and heat treatments. Unalloyed or low alloyed steels are produced by normalizing where strength level is usually moderate to low (up to grade 70). However, the contribution of strengthening mechanism comes from alloying elements i.e., mainly carbon, silicon, manganese, and sometimes other elements e.g., Cu, Ni etc. By exploiting other strengthening mechanisms, as performed by applying Thermomechanical Control Process (TMCP) or Quenching & Tempering (QT), requirement of alloy addition can be controlled to achieve higher strength which minimizes susceptibility to HIC. Normalized and QT steels are generally medium carbon steels having ferrite-pearlite or tempered martensitic microstructure, whereas, TMCP steels are low carbon grades with microstructures which depend on heat treatment in manufacturing process, often a combination of phases with various precipitates are observed in microstructures. The microstructure, grain size, volume fraction of inclusions and precipitates, and dislocation density can vary within a particular strength grade. Studies found that microstructure plays important role in hydrogen assisted cracking of steels. Uniform microstructure with minimum defects, improves HIC resistance. Susceptibility to HIC is particularly related to steel composition, deoxidation practice and processing history, as these parameters affect nonmetallic inclusions (type, size, morphology) and the material’s ability to accommodate hydrogen. Large inclusions such as elongated Manganese Sulfides (MnS) and clusters or stringers of oxides increase the HIC susceptibility in steel. It is found that the hot rolling produces the most susceptible structure to HIC degradation as hot rolling produces planer

defects which are favorable locations for hydrogen entrapment and initiation of HIC. Steels containing $S > 0.002$ were found to be susceptible HIC as MnS forms planer defects in hot rolling which act as traps for hydrogen to initiate HIC. Normalizing- quenching & tempering had shown to reduce susceptibility of steels to HIC, particularly in low sulfur steels. Banded Ferrite Pearlite was identified as one of the most susceptible microstructures in several studies. HIC is found to initiate at interfaces of ferrite and pearlite bands. Hydrogen degradation effect was found to be enhanced in banded ferrite-pearlite in fracture toughness study with different microstructures. Control of phosphorus and carbon content increases HIC resistance by lowering microsegregation and thereby reducing banding in steels. However, researcher also observed that there was no significant effect of microstructural banding on HIC for special clean steel (A516-60, $S < 0.008\%$); although, it was not investigated in the study if diffusible hydrogen trapped in banding in special clean steel was not enough to reach to a critical level to initiate HIC in absence of other type of microstructural defects. Thermo-mechanically controlled processed (TMCP) steels with low sulfur content and low carbon equivalent had shown significant resistance to HIC cracking. The effect was considered as a result of reduction in ferrite/pearlite banding in steels. Carbide rich bands were considered as secondary sites which also initiated HIC in low sulfur containing steels. Generally, rolling schedule is targeted in TMCP steels to produce microstructure of fine grain, mixture of massive pearlite and low carbon bainite without pearlite or bainite bands, and reheating is usually selected to dissolve large carbonitrate inclusions to increase cracking resistance. Refined and homogeneously quenched and tempered bainite/martensite microstructure was found to have better performance for HIC than ferrite-pearlite microstructure in pipeline steel. Researcher also believed that lower bainite could offer lower susceptibility to Hydrogen cracking than quenched and tempered martensite. However, it was found that segregated zones with bainitic and martensitic structures had a high tendency for crack initiation and HIC susceptibility. Study found that high strength granular bainite had lower intrinsic hydrogen embrittlement (HIC) resistance than tempered martensitic steel. It was postulated that hydrogen in granular bainite might concentrate at microstructures composed of martensite islands and retained-austenite locations. Researcher has observed that the retained austenite itself in M/A constituents did not trap hydrogen significantly, but the interfaces between the

retained austenite and martensitic layer might be the possible trapping sites. Interface area of cementites in bainitic structure will be larger than that in pearlite and it could increase the reversible hydrogen trapping efficiency of bainitic structure. However, granular bainite steel showed higher extrinsic resistance than conventional tempered martensite steel because of granular bainite steel reportedly trapping less hydrogen than tempered martensite steel. The effect of hydrogen in microstructure appears to change in dual phase microstructures as apparent from several investigations. Investigation by Xian-bo SHI et al., on effect of microstructure on HIC in experiment with X80 pipeline steel for three different dual phases i.e., ferrite+bainite, ferrite+martensite/austenite-islands, and ferrite+martensite respectively, found that ferrite+bainite and ferrite+martensite/austenite-islands(M/A) both had higher deformability and HIC resistance, whereas, harder microstructure of ferrite+martensite (F+M) had the worst HIC resistance. The hard martensite phase existed in bands and believed to be responsible for HIC susceptibility. It is concluded that dual phase containing a softer phase exhibit higher straining capacity and superior deformability.

Park et al., considered that generally lower bainite offered higher resistance than quenched and tempered martensite at comparable strength levels, but no study was made to compare acicular ferrite with bainite with respect to hydrogen diffusion. Jing Li et al., observed in experiment with X80 pipeline steel that granular bainite+acicular ferrite, as well as, quasi polygonal ferrite microstructure presented excellent HIC resistance, whereas, lath bainite+granular bainite microstructure containing bainite lath and martensite/austenite phases showed poor HIC resistance. The mechanism of formation of dual phases was postulated by Mohtadi et al., that in the acicular ferrite+granular bainite microstructure, acicular ferrite nucleates intragranularly in deformed austenite, and the formation requires sufficient deformation ratio in the non-recrystallization zone. The formation of M/A constituents is influenced by acicular ferrite transformation and ability of carbon atoms to diffuse. Residual austenite becomes more stable due to increasing impingement effect between ferrite laths induced by increasing nucleation sites for acicular ferrite. However, the impingement effect during bainite transformation produces a higher amount of residual austenite which subsequently transforms to M/A constituents. Huang et. al., observed in review (studies with X120 steel) that, investigation of the HIC process by different

researchers was focused on formation process of cracks, not on combined effect of different microstructures and presence of hydrogen, and the cracking nature of HIC/SSC has not been clearly explained in literature. Koh et al., in experiment observed that HIC did not occur in ferrite/acicular ferrite microstructure for a wide range of diffusible hydrogen content and HIC susceptibility was found proportional in ferrite/bainite microstructure, implying that ferrite/bainite microstructure was prone to HIC whereas, ferrite/acicular ferrite was the best microstructure for HIC resistance. Researchers found that acicular ferrite and ultra-fine ferrite had optimum HIC resistance and mechanical properties (SSCC resistance is better in ultrafine ferrite than acicular ferrite) as observed by Park et al. which was also supported by studies of several other researchers. It was postulated that acicular ferrite possessed high yield strength & toughness due to dispersed precipitation of carbonitrides and was considered as the most preferable microstructure for HIC resistance. Acicular ferrite phase had randomly oriented grain boundaries and high dislocation density, which improved hydrogen trapping efficiency than other microstructures. However, Huang et al. observed in review that the role of acicular ferrite had not been properly explained in enhancement of Sulfide Stress Cracking (SSC) resistance, which was likely to be closely related to hydrogen diffusion. Costin et al., investigated acicular ferrite from weld of X70 pipeline material (E6010 weld) with micro-cantilever structure for intrinsic HAC properties. Previous investigations reported that acicular ferrite seems to have most beneficial impact on strength, toughness, as well as, HAC resistance including welds. The outcome demonstrated that threshold stress intensity factor (K_{th}) to initiate crack propagation in acicular ferrite ranged between 1.56 MPa \sqrt{m} and 4.36 MPa \sqrt{m} . The range is significantly lower than K_{th} reported for various ferrous alloys in standard macro tests. This indicates that subcritical hydrogen assisted cracks can grow at microscale at stress intensity factors well below the stress intensity factor threshold measured with conventional tests at macro-scale. The findings indicate that mechanisms and resistance to HAC at micro-scale could be significantly different than at macro-scale as not all fracture toughening mechanisms may be activated at this scale level. The inherent difference was attributed to small grain size and high density of high angle grain boundaries, which apparently increased the resistance to cleavage like

fracture and simultaneously acted as a hydrogen trap, thereby preventing the hydrogen to diffuse to more HAC susceptible regions. Plasticity induced closure of cracks also might form part of the mechanism, needs further investigation”.

Current Evaluation

Specific observations as found in the current research, are discussed below- Metallographic analysis revealed that sample A and D consisted of ferrite and pearlite while sample E consists of ferrite bainite microstructure with M/A constituents. Ferrite-pearlite microstructure is generally found to be susceptible to HIC, while, bainitic microstructure is known to be resistant to HIC which matches with observations of samples A,D and E.

- **Discussion of Result on HIC Susceptibility:**

Chemical composition of materials play major role in determining HIC susceptibility. Each element has its specific effect, as well as, combined effect, on properties of the materials. Table 3.2, shows chemical composition of samples analyzed by Optical Emission Spectrometry. Chemical composition of the samples of A, D and E show that the elements are present within the range of specifications. Specifications of the samples are shown in table -3.3. Effect of different elements on HIC as found in testing is discussed below-

CARBON (C): Carbon is probably the first element which any steels inherit by virtue of steel making process, and controlling of C content to the desired level primarily decides mechanical properties of steels. Carbon content has significant effect on corrosion properties of steels also. Carbon, forming cementite (Fe₃C), precipitate in steels and/or carbon remain dissolved in solid solution, are primary forms of carbon that exists in steels.

This can be altered with heat treatment to form pearlite, bainite or martensite which finally imparts properties to steels. Commonly used engineering steels are often called mild steels which contain around 0.2 wt% Carbon. Normalized grades of pipeline steels which have been traditionally used in the industry for fabrication of pressure vessels or pipelines, also contain carbon in the similar range. To reduce HIC tendency in steels, improved grades of steels have been manufactured by Thermo-Mechanically-Controlled-Process (TMCP) where carbon content can be reduced substantially, usually below 0.1 wt% and microalloying elements e.g., Ti, V etc are added to supplement strength of the material. Increased quantity of carbon promotes segregation in materials along with other elements disturbing homogeneity of microstructure. Homogeneity of microstructure has also significant effect on HIC of steels.

It is evident that sample 'E' contains 0.09 wt% carbon which is significantly lower than carbon content, found in sample 'A' and sample 'D'. The combined effect of C-Mn-P as explained in Chapter-2 in literature review, fig-2.37(a) shows that segregation in steels increase as carbon content and segregation may lead to banding in microstructures. Micrograph #3.13 (sample #A), shows considerable segregation (centerline) in steel and micrograph #3.15 (sample #D), shows banding in microstructure, both the steels have relatively high carbon content, whereas, sample #E shows minimal banding or segregation which has relatively less carbon content. Anisotropy index is found to be 1.07 for sample #A, 1.08 for sample #D and 1.03 for sample #E.

Carbon, along with nitrogen, can form inclusions in presence of microalloying elements viz. Ti, Nb etc. which can be initiation locations for HIC in microalloyed steels. This has been discussed over inclusions found in SEM images, in chapter – 4.

Niobium (Nb) and Titanium (Ti) are present in sample #E, which are not present in sample #A and #D. No carbo-nitride inclusions found in HIC in sample #E which indicates that stoichiometric ratio of the elements (Nb, Ti, C, N) are maintained in well balanced condition in the matrix, however oxides of silicon could be identified in HIC samples which are discussed in chapter-4.

The quantitative evaluation of HIC could not focus any conclusive evidence on role of carbon on HIC from evaluation of sample #A, #D or #E.

Manganese (Mn): Manganese plays important role in providing strength and toughness in steels. Generally, steels contain 1.20 wt% – 1.60 wt% Mn which provides desired strength of the material. Lower Mn content will reduce strength, whereas, higher quantity may increase strength and hardenability in steels. Mn acts in combination with other elements as shown in fig 2.37 b, and promotes segregation in steels. In current study, Mn is found in close range of 1.09 wt% to 1.45 wt% and considered to have similar effect on HIC susceptibility for all the three steel samples i.e. sample #A, #D and #E.

Sulfur (S): Sulfur content is restricted in steel, which are intended to be used in sour service as sulfur contributes to formation of MnS inclusions in steels. While hot rolling, sulfur inclusions, mainly MnS inclusions create planer defects inside metal thickness which act as initiation sites for HIC. As per guiding standard, Sulfur is recommended to be restricted to 0.003 for manufacturing of steels where extent of cracks by HIC can be acceptable [NACE MR-0175]. In the current analysis, it is found that Sulfur content is in close range between 0.012 wt% - 0.013 wt% which might generate more HIC cracks than steels with lower sulfur content. However, since all the samples have

similar Sulfur content, therefore the effect of sulfur on cracking can be considered as uniform.

Silicone (Si): Silicone primarily imparts strength in steels, however high silicone can improve hardenability of steels and promote brittle fracture. Therefore, higher limit of silicone is important for steels to maintain hardness acceptable in sour service. Silicone is found in the range 0.188 – 0.336 in the steel samples which complied to the mechanical properties as mentioned in table #3.3 to comply to specifications for each sample. Silicone can promote inclusions in steel which can be initiation locations for HIC. In the metallographic analysis, it is observed that sample #A, fig-4.1, sample #D fig 4.4, and sample E fig 4.8 SEM analysis indicated presence of silicone oxide in HIC. Therefore, it appears that presence of silicone oxides may be a necessary for initiation or propagation of HIC in steels.

Chromium (Cr) & Nickel (Ni): Chromium may be added in minor quantity in pipeline steels to promote strength, higher quantity is often added to enhance corrosion resistance of steels. Nickel is austenite stabilizer and mainly promotes toughness in steels. Higher quantity of Ni can promote distinct austenite phase in ferritic steels.

Cr also increases hardenability of the steel, whereas, addition of nickel maintains equilibrium of mechanical properties viz. strength and toughness in the material. In the current samples #A, #D and #E, Chromium content is in the range of 0.067 wt% to 0.083 wt% and Nickel content is in the range of 0.02 wt% to 0.029 wt%. The strength and hardness of the samples were found within the limits of respective specifications. The SEM micrographs also did not reveal unusual presence of Cr or Ni inclusions. Therefore, role of Cr and Ni, as present in the samples

shall not be considered to be detrimental for HIC initiation in the specimens.

Copper (Cu): Copper is sometimes added in small quantities to promote corrosion resistance, as well as, resistance to hydrogen embrittlement, in steels as discussed and shown in fig #2.45 to #2.48 in literature review. In the current analysis of specimens, Cu is found to contain 0.022 wt% in sample #D and 0.011 wt% in sample #E and sample #A has insignificant quantity. Normally, Cu is added up to 0.4 wt% in steels, used in sour environment [51]. Effect of Cu on hydrogen permeation can be considered as insignificant for the samples as identified quantity is considerably low.

Titanium (Ti) & Niobium (Nb): Thermomechanically processed steels (TMCP) are usually microalloyed with Ti and Nb. Titanium primarily has the grain refining effect and it generates TiN and Ti(C,N) inclusions in steels. The inclusions act as initiating sites for HIC in steels, of course, fine dispersed Ti(C,N) is found to resist HIC by controlling hydrogen diffusion, but coarse Ti(C,N) and TiN are found to promote HIC [88]. Nb contributes to precipitation hardening and grain refinement, as well as, strengthening effect. Nb(CN) precipitates in ferrite phase which elevates tensile strength of the steel. Addition of Nb has been found to decrease HIC resistance in steels in experiment. Addition of Nb could retard the recrystallization of austenite and increased the nucleation sites, as well as, nucleation rates during ferrite transformation [96]. In the current evaluation only sample E is found to contain Nb & Ti in chemical analysis as shown in table 3.2.

Any identification of inclusion containing Ti or Nb has been discussed in chapter-4 in metallographic section.

Carbon equivalent (CE): Generally, different formulae are followed for evaluating carbon equivalent based on carbon content and other elements which contribute to hardenability and can be detrimental for Sulfide Stress Cracking (SSC) of steels. If carbon content is more than 0.12 wt%, formula as provided by IIW is followed, whereas, if carbon content in steel is less than 0.12 wt%, formula provided by Pcm is considered [60]. In the current case, CE found for sample #A as 0.44 which is towards the higher limit for acceptance, however CE is not directly correlated with HIC in steels, this is reported more for information and understanding chemical composition of the steels with respect to specifications as mentioned.

- **Hardness:**

Hardness testing of specimens were carried out according to ASTM A370 [97] and NACE MR-0175 / ISO 15156 [54]. Hardness in steels often play a major role in cracking, however, role of hardness in HIC has not been conclusively established. Low hardness is believed to favor pure HIC in steels, i.e, without any component of Sulfide Stress Cracking (SSC) or Stress Oriented Hydrogen Induced Cracking (SOHIC) in cracking mechanism. The average hardness values measured for the samples as 147 BHN for sample 'A', 128 BHN for sample 'D' and 178 BHN for sample 'E', are acceptable as per respective materials manufacturing specification, as well as, within acceptable limits provided in industry standard (NACE MR 0175/ISO-15156) of stress corrosion cracking in sour service condition. Predominantly Bainite (with some amount of martensite) phase in sample #E contribute to higher hardness than ferrite pearlite microstructure in sample #A and #D. Sample #D having lowest hardness, would favor HIC as observed in tested samples, however, the average %CLR for sample D is close to highest (22.33%) among tested samples which matches with established theory in this regard. The

hardness values measured for sample #A, #D and #E are shown below in table #3.41 (data reproduced from table #3.3).

Table # 3.41: Brinell Hardness Number (BHN) as measured for samples A, D and E are shown in table against average% CLR.

HARDNESS vs HIC		
Sample #	Hardness – BHN	Avg% CLR
D	128	22.33
A	147	12.2
E	178	22.71

High hardness is found to favor hydrogen assisted cracking as discussed in literature review in chapter-2, which strictly does not include HIC. However, in the current study, no clear correlation could be found between hardness values and HIC cracking susceptibility of the steels.

- **Banding:**

Several published technical paper identified banding as a contributing factor for HIC in steels, however, several researches also contradicted the understanding by their researches [98].

Banding was evaluated for the samples #A, D and #E in the current research and Anisotropy indices were found as 1.07, 1.08 and 1.03 respectively. The average CLR for samples #A, #D and #E have been plotted against Anisotropy Index to reflect effect of banding on HIC, as shown below.

Table – 3.42: Anisotropy Index as calculated based on ASTM E 1268 for samples #A, #D and #E are shown in table.

ANISOTROPY INDEX & AVERAGE %CLR FOR SAMPLE E-A-D		
Sample	Anisotropy Index (Increasing order)	CLR Average
E	1.03	22.71
A	1.07	12.2
D	1.08	22.33

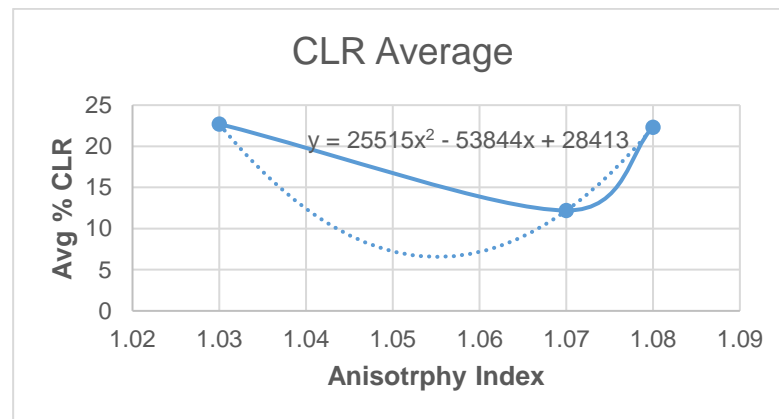


Fig- 3.64: Average %CLR are plotted against Anisotropy Index for samples #E, #A and #D (increasing order).

In the current research, the trend curve in fig-3.64 indicates an increasing trend for HIC with respect to Anisotropy Index which conforms to general understanding that banding contributes to HIC in steels.

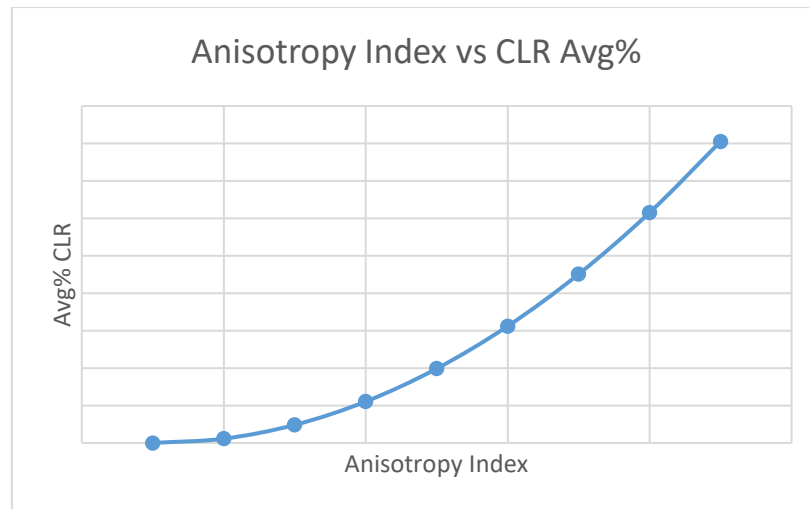


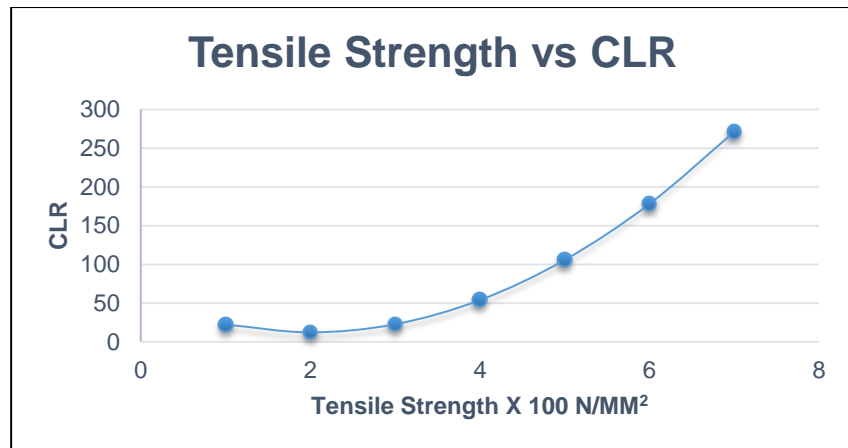
Fig- 3.65: Trend analysis from fig-3.64, indicates an increasing trend for HIC with respect to Anisotropy Index.

- **Strength:**

Tensile testing of the specimens from sample #A, #D and #E were carried out according to ASTM A370 for determining tensile and yield strength of the materials before carrying out HIC testing. It is found that tensile strength of sample #A was 531 N/mm², for sample #D it was 475 N/mm², and for sample #E tensile strength was 552 N/mm² which were found within the limits of specification of respective grade of materials as mentioned in table 3.3.. Besides composition, manufacturing process which determines the final microstructure, impacts strength of the material. Martensitic microstructure usually has highest strength, followed by bainite and ferrite in steels. In the current study, sample #E has bainitic structure and found to have higher strength than ferrite & pearlite microstructure in sample #A and #D respectively.

Effect of strength on HIC has been specifically analyzed as shown in fig#3.55 - #3.58 in the thesis.

The following trend curve (ref, fig-3.56) shows trend of hydrogen induced cracking with respect to tensile strength of the samples tested.



(Reproduced Fig-3.56 for discussion).

It can be inferred from the above trend curve that tensile strength of the rolled steels up to approximately 300 N/MM² did not have any significant effect on initiating or propagating HIC in steels. But, the influence of strength of the material has pronounced effect above 300 N/MM² TS of the steels. The HIC tendency exponentially increases as strength of the material increase above approximately 300 N/MM², and the trend follows $Y = 3.245 x^2 - 16.575x + 22.67$ which indicates that higher strength materials should be avoided in sour service to avoid HIC in rolled steels.

- **Cracking Trend Analysis in HIC Testing:**

It shall be noted in HIC trend analysis that the rising trends represented by the curves indicate increase in CLR values with respect to time which are physically possible cases, however, in some cases the trend curves show an initial rising trend, and subsequently a downtrend or vice-versa. The downtrend of CLR is physically not realistic scenario, as cracks once initiated, would not decrease in length with respect to duration, therefore the downtrend part shall be discarded in such cases in evaluation.

The CLR, CTR and CSR were determined by metallography at the cross section of the sectioned specimens as per NACE TM 0284. The trend analysis indicates following-

Sample-A: The HIC parameters (CLR, CTR and CSR) have marginal downtrend up to approx. 96 Hrs. (48x2 hrs) followed by exponential upward trend. The initial segment (up to 96 Hrs), can be considered as time required for initiation of the cracks which is relatively slow, but after initiation, the propagation is considerably fast as seen in fig-3.19.

Fig-3.35 indicates trend of HIC with respect to pH in testing. The peak value of HIC is found at approximately, pH 2.4. This indicates that maximum HIC susceptibility for the material is at environmental pH of 2.4.

Sample-D: The trend for HIC for sample #D indicates initiation of HIC in less than 96 Hrs and extremely fast propagation after initiation as found in fig- 3.23. The severity of cracking for such steels having banded ferrite and pearlite microstructure can be expected to be considerably severe.

Fig-3.39 indicates trend of HIC with respect to pH in testing for sample #D. The peak value of HIC is found at approximately, pH 2.7. This indicates that maximum HIC susceptibility for the material is at environmental pH of 2.7 (which is commonly the accepted environmental condition for testing according to NACE TM 0177)[99].

Sample-E: The CLR trend curve in fig-3.26 indicates that there has been an initial parabolic rise of HIC with respect to exposure duration which reached peak at approximately 125 Hrs (2.6x48). The downtrend of the curve after teal, can be discarded as discussed earlier.

Fig-3.43 indicates trend of HIC with respect to pH for sample #E. The trend curve is rising in nature, and no definite pH can be identified for highest value of HIC for this specific sample.

However, the trend curve indicated that up to pH 2.0 (approximately), HIC did not occur.

Overall Trend of HIC

The overall trend curve of HIC over duration of testing, in fig-3.31 shows that the HIC steadily follows an upward trend since initiation according to trajectory which can be mathematically formulated as below-

$$Y = 3.3817x^2 - 2.5417x + 8.8467.....(1)$$

The overall trend curve of HIC over pH of testing, in fig-3.47 shows that the HIC steadily follows an upward trend since initiation up to approximately, 3.4.

The mathematical expression of the trajectory is as below-

$$Y = -1.6969x^2 + 10.992x + 5.0714.....(2)$$

The above trend analysis indicates that generally, the trend analysis of HIC test results demonstrated HIC initiation and propagation for the samples, however, samples #A and #D showed long initiation stage, followed by propagation; whereas, sample #E behaved in a different way in exposure to similar testing conditions, sample #E did not show any initiation period, unlike sample #A and #D. Several differences could be identified in chemical analysis and microstructural features between sample #E and #A, as well as, #D.

- **Special Observation**

Ultrasonic Measurement (UT):

Industry practice is to determine CLR, CTR and CSR by metallography at the cross section of the sectioned specimens as per NACE TM 0284. For academic interest, ultrasonic measurement of tested samples were carried out to check the actual crack lengths which occurred by HIC in each specimen. The UT measurement was found as mentioned in table-3.32. The trending of CLR measured by UT, has been compared with trending of CLR measured by metallography also. The UT

measured CLR values were found comparatively higher than CLR values measured by metallography, the trend reflected as follows-

- A – CLR:
 - Hrs Exposure: $y = 1E-04x^2 - 0.0127x + 0.64$
 - pH of environment: $y = -0.0099x^2 - 0.0596x + 0.7428$
- D – CLR:
 - Hrs Exposure: $y = 0.0001x^2 - 0.0223x + 1.3167$
 - pH of environment: $y = -0.0725x^2 + 0.3447x + 0.1844$
- E – CLR:
 - Hrs Exposure: $y = -4E-05x^2 + 0.0111x + 0.175$
 - pH of environment: $y = 0.0766x^2 - 0.2951x + 0.9352$
- Overall CLR:
 - Hrs Exposure: $y = 6E-05x^2 - 0.008x + 0.7106$
 - pH of environment: $y = -0.0019x^2 - 0.0033x + 0.6208$
 - CLR measured by UT: $y = 12.3x^2 - 32.5x + 66.8$

Shift of pH in HIC Testing:

As HIC testing is carried out in hydrogen sulfide saturated acidic condition, there will be corrosion of the carbon steel specimens during the testing. As the steel corrodes, pH of the solution tends to increase. The same has been measured while testing to indicate susceptibility of different steel samples to corrosion in the test medium which is shown below.

Table-3.43: Special observation: Shift in pH has been recorded for each test between starting of the test and finishing of the test as mentioned below.

TEST #	H ₂ S SATURATION pH	FINISHING pH	SHIFT IN pH	AVG pH SHIFT	HRS TESTING
A1/D1/E1	1.21	3.45	2.24	2.18	48
A2/D2/E2	1.13	3.34	2.21		96
A3/D3/E3	1.24	3.34	2.1		144
A4/D4/E4	2.86	3.51	0.65	0.54	48
A5/D5/E5	2.85	3.56	0.71		96
A6/D6/E6	3.02	3.3	0.28		144
A7/D7/E7	4.09	4.1	0.01	0.01	48
A8/D8/E8	4.05	4.08	0.03		96
A9/D9	4.08	4.07	-0.01		144

The shift of pH is observed maximum in testing in lowest pH i.e., close to 1.0. The shift has reduced progressively as the testing pH was increased up to 4.0 (approx). This indicates that the samples have corroded significantly releasing metal ions in solution with lower pH which have increased the pH significantly. The rate of corrosion in tests with higher pH, is relatively less, accordingly the resultant pH shift is less.

CHAPTER FOUR

4.1 Scanning Electron Microscopy

Inclusion Characterization & HIC Crack Propagation

Scanning electron microscopy and Energy dispersive X-ray have been carried out on HIC affected specimens of A, D and E, found to have specific features as described following.

METAL SAMPLE-A:

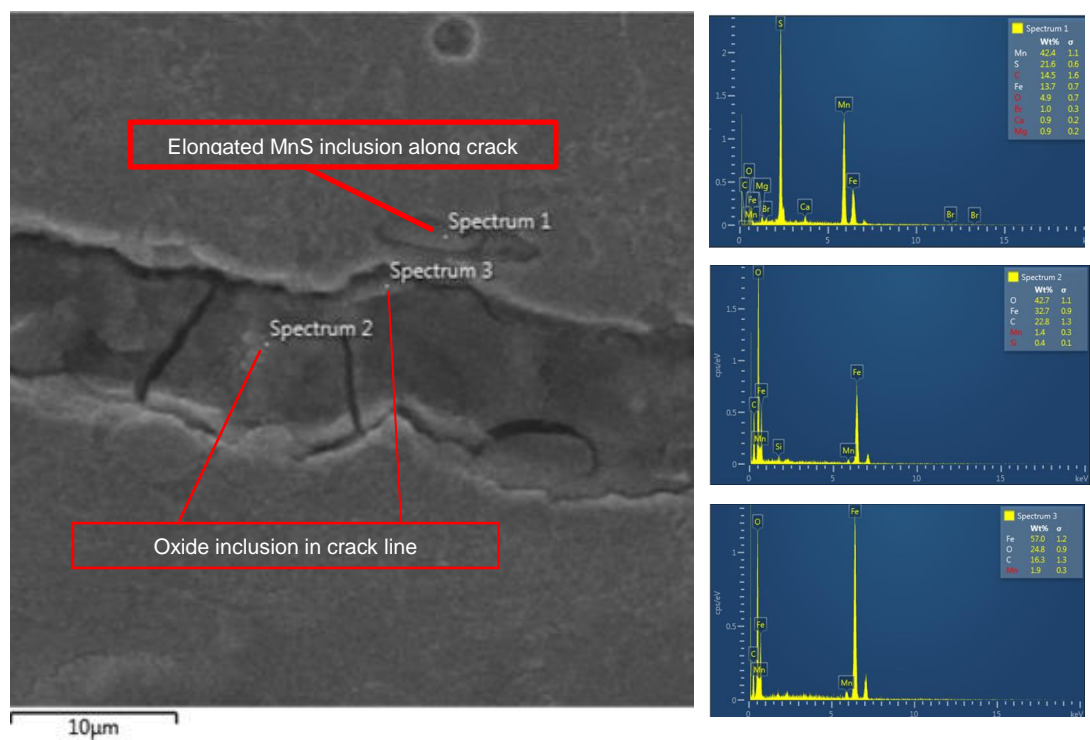


Figure 4.1: HIC in metal sample A is found originated/propagated along inclusions, identified mainly as oxides of calcium and magnesium and silicon as seen in above SEM and EDX.

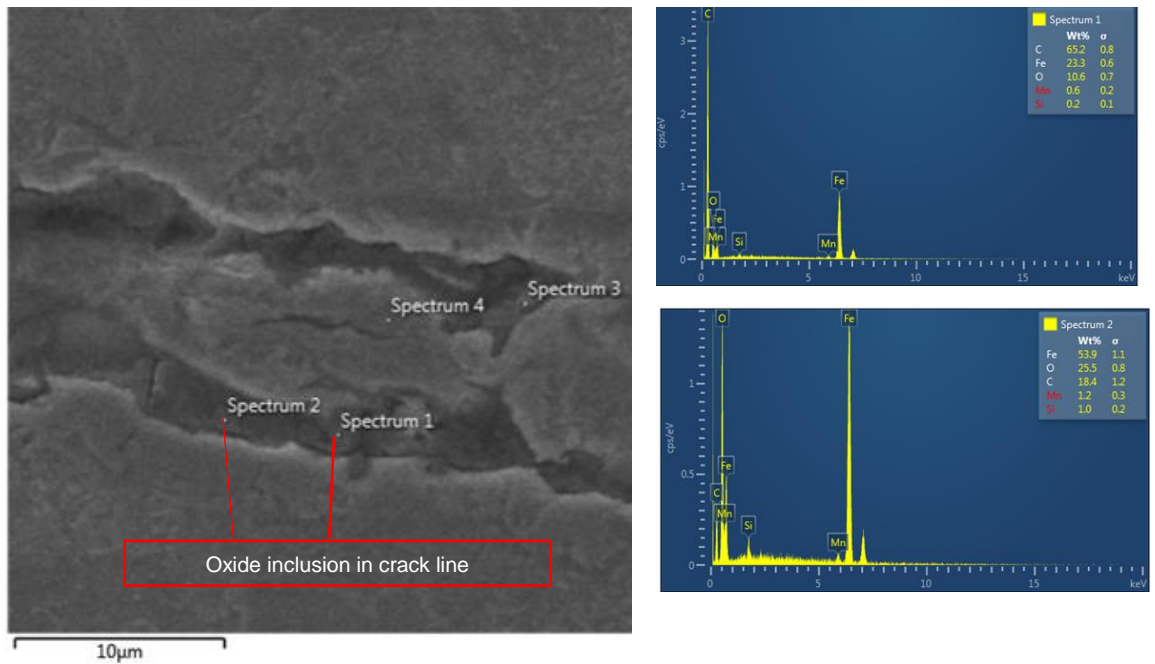


Figure 4.2: HIC in metal sample A is found originated/propagated along inclusions, identified mainly as oxide of silicon.

METAL SAMPLE-D:

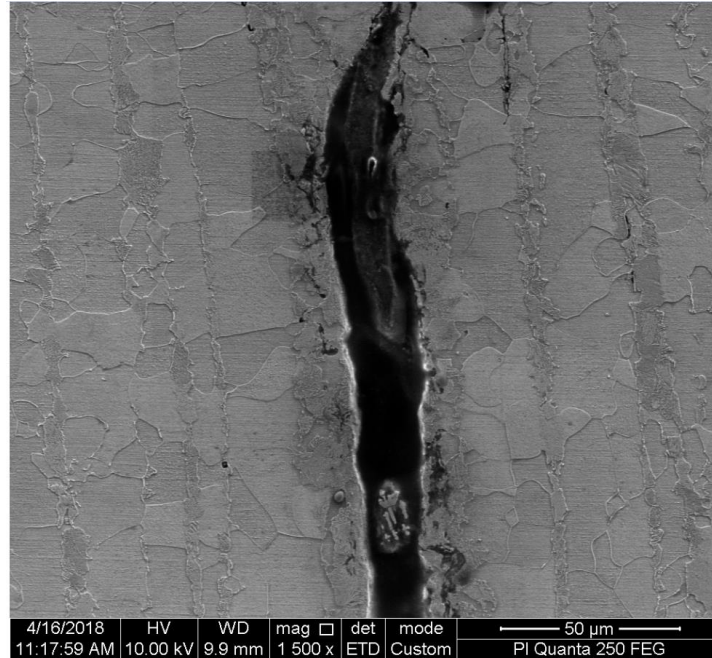


Figure 4.3: SEM image showing HIC originated/propagated along inclusions and propagated transgranularly in metal matrix.

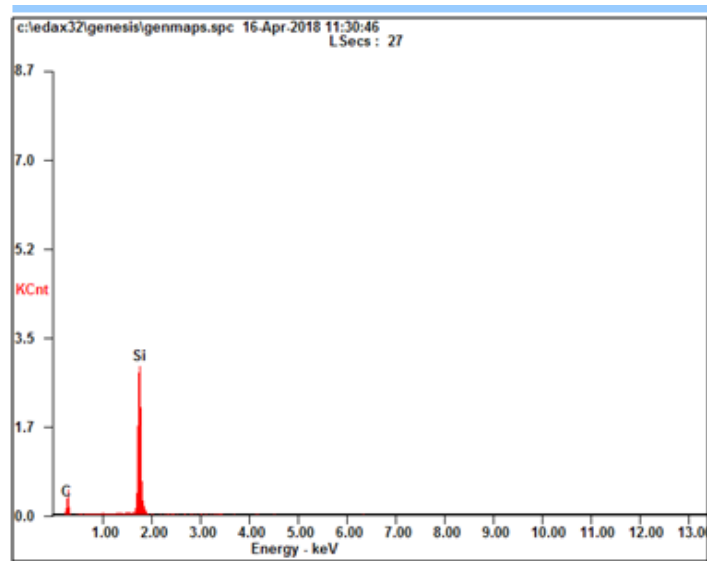
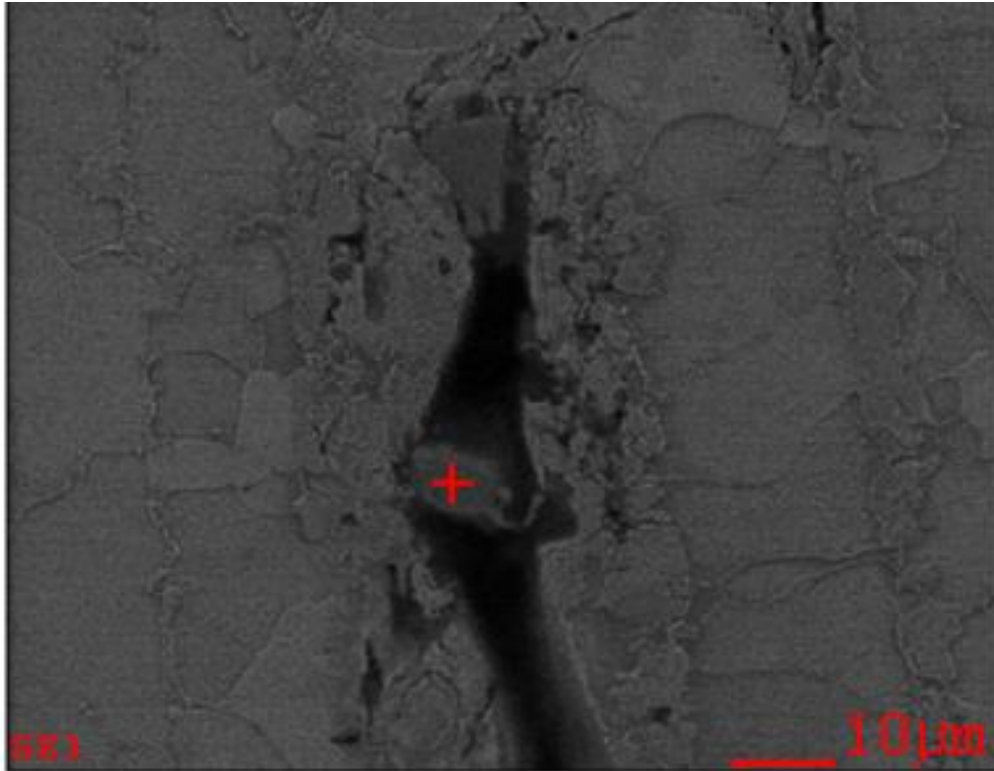


Figure 4.4: SEM and EDX images shows that HIC in metal sample D originated and propagated along inclusions. The EDX analysis shows inclusion possibly is compound of Carbon and silicon.

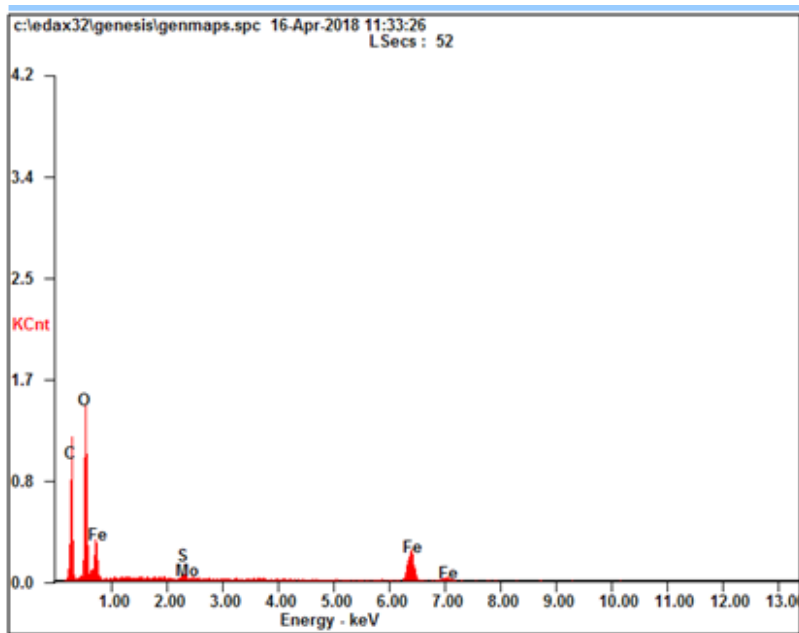
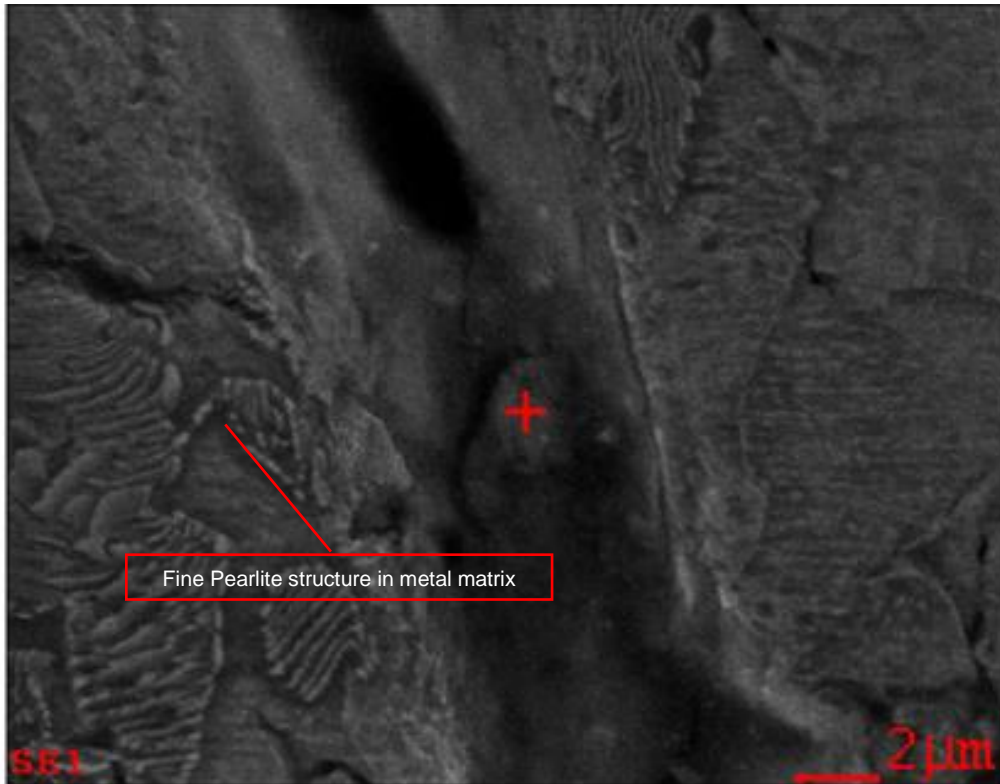


Figure 4.5: Inclusion can be seen right in HIC trajectory in metal sample D. EDX analysis indicates inclusion to consist of Oxygen, Sulfur and Mo which are known to contribute to hydrogen assisted cracking in metals. The matrix consists of Ferrite-pearlite microstructure. Large pearlite colonies can be seen in the SEM image.

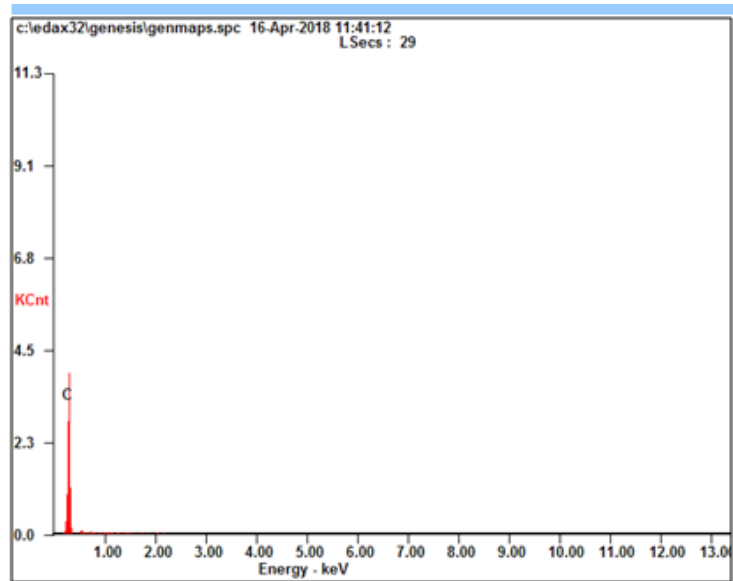
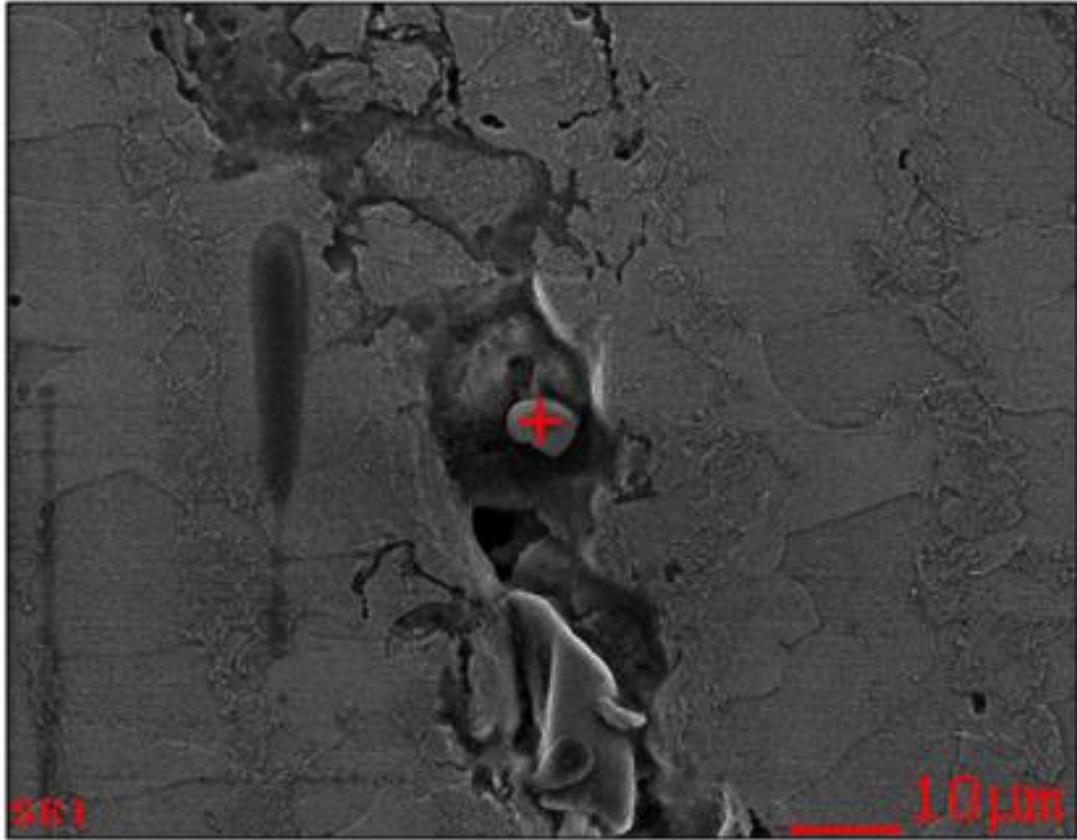


Figure 4.6: Inclusion in HIC in metal sample D did not reveal any significant elements for the inclusion other than carbon which might have transformed in morphology in steel making and rolling practice at high temperature.

METAL SAMPLE- E:

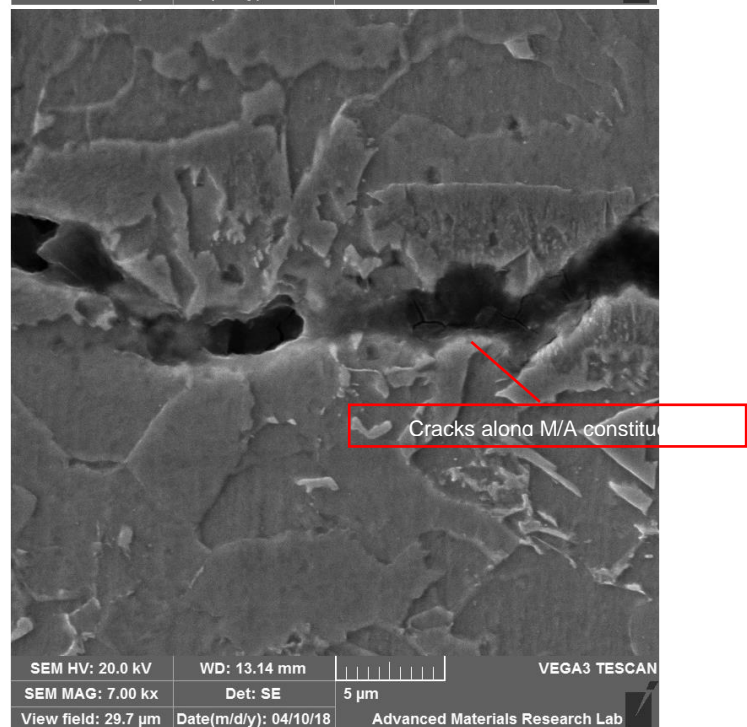
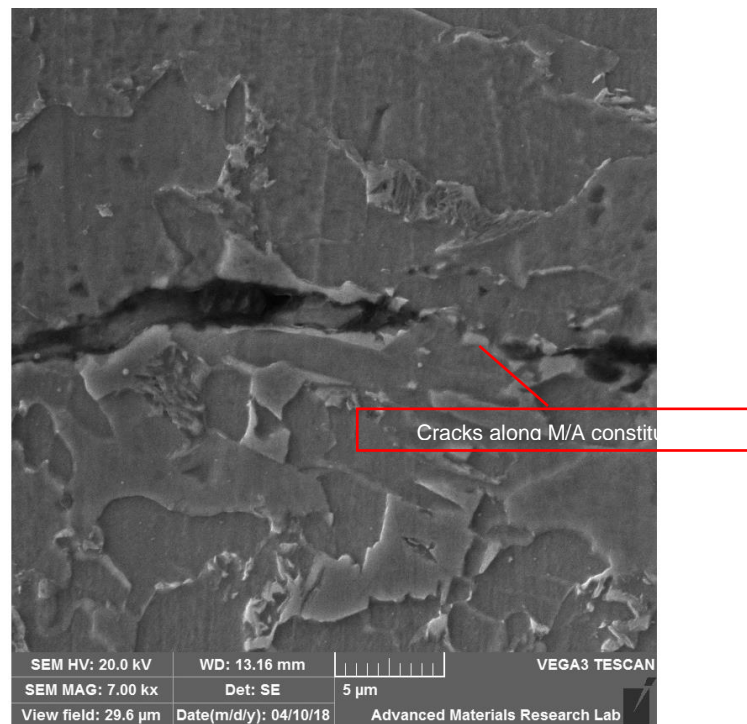


Figure 4.7 A, B: HIC in metal sample E is found originated/propagated along inclusions and fractured M/A (martensite/austenite) constituents which are known as brittle precipitates, susceptible to HIC.

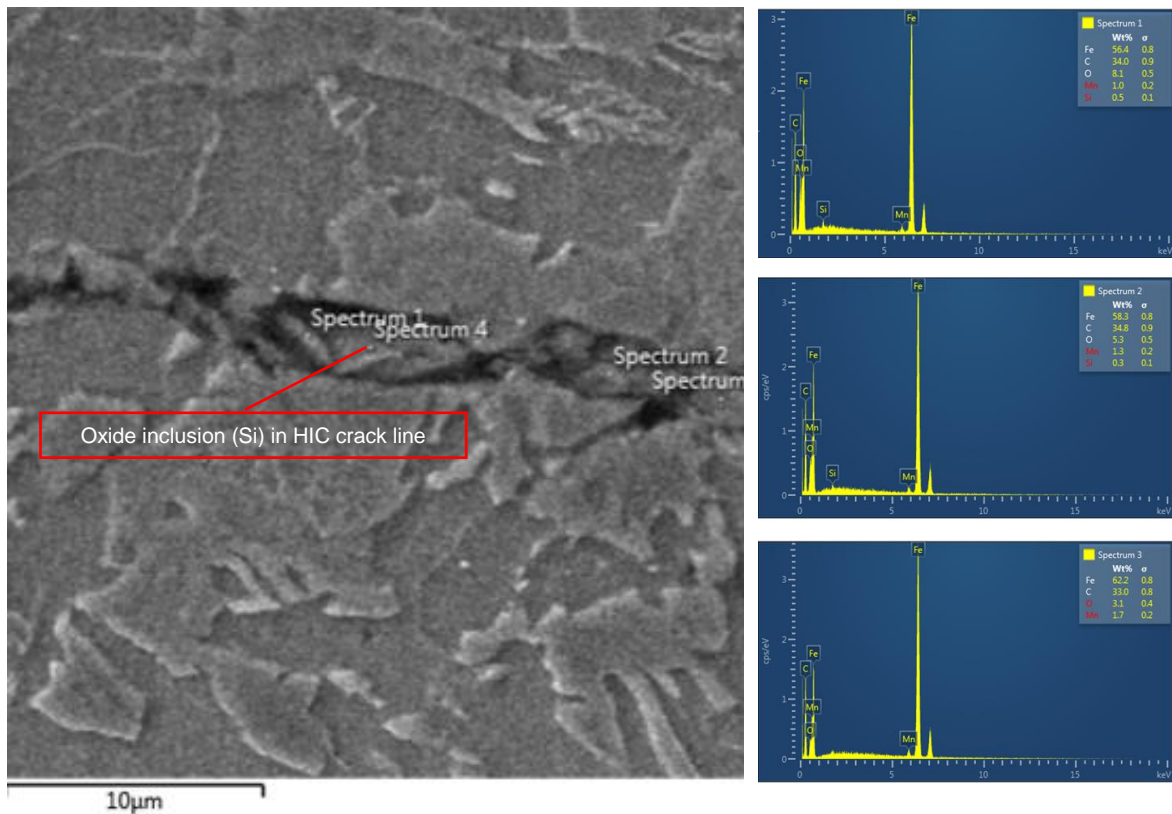


Figure 4.8: HIC in metal sample E is found originated/propagated along inclusions constituting of oxides of silicon and fractured M/A constituents.

OVERALL MICROSTRUCTURAL REVIEW

Sample-A:

Optical micrographs shown in fig-3.3, 3.12 & #3.13 reveal following for metal sample #A:

Metal sample #A, consists of fine ferrite-pearlite microstructure for ASTM A 234 WPB material. This is a conventional hot rolled medium carbon steel material. The processing induced large banding in the material as can be seen in optical micrograph #3.3 and 3.13, however, the HIC is found limited to centerline only as can be seen in optical micrograph #3.12. Fig-3.13 shows considerable centerline segregation in the metal matrix.

SEM & EDX images in fig- 4.1 and 4.2 shows that MnS and SiO are in the trajectory of Hydrogen Induced Crack, possibly inclusions consisting of MnS and Si-O are necessary requirements for the damage mechanism to occur in the steel.

Sample-D:

Optical micrographs shown in fig-3.4, 3.14 & #3.15 reveal following for metal sample #D:

Metal sample #D, consists of fine ferrite-pearlite microstructure for ASTM A 234 WPB material similar to sample #A, but the steel has relatively less carbon content (0.156 wt%) with respect to sample #A (0.185 wt%) which is evident from larger ferrite grains in the microstructure of the metal sample. Banding, similar to sample #A can be seen in metal microstructure #3.4 and #3.15. Classic HIC features are seen in the micrograph in fig#3.15 unlike in metal sample A which was limited to centerline segregation only. The HIC features in fig #3.14 indicate that the crack-ends (or edges) incline towards the preceding or following crack which eventually joins the individual crack to cause a through-thickness crack in the metal membrane. This is the typical HIC failure mechanism in the pressure vessels or pipeline steels used in sour service.

SEM & EDX images in fig 4.3- 4.6 reveal presence of inclusions right in HIC trajectory in metal sample D. EDX analysis indicates inclusion to consist of Oxygen, Sulfur and Mo which are known to contribute to hydrogen assisted cracking in metals. Besides inclusions of oxides, possibility of contribution from elongated MnS cannot be eliminated from the constituents found in EDX analysis. The matrix consists of Ferrite-pearlite microstructure. Large pearlite colonies can be seen in the SEM image.

Sample-E:

Optical micrographs shown in fig-3.5, #3.16 & #3.17 reveal following for metal sample #E:

Metal sample #E, as can be seen from the micrograph #3.5, consists of, predominantly, ferrite-bainite. Minor segregation and banding can be seen in the microstructure in fig #3.17. The HIC features in fig #3.16 indicate that the individual cracks are long and limited towards center of thickness of the material, however the cracks cover a wider area across thickness in the metal than seen in sample #A (ref: fig-3.12) .

SEM & EDX images in fig 4.7 & 4.8 shows presence of inclusions right in HIC trajectory in metal sample E. EDX analysis indicates inclusion consisting of

silicone oxide in the trajectory of the HIC. M/A particles are also seen in the cracked areas which are known to contribute to HIC in steels.

4.2 Conclusion

Extensive analysis of all test results in previous sections established following relationships for HIC in steels used for pressure vessels and pipelines fabrication-

- Relationship between Duration of Exposure and Hydrogen Induced Cracking (HIC)-
- Relationship between pH of Environment and Hydrogen Induced Cracking (HIC),
- Relationship between Tensile Strength and Hydrogen Induced Cracking (HIC),
- Microstructures and susceptibility to HIC, including types of inclusions and precipitates promoting HIC.

Quantitative analysis provided following relationship among variables which represent their combined effect on HIC.

Duration of Exposure and HIC

The overall trend of HIC (sample A, D & E) with respect to duration of exposure is found increasing with following relationship-

- CLR: $y = 3.3817x^2 - 2.5417x + 8.8467$
- CTR: $y = 2.5917x^2 - 6.6383x + 6.1967$
- CSR: $y = 0.9733x^2 - 2.59x + 1.8167$

The increasing trend of HIC which is represented by all the above parameters, e.g., CLR, CTR and CSR, primarily indicate that extent of hydrogen induced cracking in flat rolled steels will increase as the steels will be more exposed to sour service acidic environment.

Testing were carried out at aggressive conditions to identify if susceptible materials would be affected by HIC depending on the duration of exposure of the steel samples to sour conditions. Based on the outcome of tests, it can be postulated that duration of exposure of sour environment shall have direct increasing effect on HIC of flat rolled steels.

pH of Environment and HIC

The overall trend analysis of HIC with respect to pH of the environments is found, as mentioned below-

- CLR: $y = -1.6969x^2 + 10.992x + 5.0714$
- CTR: $y = -0.3732x^2 + 1.9924x + 2.9207$
- CSR: $y = -0.1191x^2 + 1.0877x - 0.6486$

The CLR and CTR show all-through upward trend between pH 1 and pH 2.7, followed by downward trend between pH 2.7 and pH 4. The CSR showed a downtrend all through between pH 1 and pH 4.

The above signifies that HIC initiates at pH 1, the length and number of cracks continue to increase up to pH 2.7, whereas the same decreases between pH 2.7 and pH 4. Close to pH 7, HIC initiation and growth stops, as negative CLR is not possible in reality.

Higher pH is less aggressive in corroding steel samples. HIC is related to corrosion of specimens as availability of hydrogen for HIC to occur in material, originate from cathodic reaction which is part of electro-chemical corrosion reaction. In current experiments, it is found that CLR values reduce above pH 2.7, indicating reduction in severity with increase of pH of the environment above pH 2.7.

The lesser value of CLR at pH values less than 2.7, are probably due to fast formation of protective scales on steel samples at too aggressive environments which are also dependent on chemical composition and microstructural morphology of the samples. The adhering scales to the surface of the specimen

will cause reduction of hydrogen charging in steels and consequently, reduction in HIC in specimens. The phenomenon was prominent in trend curves for sample #A & #D. sample #A and #D have ferrite-pearlite microstructure, whereas, sample #E having bainitic microstructure, showed different trend in HIC vs pH evaluation.

Recommended Operating Conditions to Resist HIC

The overall trend analysis (samples #A, #D & #E) of HIC cracking with respect to pH for the samples has been described above. Accordingly, it is recommended to use the materials above pH 2.7 and, as close as practicable, to pH 6 to minimize effect of HIC. If required, environment pH shall be modified with application of inhibitors to increase pH to reduce risk of HIC damage of pipeline and pressure vessel steels in acidic sour service environment.

Crack length verification by ultrasonic scanning (scan A) for the HIC tested samples, shall be considered for information only in this research.

Tensile Strength and HIC

It was found through the trend curve that tensile strength of the rolled steels, up to approximately, 300 N/MM² did not have any significant effect on initiating or propagating HIC in steels, but steels having tensile strength above 300 N/MM² showed HIC susceptibility increased significantly with strength following the exponential expression-

$$Y = 3.245 x^2 - 16.575x + 22.67$$

This indicates that higher strength materials should be avoided in sour service to avoid HIC in rolled steels.

Microstructural Features Responsible for HIC

The microstructures of sample #A and #D are ferrite-pearlite and sample #E is found as bainite.

Optical micrographs also show considerable centerline segregation in the metal matrix of sample #A and banding in sample #A and #D. Centerline segregation and banding are found considerably less for sample #E .

SEM & EDX images show that MnS and SiO are in the trajectory of all Hydrogen Induced Cracks. It appears that inclusions, consisting of MnS and Si-O, are necessary ingredients in steel microstructure for the HIC mechanism to occur in steels. Bainitic structure will be preferred than pearlitic structure as steel samples with bainitic structure showed comparatively less segregation and banding as well which indirectly influence HIC in steels.

4.4 Future Work

Extensive research and analysis has been carried out in the current project to achieve the objectives. However, following areas will require more precise understanding in future work to resist HIC-

- Resistance of mixed microstructures to HIC initiation and propagation tendency in steels,
- Effect of thickness on HIC initiation and propagation in different steel microstructures

More research is also warranted to determine appropriate test duration and pH condition to decide optimum HIC test condition for the industry.

References

- [1] P. Toussaint and R. De Chatelet, "09352 2009," *NACE Corros. 2009 Conf. Expo*, no. 09352, pp. 1–18, 2009.
- [2] C. Christensen, P. Alle, and R. T. Hill, "Paper No. 422," no. 422, 2020.
- [3] C. Bosch, V. Smith, and J. Kittel, "Paper No. 3893," no. 3893, pp. 1–16.
- [4] V. Schwinn et al, "Paper No. 583," in *Characteristics marks and production methods of HIC resistant pressure vessel steel*, no. 583.
- [5] George E. Dieter, *Mechanical Metallurgy*. McGraw - Hill Kogakusha, Ltd.
- [6] R. D. Kane and M. S. Cayard, "NACE COMMITTEE REPORT 8X294: REVIEW OF PUBLISHED LITERATURE ON WET H₂S CRACKING."
- [7] DNVGL, "OS-F101 - Submarine Pipeline Systems," no. Outubro, p. 367, 2013.
- [8] Norsok, "NORSOK Materials selection M-001," *NORSOK Stand.*, no. August, 2002.
- [9] "CAPCIS TEST FOR PIPELINE-OTI 95635 Sour Testing.pdf." .
- [10] "53-EFC-16.pdf." .
- [11] R. D. Kane and M. S. Cayard, "274 ROLES OF H₂S IN THE BEHAVIOR OF ENGINEERING ALLOYS: A REVIEW OF LITERATURE AND EXPERIENCE."
- [12] R. J. Pargeter, "Susceptibility to SOHIC for Linepipe and Pressure Vessel Steels – Review of Current Knowledge."
- [13] "99416 DETECTION REPAIR AND MITIGATION OF WET H₂S CRACKING AN OVERVIEW OF RP0296 (51300-99416-SG) (1)."
- [14] H. B. Xue and Y. F. Cheng, "Characterization of inclusions of X80

- pipeline steel and its correlation with hydrogen-induced cracking,” *Corros. Sci.*, vol. 53, no. 4, pp. 1201–1208, 2011.
- [15] “13-99416 DETECTION REPAIR AND MITIGATION OF WET H₂S CRACKING AN OVERVIEW OF RP0296 (51300-99416-SG).”
- [16] J. Ning, Y. Zheng, D. Young, B. Brown, and S. Nešić, “Thermodynamic Study of Hydrogen Sulfide Corrosion of Mild Steel,” *NACE Int.*, vol. 70, no. 4, pp. 375–389, 2014.
- [17] R. Serna, S., Albarran, J.L., and Perez, “Effect of Wet Hydrogen Sulfide Environments on The Cracking Susceptibility of Medium-Strength Micro Alloyed Pipeline Steels for Oil and Gas Transport,” *Corrosion-2003*, no. 03530, p. 10, 2003.
- [18] W. K. Kim, S. U. Koh, B. Y. Yang, and K. Y. Kim, “Effect of environmental and metallurgical factors on hydrogen induced cracking of HSLA steels,” *Corros. Sci.*, vol. 50, no. 12, pp. 3336–3342, 2008.
- [19] H. B. Xue and Y. F. Cheng, “Characterization of inclusions of X80 pipeline steel and its correlation with hydrogen-induced cracking,” *Corros. Sci.*, 2011.
- [20] S. P. Lynch, “Mechanisms and kinetics of environmentally assisted cracking: Current status, issues, and suggestions for further work,” in *Metallurgical and Materials Transactions A: Physical Metallurgy and Materials Science*, 2013.
- [21] Y. Ogawa *et al.*, “Multi-scale observation of hydrogen-induced, localized plastic deformation in fatigue-crack propagation in a pure iron,” *Scr. Mater.*, vol. 140, pp. 13–17, 2017.
- [22] X. Xing, M. Yu, W. Chen, and H. Zhang, “Atomistic simulation of hydrogen-assisted ductile-to-brittle transition in α -iron,” *Comput. Mater. Sci.*, vol. 127, pp. 211–221, 2017.
- [23] J. A. Lee *et al.*, “Hydrogen-induced toughness drop in weld coarse-grained heat-affected zones of linepipe steel,” *Mater. Charact.*, vol. 82,

pp. 17–22, 2013.

- [24] J. G. Sezgin, C. Bosch, A. Montouchet, G. Perrin, and K. Wolski, “Modelling of hydrogen induced pressurization of internal cavities,” *Int. J. Hydrogen Energy*, vol. 42, no. 22, pp. 15403–15414, 2017.
- [25] S. U. Koh, H. G. Jung, K. B. Kang, G. T. Park, and K. Y. Kim, “Effect of microstructure on hydrogen-induced cracking of linepipe steels,” *Corrosion*, 2008.
- [26] H. Y. Liou, R. I. Shieh, F. I. Wei, and S. C. Wang, “Roles of microalloying elements in hydrogen induced cracking resistant property HSLA steel,” *Corrosion*, vol. 49, no. 5, pp. 389–398, 1993.
- [27] X. S. Du, W. B. Cao, C. D. Wang, S. J. Li, J. Y. Zhao, and Y. F. Sun, “Effect of microstructures and inclusions on hydrogen-induced cracking and blistering of A537 steel,” *Mater. Sci. Eng. A*, vol. 642, pp. 181–186, 2015.
- [28] J. Nieto et al, “Journal of Materials Engineering and Performance,” *ASM Int.*, vol. Vol-22(9).
- [29] H. Takabe *et al.*, “The Effect of Alloying Elements on Environmental Cracking Resistance of Stainless Steels in CO₂ Environments with and without Small Amount of H₂S Hideki C2012-0001277,” *Corros. 2012*, 2012.
- [30] H. H. Tang and M. S. Cayard, “TEST METHODS FOR THE EVALUATION OF MATERIALS FOR WET H₂S SERVICE.”
- [31] D. I. N. E. N. Iso, E. N. Iso, and D. I. N. E. N. Iso, “October 2014,” no. October 2014, 2019.
- [32] G. T. Park, S. U. Koh, H. G. Jung, and K. Y. Kim, “Effect of microstructure on the hydrogen trapping efficiency and hydrogen induced cracking of linepipe steel,” *Corros. Sci.*, 2008.
- [33] M. Elboujdaini, R. W. Revie, C. Derushie, and N. R. Canada, “Paper No. 03528,” *Analysis*, no. 03528, pp. 1–13, 2003.

- [34] F. Gui, T. Ramgopal, and M. G. Muller, "Role of sour environments on the corrosion fatigue growth rate of x65 pipe steel," *Corrosion*, vol. 68, no. 8, pp. 730–738, 2012.
- [35] N. Loukachenko, P. Bourges, K. E. Orie, C. Chauvy, and L. Coudreuse, "09352 - Recent experience on sour service resistant steels behavior."
- [36] Y. Zheng, J. Ning, B. Brown, and S. Nešić, "Electrochemical model of mild steel corrosion in a mixed H₂S/CO₂ aqueous environment in the absence of protective corrosion product layers," *Corrosion*, vol. 71, no. 3, pp. 316–325, 2015.
- [37] R. W. Revie, V. S. Sastri, G. R. Hoey, R. R. Ramsingh, D. K. Mak, and M. T. Shehata, "Hydrogen-induced cracking of linepipe steels part 1- threshold hydrogen concentration and pH," *Corrosion*, 1993.
- [38] R. W. Revie, V. S. Sastri, R. R. Ramsingh, Y. Lafreniere, and M. Elboudjaini, "Hydrogen-induced cracking of line pipe steels used in sour service," *Corrosion*, vol. 49, no. 7, pp. 531–535, 1993.
- [39] M.G.Hay et al, "Fitness for purpose material testing for sour gas service-An Overview," *Corrosion*, no. March, 2001.
- [40] A. Traidia, M. Alfano, G. Lubineau, S. Duval, and A. Sherik, "An effective finite element model for the prediction of hydrogen induced cracking in steel pipelines," *Int. J. Hydrogen Energy*, vol. 37, no. 21, pp. 16214–16230, 2012.
- [41] D. Mizuno *et al.*, "Paper No. 7333," no. 7333, pp. 1–11.
- [42] M. A. Mohtadi-Bonab, J. A. Szpunar, and S. S. Razavi-Tousi, "A comparative study of hydrogen induced cracking behavior in API 5L X60 and X70 pipeline steels," *Eng. Fail. Anal.*, vol. 33, pp. 163–175, 2013.
- [43] D. P. Dunne, D. Hejazi, A. A. Saleh, A. J. Haq, A. Calka, and E. V. Pereloma, "Investigation of the effect of electrolytic hydrogen charging of X70 steel: I. The effect of microstructure on hydrogen-induced cold

- cracking and blistering,” *Int. J. Hydrogen Energy*, vol. 41, no. 28, pp. 12411–12423, 2016.
- [44] R. W. Revie, V. S. Sastri, R. R. Ramsingh, Y. Lafreniere, and M. Elboujdaini, “Hydrogen-induced cracking of line pipe steels used in sour service,” *Corrosion*, 1993.
- [45] Y. Ogawa, H. Matsunaga, J. Yamabe, M. Yoshikawa, and S. Matsuoka, “Unified evaluation of hydrogen-induced crack growth in fatigue tests and fracture toughness tests of a carbon steel,” *Int. J. Fatigue*, vol. 103, pp. 223–233, 2017.
- [46] T. H. Hyodo, M. Iino, a Ikeda, M. Kimura, and M. Shimizu, “The Hydrogen Permeation and Hydrogen - Induced Cracking Behavior of Linepipe Dynamic Full Scale Tests,” *Corros. Sci.*, vol. 27, no. 10, pp. 1077–1098, 1987.
- [47] J. Xie, L. Yang, B. Worthingham, and F. King, “Hydrogen Effects on High Strength Pipeline Steels,” *Corrosion*, no. 09120, pp. 1–15, 2009.
- [48] S. P. Lynch, H. G. Jung, K. B. Kang, G. T. Park, and K. Y. Kim, “Mechanisms and kinetics of environmentally assisted cracking,” *Metall. Mater. Trans. A*, vol. 44A, no. 7, pp. 574–585, 2013.
- [49] A. J. Haq, K. Muzaka, D. P. Dunne, A. Calka, and E. V. Pereloma, “Effect of microstructure and composition on hydrogen permeation in X70 pipeline steels,” *Int. J. Hydrogen Energy*, vol. 38, no. 5, pp. 2544–2556, 2013.
- [50] J. Kittel, V. Smanio, M. Fregonese, L. Garnier, and X. Lefebvre, “Hydrogen induced cracking (HIC) testing of low alloy steel in sour environment: Impact of time of exposure on the extent of damage,” *Corros. Sci.*, vol. 52, no. 4, pp. 1386–1392, 2010.
- [51] J. Kittel, V. Smanio, M. Fregonese, L. Garnier, and X. Lefebvre, “Hydrogen induced cracking (HIC) testing of low alloy steel in sour environment: Impact of time of exposure on the extent of damage,” *Corros. Sci.*, 2010.

- [52] W. K. Kim, S. U. Koh, and K. Y. Kim, "Paper No. 07500," *Corros.* 2007, no. 07500, p. paper 500, 2007.
- [53] M. A. Mohtadi-Bonab, J. A. Szpunar, L. Collins, and R. Stankievech, "Evaluation of hydrogen induced cracking behavior of API X70 pipeline steel at different heat treatments," *Int. J. Hydrogen Energy*, vol. 39, no. 11, pp. 6076–6088, 2014.
- [54] NACE, "NACE MR0175/ISO 15156-1/2001: Petroleum and natural gas industries — Materials for use in H₂S-containing environments in oil and gas production — Part 1 : General principles for selection of cracking-resistant materials," *Transportation (Amst.)*, no. 21307, 2005.
- [55] F. Huang, X. G. Li, J. Liu, Y. M. Qu, J. Jia, and C. W. Du, "Hydrogen-induced cracking susceptibility and hydrogen trapping efficiency of different microstructure X80 pipeline steel," *J. Mater. Sci.*, vol. 46, no. 3, pp. 715–722, 2011.
- [56] R. J. Pargeter, "Susceptibility to SOHIC for Linepipe and pressure vessel- Review of current knowledge," *NACE Corros.*, no. 07115, pp. 1–27, 2007.
- [57] G. Domizzi, G. Anteri, and J. Ovejero-García, "Influence of sulphur content and inclusion distribution on the hydrogen induced blister cracking in pressure vessel and pipeline steels," *Corros. Sci.*, vol. 43, no. 2, pp. 325–339, 2001.
- [58] ASTM standard A841/841M, "Standard Specification for Steel Plates for Pressure Vessels , Produced by Thermo- Mechanical Control Process (TMCP)," *Annu. B. ASTM Stand.*, vol. i, no. Reapproved 2007, pp. 1–5, 2011.
- [59] ASTM, "Standard Specification for Pressure Vessel Plates , Carbon Steel , for Moderate- and Lower-Temperature Service," *Annu. B. ASTM Stand.*, pp. 1–4, 2011.
- [60] "Specification for line pipe," *Br. Corros. J.*, vol. 20, no. 3, pp. 106–106, 2013.

- [61] M. Masoumi, C. C. Silva, and H. F. G. de Abreu, "Effect of crystallographic orientations on the hydrogen-induced cracking resistance improvement of API 5L X70 pipeline steel under various thermomechanical processing," *Corros. Sci.*, vol. 111, pp. 121–131, 2016.
- [62] M. Y. Matrosov, O. N. Sychev, A. M. Korchagin, and O. P. Talanov, "Corrosion Resistant Plates for Pipes Operated in Sour Environments," *Mater. Sci. Forum*, vol. 854, pp. 106–111, 2016.
- [63] J. Li, X. Gao, L. Du, and Z. Liu, "Relationship between microstructure and hydrogen induced cracking behavior in a low alloy pipeline steel," *J. Mater. Sci. Technol.*, no. 2010, 2017.
- [64] J. Moon *et al.*, "Influence of precipitation behavior on mechanical properties and hydrogen induced cracking during tempering of hot-rolled API steel for tubing," *Mater. Sci. Eng. A*, vol. 652, pp. 120–126, 2016.
- [65] M. S. Cayard, R. D. Kane, and D. L. Cooke, "An Exploratory Examination Of The Effect Of SOHIC Damage On The Fracture Resistance Of Carbon Steels," *Corrosion*, no. 525, pp. 1–16, 1997.
- [66] G. T. Park, S. U. Koh, H. G. Jung, and K. Y. Kim, "Effect of microstructure on the hydrogen trapping efficiency and hydrogen induced cracking of linepipe steel," *Corros. Sci.*, vol. 50, no. 7, pp. 1865–1871, 2008.
- [67] R. A. Carneiro, R. C. Ratnapuli, and V. de Freitas Cunha Lins, "The influence of chemical composition and microstructure of API linepipe steels on hydrogen induced cracking and sulfide stress corrosion cracking," *Mater. Sci. Eng. A*, vol. 357, no. 1–2, pp. 104–110, 2003.
- [68] W. L. Costin, O. Lavigne, A. Kotousov, R. Ghomashchi, and V. Linton, "Investigation of hydrogen assisted cracking in acicular ferrite using site-specific micro-fracture tests," *Mater. Sci. Eng. A*, vol. 651, pp. 859–868, 2016.

- [69] K. O. Findley, M. K. O'Brien, and H. Nako, "Critical assessment 17: Mechanisms of hydrogen induced cracking in pipeline steels," *Mater. Sci. Technol. (United Kingdom)*, vol. 31, no. 14, pp. 1673–1680, 2015.
- [70] M. Lobatón, P. Raffinage, and P. Couronne-Prpc, "Managing wet H₂S Cracking in Refineries."
- [71] R. W. Revie, V. S. Sastri, G. R. Hoey, R. R. Ramsingh, D. K. Mak, and M. T. Shehata, "Hydrogen-induced cracking of linepipe steels part 1- threshold hydrogen concentration and pH," *Corrosion*, vol. 49, no. 1, pp. 17–23, 1993.
- [72] H. Lukito and Z. Szklarska-Smialowska, "Susceptibility of medium-strength steels to hydrogen-induced cracking," *Corros. Sci.*, vol. 39, no. 12, pp. 2151–2169, 1997.
- [73] M. A. Al-Anezi and S. Rao, "Challenges in procurement of HIC resistant steel pipes," *J. Fail. Anal. Prev.*, vol. 11, no. 4, pp. 385–392, 2011.
- [74] V. Venegas, F. Caleyó, T. Baudin, J. H. Espina-Hernández, and J. M. Hallen, "On the role of crystallographic texture in mitigating hydrogen-induced cracking in pipeline steels," *Corros. Sci.*, vol. 53, no. 12, pp. 4204–4212, 2011.
- [75] M. A. Mohtadi-Bonab, M. Eskandari, and J. A. Szpunar, "Texture, local misorientation, grain boundary and recrystallization fraction in pipeline steels related to hydrogen induced cracking," *Mater. Sci. Eng. A*, vol. 620, pp. 97–106, 2014.
- [76] T. Fujishiro, N. Steel, S. M. Corporation, T. Hara, N. Steel, and S. M. Corporation, "Paper No. 10665," no. 10665, pp. 1–11.
- [77] K. E. Orie, "Paper No. 632," no. 632, 2017.
- [78] L. Coudreuse, C. Zmudzinski, P. Bocquet, U. Industeel, A. Gingell, and A. Cheviet, "Corrosion 01105 2001," *Corrosion*, 2001.
- [79] T.E. PEREZ, "Paper no 121, Corrosion 98," 1998.

- [80] L. Coudreuse, C. Zmudzinski, P. Bocquet, A. Gingell, and A. Cheviet, "APPLICATION OF NORMALISED AND QUENCHED AND TEMPERED PRESSURE VESSEL STEELS AS A FUNCTION OF SOUR SERVICE SEVERITY."
- [81] K. Baba, D. Mizuno, K. Yasuda, H. Nakamichi, and N. Ishikawa, "Effect of Cu addition in pipeline steels on prevention of hydrogen permeation in mildly sour environments," *Corrosion*, vol. 72, no. 9, pp. 1107–1115, 2016.
- [82] X. Shi, W. Yan, W. Wang, Y. Shan, and K. Yang, "Novel Cu-bearing high-strength pipeline steels with excellent resistance to hydrogen-induced cracking," *Mater. Des.*, vol. 92, pp. 300–305, 2016.
- [83] T. Hvodo, M. Iino, A. Ikeda, M. Kimura, and M. Shimizu, "THE HYDROGEN PERMEATION AND HYDROGEN-INDUCED CRACKING BEHAVIOUR OF LINEPIPE IN DYNAMIC FULL SCALE TESTS," *Corros. Sci.*, vol. 27, no. 1011, pp. 1077–1098, 1987.
- [84] N. Winzer *et al.*, "Hydrogen diffusion and trapping in Ti-modified advanced high strength steels," *Mater. Des.*, vol. 92, pp. 450–461, 2016.
- [85] C. Bosch, T. Haase, A. Liessem, and M. Ruhr GERMANY J-P Jansen, "08109 - EFFECT OF NACE TM0284 TEST MODIFICATIONS ON THE HIC PERFORMANCE OF LARGE-DIAMETER PIPES."
- [86] T. F. Elf, "Corrosion 01067 2001," 2001.
- [87] F. Huang, J. Liu, Z. J. Deng, J. H. Cheng, Z. H. Lu, and X. G. Li, "Effect of microstructure and inclusions on hydrogen induced cracking susceptibility and hydrogen trapping efficiency of X120 pipeline steel," *Mater. Sci. Eng. A*, vol. 527, no. 26, pp. 6997–7001, 2010.
- [88] S. U. Koh, B. Y. Yang, and K. Y. Kim, "Effect of Cr and Mo on Susceptibility to Sulfide Stress Cracking of API X70 Grade Line Pipe Steels.pdf," no. March, pp. 262–274, 2004.

- [89] M. A. Al-Anezi, G. S. Frankel, and A. K. Agrawal, "Susceptibility Of Conventional Pressure Vessel Steel To HIC And SOHIC In H₂S Diglycolamine Solutions," *Corrosion*, vol. 55, no. 11, pp. 1101–1109, 1999.
- [90] G. Herbsleb, R. Poepperling, and W. Schwenk, "Occurrence and Prevention of Hydrogen Induced Stepwise Cracking and Stress Corrosion Cracking of Low Alloy Pipeline Steels," *Corrosion*, vol. 36, no. 5, pp. 247–256, 1981.
- [91] S. J. Suess, S. Technimet, and N. Berlin, "Paper No.," no. 07, pp. 1–26.
- [92] M. A. Mohtadi-Bonab, J. A. Szpunar, and S. S. Razavi-Tousi, "Hydrogen induced cracking susceptibility in different layers of a hot rolled X70 pipeline steel," *Int. J. Hydrogen Energy*, vol. 38, no. 31, pp. 13831–13841, 2013.
- [93] B. Crowder, S. Mishael, J. Buchanan, and R. Shockley, "11105: Sulfide Stress Cracking Susceptibility of Local Hard Areas in Carbon Steel Weld Heat Affected Zones."
- [94] A. S. F. T. A. MATERIALS, "ASTM A 234 / A 234M - 99 : Standard specification for piping fittings of wrought carbon steel and alloy steel for moderate and high temperature service," 1999.
- [95] A. S. F. T. A. MATERIALS, "ASTM A 370-97a : Standard test methods and definitions for mechanical testing of steel products," 1997.
- [96] H. Y. Liou, R. I. Shieh, F. I. Wei, and S. C. Wang, "Roles of microalloying elements in hydrogen induced cracking resistant property HSLA steel," *Corrosion*, 1993.
- [97] ASTM E8M-04, "A 370-06 Standard Test Methods and Definitions for Mechanical Testing of Steel Products," *Annu. B. ASTM Stand.*, no. October, pp. 1–54, 2006.
- [98] B. S. Kulesza, J. E. Shick, F. B. Fletcher, and E. E. McDowell, "Paper No. 7498," no. 7498, pp. 1–11.

- [99] N. S. Tm and I. No, "Standard Test Method Laboratory Testing of Metals for Resistance to Sulfide Stress Cracking and Stress Corrosion Cracking in H₂S Environments," 1997.

APPENDIX-1

PUBLICATION-1:

ScienceDirect Engineering Fracture Mechanics journal

Hydrogen induced cracking of pipeline and pressure vessel steels- A review

Goutam Ghosh, Paul Rostron, Rajnish Garga, Ashoutosh Pandaya

University of Petroleum and Energy Studies, Dehradun, India

The Petroleum Institute, Khalifa University, Abu Dhabi, United Arab Emirates

ARTICLE INFO

Keywords:

Hydrogen Induced Cracking (HIC)

Inclusion

Microstructure

Diffusion

ABSTRACT

Pipelines and pressure vessels made of carbon and low alloy steels have suffered from Hydrogen

Induced Cracking (HIC) in wet hydrogen sulfide environment in the oil & gas industry. Hydrogen which is produced at cathode due to corrosion reaction, diffuses into the steel and result in cracking in wet hydrogen sulfide environment. Hydrogen assisted cracking usually manifests in carbon and low alloy steels with unique crack initiation and propagation characteristics. The origin and morphology of cracks are dependent on various factors viz., mechanical properties & composition of the material, manufacturing process including heat treatment, applicable stresses etc. Hydrogen assisted cracking is commonly classified into three categories based on initiation, morphology and stress requirement in cracking as, Hydrogen Induced Cracking (HIC), Sulfide Stress Cracking (SSC) and Stress Oriented Hydrogen Induced Cracking (SOHIC).

The current paper discusses the metallurgical factors which play a major role in Hydrogen

Induced Cracking of flat rolled steels commonly used in manufacturing of pipelines and pressure

vessels in oil & gas industry as found in several studies.

<https://doi.org/10.1016/j.engfracmech.2018.06.018>

Received 7 March 2018; Received in revised form 18 April 2018; Accepted 13 June 2018

* Corresponding author.

E-mail addresses: goutamkw@gmail.com (G. Ghosh), prostron@pi.ac.ae (P. Rostron), rgarg@ddn.upes.ac.in (R. Garg), apanday@ddn.upes.ac.in (A. Panday).

Engineering Fracture Mechanics 199 (2018) 609–618

Available online 15 June 2018

0013-7944/ © 2018 Published by Elsevier Ltd.

PUBLICATION-2:

International Journal of Applied Engineering Research
ISSN 0973-4562 Volume 13, Number 11 (2018) pp. 9053-9059 ©
Research India Publications. <http://www.ripublication.com> 9053

**Effect of Change of Acidic Condition (pH) and Test Duration on
Hydrogen Induced Cracking of Flat Rolled Steels**

1Mr. Goutam Ghosh, 2Dr. Paul Rostron, 3Dr. Rajnish Garg, 4Dr. Ashoutosh
Panday

*1,*University of Petroleum and Energy Studies, Dehradun, India.*

(Corresponding author)*

2Khalifa University, Abu Dhabi, UAE.

3University of Petroleum and Energy Studies, Dehradun, India.

4University of Petroleum and Energy Studies, Dehradun, India.

Abstract

Flat rolled steel products are found to suffer from Hydrogen Induced cracking in sour condition in oil and gas industry. Typically, Hydrogen Induced cracking or HIC is caused by trapped hydrogen atoms at defect locations. The role of stress differs in different hydrogen assisted cracking mechanisms e.g., in Sulfide Stress Cracking (SSC) and Stress Oriented Hydrogen Induced Cracking (SOHIC) where additional stress is considered as necessary to initiate cracking, whereas, in case of HIC, external load is not considered as a prerequisite, rather, internal stress generated by the hydrogen molecules accumulated in defect locations inside the metal thickness, finally causes cracking.

To avoid unwarranted failure by HIC in service, steels are tested in manufacturing, as well as, fabrication of equipment. HIC testing is commonly carried out according to NACE TM 0284 standard[1]. The standard provides test conditions including, duration for testing and methodology for evaluation of HIC, however the acceptance limits of HIC usually remains with the owner of the equipment as HIC free steel may be significantly challenging to manufacture in the industry and some extent of HIC is accepted in material

qualification. HIC cracking is found to vary in intensity with change of acidic condition and duration of testing. The current paper describes the study and the results obtained to highlight the effect of change of acidic condition (represented by pH) and duration of testing on HIC of flat rolled steels.

Keywords: Hydrogen Induced Cracking (HIC), Crack Length Ratio (CLR), Crack Thickness Ratio (CTR), Crack Sensitivity Ratio (CSR).

APPENDIX- 2

HIC TEST RESULT FOR EACH SPECIMEN

GLOSSARY

Sour Service:

Exposure to oil field environment that contain sufficient hydrogen sulfide (H₂S) to cause cracking of materials. As per NACE MR-0175/ISI-15156, the service is called 'sour service' if partial pressure of hydrogen sulfide in a system exceeds or equal to 0.3 KPa (0.05 Psi),.

Hydrogen Induced Cracking

Typical planer cracking occurring largely in, flat rolled steels in sour service due to hydrogen trapping at planner defect sites.

Sulfide Stress Cracking:

Cracking of susceptible metals in presence of tensile stress (residual and / or applied), water and hydrogen sulfide (H₂S).

Hydrogen Embrittlement:

Degradation of material properties in presence of hydrogen. The main characteristics include temperature dependence, strain rate sensitivity and susceptibility to delayed fracture. Hydrogen embrittlement is enhanced by slow strain rates.

pH

pH indicates the [acidity](#) or [basicity](#) of an [aqueous solution](#), in a [logarithmic scale](#) measurement. It is (approximately) the negative of the base 10 [logarithm](#) of the [molar concentration](#), measured in units of [moles](#) per liter, of [hydrogen ions](#). Precisely, it is the negative of the base 10 logarithm of the [activity](#) of the hydrogen ion.^[1] Solutions with a pH less than 7 are acidic and solutions with a pH greater than 7 are [basic or alkaline](#). [Pure water](#) is measured as pH 7 (25 °C), considered as

neutral i.e., neither an acid nor a base. The pH value can be less than 0 or greater than 14 for very strong acids and bases, respectively.^[2]

.....**THE END**.....